VOLUME 87, NO. EM
DECEMBER 1961
PART 1

JOURNAL of the

Engineering Mechanics Division

PROCEEDINGS OF THE
AMERICAN SOCIETY
OF CIVIL ENGINEERS

Vol. 87 No. EM 6

Journal of the
ENGINEERING MECHANICS DIVISION
Proceedings of the American Society of Civil Engineers

CONTENTS

December, 1961

Papers

(over)

Note.—Part 2 of this Journal is the 1961-45 Newsletter of the Engineering Mechanics Division.

The three preceding issues of this Journal are dated June 1961, August 1961, and October 1961.

DISCUSSION

Journal of the
ENGINEERING MECHANICS DIVISION
Proceedings of the American Society of Civil Engineers

EQUATIONS FOR PLATE-BEAM SYSTEMS IN TRANSVERSE BENDING

By Alfredo H.-S. Ang[1] and Wallace Prescott,[2] Associate Members, ASCE

SYNOPSIS

Recurrent equations for combined plate-beam systems are derived on the basis of a discrete model that has previously been shown to be the finite difference analog of the continuum model of a plate. The equations presented include the effects of flexural and torsional stiffnesses of the beams.

INTRODUCTION

Many problems that are of interest to engineers involve boundaries or constraints that are not readily suitable for analytic solution. Such situations may be resolved by numerical techniques that provide approximate solutions to these problems.

The method of finite differences is one of the methods. This method has been used increasingly in many applied fields since the advent of modern digital computers. There are two basic approaches in seeking approximate solutions to physical problems of continuum by the method of finite differences. One approach is to derive the governing differential equation of the continuum and subsequently approximate the differential equation by a system of finite difference equations. The other approach is to introduce a discrete model to approximate the continuum, with the restriction that in the limit the discrete

Note.—Discussion open until May 1, 1962. To extend the closing date one month, a written request must be filed with the Executive Secretary, ASCE. This paper is part of the copyrighted Journal of the Engineering Mechanics Division, Proceedings of the American Society of Civil Engineers, Vol. 87, No. EM6, December, 1961.

[1] Asst. Prof. of Civ. Engrg., Univ. of Illinois, Urbana, Ill.

[2] Graduate Student in Civ. Engrg., Univ. of Illinois, Urbana, Ill.; on leave from Tennessee Poly. Inst., Cookeville, Tenn.

model approaches the continuum (at least in an intuitive sense). The latter approach is used herein to derive the governing recurrent equations for plate-beam systems. Using this approach, difficulties due to discontinuities and special boundary conditions that would otherwise be encountered, are circumvented and the governing equations are readily derived. The discrete model used is an extension of the plate model first proposed by Nathan M. Newmark,[3] F. ASCE.

The application of finite differences to problems of bending of plates are not new and may be found in many places in the literature. What is claimed to be new, however, is the use of the approach described herein (including the use of fictitious deflections) that makes possible the derivation of the equations for plate-beam systems (based on central differences) wherein the beams have combined torsional and flexural stiffnesses. In addition, most of the equations, particularly those pertaining to corner boundaries with beams, are presented for the first time.

The object of the paper is twofold: To demonstrate that a physical model can be used to great advantage in supplementing a purely mathematical approach, thus making possible solutions to problems involving complex boundary conditions and constraints; and to describe the derivation of and present equations that can be used by engineers in the analysis of plate-beam systems involving beams with torsional and flexural stiffnesses.

The analysis of plate-beam systems is based on the ordinary theories of flexure of beams and plates. In addition, the neutral axes of the beams are assumed to coincide with the middle plane of the plate. Torsion in the beam is assumed to be uniform between node points, and effects of warping are neglected. A beam is represented by a line.

Notation.—The terms adopted for use in this paper are defined where they first appear and are listed alphabetically, for convenience of reference, in the Appendix.

DERIVATION OF EQUATIONS

Although the analysis of plate-beam systems requires finite difference recurrent equations for plates, these equations will not be presented herein. They can be found in a number of places in the literature.[4] Recurrent equations that are peculiar only to combined plate-beam systems are derived. This is done in some detail for one case whereas others are presented without ramifications except notes concerning their applications.

The equations are derived for equal grid distances and are, therefore, restricted to square nets with straight boundaries. However, equations for rectangular nets can be similarly derived without special difficulties. For other coordinate systems, models similar to the one used must be devised and corresponding equations derived therefrom.

---

3 "A Numerical Procedure for the Analysis of Continuous Plates," by A. H. -S. Ang and N. M. Newmark, Proceedings, 2nd ASCE Conf. on Electronic Computation, September, 1960, p. 379.

4 "Analysis of Skew Slabs," by V. P. Jensen, Bulletin No. 332, Univ. of Illinois Engrg. Experiment Sta., 1941.

Central differences are used throughout. The inaccuracy involved in using the equations, therefore, is a result of the error inherent in the central difference approximation.[5]

Effects of Beam Stiffness.—Beams with only flexural stiffness have been considered before.[6] The effects of beams with combined flexural and torsional stiffnesses will be described.

Fig. 1 shows a plate stiffened with an interior beam. If the beam has torsional stiffness there will be discontinuity at the junction between the plate and the beam; that is, the curvatures of the plate normal to the axis of the beam will be different at the two faces of the beam. Referring to Fig. 1, these curvatures at joint o, by the three-point formula, are as follows:

$$\left(\frac{\partial^2 w}{\partial y^2}\right)_{on} = \frac{w_n - 2w_o + w_{\bar{s}}}{\lambda^2} \quad \ldots\ldots\ldots\ldots\ldots (1a)$$

and

$$\left(\frac{\partial^2 w}{\partial y^2}\right)_{os} = \frac{w_{\bar{n}} - 2w_o + w_s}{\lambda^2} \quad \ldots\ldots\ldots\ldots\ldots (1b)$$

in which $w_{\bar{n}}$ and $w_{\bar{s}}$ are fictitious deflections at points n and s, respectively, and λ is the distance between node points. The two fictitious deflections $w_{\bar{n}}$ and $w_{\bar{s}}$ are related by the fact that the angle of twist of the beam at o can be expressed as

$$\left(\frac{\partial w}{\partial y}\right)_o = \frac{w_n - w_{\bar{s}}}{2\lambda} = \frac{w_{\bar{n}} - w_s}{2\lambda} \quad \ldots\ldots\ldots\ldots (2)$$

Therefore

$$w_{\bar{s}} = w_n + w_s - w_{\bar{n}} \quad \ldots\ldots\ldots\ldots\ldots (3)$$

The curvatures given as Eq. 1 produce plate bending moments normal to the two faces of the beam that, in general, are not equal. This difference in bending moments about the axis of the beam acting at joint o is equilibrated by the torsional moments in the beam at o, as shown in Fig. 2(a). That is

$$(m_{on} - m_{os}) + (T_{oe} - T_{ow}) = 0 \quad \ldots\ldots\ldots\ldots (4)$$

In terms of deflections, these moments are

$$m_{on} = -N\lambda\left(\frac{w_n - 2w_o + w_{\bar{s}}}{\lambda^2} + \mu\,\frac{w_e - 2w_o + w_w}{\lambda^2}\right) \ldots\ldots (5a)$$

---

5 "Numerical Methods in Engineering," by M. G. Salvadori and M. L. Baron, Prentice-Hall, Inc., Englewood Cliffs, N. J., 1952.

6 "Moments in Simply Supported Skew I-Beam Bridges," by T. Y. Chen, C. P. Siess, and N. M. Newmark, Bulletin No. 439, Univ. of Illinois Engrg. Experiment Sta., 1957.

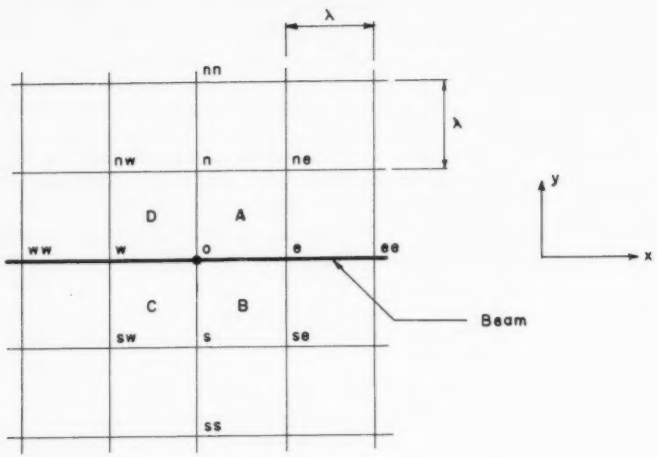

FIG. 1.—STANDARD DESIGNATION OF POINTS RELATIVE TO POINT O

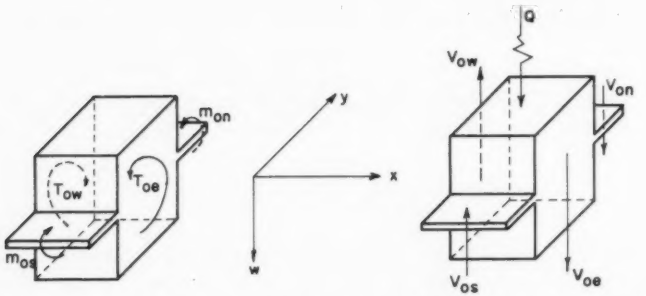

(a.) Moments about x-axis at joint O. (b.) Shear forces at joint O.

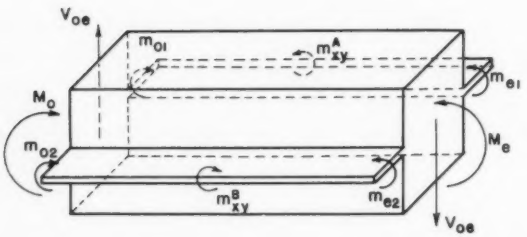

(c.) Moments about y-axis in bar oe.

FIG. 2.—EQUILIBRIUM OF JOINT AND BAR IN A PLATE-BEAM SYSTEM

$$m_{os} = - N \lambda \left(\frac{w_{\overline{n}} - 2w_o + w_s}{\lambda^2} + \mu \frac{w_e - 2w_o + w_w}{\lambda^2} \right) \quad \ldots . (5b)$$

$$T_{oe} = - J N \lambda \left(\frac{w_{ne} - w_{\overline{se}}}{2 \lambda^2} - \frac{w_n - w_{\overline{s}}}{2 \lambda^2} \right) \quad \ldots \ldots . (5c)$$

and

$$T_{ow} = - J N \lambda \left(\frac{w_n - w_{\overline{s}}}{2 \lambda^2} - \frac{w_{nw} - w_{\overline{sw}}}{2 \lambda^2} \right) \quad \ldots \ldots . (5d)$$

in which

$$N = \frac{E h^3}{12 (1 - \mu^2)} \quad \ldots \ldots \ldots \ldots \ldots (5e)$$

stiffness per unit width of plate, and

$$J = \frac{G C}{N \lambda} \quad \ldots \ldots \ldots \ldots \ldots \ldots (5f)$$

a measure of the torsional stiffness of the beam. Substituting these expressions into Eq. 4 and using Eq. 3 to eliminate the fictitious deflections below the beam, gives the equilibrium of moments about the axis of the beam in terms of deflections as follows:

$$- 2 w_n - J w_s + J/2 \left(w_{se} + w_{sw} - w_{\overline{ne}} - w_{\overline{nw}} \right) + (2 + J) w_{\overline{n}} = 0 \ldots (6)$$

or, in pattern form

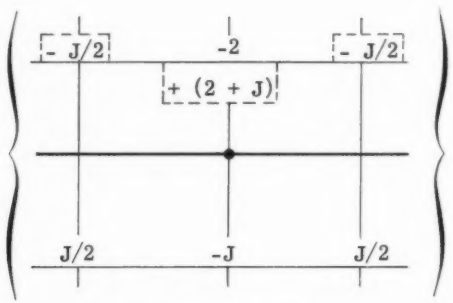

$$w = 0 \quad \ldots . . (7)$$

The presence of a beam with torsional stiffness, therefore, imposes an additional requirement for the joints on the beam as given by Eq. 7. The values inside the dotted boxes are coefficients of the fictitious deflections at the indicated points. These fictitious deflections, in general, do not coincide with the real deflections at the same points. Eq. 7, and similar equations to be derived, are to be used either to eliminate the fictitious deflections or to provide additional equations for determining the fictitious deflections. The latter procedure is usually preferable, because the fictitious deflections are required for finding the plate bending moments at, and normal to, the faces of the beam, as well as for finding the torsional moments in the beam.

The fictitious deflections can be considered as providing a means of specifying the angle of twist of a beam at a given point. The use of fictitious deflections, therefore, makes possible the use of central difference approximation in deriving the governing equations for a plate-beam system involving beam torsion.

Joints on or Near an Interior Beam.—Referring to Fig. 2(b), the equilibrium of forces normal to the middle-plane of the plate for a joint on an interior beam is given by

$$V_{oe} + V_{on} - V_{ow} - V_{os} + Q = 0 \quad \ldots\ldots\ldots\ldots (8)$$

in which Q is the equivalent concentrated load at the joint.[7] The other terms in Eq. 8 representing shears are, for example [see Fig. 2(c)]

$$V_{oe} = \frac{1}{\lambda}\left(M_e - M_o\right) + \frac{\left(m_{e1} + m_{e2}\right) - \left(m_{o1} + m_{o2}\right)}{\lambda} + \frac{\left(m_{xy}^{A} - m_{xy}^{B}\right)}{\lambda} \quad \ldots\ldots\ldots\ldots\ldots (9)$$

in which, for instance

$$M_o = - E I \left(\frac{w_e - 2w_o + w_w}{\lambda^2}\right) = - H N \lambda \left(\frac{w_e - 2w_o + w_w}{\lambda^2}\right) \ldots (10a)$$

$$m_{o1} = - N \frac{\lambda}{2}\left(\frac{w_e - 2w_o + w_w}{\lambda^2}\right) + \mu\left(\frac{w_n - 2w_o + w_s}{\lambda^2}\right) \quad \ldots (10b)$$

$$m_{o2} = - N \frac{\lambda}{2}\left(\frac{w_e - 2w_o + w_w}{\lambda^2} + \mu \frac{w_{\overline{n}} - 2w_o + w_s}{\lambda^2}\right) \ldots . (10c)$$

$$m_{xy}^{A} = - N \frac{\lambda}{2}(1 - \mu)\left(\frac{w_{ne} - w_n}{\lambda^2} - \frac{w_e - w_o}{\lambda^2}\right) \ldots . . (10d)$$

and

$$H = \frac{E I}{N \lambda} \quad \ldots\ldots\ldots\ldots\ldots\ldots (10e)$$

a measure of the flexural stiffness of the beam. Note the use of fictitious deflections in m_{o1} and m_{o2}. The other terms in Eq. 8 can be similarly expressed in terms of deflections. Substituting these expressions into Eq. 8 and making use of Eq. 3 gives the equation of equilibrium of normal forces for a joint on an interior beam, as follows:

---

7 "Numerical Procedure for Computing Deflections, Moments, and Buckling Loads," by N. M. Newmark, Transactions, ASCE, Vol. 108, 1943, p. 1161.

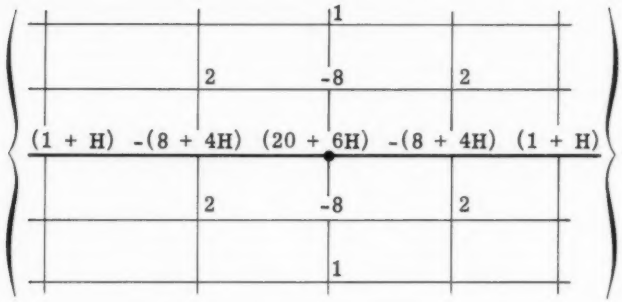

$$w = \frac{Q\lambda^2}{N} \quad \ldots(11)$$

Eq. 11 does not contain any fictitious deflections. However, this is not the case in the corresponding equation for the joints immediately adjacent to the beam as shown in Eq. 12, in which the value inside the dotted box is the coefficient of the fictitious deflection.

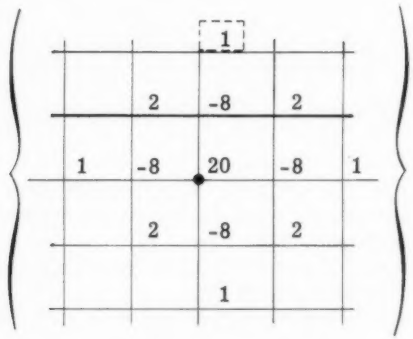

$$w = \frac{Q\lambda^2}{N} \quad \ldots\ldots\ldots(12)$$

Eq. 7 applied to every joint on an interior beam provides additional equations for determining the values of the fictitious deflections, that resulted from Eq. 12.

Joints on or Near an Exterior Beam.—Equilibrium of normal forces, for joints on an exterior beam and immediately adjacent to it are described, respectively, by Eqs. 13 and 14.

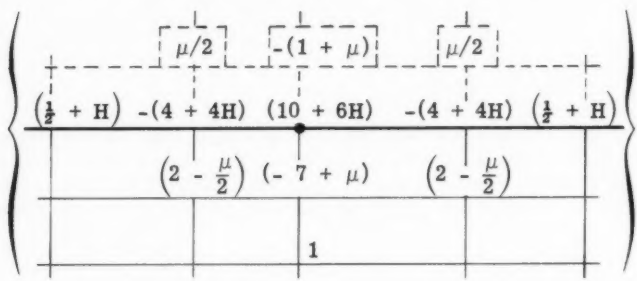

$$w = \frac{Q\lambda^2}{N} \quad \ldots(13)$$

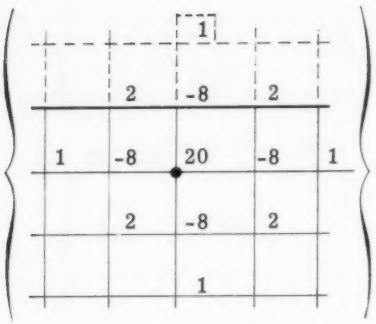

$$w = \frac{Q\,\lambda^2}{N} \quad \ldots\ldots\ldots (14)$$

The equilibrium of moments about the axis of the beam for a joint on the exterior beam is given by

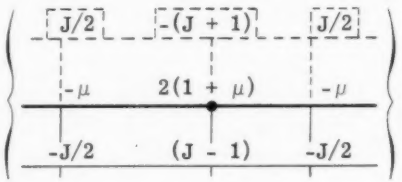

$$w = 0 \quad \ldots\ldots\ldots (15)$$

Eq. 15 should be applied to every joint on the exterior beam to provide the necessary additional equations for determining the fictitious deflections of the points outside the plate, as indicated in Eqs. 13 and 14.

Joints on Corners with Beams.—Two types of corners with beams are considered, a sharp corner and a re-entrant corner.

For a sharp corner, the equilibrium of normal forces is given by

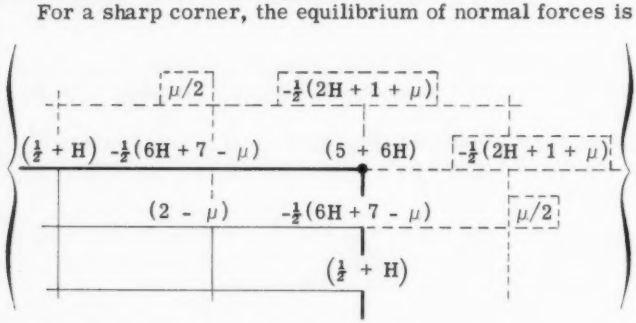

$$w = \frac{Q\,\lambda^2}{N} \quad \ldots\ldots (16)$$

For this case, there are two moment equilibrium conditions to be satisfied, that are

$$\sum M_x = 0 \text{ and } \sum M_y = 0 \quad \ldots\ldots\ldots\ldots\ldots (17)$$

and in terms of deflections are, respectively

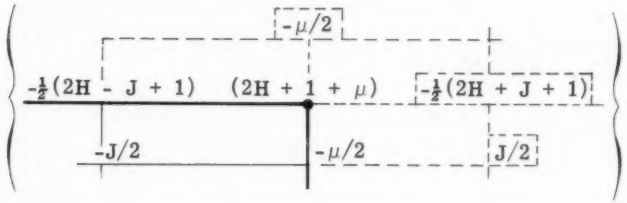

$$w = 0 \quad \ldots(18)$$

and

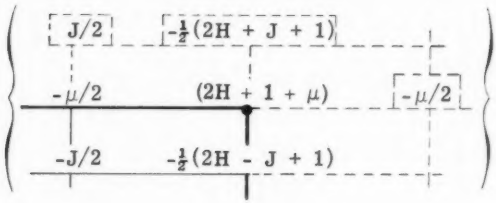

$$w = 0 \quad \ldots\ldots\ldots(19)$$

For a re-entrant corner, equilibrium of normal forces is given by

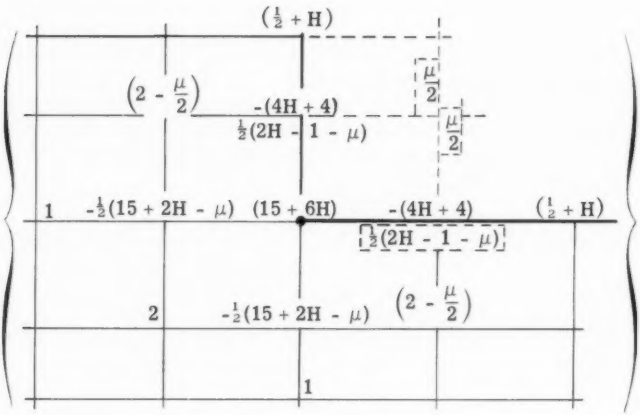

$$w = \frac{Q\,\lambda^2}{N} \quad \ldots(20)$$

In general, there are two fictitious deflections at point ne. These are necessary because the angles of twist of the two beams that are defined by the deflections at ne are generally different.

The two moment equilibrium requirements corresponding to Eq. 17 are, respectively

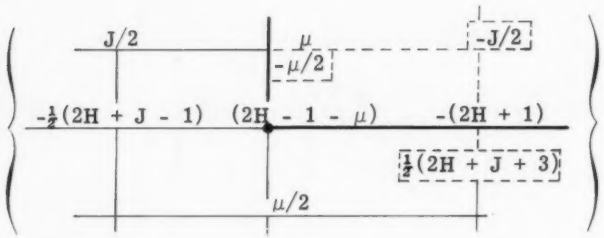

$$w = 0 \quad \ldots\ldots(21)$$

and

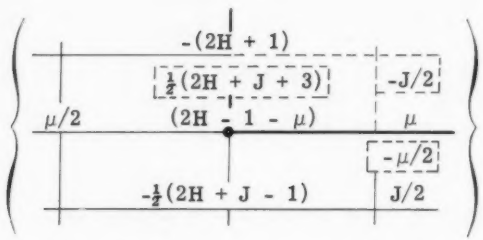

$$w = 0 \quad \ldots\ldots\ldots(22)$$

The two fictitious deflections at point ne in Eqs. 21 and 22 are also different. The one in Eq. 21 defines the angle of twist of the beam oriented in the y-direction, whereas that in Eq. 22 defines the angle of twist of the beam oriented in the x-direction.

Eqs. 18 and 19 and Eqs. 21 and 22 provide the necessary equations for determining the corresponding fictitious deflections.

In the derivation of Eqs. 20 through 22 there are certain characteristics peculiar to a re-entrant corner that deserve further explanations. For this purpose, it will suffice to investigate some of the plate bending moments acting at such a corner as follows (see Fig. 3):

$$m_{o1} = -N\frac{\lambda}{2}\left(\frac{w_{\overline{e}} - 2w_o + w_w}{\lambda^2} + \mu\,\frac{w_{\overline{n}} - 2w_o + w_s}{\lambda^2}\right) \ldots(23a)$$

$$m_{o2} = -N\frac{\lambda}{2}\left(\frac{w_{\overline{e}} - 2w_o + w_w}{\lambda 2} + \mu\,\frac{w_n - 2w_o + w_{\overline{s}}}{\lambda^2}\right) \ldots.(23b)$$

and

$$m_{o3} = -N\frac{\lambda}{2}\left(\frac{w_e - 2w_o + w_{\overline{w}}}{\lambda^2} + \mu\,\frac{w_{\overline{n}} - 2w_o + w_s}{\lambda^2}\right) \ldots.(23c)$$

Note that in m_{o1} and m_{o2} the x-curvatures are identical for the two moments while the y-curvatures are different; that is, the y-curvature of m_{o1} is the y-curvature of the plate at the corner while the y-curvature of m_{o2} is the same

as the curvature of the beam oriented in the y-direction. Furthermore, the x-curvature in m_{o3} is the same as that of the other beam, but the y-curvature is the same as the corresponding curvature of m_{o1}.

ILLUSTRATIVE PROBLEMS

Two example problems are given to illustrate the use of the equations derived herein. These problems are also intended to give some indications of the type of complex boundary-value problems of plate-beam systems that can be solved. However, extensive results and analysis of the variables in plate-beam systems are not within the scope of the paper.

The application of certain equations may require clarification. For this purpose, some of the equations are explicitly written for the two problems using $\mu = 0$. Results in the form of bending moments at certain sections of the

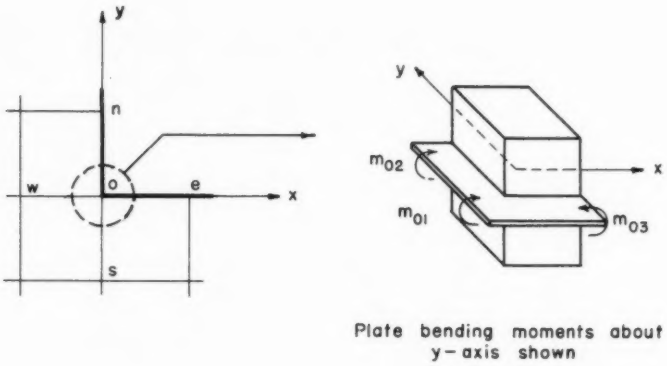

FIG. 3.—JOINT AT RE-ENTRANT CORNER

plates are shown in Figs. 4 and 5. In both problems, a uniformly distributed transverse load is applied and $\mu = 0$ is used.

Example 1.—One quarter of the structure analyzed in the first problem is shown in Fig. 4(a), which is a square plate with two opposite edges fixed and the remaining edges stiffened with beams. One flexural stiffness of the beams (H = 20) and three different values of torsional stiffness (J = 0, 10, 20)are used.

Referring to Fig. 4(a), note that points 1 through 5 and $\overline{16}$ through $\overline{20}$ represent points having fictitious deflections.

Applying Eq. 12 to point 18 and making use of Eq. 3 give

$$21w_{18} - 8\left(w_{13} + w_{17} + w_{19} + w_{23}\right) + 2\left(w_{12} + w_{14} + w_{22} + w_{24}\right)$$

$$+ \left(w_8 + w_{16} + w_{20} + w_{28}\right) - w_{\overline{18}} = \frac{q\,\lambda^4}{N}$$

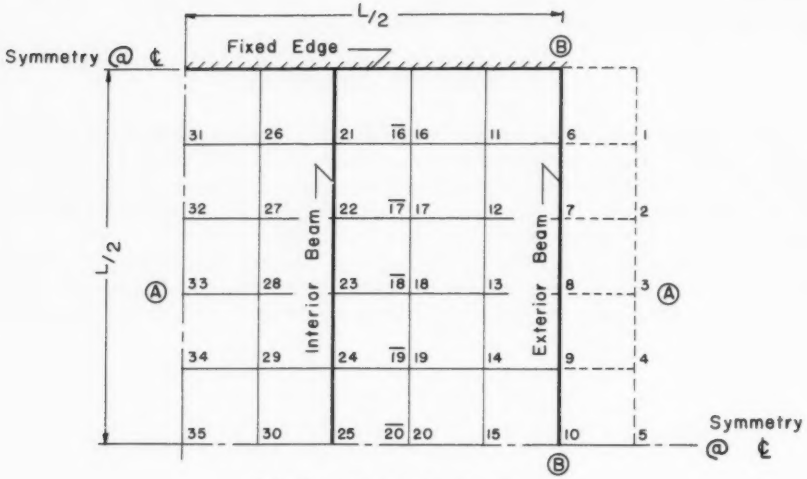

(a.) Structure Analyzed

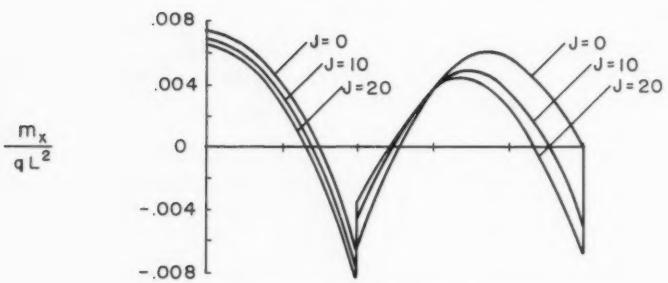

(b.) Plate Moments (m_x) Along Line A–A

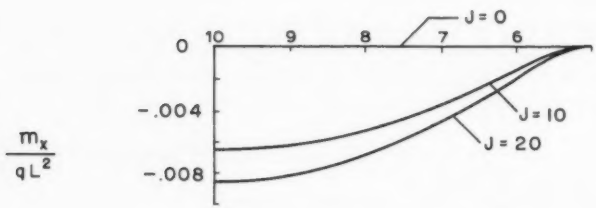

(c.) Plate Moments (m_x) Across Section B–B

FIG. 4.—EXAMPLE PROBLEM I

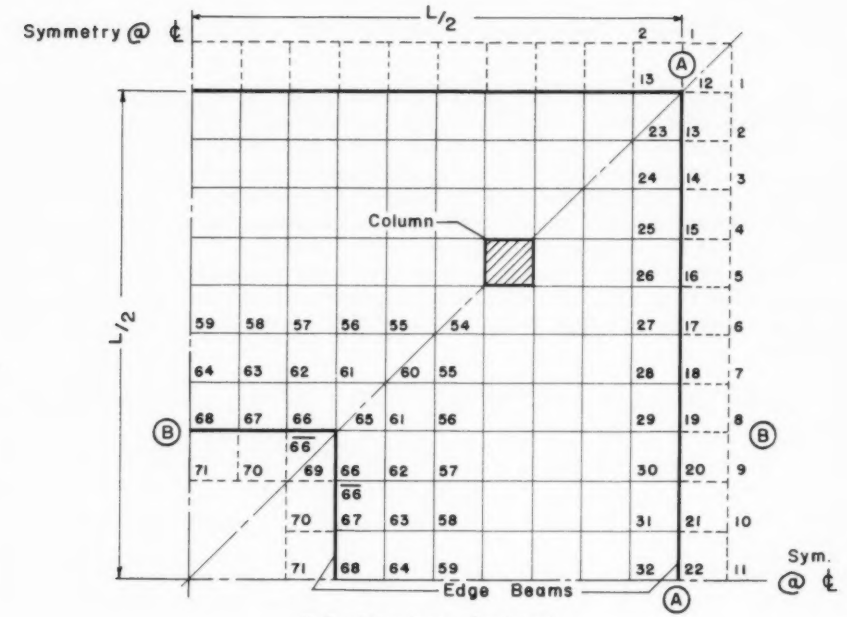

(a.) Structure Analyzed

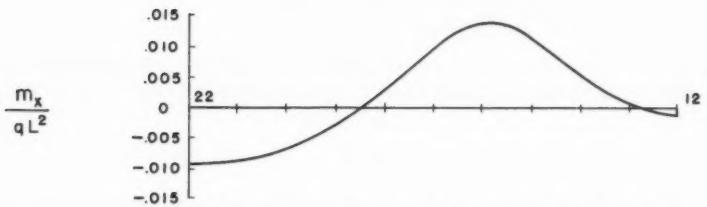

(b) Plate Moments (m_x) Across Section A – A

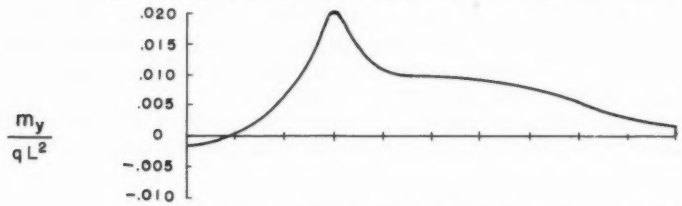

(c) Plate Moments (m_y) Across Section B – B

FIG. 5.—EXAMPLE PROBLEM II

Applying Eq. 7 to point 23 yields

$$- 2w_{18} + \frac{J}{2}\left(w_{27} - 2w_{28} + w_{29}\right) + (2 + J)\, w_{\overline{18}} - \frac{J}{2}\left(w_{\overline{17}} + w_{\overline{19}}\right) = 0$$

The application of the other equations, such as Eq. 11 for points 21 through 25 and Eqs. 13 and 15 to points 6 through 10, needs no further explanation.

Example 2.—Fig. 5(a), shows one quarter of the structure analyzed in this problem. The structure is a square plate supported on four infinitely rigid columns, with a square opening at the center. The edges of the opening as well as all the exterior edges are stiffened with beams having flexural and torsional stiffnesses of H = J = 20.

Taking into consideration the symmetry of the structure, Eqs. 16 and 18 when applied to point 12 are straight-forward and do not require further comments. Applying both Eqs. 20 and 21 to point 65 yields, respectively, the following:

$$(15 + 6H)\, w_{65} - 8\,(1 + H)\, w_{66} - (2H + 15)\, w_{61} + (1 + 2H)\, w_{67}$$

$$+ 2\, w_{60} + 2\, w_{56} + 4\, w_{62} + (2H - 1)\, w_{\overline{66}} = 0.75\, \frac{q\,\lambda^4}{N}$$

and

$$(2H - 1)\, w_{65} - \frac{1}{2}\,(2H + J - 1)\, w_{61} - (1 + 2H)\, w_{66} + \frac{J}{2}\, w_{62}$$

$$- \frac{J}{2}\, w_{69} + \frac{1}{2}\,(2H + J + 3)\, w_{\overline{66}} = 0$$

It should be emphasized that in any problem, the number of equations is equal to the number of unknown deflections including the fictitious deflections.

CONCLUSIONS

By introducing approximations in the physical model itself, rather than in the governing differential equation, finite difference recurrent equations for plate-beam systems can be derived without the difficulties due to discontinuities that would otherwise be encountered. These recurrent equations when used in conjunction with the equations for plates provide a means of obtaining numerical solutions to combined plate-beam systems.

The equations contained herein were derived on the basis of a plate model that has been shown to be the finite difference equivalent of a continuum.[3]

ACKNOWLEDGMENTS

The results presented were obtained as part of a program supported by a National Science Foundation grant.

APPENDIX.—NOTATION

The following notation, adopted for use in this paper, is listed here for ease of reference and for the convenience of discussers:

$H = \frac{E\,I}{N\,\lambda}$, a measure of the flexural stiffness of a beam;

$J = \frac{G\,C}{N\,\lambda}$, a measure of the torsional stiffness of a beam;

M = bending moment in a beam;

m = moment per given width of plate;

$N = \frac{E\,h^3}{12\,(1 - \mu^2)}$, stiffness per unit width of plate;

Q = equivalent concentrated load at a joint;

q = intensity of uniformly distributed load;

T = torsional moment in a beam;

V = shear force;

w = deflection normal to the plane of a plate;

x,y = Cartesian reference axes;

λ = distance between joints or node points; and

μ = Poisson's ratio.

Journal of the
ENGINEERING MECHANICS DIVISION
Proceedings of the American Society of Civil Engineers

ELECTRONIC ANALOG COMPUTERS FOR LAMINAR FLOW PROBLEMS

By Donald F. Young[1]

SYNOPSIS

A simple technique is presented for the use of an electronic analog computer to determine velocity distributions in both steady and unsteady uniform laminar flow problems. Three specific examples are given, and a comparison of the computer solutions with the theoretical solutions indicates the satisfactory accuracy of the technique.

INTRODUCTION

Electronic differential analyzers, or more simple "analog computers," are now being used extensively in practically every branch of engineering, particularly for problems in which the independent variable is time. Because the analog computer integrates with respect to the single variable time, it is well suited for this type of problem. However, for many problems in areas such as mechanics, heat transfer, aerodynamics, and nuclear engineering, solutions to partial differential equations containing two or more independent variables are required. Two techniques are currently available for solving partial differential equations with the analog computer. In certain instances, the partial differential equation can be reduced by separation of variables to a system of ordinary differential equations, each involving a single independent variable. These equations can then be solved on the computer. However, a frequently

Note.—Discussion open until May 1, 1962. To extend the closing date one month, a written request must be filed with the Executive Secretary, ASCE. This paper is part of the copyrighted Journal of the Engineering Mechanics Division, Proceedings of the American Society of Civil Engineers, Vol. 87, No. EM 6, December, 1961.

[1] Prof. of Theoretical and Applied Mechanics, Dept. of Nuclear Engrg., Iowa State Univ., Ames, Iowa.

simpler and more general technique is one of replacing the original partial derivatives by their finite-difference approximations, thereby reducing the original differential equation to a form that can be solved on the computer. This method was first described by T. A. Rogers[2] and R. M. Howe and V. S. Haneman[3] and has been used for the solution of several different types of partial differential equations.

Although conventional electrical analogies, such as systems utilizing conductive solids or liquids, or resistance networks, have been widely used for the study of fluid mechanics problems, particularly in the study of the flow of ideal fluids (see for example the work by Malavard[4]), no reference to studies in which an electronic analog computer had been used to investigate the steady or unsteady viscous flow of an incompressible fluid through or between various regular geometries such as flat plates, circular tubes, or rectangular tubes was found. Because the governing partial differential equation for this type of problem is similar to the heat equation which has been studied by the use of an electronic analog computer,[2] laminar flow problems can also be treated in this manner. It should be noted that passive analog computers, as demonstrated by J. L. Shearer,[5] can also be used for this type of problem. However, it was the purpose of the present investigation to demonstrate the applicability of the use of electronic analog computers to various types of laminar flow problems. In this study three specific problems were considered (Fig. 1):

(1) Starting flow between infinite parallel plates;
(2) flow between infinite parallel plates under the influence of a pulsating pressure gradient; and
(3) flow near an oscillating infinite plate.

These three relatively simple cases were selected so that the analog solutions could be compared with the theoretical solutions. However, as noted in the last section of this paper the general method of approach can be extended to flow through tubes of various cross sections.

Notation.—The letter symbols adopted for use in this paper are defined where they first appear, in the illustrations or in the text, and are arranged alphabetically, for convenience of reference, in the Appendix.

FINITE DIFFERENCE APPROXIMATION

The differential equation for laminar flow between parallel plates is

$$\nu \frac{\partial^2 u}{\partial y^2} = \frac{\partial u}{\partial t} + \frac{1}{\rho} \frac{\partial p}{\partial x} \quad \ldots\ldots\ldots\ldots\ldots\ldots (1)$$

---

2 "Electronic Analog Computers and Partial Differential Equation Solutions," by T. A. Rogers, Memorandum to Dept. of Engrg., Univ. of California, Los Angeles, 1952. (Noted in reference 3. Memorandum no longer available)

3 "The Solution of Partial Differential Equations by Difference Methods Using the Electronic Differential Analyzer," by R. M. Howe and V. S. Haneman, Proceedings, IRE, Vol. 41, 1953, p. 1497.

4 "The Use of Rheoelectrical Analogies in Aerodynamics," by L. C. Malavard, AGARD 18, 1956.

5 "Electric Network Analog Study of Viscous Flow Normal to Parallel Evenly Spaced Cylinders," by J. L. Shearer, Textile Research Journal, Vol. 29, 1959, p. 467.

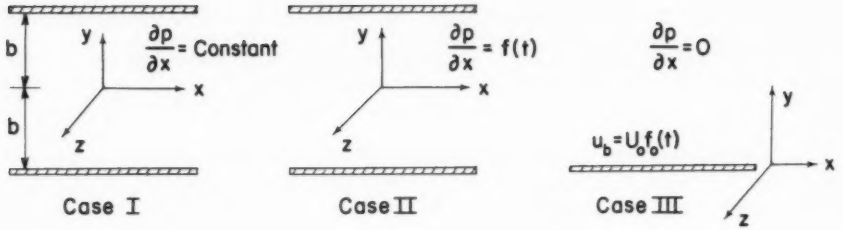

FIG. 1.—BOUNDARY GEOMETRY AND COORDINATE SYSTEM FOR PROBLEMS STUDIED

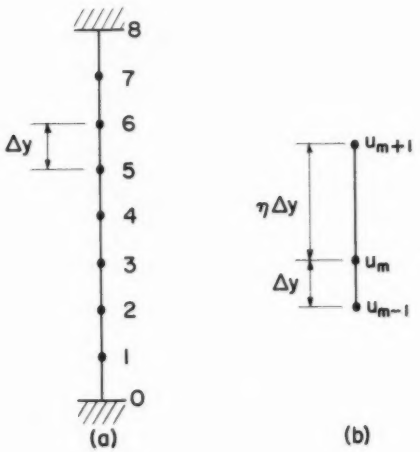

FIG. 2.—FINITE-DIFFERENCE GRID

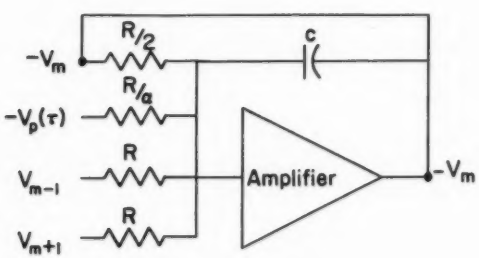

FIG. 3.—BASIC AMPLIFIER CIRCUIT

in which ν is the kinematic viscosity, u denotes the velocity component in the x-direction, t is time, ρ is fluid density, and $\frac{\partial p}{\partial x}$ is the pressure gradient.

The boundary conditions for this problem are simply that fluid velocities at the boundaries are the same as the velocity of the boundary; that is, for a fixed boundary $u_b = o$, or for a moving boundary $u_b = U_o f_o(t)$ as illustrated in Case III of Fig. 1.

To rewrite Eq. 1 in terms of its finite difference approximation the flow field is subdivided into a number of intervals (Fig. 2). The average velocity gradient between, for example, nodes 4 and 5, is

$$\left(\frac{\partial u}{\partial y}\right)_{4\to5} \cong \frac{u_5 - u_4}{\Delta y} \quad \ldots\ldots\ldots\ldots\ldots\ldots (2)$$

and between 5 and 6

$$\left(\frac{\partial u}{\partial y}\right)_{5\to6} \cong \frac{u_6 - u_5}{\Delta y} \quad \ldots\ldots\ldots\ldots\ldots\ldots (3)$$

The second derivative at node 5 can be approximated as

$$\left(\frac{\partial^2 u}{\partial y^2}\right)_5 \cong \frac{1}{\Delta y}\left[\left(\frac{\partial u}{\partial y}\right)_{5\to6} - \left(\frac{\partial u}{\partial y}\right)_{4\to5}\right] \cong \frac{1}{(\Delta y)^2}\left[u_6 + u_4 - 2\,u_5\right] \quad \ldots (4)$$

Therefore, at node 5 the differential equation can be approximated as

$$\frac{\nu}{(\Delta y)^2}\left[u_6 + u_4 - 2\,u_5\right] \cong \frac{\partial u_5}{\partial t} + \frac{1}{\rho}\frac{\partial p}{\partial x} \quad \ldots\ldots\ldots (5)$$

and, in general, the finite difference equation for any node m is

$$\frac{\nu}{(\Delta y)^2}\left[u_{m+1} + u_{m-1} - 2\,u_m\right] \cong \frac{\partial u_m}{\partial t} + \frac{1}{\rho}\frac{\partial p}{\partial x} \quad \ldots\ldots\ldots (6)$$

Eq. 6 is valid for any node point around which the spacing Δy is equal. In certain instances it is convenient to use unequal spacing, and the finite difference equation must be modified accordingly. For the example illustrated in Fig. 2(b) the approximation for the second derivative becomes

$$\left(\frac{\partial^2 u}{\partial y^2}\right)_m \cong \frac{1}{(\Delta y)^2}\left[\frac{u_{m+1}}{\frac{\eta}{2}(1+\eta)} + \frac{u_{m-1}}{\frac{1}{2}(1+\eta)} - \frac{2\,u_m}{\eta}\right] \quad \ldots\ldots\ldots (7)$$

in which η is some constant multiplier of Δy.

For the particular flow problems studied eight intervals were used. For Cases I and II (Fig. 1) the intervals were equally spaced, but the spacing for Case III was not equal because this would obviously require an infinite number

of intervals. The spacing for Case III was arbitrarily selected so that intervals between nodes 0 and 5 were equally spaced, the interval between 5 and 6 equal to 2 Δ y, between 6 and 7 equal to 8 Δ y, and between 7 and 8 equal to η Δ y in which $\eta >> 8$. The actual method used to simulate this condition will be examined in the following section.

COMPUTER SETUP

If Eq. 6 is rewritten as

$$u_m = \int_o^t \frac{\nu}{(\Delta y)^2} \left[u_{m+1} + u_{m-1} - 2\,u_m - \frac{(\Delta y)^2}{\nu} F(t) \right] dt \quad \ldots (8)$$

in which $F(t) = \frac{1}{\rho} \frac{\partial p}{\partial x}$ and compared with the equation for the output voltage of the operational amplifier of Fig. 3, the similarity between the equations is immediately apparent. The equation for the output of the amplifier of Fig. 3 is

$$V_m = \int_o^\tau \frac{1}{R\,C} \left[V_{m+1} + V_{m-1} - 2\,V_m - \alpha\, V_p(\tau) \right] d\tau \quad \ldots (9)$$

in which V represents voltage, R resistance, C capacitance, α an arbitrary constant, and τ computer time. Thus it is noted that, if the correct inputs are fed into the amplifier, the output can be made proportional to u_m. This can be accomplished by letting

$$V = n_1\, u \quad \ldots (10)$$

$$\tau = n_2\, t \quad \ldots (11)$$

and

$$\alpha\, V_p(\tau) = \frac{n_1 (\Delta y)^2 F(t)}{\nu} \quad \ldots (12)$$

in which n_1 and n_2 are constants.

Substitution of Eqs. 10, 11, and 12 into Eq. 8 indicates that if

$$R\,C = n_2 \frac{(\Delta y)^2}{\nu} \quad \ldots (13)$$

then the voltage is proportional to velocity as indicated by Eq. 10. The constant of integration has been omitted from Eq. 8, because for all flow cases it was assumed that at t=o, u=o. In the computer setup this corresponded to having no initial charge on the capacitors. The complete basic computer circuit that was used is shown in Fig. 4. The velocities correspond to the output voltages of the amplifiers but are the negatives of the voltages for amplifiers A_1, A_3 A_5, and A_7. This is due to the inherent characteristic of the amplifier to change the sign of the input voltage. If desired, sign changers could be incorporated into the circuit, but this would require four additional amplifiers. The equipment used in the investigation consisted primarily of a Heath table top

analog computer, a Hewlett Packard low frequency function generator, and Brush recording equipment.

Because each of the cases studied required some modification of the basic computer set-up, the details of the computer circuit for each will be considered. The actual computer results are given in the next section.

(a) Case I.—For this problem the boundary conditions are $u(\pm b, t) = 0$ which corresponds to $V_0 = V_8 = 0$, and the pressure gradient is constant so that the input voltage, V_p, is a constant. Because the transient flow was of interest for this case, the procedure followed was to apply the constant voltage V_p suddenly, and to record the output voltages of all the amplifiers continuously until a steady state condition was attained.

(b) Case II.—As for Case I the voltages V_0 and V_8 were held at ground potential. However, the voltage V_p was a function of time and for the particular

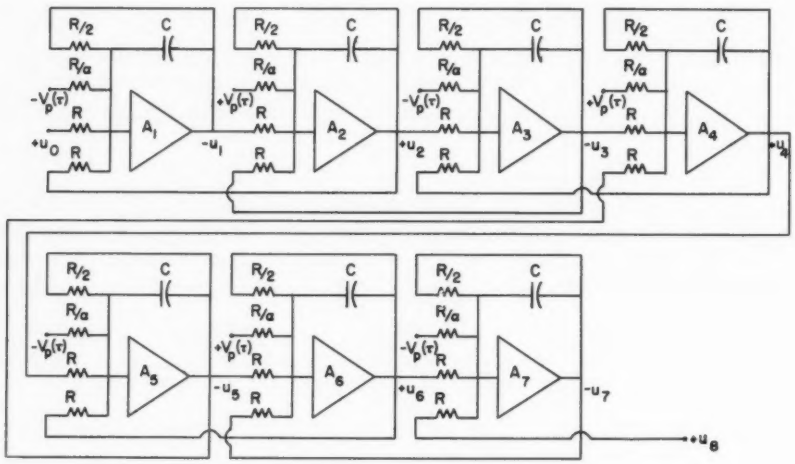

FIG. 4.—BASIC COMPUTER CIRCUIT

problem studied varied sinusoidally. This voltage was generated by the low frequency function generator and, as before, the output voltages of all amplifiers were recorded.

(c) Case III.—For this problem the boundary at y = o is moving with some prescribed velocity $u_b = U_0 f_0(t)$ and the pressure gradient $\frac{\partial p}{\partial x} = 0$. Therefore, the voltage, V_0, was made to vary in the same manner as $f_0(t)$ with $V_p = 0$. For the particular problem considered the voltage V_0 varied sinusoidally. The difficulty encountered in this case was that y approached infinity and therefore the nodes could not be equally spaced. However, an inspection Eq. 17 indicated that if $\eta \neq 1$ then the u_{m+1}, u_{m-1}, u_m terms must be modified by factors that are functions of η. In the computer circuit this corresponds to modifying the input voltages by these factors. This can be readily accomp-

lished through the use of the coefficient potentiometers. As previously mentioned, it was desirable to make η very large. For the particular problem studied, the actual value of η did not appear to be too critical for this last interval.

THEORETICAL SOLUTION

To gain some insight into the accuracy of the computer solutions, it was thought advisable to compare these solutions with the theoretical solutions. The basic problem is to obtain a solution to Eq. 1 subject to certain boundary and initial conditions. The general solutions are presented here, and the specific problems of interest are treated as special cases. For Cases I and II, in which the boundaries are fixed, the solution can be formulated in the following manner:

$$u = u_t + u_s \quad \ldots\ldots\ldots\ldots\ldots\ldots (14)$$

in which u_t is the transient part of u, and u_s is the steady state part of u. It was assumed that the pressure gradient was a periodic function of time and could be expressed as

$$\frac{\partial p}{\partial x} = f(t) = A_o + \sum_{n=1}^{\infty} A_n \cos n\omega t + \sum_{n=1}^{\infty} B_n \sin n\omega t \quad \ldots\ldots\ldots (15)$$

in which ω is the angular frequency and n = 1, 2, 3 . . . . . .
L. J. Kastner and S. H. Shih[6] have given the details of the steady state solution

$$u_s = \alpha_o(y) + \sum_{n=1}^{\infty} \alpha_n(y) \cos n\omega t + \sum_{n=1}^{\infty} \beta_n(y) \sin n\omega t \quad \ldots\ldots (16)$$

It then follows that

$$u_s = -\frac{A_o}{2\mu}\left(b^2 - y^2\right) - \frac{1}{2\mu}\sum_{n=1}^{\infty}\left\{\left[A_n S_n(y) + B_n C_n(y)\right]\cos n\omega t + \left[B_n S_n(y) - A_n C_n(y)\right]\sin n\omega t\right\} \quad \ldots\ldots\ldots\ldots\ldots\ldots (17)$$

in which μ is the absolute viscosity and

$$S_n(y) = \frac{\sin q(b+y)\ \sinh q(b-y) + \sin q(b-y)\ \sinh q(b+y)}{q^2(\cos 2qb + \cosh 2qb)} \quad \ldots\ldots (18)$$

$$C_n(y) = \frac{\cos q(b+y)\ \cosh q(b-y) + \cos q(b-y)\ \cosh q(b+y) - \cos 2qb - \cosh 2qb}{q^2(\cos 2qb + \cosh 2qb)} \quad \ldots (19)$$

---

6 "Critical Reynolds Numbers for Steady and Pulsating Flow," by L. J. Kastner and S. H. Shih, Engineering, Vol. 172, 1951, p. 389.

and

$$q = \sqrt{\frac{n\omega}{2\nu}} \quad \ldots\ldots\ldots\ldots\ldots\ldots\ldots\ldots (20)$$

For the special case of interest in the present investigation

$$\frac{\partial p}{\partial x} = A_o + A_1 \cos \omega t \quad B_n = 0 \quad \ldots\ldots\ldots\ldots (21)$$

and, thus,

$$u_s = -\frac{A_o}{2\mu b^2}\left[1 - \frac{y^2}{b^2}\right] - \frac{A_1}{2\mu q^2}\left[S(y)\cos \omega t - C(y)\sin \omega t\right]. \quad (22)$$

in which

$$S(y) = \frac{\sin qb\left(1+\frac{y}{b}\right)\sinh qb\left(1-\frac{y}{b}\right) + \sin qb\left(1-\frac{y}{b}\right)\sinh qb\left(1+\frac{y}{b}\right)}{\cos 2qb + \cosh 2qb} \quad . . (23)$$

$$C(y) = \frac{\cos qb\left(1+\frac{y}{b}\right)\cosh qb\left(1-\frac{y}{b}\right) + \cos qb\left(1-\frac{y}{b}\right)\cosh qb\left(1+\frac{y}{b}\right) - \cos 2qb - \cosh 2qb}{\cos 2qb + \cosh 2qb} \quad . . (24)$$

The transient solution is obtained from the equation

$$\nu \frac{\partial^2 u_t}{\partial y^2} = \frac{\partial u_t}{\partial t} \quad \ldots\ldots\ldots\ldots\ldots\ldots (25)$$

by separation of variables. This solution is

$$u_t = \sum_{n=1}^{\infty} A_n \, e^{-(2n-1)^2\left(\frac{\pi}{2}\right)^2 \frac{\nu t}{b^2}} \cos (2n-1)\left(\frac{\pi}{2}\right)\frac{y}{b} \quad \ldots\ldots (26)$$

To satisfy the initial condition $u(y,o) = o$

$$A_n = \frac{2}{b}\int_o^b - u_s(y_1 o) \cos (2n-1)\left(\frac{\pi}{2}\right)\frac{y}{b}\, dy \quad \ldots\ldots\ldots (27)$$

The solution given by the sum of Eqs. 17 and 26 thus represents the general solution to the problem for which the pressure gradient is an arbitrary periodic function of time; and the sum of Eqs. 22 and 26 gives the solution for the special case in which the pressure gradient consists of a constant component that fluctuates harmonically.

A computer solution was first obtained for the transient flow developed when the fluid is subjected suddenly to a constant pressure gradient. This type of flow is commonly called "starting flow" and is referred to herein as Case I. The theoretical solution for this case is obtained from Eq. 26 in which the coef-

ficients are obtained from Eq. 27 with

$$u_s = -\frac{A_o}{2\mu b^2}\left(1 - \frac{y^2}{b^2}\right) \quad \ldots\ldots\ldots\ldots\ldots\ldots (28)$$

A comparison of the results obtained by the theoretical solution with those obtained from the computer is shown in the dimensionless plot of Fig. 5 for three representative times. The agreement between the two solutions appears to be satisfactory.

As noted previously for the problem in which the pressure gradient is a function of time the general solution is given by the sum of Eqs. 17 and 26. Eq. 17 indicates that the "steady" part of the solution consists of an oscillating component of the velocity plus the characteristic parabolic distribution. A computer solution was obtained for Case II with

$$A_o = 0\,,\ B_n = 0\,,\ \frac{\partial p}{\partial x} = A_1 \cos \omega t \quad \ldots\ldots\ldots (29)$$

A comparison of the computer solution with the theoretical solution is shown in the dimensionless plot of Fig. 6. Only the results for the steady oscillating part of the solutions are shown. However, it should be emphasized that the transient part of the solution can be readily obtained from the computer. The parameter qb was arbitrarily selected, and the velocity profile at the instant when the velocity at the midpoint between two plates is a maximum is shown in Fig. 6. As in the previous case, the two solutions agree closely.

The theoretical solution for Case III can be formulated in a manner similar to that of the first two examples. For this case the fluid extends to infinity in the positive y-direction and is bounded by an infinite plate having a prescribed periodic motion in the x-direction. In general this motion can be specified as

$$u_{y=o} = \sum_{n=1}^{\infty} C_n \cos n\omega t + \sum_{n=1}^{\infty} D_n \sin n\omega t \quad \ldots\ldots\ldots (30)$$

The other boundary condition is $u(\infty, t) = o$, and the steady state solution can be written as

$$u_s = \sum_{n=1}^{\infty} \phi_n(y) \cos n\omega t + \sum_{n=1}^{\infty} \theta_n(y) \sin n\omega t \quad \ldots\ldots\ldots (31)$$

It then follows that

$$u_s = e^{-\sqrt{\frac{\beta}{2}}\,y} \left\{ \sum_{n=1}^{\infty} \left[-D_n \sin\sqrt{\frac{\beta}{2}}\,y + C_n \cos\sqrt{\frac{\beta}{2}}\,y \right] \cos n\omega t \right.$$

$$\left. + \sum_{n=1}^{\infty} \left[D_n \cos\sqrt{\frac{\beta}{2}}\,y + C_n \sin\sqrt{\frac{\beta}{2}}\,y \right] \sin n\omega t \right\} \quad \ldots\ldots\ldots\ldots (32)$$

in which

$$\beta = \frac{n\omega}{\nu} \quad \ldots\ldots\ldots\ldots\ldots\ldots (33)$$

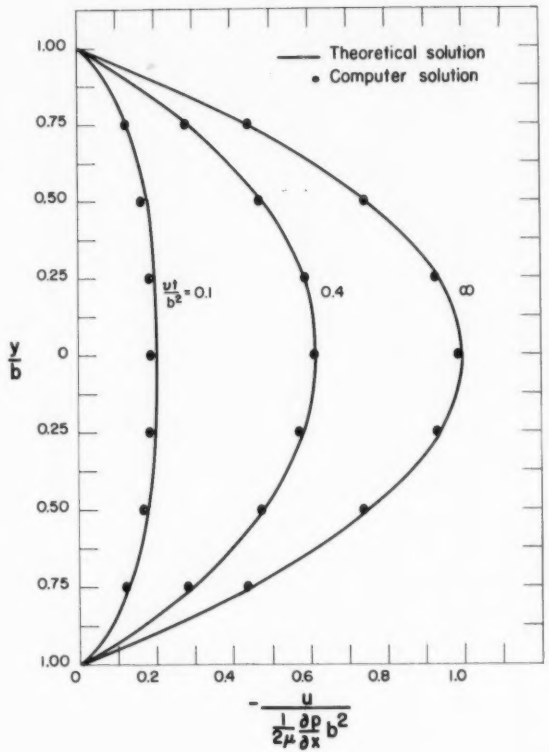

FIG. 5.—COMPARISON OF THEORETICAL AND COMPUTER SOLUTIONS FOR CASE I

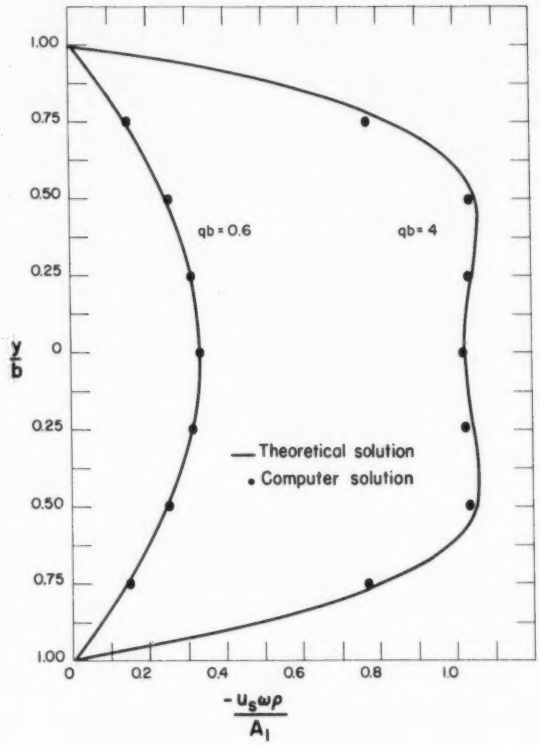

FIG. 6.—COMPARISON OF THEORETICAL AND COMPUTER SOLUTIONS FOR CASE II

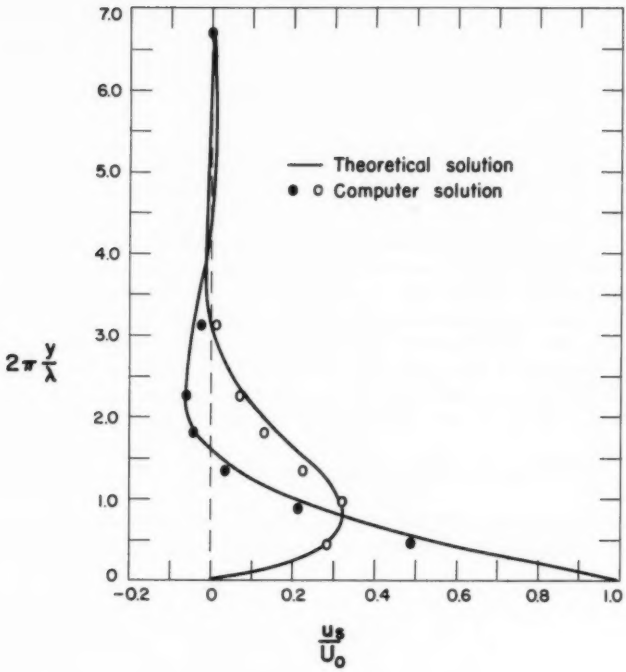

FIG. 7.—COMPARISON OF THEORETICAL AND COMPUTER SOLUTIONS FOR CASE III

The transient part of the solution can be obtained in a manner similar to that described for Case I. However, after an interval of time this part of the solution does not contribute significantly to the velocity.

For the special case with $D_n = 0$, $C_n = U_o$, and $n = 1$, the steady state solution becomes

$$u_s = U_o e^{-y\sqrt{\beta/2}} \cos\left(\omega t - \sqrt{\frac{\beta}{2}}\, y\right) \quad \ldots\ldots\ldots\ldots (34)$$

A dimensionless plot of the velocity profiles for the times when the velocity at y = o is a maximum and when equal to zero is shown in Fig. 7. The parameter λ is the wave length and is equal to $2\pi/\sqrt{\frac{\beta}{2}}$. The computer solution is also shown. The agreement between the two solutions is reasonably good, but not as close as for the two previous cases.

CONCLUSIONS

Although the specific examples considered in this investigation are relatively simple, the same technique can be used for more involved problems, that is,

for more general types of pressure gradient fluctuations or boundary motions. As far as the computer solution is concerned, the only requirement is that a voltage to simulate these variations can be generated. Of course, as noted from the general solutions presented, theoretical solutions can also be obtained for more involved problems. However, the major advantages of the computer solutions lie in the ease with which the various problems can be solved and the parameters changed, and in the complete picture of the solution which is obtained, that is, a continuous record of the velocities, including both the transient and steady state components. The results of this study (as illustrated by Figs. 5, 6, and 7) indicate that a reasonable degree of accuracy can be obtained with a relatively simple computer circuit and by using a small number of intervals in setting up the finite difference approximation. As the problem was set up on the computer, one amplifier per node was required. However, for problems in which symmetry exists, there is really only a need to solve the problem for a portion of the field.[3] For example in Case I it is recognized that, due to the geometry of the system, the velocity distribution is symmetrical with respect to the xz plane. Thus, if the appropriate boundary condition is used, namely $\left(\frac{\partial u}{\partial y}\bigg|_{y=o} = 0\right)$ the number of amplifiers actually required can be reduced.

The technique discussed herein can be readily extended to uniform two-dimensional laminar flow problems. The basic differential equation for this case is

$$\nu\left[\frac{\partial^2 u}{\partial y^2} + \frac{\partial^2 u}{\partial z^2}\right] = \frac{\partial u}{\partial t} + \frac{1}{\rho}\frac{\partial p}{\partial x} \quad \ldots\ldots\ldots\ldots\ldots (35)$$

As before the left side of Eq. 35 can be approximated by an appropriate finite difference expression. For this type of problem it is important to take advantage of symmetry so that the number of amplifiers required can be held at a reasonable figure. This procedure has been successfully applied to two-dimensional heat transfer problems.[3] Although theoretical solutions to Eq. 35 are available for various boundary geometries, they are rather involved, and as mentioned previously, the simplicity and flexibility of the computer solutions make this approach particularly attractive.

ACKNOWLEDGMENTS

The investigation reported in this paper was supported by the Iowa State University Engineering Experiment Station.

APPENDIX.—NOTATION

The following symbols are adopted for use in this paper:

A_n, B_n = Coefficients of Fourier series used to describe pressure gradient;

b = half-width between boundaries;

C = capacitance;

C_n, D_n = coefficients of Fourier series used to describe boundary motion for Case III;

n_1 = constant of proportionality between velocity and voltage;

n_2 = constant of proportionality between actual time and computer time;

p = pressure;

q = frequency parameter $q = \sqrt{\frac{n\,\omega}{z\,\nu}}$;

R = resistance;

t = time;

u = velocity;

u_b = velocity of boundary;

u_s = steady state component of velocity;

u_t = transient component of velocity;

V = voltage;

V_p = variable input voltage;

x, y, z = rectangular coordinates;

α = multiplier for input voltage;

α_n, β_n = coefficients of Fourier series used to describe steady state velocity for Cases I and II;

β = frequency parameter $\beta = \sqrt{\frac{n\,\omega}{\nu}}$;

η = multiplier for increments Δy;

θ_n, ϕ_n = coefficients of Fourier series used to describe steady state velocity for Case III;

λ = wave length;

μ = absolute viscosity;

ν = kinematic viscosity;

ρ = fluid density;

τ = computer time; and

ω = angular frequency.

Journal of the
ENGINEERING MECHANICS DIVISION
Proceedings of the American Society of Civil Engineers

BENDING AND STRETCHING OF LAMINATED AEOLOTROPIC PLATES[a]

By Yehuda Stravsky[1]

SYNOPSIS

A linear theory is established for a general multi-layer aeolotropic plate subject to in-plane forces and transverse loading. It is shown that a coupling phenomenon occurs, between in-plane forces and transverse bending, in the differential equations as well as in the boundary conditions. Some special types of heterogeneity are indicated for which the coupling of stretching and bending disappears. The general results of the paper are illustrated by means of explicit solutions for some plate problems.

INTRODUCTION

In the following, a linear theory is established for the bending and stretching of a thin, elastic, aeolotropic, multi-layer plate.

It has been shown[2] that, for a special class of heterogeneous aeolotropic plates a coupling phenomenon occurs between in-plane stretching and transverse bending.

Note.—Discussion open until May 1, 1962. To extend the closing date one month, a written request must be filed with the Executive Secretary, ASCE. This paper is part of the copyrighted Journal of the Engineering Mechanics Division, Proceedings of the American Society of Civil Engineers, Vol. 87, No. EM 6, December, 1961.

[a] Revised and extended version of paper presented at the October, 1960, ASCE Annual Meeting at Boston, Mass., based on a part of a thesis presented to the Massachusetts Inst. of Tech., Cambridge, Mass., in September, 1959, in partial fulfilment of the requirements for the degree of Doctor of Philosophy.

[1] Senior Lecturer, Dept. of Mechanics, Israel Inst. of Tech., Haifa, Israel; formerly, asst. Prof. of Structural Engrg., M. I. T., Cambridge, Mass.

[2] "Bending and Stretching of Certain Types of Heterogeneous Aeolotropic Elastic Plates," by E. Reissner and Y. Stavsky, Journal of Applied Mechanics, No. 61, APM, 21.

A similar coupling was previously observed[3] for an asymmetrically laminated orthotropic shell. At the time the present paper was written a relevant paper appeared,[4] in which the coupled differential equations were derived for a multi-layer isotropic plate considering non-linear strain-displacement relations. It was concluded that "in the small deflection theory the in-plane forces and transverse deflection are incoupled. . . solutions may be obtained directly from the single-layer plate by transposition."

The linear theories presented elsewhere[2,3,4] are obtained as special cases of the general theory developed herein, and can be applied to the analysis of a plate laminated of aeolotropic, orthotropic, and isotropic layers.

It becomes clear that even for the small deflection theory of K. S. Pister and S. B. Dong,[4] no simple "transposition of single layer plate theory" is possible, because stretching and bending are still coupled in the boundary conditions, although the differential equations are discoupled.

FORMULATION OF THE PROBLEM

Consider a thin, elastic plate composed of homogeneous aeolotropic sheets, conveniently, the bottom sheet is designated as "layer 1," the top sheet as "layer n," and the origin of the coordinates is chosen to coincide with an arbitrary point at the lower face of layer 1, that also contains the x,y axes.

Taking the positive direction of the thickness coordinate, z, upward the geometry of layer m, for example, is defined by its bottom plane, $z = h_{m-1}$, and its top plane, $z = h_m$, with thickness $(h_m - h_{m-1})$. The total thickness of the composite plate is h_n or, simply, h.

Defining stress resultants, stress couples, reference surface strains (at $z = 0$), and bending curvatures, as is usual in plate theory, the following equilibrium equations and strain-displacement relations of linear plate theory, based on the Euler-Bernoulli hypothesis are possible:

$$N_{x,x} + N_{xy,y} + P_x = 0 \ , \quad N_{xy,x} + N_{y,y} + P_y = 0 \quad \ldots\ldots\ldots (1)$$

$$M_{x,x} + M_{xy,y} - Q_x = 0 \ , \quad M_{xy,x} + M_{y,y} - Q_y = 0 \quad \ldots\ldots\ldots (2)$$

$$Q_{x,x} + Q_{y,y} + p = 0 \quad \ldots\ldots\ldots\ldots\ldots\ldots (3)$$

$$\epsilon_x = \epsilon_x^o + z\,\kappa_x \ , \quad \epsilon_y = \epsilon_y^o + z\,\kappa_y \ , \quad \epsilon_{xy} = \epsilon_{xy}^o + z\,\kappa_y \quad \ldots\ldots (4)$$

$$\epsilon_x^o = u_{,x} \ , \qquad \epsilon_y^o = v_{,y} \ , \qquad \epsilon_{xy}^o = u_{,y} + v_{,x} \quad \ldots\ldots (5)$$

and

$$\kappa_x = -w_{,xx} \ , \qquad \kappa_y = -w_{,yy} \ , \qquad \kappa_{xy} = -2w_{,xy} \quad \ldots\ldots (6)$$

---

3 "The Calculation of Laminated Anisotropic Shells," by S. A. Ambartsumtan, Izv. Akad. Nauk ArmSSR, Ser. Fiz. - Matem., Estestv Tekhn. Nauk 6, 3, 15-35, 1953.

4 "Elastic Bending of Layered Plates," by K. S. Pister and S. B. Dong, Proceedings, ASCE, Vol. 85, No. EM 4, 1959, p. 1.

The components of strain, according to S. G. Lekhnitsky,[5] define components of stress through stress strain relations that can be written, for example, for layer m, using a convenient notation for the elastic moduli in the form:

$$\begin{bmatrix} \tau_x^m \\ \tau_y^m \\ \tau_{xy}^m \end{bmatrix} = \begin{bmatrix} E_{xx}^m & E_{xy}^m & E_{xs}^m \\ E_{yx}^m & E_{yy}^m & E_{ys}^m \\ E_{sx}^m & E_{sy}^m & E_{ss}^m \end{bmatrix} \begin{bmatrix} \epsilon_x \\ \epsilon_y \\ \epsilon_{xy} \end{bmatrix} \quad \ldots\ldots\ldots\ldots (7)$$

Generalizing the examination by E. Reissner and the writer,[2] it is assumed that E_{ij}^m varies arbitrarily from layer to layer but follows the symmetry relations $E_{ji}^m = E_{ij}^m$ (i,j = x,y,s).

In order to obtain a complete system of plate equations, Eq. 7 is introduced, in view of Eqs. 4 and 6, into the definitions $N_x = \int_0^h \tau_x \, dz$, $M_x = \int_0^h \tau_x \, z \, dz$, and so forth, for stress resultants and couples. It should be noted that the couples are computed with regard to the reference plane, z = 0.

A system of plate stress-strain relations is obtained as follows:

$$\begin{bmatrix} N_x \\ N_y \\ N_{xy} \\ M_x \\ M_y \\ M_{xy} \end{bmatrix} = \left[\begin{array}{ccc:ccc} A_{xx} & A_{xy} & A_{xs} & B_{xx} & B_{xy} & B_{xs} \\ A_{yx} & A_{yy} & A_{ys} & B_{yx} & B_{yy} & B_{ys} \\ A_{sx} & A_{sy} & A_{ss} & B_{sx} & B_{sy} & B_{ss} \\ \hdashline B_{xx} & B_{xy} & B_{xs} & D_{xx} & D_{xy} & D_{xs} \\ B_{yx} & B_{yy} & B_{ys} & D_{yx} & D_{yy} & D_{ys} \\ B_{sx} & B_{sy} & B_{ss} & D_{sx} & D_{sy} & D_{ss} \end{array}\right] \begin{bmatrix} \epsilon_x \\ \epsilon_y \\ \epsilon_{xy} \\ \kappa_x \\ \kappa_y \\ \kappa_{xy} \end{bmatrix} \quad \ldots\ldots (8)$$

The elastic areas, the elastic statical moments, and the elastic moments of inertia are given, correspondingly, by

$$\left(A_{xx}, B_{xx}, D_{xx}\right) = \sum_{m=1}^{n} \int \left(1, z, z^2\right) E_{xx}^m \, dz \text{ , etc.} \quad \ldots\ldots (9)$$

---

5 "Bending of a Nonhomogeneous Anisotropic Thin Plate of Symmetrical Construction," by S. G. Lekhnitsky, Journal of Mathematics and Mechanics, PMM, Vol. 1, 1941. p. 71.

It is clear that whenever E_{ij} are continuous functions of z, no summation will be necessary in Eq. 9, and the integral limits will be z = 0 and z = h.

Eqs. 8 may also be written with the use of suitable auxiliary matrices in the form

$$\begin{bmatrix} N \\ M \end{bmatrix} = \left[\begin{array}{c|c} A & B \\ \hline B & D \end{array}\right] \begin{bmatrix} \epsilon \\ \kappa \end{bmatrix} \quad \ldots\ldots\ldots\ldots (10)$$

Eqs. 1, 2, and 3 together with Eq. 8 constitute a system of eleven equations for eleven unknowns N_x, N_y, N_{xy}, Q_x, Q_y, M_x, M_y, M_{xy}, u,v,w. An Airy stress function F, defined by

$$N_x = F_{,yy} + \Omega\,, \quad N_y = F_{,xx} + \Omega\,, \quad N_{xy} = F_{,xy} \quad \ldots\ldots\ldots (11)$$

is introduced next and assumes that the body forces p_x, p_y in Eqs. 1 are restricted so as to be derivable from a potential, Ω, as $p_x = -\Omega_{,x}$, $p_y = -\Omega_{,y}$.

Following the same method that appears in section 3 of the work of Reissner and the writer,[2] Eqs. 3 and 8 are reduced to two simultaneous fourth order equations in terms of w and F:

$$L_1\, w - L_3\, F = p - L_{B^*}\, \Omega \quad \ldots\ldots\ldots\ldots (12a)$$

and

$$L_2\, F + L_3\, w = - L_{A^*}\, \Omega \quad \ldots\ldots\ldots\ldots (12b)$$

The operators, L_i, are as follows:

$$L_1 = D^*_{xx} \frac{\partial^4}{\partial x^4} + 4\, D^*_{xs} \frac{\partial^4}{\partial x^3 \partial y} + 2\left(D^*_{xy} + 2\, D^*_{ss}\right) \frac{\partial^4}{\partial x^2 \partial y^2} + 4\, D^*_{ys} \frac{\partial^4}{\partial x \partial y^3} + D^*_{yy} \frac{\partial^4}{\partial y^4} \quad \ldots\ldots\ldots\ldots (13)$$

$$L_2 = A^*_{yy} \frac{\partial^4}{\partial x^4} - 2\, A^*_{ys} \frac{\partial^4}{\partial x^3 \partial y} + \left(2\, A^*_{xy} + A^*_{ss}\right) \frac{\partial^4}{\partial x^2 \partial y^2} - 2\, A^*_{xs} \frac{\partial^4}{\partial x \partial y^3} + A^*_{xx} \frac{\partial^4}{\partial y^4} \quad \ldots\ldots\ldots\ldots (14)$$

$$L_3 = B^*_{yx}\frac{\partial^4}{\partial x^4} + \left(2B^*_{ys} - B^*_{sx}\right)\frac{\partial^4}{\partial x^3 \partial y} + \left(B^*_{xx} + B^*_{yy} - 2B^*_{ss}\right)\frac{\partial^4}{\partial x^2 \partial y^2} + \left(2B^*_{xs} - B^*_{sy}\right)\frac{\partial^4}{\partial x \partial y^3} + B^*_{xy}\frac{\partial^4}{\partial y^4} \quad \ldots\ldots\ldots (15)$$

$$L_{A^*} = \left(A^*_{yx} + A^*_{xx}\right)\frac{\partial^2}{\partial x^2} - \left(A^*_{sx} + A^*_{sy}\right)\frac{\partial^2}{\partial x \partial y} + \left(A^*_{xx} + A^*_{xy}\right)\frac{\partial^2}{\partial y^2} \quad \ldots\ldots\ldots\ldots\ldots\ldots (16)$$

and

$$L_{B^*} = \left(B^*_{xx} + B^*_{yx}\right)\frac{\partial^2}{\partial x^2} + 2\left(B^*_{xs} + B^*_{ys}\right)\frac{\partial^2}{\partial x \partial y} + \left(B^*_{xy} + B^*_{yy}\right)\frac{\partial^2}{\partial y^2} \quad \ldots\ldots\ldots\ldots\ldots\ldots (17)$$

The starred matrices are given in terms of the unstarred submatrices, and their inverses are as follows:

$$\left[A^*\right] = \left[A^{-1}\right], \left[B^*\right] = -\left[A^{-1}\right]\left[B\right], \left[D^*\right] = \left[D\right] - \left[B\right]\left[A^{-1}\right]\left[B\right] \ldots (18)$$

It is noted that although A^* and D^* are symmetric matrices, the same need not be true for B^*. Eqs. 12 through 17 are remarkable for two specific properties:

1. There is a coupling between transverse bending and in-plane stretching that is governed by the L_3-operator, the structure of which is connected with the B-matrix in the stress strain relations in Eq. 8. In generalization of the type of heterogeneous plates analyzed by Reissner and the writer,[1] all the elements in the B-matrix are regularly obtained and, consequently, all terms appear in the L_3-operator. This means that in this case, even for one dimensional problems, w and F are still coupled.
2. The operator, L_1, involves the elements of the matrix, D^*, rather than the elements of the matrix, D, when transferred to the middle surface of the plate.

Four boundary conditions, along a boundary $f_b(x,y) = 0$, are associated with the system in Eqs. 12, and take the following form when displacements or stresses are prescribed:

$$\left.\begin{aligned} U_n &= \overline{U}_n \quad \text{or} \quad N_n = \overline{N}_n \\ U_s &= \overline{U}_s \quad \text{or} \quad N_{ns} = \overline{N}_{ns} \\ w &= \overline{w} \quad \text{or} \quad V_n + M_{ns,s} = \overline{V}_n + \overline{M}_{ns,s} \\ w_{,n} &= \overline{w}_{,n} \quad \text{or} \quad M_n = \overline{M}_n \end{aligned}\right\} \qquad \ldots\ldots\ldots (19)$$

In view of Eqs. 5, 6, and 8 the coupling of w and F enters, not only into the differential Eqs. 12, but into the boundary conditions of Eq. 19 as well.

Once the system of Eqs. 12 is solved and subjected to suitable boundary conditions of Eq. 19, all other unknowns can be determined directly. The stress resultants are given by Eqs. 11, the couples by Eqs. 4 through 6 and 8, and the transverse shear resultants by Eqs. 2. The strain components are given by Eqs. 4 through 6, and the stress components are obtained from Eqs. 7.

GENERALIZED STRESS FUNCTION Φ

When body forces are not considered it is convenient, in some problems, to transform the system of two simultaneous differential equations for w and F as in Eqs. 12 into a single equation of the eighth order, in terms of a generalized stress function, $\Phi = \Phi(x,y)$. Let

$$w = L_2\,\Phi\,, \quad F = -\,L_3\,\Phi \qquad \ldots\ldots\ldots\ldots\ldots (20)$$

and introduce into Eqs. 12, noting that the second one is identically satisfied, while the first one reads

$$L\,\Phi = p \qquad \ldots\ldots\ldots\ldots\ldots\ldots\ldots (21)$$

in which

$$L = L_1\,L_2 + L_3{}^2 \qquad \ldots\ldots\ldots\ldots\ldots\ldots\ldots (22)$$

which can be rewritten in view of Eqs. 13 through 15 as

$$L = A_1 \frac{\partial^8}{\partial x^8} + A_3 \frac{\partial^8}{\partial x^7 \partial y} + A_5 \frac{\partial^8}{\partial x^6 \partial y^2} + A_7 \frac{\partial^8}{\partial x^5 \partial y^3}$$

$$+ A_9 \frac{\partial^8}{\partial x^4 \partial y^4} + A_8 \frac{\partial^8}{\partial x^3 \partial y^5} + A_6 \frac{\partial^8}{\partial x^2 \partial y^6} + A_4 \frac{\partial^8}{\partial x \partial y^7} + A_2 \frac{\partial^8}{\partial y^8} \qquad \ldots (23)$$

in which

$$A_1 = A^*_{yy}\,D^*_{xx} + \left(B^*_{yx}\right)^2 \qquad \ldots\ldots\ldots\ldots\ldots\ldots\ldots\ldots (24)$$

$$A_2 = A^*_{xx}\, D^*_{yy} + \left(B^*_{xy}\right)^2 \quad \ldots\ldots\ldots\ldots\ldots\ldots\ldots\ldots\ldots\ldots (25)$$

$$A_3 = -\,2\,A^*_{ys}\, D^*_{xx} + 4\,A^*_{yy}\, D^*_{xs} + 2\,B^*_{yx}\left(2\,B^*_{ys} - B^*_{sx}\right) \ldots\ldots\ldots\ldots (26)$$

$$A_4 = -\,2\,A^*_{xs}\, D^*_{yy} + 4\,A^*_{xx}\, D^*_{ys} + 2\,B^*_{xy}\left(2\,B^*_{xs} - B^*_{sy}\right) \ldots\ldots\ldots\ldots (27)$$

$$A_5 = \left(2\,A^*_{xy} + A^*_{ss}\right) D^*_{xx} - 8\,A^*_{ys}\, D^*_{xs} + 2\,A^*_{yy}\left(D^*_{xy} + 2\,D^*_{ss}\right)$$
$$+ 2\,B^*_{yx}\left(B^*_{xx} + B^*_{yy} - 2\,B^*_{ss}\right) + \left(2\,B^*_{ys} - B^*_{sx}\right)^2 \ldots\ldots\ldots\ldots (28)$$

$$A_6 = \left(2\,A^*_{xy} + A^*_{ss}\right) D^*_{yy} = 8\,A^*_{xs}\, D^*_{ys} + 2\,A^*_{xx}\left(D^*_{xy} + 2\,D^*_{ss}\right)$$
$$+ 2\,B^*_{xy}\left(B^*_{xx} + B^*_{yy} - 2\,B^*_{ss}\right) + \left(2\,B^*_{xs} - B^*_{sy}\right)^2 \ldots\ldots\ldots\ldots (29)$$

$$A_7 = -\,2\,A^*_{xs}\, D^*_{xx} + 4\left(2\,A^*_{xy} + A^*_{ss}\right) D^*_{xs} - 4\,A^*_{ys}\left(D^*_{xy} + 2\,D^*_{ss}\right)$$
$$+ 4\,A^*_{yy}\, D^*_{ys} + 2\,B^*_{yx}\left(2\,B^*_{xs} - B^*_{sy}\right)$$
$$+ 2\left(2\,B^*_{ys} - B^*_{sx}\right)\left(B^*_{xx} + B^*_{yy} - 2\,B^*_{ss}\right) \ldots\ldots\ldots\ldots\ldots\ldots (30)$$

$$A_8 = -\,2\,A^*_{ys}\, D^*_{yy} + 4\left(2\,A^*_{xy} + A^*_{ss}\right) D^*_{ys} - 4\,A^*_{xs}\left(D^*_{xy} + 2\,D^*_{ss}\right)$$
$$+ 4\,A^*_{xx}\, D^*_{xs} + 4\,A^*_{xx}\, D^*_{xs} + 2\,B^*_{xs}\left(2\,B^*_{ys} - B^*_{sx}\right)$$
$$+ 2\left(2\,B^*_{xs} - B^*_{sy}\right)\left(B^*_{xx} + B^*_{yy} - 2\,B^*_{ss}\right) \ldots\ldots\ldots\ldots\ldots\ldots (31)$$

and

$$A_9 = A^*_{xx}\, D^*_{xx} - 8\,A^*_{xs}\, D^*_{xs} + 2\left(2\,A^*_{xy} + A^*_{ss}\right)\left(D^*_{xy} + 2\,D^*_{ss}\right)$$
$$- 8\,A^*_{ys}\, D^*_{ys} + A^*_{yy}\, B^*_{yy} + 2\,B^*_{xy}\, B^*_{yx}$$
$$+ 2\left(2\,B^*_{ys} - B^*_{sx}\right)\left(2\,B^*_{xs} - B^*_{sy}\right) + \left(B^*_{xx} + B^*_{yy} - 2\,B^*_{ss}\right)^2 \ldots\ldots (32)$$

Similarly, the boundary conditions in Eq. 19 can be expressed in terms of Φ and so the problem is completely defined.

CYLINDRICAL BENDING OF LONG RECTANGULAR PLATES

Insight into some of the consequences of the general elastic heterogeneity considered here may be obtained by determining the state of stress and deformation in long rectangular plates subject to cylindrical bending.

Consider plates composed of layers that follow the stress strain relations given in Eqs. 7. Let the y-axis coincide with one of the longitudinal edges of the plate, and let l be the free span of the heterogeneous plate. The edges x = 0,l are assumed to be simply supported, and the edge x = l is free to move in the x-direction while the other one is fixed in place.

Supposing that the plate is also supported at $y = \pm\infty$, it is clear that the behavior of the laminated structure under the load $p = p(x)$ will be independent of y; the problem is, therefore, one-dimensional.

This simplification permits an immediate integration of Eq. 21, which takes now the following form:

$$A_1 \frac{d^8 \Phi}{dx^8} = p \quad \ldots\ldots\ldots\ldots\ldots\ldots (33)$$

in which A_1 is given by Eq. 24.

The solution of Eq. 33 is subject to the following boundary conditions:

$$x = 0, l: \quad N_x = N_{xy} = w = M_x = 0 \quad \ldots\ldots\ldots\ldots (34)$$

Integrating Eq. 33 it is found that for p = constant

$$\Phi = \frac{p}{A_1} \frac{x^8}{56 \times 720} + C1 \frac{x^7}{7 \times 720} + C_2 \frac{x^6}{720} + C_3 \frac{x^5}{120} + C_4 \frac{x^4}{24}$$

$$+ C_5 \frac{x^3}{6} + C_6 \frac{x^2}{2} + C_7 x + C_8 \quad \ldots\ldots\ldots\ldots\ldots\ldots (35)$$

In view of Eqs. 20, 4, 5, 6, 8, and 34 the following is obtained:

$$w = \frac{A^*_{yy}}{24 A_1} p l^4 \left[\left(\frac{x}{l}\right)^4 - 2\left(\frac{x}{l}\right)^3 + \left(\frac{x}{l}\right)\right] \ldots\ldots\ldots (36)$$

$$F = -\frac{B^*_{yx}}{24 A_1} p l^4 \left[\left(\frac{x}{l}\right)^4 - 2\left(\frac{x}{l}\right)^3 + \left(\frac{x}{l}\right)\right] \ldots\ldots\ldots (37)$$

$$N_x = N_{xy} = 0 \quad \ldots\ldots\ldots\ldots\ldots\ldots\ldots\ldots (38)$$

$$N_y = B^*_{yx} \frac{p}{2 A_1} x(1 - x) \ldots\ldots\ldots\ldots\ldots\ldots (39)$$

$$M_x = \frac{p}{2} x(1 - x) \quad \ldots\ldots\ldots\ldots\ldots\ldots\ldots (40)$$

$$M_y = \left[B^*_{yx} B^*_{yy} + A^*_{yy} D^*_{xy}\right] \frac{p}{2 A_1} x(1 - x) \ldots\ldots\ldots (41)$$

and

$$M_{xy} = \left[B^*_{yx} B^*_{ys} + A^*_{yy} D^*_{xs}\right] \frac{p}{2 A_1} x(1 - x) \ldots\ldots\ldots (42)$$

Making use of Eqs. 4, 5, 6, 8, 36, and 37 the strain components are:

$$\epsilon_x = \left[A^*_{xy}\ B^*_{yx} + \left(z - B^*_{xx}\right)\ A^*_{yy}\right] \frac{p}{2\,A_1}\ x(1 - x) \quad \ldots\ldots(43)$$

$$\epsilon_y = 0 \quad \ldots\ldots(44)$$

and

$$\epsilon_{xy} = \left[A^*_{ys}\ B^*_{yx} - A^*_{yy}\ B^*_{sx}\right] \frac{p}{2\,A_1}\ x(1 - x) \quad \ldots\ldots(45)$$

The stress components, in view of Eqs. 7, 43, 44, and 45, take the form

$$\tau^m_x = \left\{\left[E^m_{xx}\left(A^*_{xy}\ B^*_{yx} - A^*_{yy}\ B^*_{xx}\right) + E^m_{xs}\left(A^*_{ys}\ B^*_{yx} - A^*_{yy}\ B^*_{sx}\right)\right]\right.$$

$$\left. + z\ E^m_{xx}\ A^*_{yy}\right\} \frac{P}{2\,A_1}\ x(1 - x) \quad \ldots\ldots(46)$$

$$\tau^m_y = \left\{\left[E^m_{yx}\left(A^*_{xy}\ B^*_{yx} - A^*_{yy}\ B^*_{xx}\right) + E^m_{ys}\left(A^*_{ys}\ B^*_{yx} - A^*_{yy}\ B^*_{sx}\right)\right]\right.$$

$$\left. + z\ E^m_{yx}\ A^*_{yy}\right\} \frac{P}{2\,A_1}\ x(1 - x) \quad \ldots\ldots(47)$$

and

$$\tau^*_{xy} = \left\{\left[E^m_{sx}\left(A^*_{xy}\ B^*_{yx} - A^*_{yy}\ B^*_{xx}\right) + E^m_{ss}\left(A^*_{ys}\ B^*_{yx} - A^*_{yy}\ B^*_{sx}\right)\right]\right.$$

$$\left. + z\ E^m_{sx}\ A^*_{yy}\right\} \frac{P}{2\,A_1}\ x(1 - x) \quad \ldots\ldots(48)$$

The transverse shear resultants are obtained by using Eqs. 2, 40, 41, and 42.

$$Q_x = \frac{p}{2}\left(1 - 2\,\frac{x}{l}\right) \quad \ldots\ldots(49)$$

and

$$Q_y = \left[B^*_{yx}\ B^*_{ys} + A^*_{yy}\ D^*_{xs}\right] \frac{p}{2\,A_1}\ x(1 - x) \quad \ldots\ldots(50)$$

The transverse shear components τ_{xz}, τ_{yz}, can be obtained by using the macroscopic equilibrium equations, which for the problem takes the form

$$\tau_{x,x} + \tau_{xz,z} = 0 \quad \ldots\ldots(51)$$

and

$$\tau_{xy,x} + \tau_{yz,z} = 0 \quad \ldots\ldots(52)$$

And, thus,

$$\tau_{xz}^{m} = - \left[\int_0^{h_{m-1}} \tau_{x,x} \, dz + \int_{h_{m-1}}^{z \le h_m} \tau_{x,x} \, dz \right] \ldots\ldots (53)$$

and

$$\tau_{yz}^{m} = - \left[\int_0^{h_{m-1}} \tau_{xy,x} \, dz + \int_{h_{m-1}}^{z \le h_m} \tau_{xy,x} \, dz \right] \ldots\ldots (54)$$

Or, in terms of the transverse shear resultants it is found that

$$\begin{aligned} \tau_{xz}^{m} = - \frac{V_x}{A_1} \Bigg\{ & \Bigg[\left(A_{xy}^{*} B_{yx}^{*} - A_{yy}^{*} B_{xx}^{*} \right) \sum_{i=1}^{m-1} E_{xx}^{i} \left(h_i - h_{i-1} \right) \\ & + \left(A_{ys}^{*} B_{yx}^{*} - A_{yy}^{*} B_{sx}^{*} \right) \sum_{i=1}^{m-1} E_{xs}^{i} \left(h_i - h_{i-1} \right) \\ & + A_{yy}^{*} \sum_{i=1}^{m-1} \frac{1}{2} E_{xx}^{i} \left(h_i^2 - h_{i-1}^2 \right) \Bigg] \\ & + \left(z - h_{m-1} \right) \left[E_{xx}^{m} \left(A_{xy}^{*} B_{yx}^{*} - A_{yy}^{*} B_{xx}^{*} \right) \right. \\ & \left. + E_{xs}^{m} \left(A_{ys}^{*} B_{yx}^{*} - A_{yy}^{*} B_{sx}^{*} \right) \right] + \frac{1}{2} E_{xx}^{m} \left(z^2 - h_{m-1}^2 \right) A_{yy}^{*} \Bigg\} \ldots (55) \end{aligned}$$

$$\begin{aligned} \tau_{yz}^{m} = - \frac{V_y}{B_{yx}^{*} B_{ys}^{*} + A_{yy}^{*} D_{xs}^{*}} \Bigg\{ & \Bigg[\left(A_{xy}^{*} B_{yx}^{*} \right. \\ & \left. - A_{yy}^{*} B_{xx}^{*} \right) \sum_{i=1}^{m-1} E_{xs}^{i} \left(h_i - h_{i-1} \right) \\ & + \left(A_{ys}^{*} B_{yx}^{*} - A_{yy}^{*} B_{sx}^{*} \right) \sum_{i=1}^{m-1} E_{ss}^{i} \left(h_i - h_{i-1} \right) \\ & + A_{yy}^{*} \sum_{i=1}^{m-1} \frac{1}{2} E_{xs}^{i} \left(h_i^2 - h_{i-1}^2 \right) \Bigg] \end{aligned}$$

$$+ \left(z - h_{m-1}\right)\left[E^m_{xs}\left(A^*_{xy}\, B^*_{yx} - A^*_{yy}\, B^*_{xx}\right)\right.$$

$$\left. + E^m_{ss}\left(A^*_{ys}\, B^*_{yx} - A^*_{yy}\, B^*_{sx}\right)\right]$$

$$+ \frac{1}{2} E^m_{xs}\left(z^2 - h^2_{m-1}\right) A^*_{yy} \Bigg\} \quad \ldots\ldots\ldots\ldots\ldots\ldots (56)$$

Note that in order to maintain the deformed shape in Eq. 36, a cross resultant force, N_y, will be developed in the plate in addition to the couples M_x, M_y, M_{xy} and their shear resultants, Q_x, Q_y, that occur in the homogeneous aeolotropic plate subject to cylindrical bending.

Eqs. 36 through 56 are also remarkable for the state of stress and strain that characterizes the behavior of the heterogeneous plate. Transverse bending is associated with in-plate deformations ϵ_x and ϵ_{xy} and in plane stress τ_x, τ_y, τ_{xy} of quite a complicated dependence on the elastic moduli, elastic areas, elastic statical moments, and moments of inertia of the plate.

UNIFORM DISTRIBUTION OF STRESS RESULTANTS AND COUPLES

Assumed that the plate is subjected to resultants, N, and couples, M, that are independent of x,y, an attempt is made to solve the system of Eqs. 12 for the rectangular plate bounded by x = 0,a and y = 0,b subject to the following boundary conditions:

$$\begin{aligned} x = 0,a &: N_x = \bar{n}_x,\ N_{xy} = \bar{n}_{xy},\ M_x = \bar{m}_x,\ \int_0^b R_x\, dy = 2\left[\bar{m}_{xy}\right]_0^b \\ y = 0,b &: N_y = \bar{n}_y,\ N_{xy} = \bar{n}_{xy},\ M_y = \bar{m}_y,\ R_y = 0 \end{aligned} \quad \ldots (57)$$

Because all prescribed forces and couples are constant, it is established, in view of Eqs. 2, that

$$V_x = V_y = 0 \quad \ldots\ldots\ldots\ldots\ldots\ldots (58)$$

In view of Eq. 10, when N_x, N_y, N_{xy} have constant values n_x, n_y, n_{xy}, and there are no body forces p_x, p_y

$$F = \frac{1}{2} n_x\, y^2 + \frac{1}{2} n_y\, x^2 - n_{xy}\, x\, y \quad \ldots\ldots\ldots\ldots (59)$$

In order that M_x, M_y, M_{xy} at the same time have constant values m_x, m_y, m_{xy} it is required that κ_x, κ_y, κ_{xy} have constant values k_x, k_y, k_{xy}. Accordingly, the deflection function, w, takes the form

$$w = \frac{1}{2} k_x\, x^2 + \frac{1}{2} k_y\, y^2 + k_{xy}\, x\, y \quad \ldots\ldots\ldots\ldots (60)$$

and so are Eqs. 12 identically satisfied, with $p = \Omega = 0$.

To determine the constants in Eq. 60, first invert Eqs. 8 or 10 as follows:

$$\begin{bmatrix} \epsilon^{o} \\ \kappa \end{bmatrix} = \left[\begin{array}{c|c} a & b \\ \hline c & d \end{array}\right] \begin{bmatrix} N \\ M \end{bmatrix} \quad \ldots\ldots\ldots\ldots\ldots (61)$$

in which a, b, c, d, are 3 x 3 matrices related to the matrices A, B, D by the following relations:

$$[a] = [A^{-1}] + [X]\,[Z^{-1}]\,[Y] \quad \ldots\ldots\ldots\ldots (62)$$

$$[b] = -[X]\,[Z^{-1}] = [c]^{T} \quad \ldots\ldots\ldots\ldots\ldots (63)$$

$$[c] = -[Z^{-1}]\,[Y] \quad \ldots\ldots\ldots\ldots\ldots\ldots (64)$$

and

$$[d] = [Z^{-1}] \quad \ldots\ldots\ldots\ldots\ldots\ldots\ldots (65)$$

in which

$$[X] = [A^{-1}]\,[B] \quad \ldots\ldots\ldots\ldots\ldots\ldots (66)$$

$$[Y] = [B]\,[A^{-1}] \quad \ldots\ldots\ldots\ldots\ldots\ldots (67)$$

and

$$[Z] = [D] - [Y]\,[D] \quad \ldots\ldots\ldots\ldots\ldots\ldots (68)$$

Note that a, d are symmetric matrices but b, c are, generally, not symmetric matrices.

Considering Eqs. 61 and 57 it is found that

$$[\kappa] = [c]\,[\bar{n}] + [d]\,[\bar{m}] \quad \ldots\ldots\ldots\ldots\ldots (69)$$

and, thus, the functions w and F of Eqs. 59 and 60 are uniquely determined. The strain and stress contribution can be completed by using Eqs. 61 and 4 through 7 in conjunction with Eqs. 59 and 60.

The expressions for the stress components in terms of stress resultants and couples are mentioned here:

$$[_{\tau}m] = [E^{m}]\,\left([a] + z\,[c]\right)\,[N] + [E^{m}]\,\left([b] + z\,[d]\right)\,[M] \quad \ldots (70)$$

which expresses a remarkable characteristic of heterogeneous plates: generally, each stress component is a function of all resultants and couples.

SOME SPECIAL CASES DERIVED FROM GENERAL THEORY

The specialization of the general system of Eqs. 12 to the interesting cases is indicated here:

I. For which bending and stretching are uncoupled
II. For which the cross-elasticity effect, Eq. 70, disappears

An example of case I is the symmetrically laminated aeolotropic plate. Let the plate described in section 2 be the upper half of a composite plate of total thickness, h, made up of 2n layers. For such a plate it is convenient to take the reference plane z = 0 to coincide with the symmetry plane of the plate. In view of Eq. 9 it is established that $L_3 = 0$. The system Eqs. 12 is uncoupled and takes the form

$$L_1 w = p \quad \ldots\ldots\ldots\ldots\ldots\ldots (71)$$

and

$$L_2 F = 0 \quad \ldots\ldots\ldots\ldots\ldots\ldots (72)$$

in which

$$L_1 = D_{xx} \frac{\partial^4}{\partial x^4} + 4 D_{xs} \frac{\partial^4}{\partial x^3 \partial y} + 2 \left(D_{xy} + 2 D_{ss}\right) \frac{\partial^4}{\partial x^2 \partial y^2} + 4 D_{ys} \frac{\partial^4}{\partial x \partial y^3} + D_{yy} \frac{\partial^4}{\partial y^4} \quad \ldots\ldots\ldots\ldots (73)$$

and

$$D_{ij} = 2 \sum_{m=1}^{n} \frac{1}{3} E_{ij}^m \left(h_m^3 - h_{m-1}^3\right) \quad \ldots\ldots\ldots\ldots (74)$$

and L_2 is given by Eq. 14.

The difference between Eqs. 71 and 72 and the classical equations of homogeneous aeolotropic plates lies only in the value of the constants in the operators L_1 and L_2. Known results of homogeneous plate theory can be fully utilized for the analysis of the symmetrically laminated plate, as far as solving for w and F goes. This was first shown by Lekhnitsky[5] for the bending system shown in Eq. 71.

However, it is noted that the cross-elasticity effect in Eq. 70 is still present but is simplified to

$$\left[\tau^m\right] = \left[E^m\right] \left[a\right] \left[N\right] \text{ or } \left[\tau^m\right] = z \left[E^m\right] \left[d\right] \left[M\right] \quad \ldots\ldots (75)$$

in which

$$\left[a\right] = \left[A^{-1}\right] \quad \ldots\ldots\ldots\ldots\ldots\ldots (76)$$

and

$$\left[d\right] = \left[D^{-1}\right] \quad \ldots\ldots\ldots\ldots\ldots\ldots (77)$$

and D is given by Eq. 74.

As an example of case II consider the multi-layer aeolotropic plate, for which all the elastic moduli E vary in the same manner with z. Thus

$$\left[E^m\right] = c^m \left[E^\circ\right] \quad \ldots\ldots\ldots\ldots\ldots\ldots (78)$$

In view of Eqs. 9 and 78

$$[B] = q\,[A] \qquad \ldots\ldots\ldots\ldots\ldots\ldots (79)$$

in which

$$q = \frac{\frac{1}{2}\sum_{m=1}^{n} c^m \left(h_m^2 - h_{m-1}^2\right)}{\sum_{m=1}^{n} c^m \left(h_m - h_{m-1}\right)} \qquad \ldots\ldots\ldots\ldots\ldots\ldots (80)$$

Introducing Eq. 79 into Eq. 18 it is found that

$$\begin{aligned} [A^*] &= [A^{-1}]\ ,\ [B^*] = -\,q\,[I] \\ [D^*] &= [D] - q^2\,[A] \end{aligned} \qquad \ldots\ldots\ldots\ldots\ldots\ldots (81)$$

in which I is the unit matrix.

Because B^* is a diagonal matrix with equal elements, the coupling operator L_3 vanishes identically in view of Eq. 15.

The quantity, q, given by Eq. 80 is identified as the distance of neutral surface from the reference z = 0.

The existance of a single neutral plane, at which all strain components vanish simultaneously, causes the cross-elasticity effect of Eq. 70 to disappear.

In order to show this, the reference plane z = 0 at the neutral plane of the sheet is located.

Eq. 61 takes the form

$$\begin{bmatrix} \epsilon^o \\ \\ \kappa \end{bmatrix} = \left[\begin{array}{c|c} a & o \\ \hline o & d \end{array}\right] \begin{bmatrix} N \\ \\ M \end{bmatrix} \qquad \ldots\ldots\ldots\ldots\ldots\ldots (82)$$

in which

$$[a] = [A^{-1}]\ ,\ [d] = [D^{*-1}] \qquad \ldots\ldots\ldots\ldots\ldots\ldots (83)$$

Using Eqs. 82, 78, and 70 it is found that

$$[\tau^m] = c^m\,[E^o]\left([a]\,[N] + z\,[d]\,[M]\right) \qquad \ldots\ldots\ldots\ldots (84)$$

and considering Eq. 83

$$[\tau^m] = c^m\left(\frac{[N]}{A^o} + z\,\frac{[M]}{D^o}\right) \qquad \ldots\ldots\ldots\ldots\ldots\ldots (85)$$

is finally established. Where the pseudo-elastic-weighed area and moment of inertia are respectively given by

$$A^o = \sum_{m=1}^{n} c^m \left(h_m - h_{m-1}\right) \quad \ldots\ldots\ldots\ldots (86)$$

and

$$D^o = \frac{1}{3} \sum_{m=1}^{n} c^m \left(h_m^3 - h_{m-1}^3\right) \quad \ldots\ldots\ldots\ldots (87)$$

It is noted that, although cases I and II are mathematically identical, case II is completely analogous to that of classical stretching and bending of homogeneous aeolotropic plates, but case I involves cross-stress systems, as in Eq. 75, which cannot be accounted for within the framework of classical theory. For example, bending moments M_x causes self-equilibrated stresses σ_y on the boundaries $y = 0, l_y$.

The far reaching consequences of the presence of the uncoupled cross-elasticity effect (Eq. 75) in case I show up in a plate theory that considers transverse shear and normal stress deformations. However, an examination of this problem is beyond the scope of this paper.[6]

NUMERICAL EXAMPLES

To obtain a quantitative insight into the results of uniform distributions of resultants and couples, consider first an aeolotropic heterogeneous rectangular plate with

$$E_{ij} = E_{ij}^o \left(1 + R \cos \frac{m\pi}{h} z\right) \quad \ldots\ldots\ldots\ldots (88)$$

and

$$\left[E^o\right] = E_{xx}^o \begin{bmatrix} 1 & 0.2 & 0.2 \\ 0.2 & 1 & 0.2 \\ 0.2 & 0.2 & 0.3 \end{bmatrix} \quad \ldots\ldots\ldots\ldots (89)$$

Case 1.—$R = 1$, $m - 1$ in Eq. 88.

The following results are found for a uniform axial force, N_x, applied at the middle plane of the plate $\left(z = \frac{h}{2}\right)$:

$$w = \frac{N_x}{E_{xx}^o h^2} \left[- 2.782271\, x^2 - 0.214016\, y^2 + 6.737039\, x\, y\right] \ldots (90)$$

---

6 "On the Theory of Heterogeneous Anisotropic Plates," by Y. Stavsky, thesis presented to the Massachusetts Inst. of Tech., in Cambridge, Mass., in September, 1959, in partial fulfilment of the requirements for the degree of Doctor of Philosophy.

$$\begin{bmatrix} \epsilon_x \\ \epsilon_y \\ \epsilon_{xy} \end{bmatrix} = \frac{N_x}{E^o_{xx}\, h} \left[\begin{array}{c|c|c|} -0.493945 & 2.288326 & 5.070598 \\ 0.037995 & -0.176025 & -0.390046 \\ 0.303966 & -1.408201 & -3.120368 \end{array} \right]_{z=0}^{z=\frac{h}{2}}{}_{z=h} \quad \ldots . (91)$$

and

$$\begin{bmatrix} \tau_x \\ \tau_y \\ \tau_{xy} \end{bmatrix} = \frac{N_x}{h} \left[\begin{array}{c|c|c|} -0.851104 & 1.971484 & 0 \\ 0 & 0 & 0 \\ 0 & 0 & 0 \end{array} \right]_{z=0}^{z=\frac{h}{2}}{}_{z=h} \quad \ldots . (92)$$

Analogous results for the case of a uniform bending moment, M_x, are:

$$w = -\frac{6\, M_x}{E^o_{xx}\, h^3} \left[2.288326\, x^2 - 0.176025\, y^2 - 1.408201\, x\, y \right] \ldots (93)$$

$$\begin{bmatrix} \epsilon_x \\ \epsilon_y \\ \epsilon_{xy} \end{bmatrix} = \frac{6\, M_x}{E^o_{xx}\, h^2} \left[\begin{array}{c|c|c|} -1.360902 & 0.927424 & 3.215750 \\ 0.104685 & -0.071340 & -0.244032 \\ 0.837479 & -0.570722 & -1.978923 \end{array} \right]_{z=0}^{z=\frac{h}{2}}{}_{z=h} \quad \ldots . (94)$$

and

$$\begin{bmatrix} \tau_x \\ \tau_y \\ \tau_{xy} \end{bmatrix} = \frac{6\, M_x}{h^2} \left[\begin{array}{c|c|c|} -2.344940 & 0.799012 & 0 \\ 0 & 0 & 0 \\ 0 & 0 & 0 \end{array} \right]_{z=0}^{z=\frac{h}{2}}{}_{z=h} \quad \ldots . (95)$$

A graphical representation of these results is given in Figs. 1 and 2.

Case 2.—R = 1, m = 8 in Eq. 88.

The following results are obtained for a uniform axial force N_x, applied at $z = \frac{h}{2}$:

$$w = 0 \ldots \ldots \ldots \ldots \ldots \ldots \ldots (96)$$

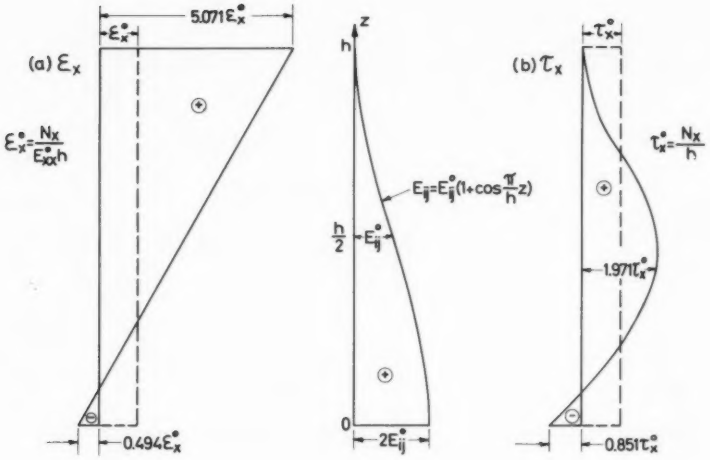

CASE 1 N_x

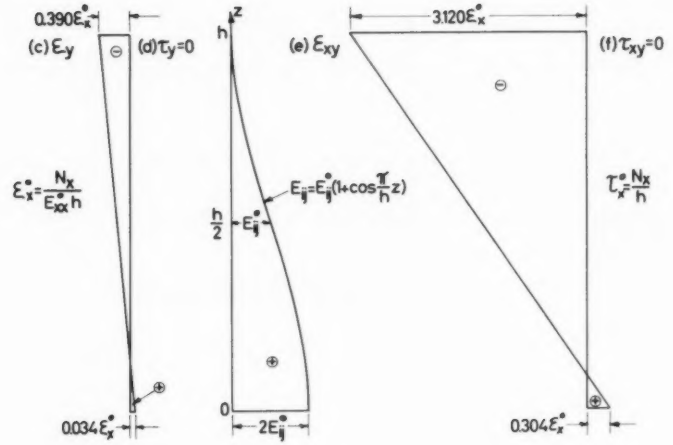

CASE 1 N_x

FIG. 1.—STRAIN AND STRESS COMPONENTS IN A HETEROGENEOUS AEOLOTROPIC PLATE, WITH THE SAME Z VARIATION OF E_{IJ}, SUBJECT TO UNIFORM AXIAL TENSION N_X

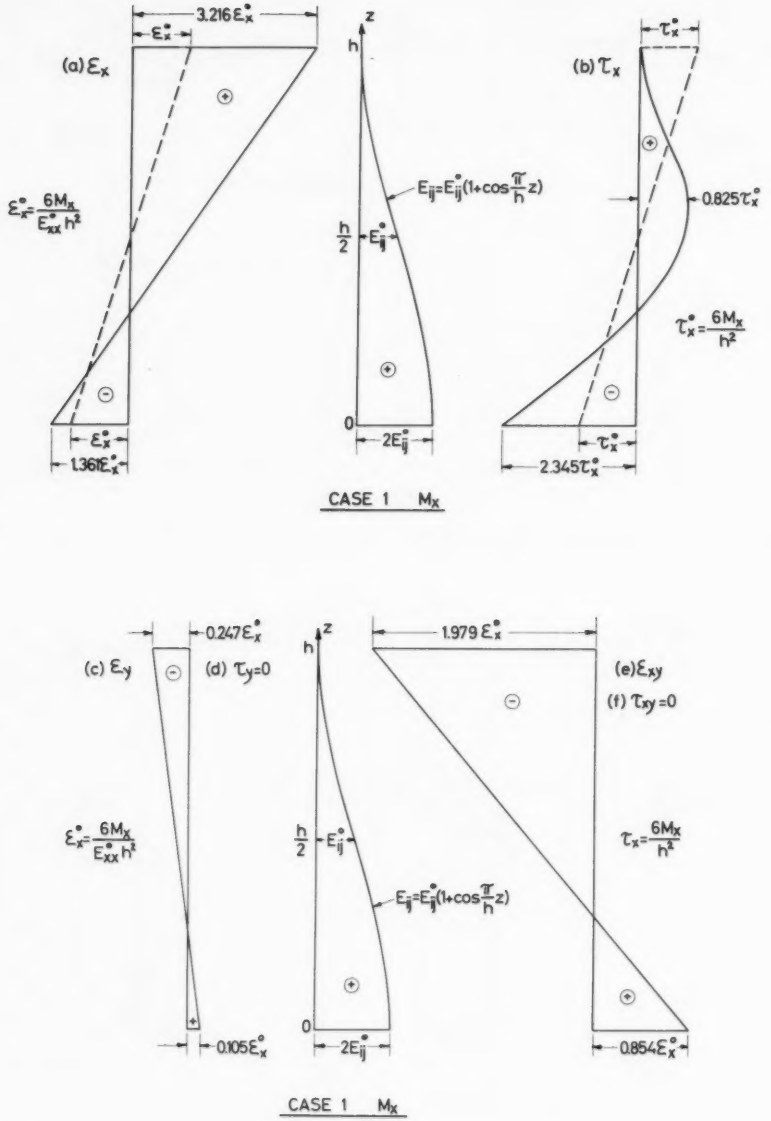

FIG. 2.—STRAIN AND STRESS COMPONENTS IN A HETEROGENEOUS AEOLOTROPIC PLATE WITH THE SAME E VARIATION OF E_{IJ}, SUBJECT TO PURE BENDING MOMENT M_X

$$\begin{bmatrix} \epsilon_x \\ \epsilon_y \\ \epsilon_{xy} \end{bmatrix} = \frac{N_x}{E^o_{xx}\, h} \begin{bmatrix} 1.160715 \\ -0.089286 \\ -0.714286 \end{bmatrix} \quad \ldots\ldots\ldots\ldots\ldots\ldots\ldots\ldots\ldots\ldots (97)$$

and

$$\begin{bmatrix} \tau_x \\ \tau_y \\ \tau_{xy} \end{bmatrix} = \frac{N_x}{h} \left[\begin{array}{c|c|c|c|c} 2.000000 & 0.190984 & 0 & & \\ 0 & 0 & 0 & & \\ 0 & 0 & 0 & & \\ \hline z=0 & z=0.1h & z=0.125h & & \end{array} \right.$$

$$\left. \begin{array}{c|c|c|c} 0.190984 & 1.309013 & 2.000000 & \\ 0 & 0 & 0 & \\ 0 & 0 & 0 & \\ \hline z=0.15h & z=0.2h & z=0.25h & \end{array} \right] \ldots (98)$$

Analogous results for the case of a uniform bending moment, M_x, are:

$$w = -\frac{6\, M_x}{E^o_{xx}\, h^3} \left[1.118227\, x^2 - 0.086017\, y^2 - 0.688140\, x\, y \right] \ldots (99)$$

$$\begin{bmatrix} \epsilon_x \\ \epsilon_y \\ \epsilon_{xy} \end{bmatrix} = \frac{6\, M_x}{E^o_{xx}\, h^2} \left[\begin{array}{c|c|c|c} -1.118227 & -0.559113 & 0 & \\ 0.086017 & 0.043008 & 0 & \\ 0.688140 & 0.344070 & 0 & \\ \hline z=0 & z=\frac{h}{4} & z=\frac{h}{2} & \end{array} \right] \ldots (100)$$

and

$$\begin{bmatrix} \tau_x \\ \tau_y \\ \tau_{xy} \end{bmatrix} = \frac{6\, M_x}{h^2} \left[\begin{array}{c|c|c|c|c|c} -1.926791 & 0 & -0.963375 & 0 & & \\ 0 & 0 & 0 & 0 & & \\ 0 & 0 & 0 & 0 & & \\ \hline z=0 & z=\frac{h}{8} & z=\frac{h}{4} & z=\frac{h}{2} & & \end{array} \right] \ldots (101)$$

A graphical representation of the results for case 2 is given in Figs. 3 and 4.

Because the cross-elasticity effect of Eq. 70 vanishes for the type of heterogeneity indicated by Eqs. 88 and 89, only τ_X stresses are developed of quite an interesting shape.

It seems striking how effectively one can control the elastic stress distribution by the type of the heterogeneity of the plate and, thus, the material is

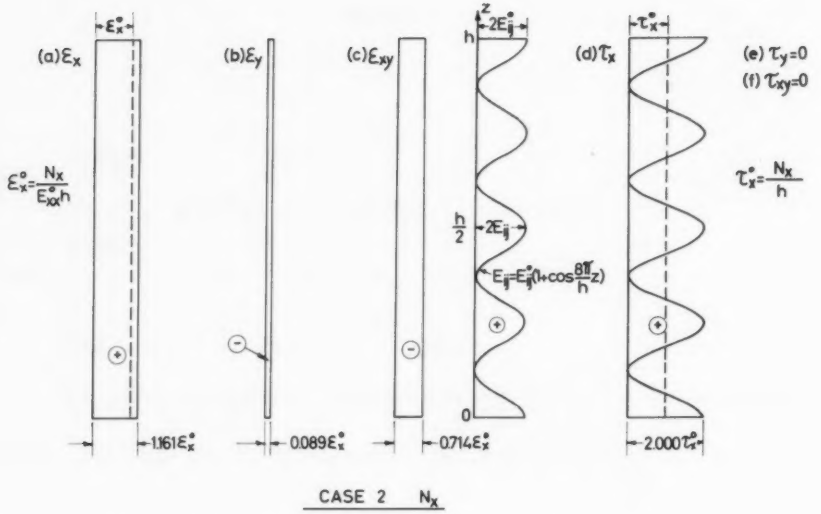

FIG. 3.—STRAIN AND STRESS COMPONENTS IN A SYMMETRICALLY HETEROGENEOUS AEOLOTROPIC PLATE WITH THE SAME Z VARIATION OF E_{IJ}, SUBJECT TO UNIFORM AXIAL TENSION N_X

utilized much more effectively in bending than in the conventional elastic homogeneous system.

So far, a special class of heterogeneity has been dealt with; namely, all elastic moduli have the same variation throughout the plate thickness. A somewhat more general case is now considered as follows:

Case 3.—

$$[E] = E_{xx}^\circ \begin{bmatrix} 1 & \left(1 + 0.6\cos\frac{\pi}{h}z\right) & 0.2 & \left(1 + 0.6\cos\frac{\pi}{h}z\right) & 0.002\left(1 + 100\cos\frac{\pi}{h}z\right) \\ 0.2 & \left(1 + 0.6\cos\frac{\pi}{h}z\right) & 1 & \left(1 + 0.6\cos\frac{\pi}{h}z\right) & 0.002\left(1 + 100\cos\frac{\pi}{h}z\right) \\ 0.002\left(1 + 100\cos\frac{\pi}{h}z\right) & & 0.002\left(1 + 100\cos\frac{\pi}{h}z\right) & & 0.4\left(1 + 0.6\cos\frac{\pi}{h}z\right) \end{bmatrix} \quad . . (102)$$

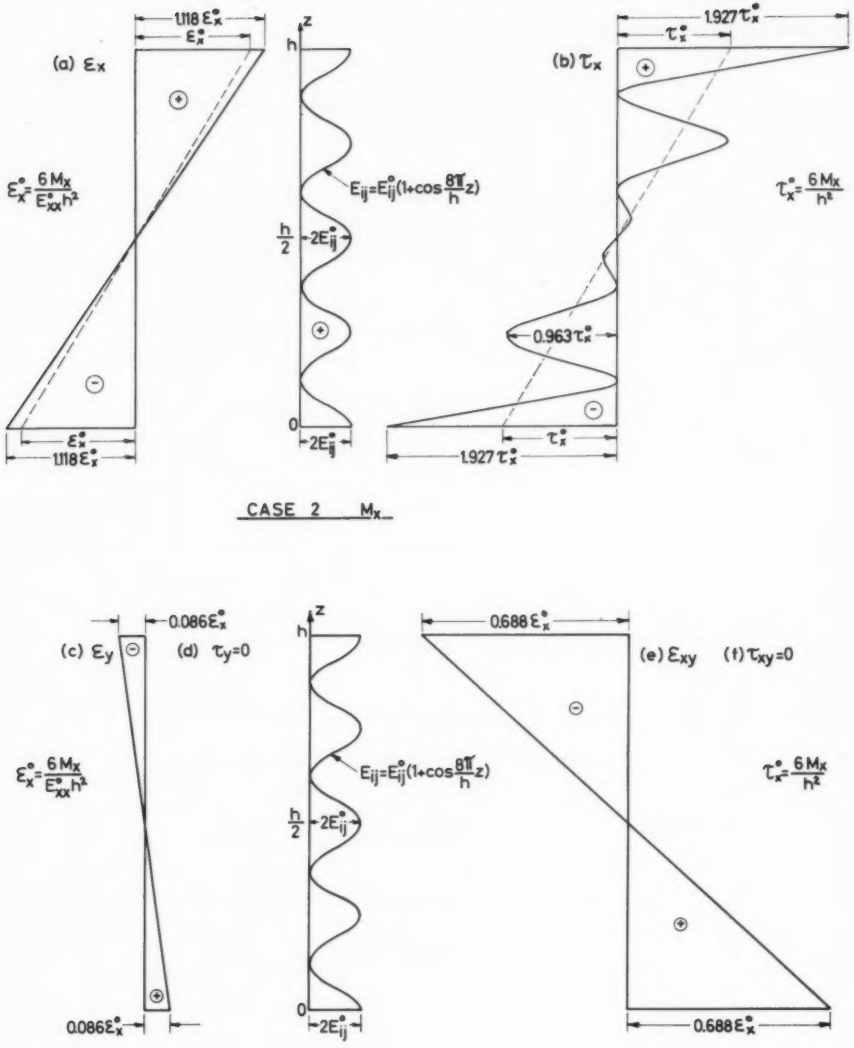

FIG. 4.—STRAIN AND STRESS COMPONENTS IN A SYMMETRICALLY HETEROGENEOUS AEOLOTROPIC PLATE WITH THE SAME Z VARIATION OF E_{IJ}, SUBJECT TO PURE BENDING MOMENT M_X

The following results were obtained for a uniformly axial force applied at the middle plane of the plate $\left(z = \frac{h}{2}\right)$:

$$w = \frac{N_x}{E^o_{xx} h^2} \left[-1.1076\, x^2 + 0.0009\, y^2 - 1.1111\, x\, y\right] \quad \ldots\ldots(103)$$

$$\begin{bmatrix} \epsilon_x \\ \epsilon_y \\ \epsilon_{xy} \end{bmatrix} = \frac{N_x}{E^o_{xx} h} \left[\begin{array}{c|c|c|c|c} 0.2776 & 0.7207 & 1.3852 & 1.8283 & 2.4929 \\ -0.1335 & -0.1338 & -0.1343 & -0.1347 & -0.1352 \\ -0.6229 & -0.1785 & 0.4882 & -0.6229 & 1.5993 \\ \hline z=0 & z=0.2h & z=0.5h & z=0.7h & z=h \end{array}\right] \quad \ldots(104)$$

$$\begin{bmatrix} \tau_x \\ \tau_y \\ \tau_{xy} \end{bmatrix} = \frac{N_x}{h} \left[\begin{array}{c|c|c|c|c} 0.275668 & 1.001515 & 1.359363 & 1.058305 & 0.669676 \\ -0.250440 & -0.013839 & +0.143710 & 0.041748 & -0.171318 \\ -0.369520 & -0.009896 & +0.197782 & 0.045780 & -0.210930 \\ \hline z=0 & z=0.2h & z=0.5h & z=0.7h & z=h \end{array}\right] \quad \ldots(105)$$

Analogous results for the case of a uniform bending moment, M_x, are:

$$w = \frac{6\, M_x}{E^o_{xx} h^3} \left[1.38525\, x^2 - 0.13431\, y^2 - 0.48820\, x\, y\right] \ldots\ldots(106)$$

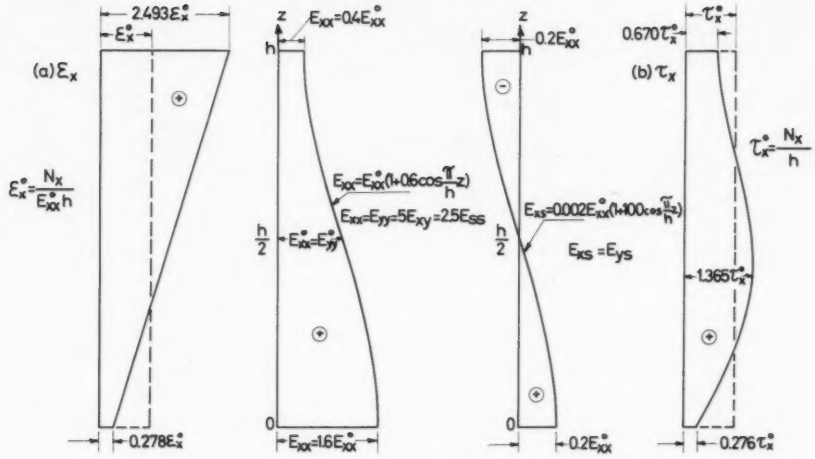

CASE 3 N_x

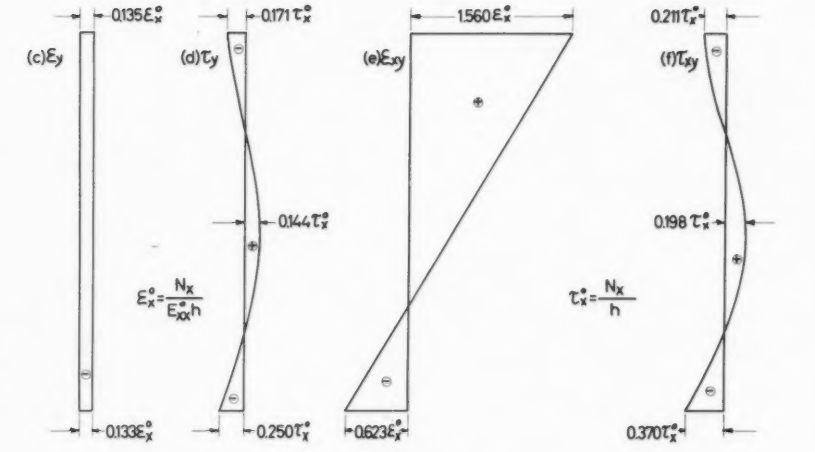

CASE 3 N_x

FIG. 5.—STRAIN AND STRESS COMPONENTS IN A NON-SYMMETRICAL HETEROGENEOUS AEOLOTROPIC PLATE SUBJECT TO UNIFORM AXIAL TENSION N_X

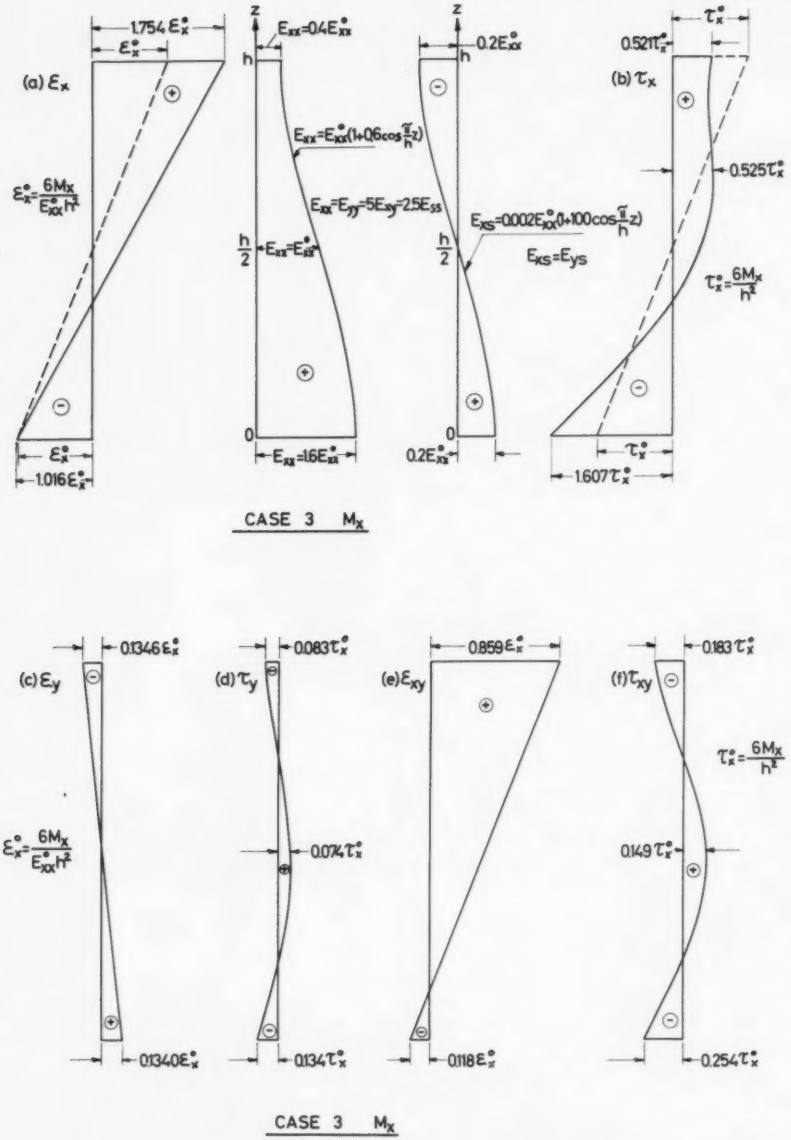

FIG. 6.—STRAIN AND STRESS COMPONENTS IN A NON-SYMMETRICALLY HETEROGENEOUS AEOLOTROPIC PLATE SUBJECT TO PURE BENDING MOMENT M_X

$$\begin{bmatrix} \epsilon_x \\ \epsilon_y \\ \epsilon_{xy} \end{bmatrix} = \frac{6\,M_x}{E^o_{xx}\,h^2} \left[\begin{array}{c|c|c|c} -1.01603 & -0.46193 & 0.36921 & \\ 0.13401 & 0.08028 & -0.00030 & \\ -0.11783 & 0.07745 & 0.37037 & \\ z=0 & z=0.2h & z=0.5h & \end{array}\right.$$

$$\left.\begin{array}{c|c|c} 0.92331 & 1.75447 & \\ -0.05403 & 0.13461 & \\ 0.56565 & 0.85857 & \\ z=0.7h & z=h & \end{array}\right] \quad \ldots(107)$$

and

$$\begin{bmatrix} \tau_x \\ \tau_y \\ \tau_{xy} \end{bmatrix} = \frac{6\,M_x}{h^2} \left[\begin{array}{c|c|c|c} -1.606578 & -0.649630 & 0.369892 & \\ -0.134513 & -0.005288 & 0.074281 & \\ -0.253584 & -0.016501 & 0.148883 & \\ z=0 & z=0.2h & z=0.5h & \end{array}\right.$$

$$\left.\begin{array}{c|c|c} 0.525328 & 0.521019 & \\ 0.019199 & -0.083486 & \\ 0.046011 & -0.183358 & \\ z=0.7h & z=h & \end{array}\right] \quad \ldots(108)$$

A graphical representation of the results for Case 3 is given in Figs. 5 and 6.

It is noted that the strain and stress distribution deviate considerably, quantitatively and qualitatively, from the corresponding results for homogeneous systems.

The occurance of cross-stresses is clearly examplified and it seems that it has to be considered in the design of laminated structures.

ACKNOWLEDGMENT

The writer gratefully acknowledges the guidance and advice that C. H. Norris, E. Reissner and A. G. H. Dietzall of the Massachusetts Institute of Technology, Cambridge, Mass., contributed throughout this work. The author is likewise indebted to S. Namyet for helpful discussions of the matrix algebra of

this paper and to S. Mauch for carrying out the numerical work on the IBM 709 digital computer at MIT.

The present results were obtained in the course of research sponsored in part by the Hebrew Technical Institute in New York, The Israel Institute of Technology, and in part by the Air Research and Development Command of the United States Air Force.

Journal of the
ENGINEERING MECHANICS DIVISION
Proceedings of the American Society of Civil Engineers

VARIATIONAL METHODS IN FLUID DYNAMICS[a]

By J. W. Delleur,[1] M. ASCE, and A. A. Sooky[2]

SYNOPSIS

A variational principle applicable to incompressible laminar flows is presented. The case in which the boundary conditions specify the velocity on one part of the boundary and the stresses on the remainder of the boundary is considered. The method is particularly well suited for machine computations. The variational principle is applied to an approximate computation of the velocity distribution for laminar flow in square and rectangular ducts. Approximate and exact solutions are compared.

INTRODUCTION

Variational procedures may be particularly useful to obtain approximate solutions to a wide variety of problems. Variational techniques make use of certain broad minimum principles. For example, in structural engineering and in elasticity the concepts of least work, minimum potential energy, minimum strain, and complementary energies are commonly used. Similar broad minimum principles applicable to fluid-mechanics problems are not presented in standard textbooks. The purpose herein is to state a variational principle that is applicable to a class of problems in fluid mechanics, and to illustrate its usefulness in solving problems by use of digital computers.

Note.—Discussion open until May 1, 1962. To extend the closing date one month, a written request must be filed with the Executive Secretary, ASCE. This paper is part of the copyrighted Journal of the Engineering Mechanics Division, Proceedings of the American Society of Civil Engineers, Vol. 87, No. EM6, December, 1961.

[a] Presented at the October, 1960 ASCE Convention in Boston, Mass.

[1] Assoc. Prof. of Hydr. Engrg., Purdue Univ., Lafayette, Ind.
[2] Research Asst., School of Civ. Engrg., Purdue Univ., Lafayette, Ind.

The basic variational principle of particle dynamics was known by Lagrange. The Lagrangean equations of motion, Bernoulli theorem, and other equations of hydrodynamics in the Lagrangean system can be derived from variational principles.[3] However, engineering problems are usually formulated in the Eulerian system. The variational principle stated herein is the Eulerian system and is applicable to laminar flows, in which inertia forces are negligible. Important features of this principle are the two boundary conditions considered:

1. The case where velocity is specified along the whole boundary or the stresses are zero along the entire boundary; and
2. The case where the boundary conditions specify the velocity on one part of the boundary and the stresses on the remainder of the boundary.

The principle was first stated by Helmholtz[4,5] and the discussion of the general equations for steady motion of a viscous incompressible fluid from a variational point of view was first given by C. B. Millikan.[6]

The equations describing laminar flows, the basic variational problem, and Euler equations will be reviewed before the principle is stated, proven, and then applied.

Notation.—The letter symbols adopted for use in this paper are defined where they first appear, in the illustrations or in the text, and are arranged alphabetically, for convenience of reference, in the Appendix.

VISCOUS-FLOW EQUATIONS

A problem in laminar flow may be formulated in terms of the differential equations describing the phenomena and the boundary conditions of the problem. The governing differential equations for incompressible fluids[7] are the equation of continuity

$$\frac{\partial u_i}{\partial x_i} = 0 \quad \ldots\ldots\ldots\ldots\ldots\ldots (1)$$

and the Navier-Stokes equations of motion

$$\frac{\partial u_i}{\partial t} + u_j \frac{\partial u_i}{\partial x_j} = -\frac{1}{\rho}\frac{\partial p}{\partial x_i} + \nu \frac{\partial^2 u_i}{\partial x_j \partial x_j} \quad \ldots\ldots\ldots\ldots (2)$$

in which u is velocity, t denotes time, ρ is density, p represents pressure, the indices i, j, and k denote the x, y, and z components, and summation should be

---

[3] "Variation Principles of Hydrodynamics," by C. Eckart, The Physics of Fluids, Vol. 3, May-June, 1960, p. 421.

[4] "Zur Theorie der Stationären Strõme in Reibenden Flüssigkeiten," by Hermann Helmholtz, Verhandlungen des naturhistorisch—medizinischen Vereins zu Heidelberg, Band V, October, 1868.

[5] "Hydrodynamics," by Horace Lamb, Dover Publications, New York, N. Y., 1945, Article 344.

[6] "On the Steady Motion of Viscous, Incompressible Fluids; with Particular Reference to a Variational Principle," by C. B. Millikan, Philosophical Magazine, Vol. 7, No. 44, April, 1929, p. 641.

[7] "Modern Development in Fluid Dynamics," by S. Goldstein, Oxford Univ. Press, Oxford, England, 1938, Chap. 3.

made over the three values of a repeated index occurring in the expression for each general term. The rates of strain in the fluid flow are expressed by

$$e_{ij} = \frac{\partial u_i}{\partial x_j} + \frac{\partial u_j}{\partial x_i} \quad \ldots\ldots\ldots\ldots\ldots\ldots (3)$$

and the corresponding stresses are

$$\sigma_{ij} = - p\ \delta_{ij} + \mu e_{ij} \quad \ldots\ldots\ldots\ldots\ldots\ldots (4)$$

in which δ_{ij} is the Kronecker delta, equal to unity when $i = j$ and equal to zero under other conditions, and μ is absolute viscosity. The rate of dissipation of energy per unit of time per unit volume is

$$\phi = \frac{1}{2}\ \mu\ e_{ij}\ e_{ji} = \frac{1}{2}\ \sigma_{ij}\ e_{ij} \quad \ldots\ldots\ldots\ldots\ldots\ldots (5)$$

CALCULUS OF VARIATIONS AND EULER-LAGRANGE EQUATIONS

The calculus of variation makes use of broad minimum principles that characterize a class of phenomena. It is then concerned with the extremization (minimization or maximization) of a quantity J by the proper choice of the entities on which J depends. For example, it is desired to find what plane curve connecting two points (x_1, y_1) and (x_2, y_2) has the shortest length. The length of the curve is given by

$$J = \int_{x_1}^{x_2} \sqrt{1 + y'^2}\ dx \quad \ldots\ldots\ldots\ldots\ldots\ldots (6)$$

in which y' denotes the derivative dy/dx (Fig. 1). Of all the curves

$$Y = y(x) + \epsilon\ \eta(x) \quad \ldots\ldots\ldots\ldots\ldots\ldots (7)$$

which pass through the given end points, the shortest one

$$y = y(x) \quad \ldots\ldots\ldots\ldots\ldots\ldots (8)$$

must be selected. The problem thus reduces to finding the function y(x) that makes the integral J a minimum. Therefore, there are two features to be considered:

1. The geometrical or physical principles which make it possible to write an expression such as Eq. 6; and
2. The mathematical condition in addition to the boundary conditions that a function such as y(x) must satisfy in order to make J a minimum.

The mathematical condition is considered first, and the physical principle will be discussed subsequently.

In order to minimize the integral

$$J = \int_{x_1}^{x_2} F(x, y, y')\ dx \quad \ldots\ldots\ldots\ldots\ldots\ldots (9)$$

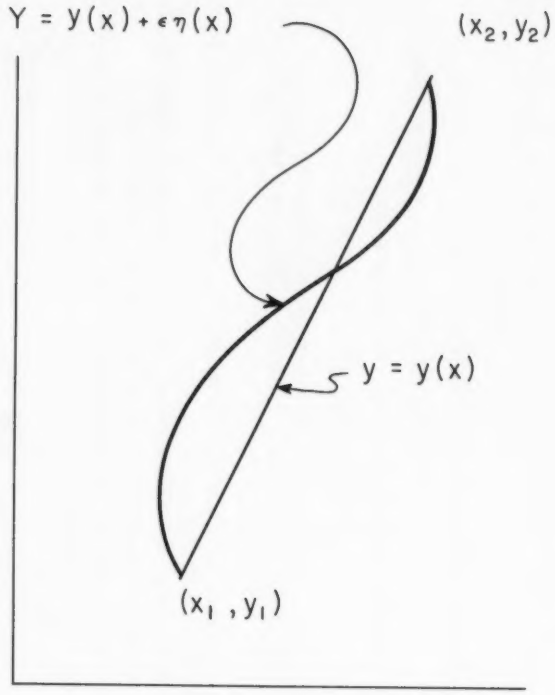

FIG. 1

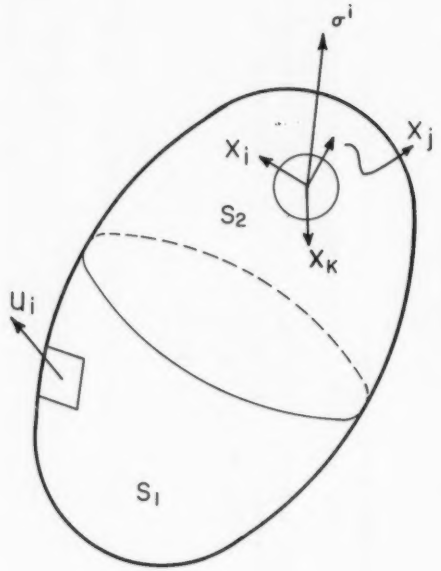

FIG. 2

the function y(x) must satisfy the boundary conditions and the Euler-Lagrange differential equation.[8,9]

$$\frac{\partial F}{\partial y} - \frac{d}{dx}\left(\frac{\partial F}{\partial y'}\right) = 0 \quad \ldots\ldots\ldots\ldots\ldots\ldots (10)$$

In fluid mechanics the velocity may be a function of two or three independent variables. The previous theorem can be extended to several dependent and independent variables. For example, in order to minimize the integral

$$J = \iint F\left(x, y, u, u_x, u_y\right) dx\, dy \quad \ldots\ldots\ldots\ldots (11)$$

(in which the subscripts denote partial derivatives), the function u(x, y) must satisfy the Euler-Lagrange differential equation

$$\frac{\partial F}{\partial u} - \frac{\partial}{\partial x}\left(\frac{\partial F}{\partial u_x}\right) - \frac{\partial}{\partial y}\left(\frac{\partial F}{\partial u_y}\right) = 0 \quad \ldots\ldots\ldots\ldots (12)$$

in addition to the boundary conditions.

VARIATIONAL PRINCIPLE

The object of the variational principle is to state a minimum principle that characterizes laminar flows. This makes possible the construction of integrals that attain their minimum when the flow is steadily uniform. The problem of determination of velocities reduces to standard methods of the calculus of variations. Once velocities are known, pressures and other quantities may be calculated by the usual methods of fluid mechanics.

The variational principle is as follows: The motion of an incompressible fluid that satisfies the equation of continuity, the equations of motion, and the boundary condition of zero stress or specified velocity along the whole boundary is such that the dissipation integral

$$J = \int_V F\, dv = \frac{1}{2}\int_V \sigma_{ij}\, e_{ij}\, dv \quad \ldots\ldots\ldots\ldots\ldots (13)$$

attains a minimum for steady uniform flow. If, instead, the boundary conditions specify the velocity on one part S_1 of the boundary, and the stresses on the remaining part S_2 of the boundary, then the following expression is a minimum:[5]

$$I = \frac{1}{2}\int_V \sigma_{ij}\, e_{ij}\, dv - 2\int_{S_2} \sigma^i\, u_i\, dS \quad \ldots\ldots\ldots\ldots (14)$$

in which I is the excess of the dissipation integral over twice the rate at which work is being done by the specified surface tractions σ^i (Fig. 2). Hence, for

[8] "Calculus of Variations with Applications to Physics and Engineering," by R. Weinstock, McGraw-Hill Book Co., Inc., New York, N. Y., 1952.

[9] "Methods of Mathematical Physics," by R. Courant and D. Hilbert, Interscience Publishers, Inc., New York, N. Y., 1943.

steady, incompressible laminar flow, the velocity distribution is to be chosen so that the boundary conditions are satisfied and the excess of the rate at which work is being done on the boundaries over the total rate of change in kinetic energy plus potential energy plus dissipation of energy within the boundaries is a minimum.

The variational principle may be justified by replacing the integrand F of the variational integral in the Euler-Lagrange equations corresponding to the variational principle stated previously, and by showing that the result obtained is equivalent to the equations of continuity and of motion describing the problem. In this fashion it can be formally proved that minimizing the integrals of Eqs. 13 or 14 is equivalent to solving the Navier-Stokes equations with the inertia terms neglected; this fact is used in the solution of problems. If the closed-form solution of the equations of motion and continuity for a given problem cannot be obtained, the problem may be transformed into the equivalent minimization of the integrals of Eqs. 13 or 14. The Euler-Lagrange differential equation does not need to be solved rigorously. Approximate methods are available, among which are the Rayleigh-Ritz and the Galerkin methods,[9] the former being illustrated in the examples.

The variational principle stated previously may also be verified by taking the variation of J or I and investigating the conditions under which they vanish.

Taking the variation of the dissipation integral (Eq. 13), one obtains

$$\delta J = \frac{1}{2} \int_V \left(\delta \sigma_{ij} \, e_{ij} + \delta e_{ij} \, \sigma_{ij} \right) dv = \int_V \sigma_{ij} \, \delta e_{ij} \, dv \quad \ldots\ldots (15)$$

because of the symmetry of the stress and strain tensors. Making use of Eq. 3 leads to

$$\delta J = \int_V \sigma_{ij} \left[\frac{\partial \left(\delta u_i \right)}{\partial x_j} + \frac{\partial \left(\delta u_j \right)}{\partial x_i} \right] dv$$

$$= \int_V \left[\frac{\partial}{\partial x_i} \left(\sigma_{ij} \, \delta u_j \right) + \frac{\partial}{\partial x_j} \left(\sigma_{ij} \, \delta u_i \right) - \delta u_j \frac{\partial \sigma_{ij}}{\partial x_i} - \delta u_i \frac{\partial \sigma_{ij}}{\partial x_j} \right] dv \quad \ldots (16)$$

and, because of symmetry

$$\delta J = 2 \int_V \left[\frac{\partial}{\partial x_j} \left(\sigma_{ij} \, \delta u_i \right) - \delta u_i \frac{\partial \sigma_{ij}}{\partial x_j} \right] dv \quad \ldots\ldots\ldots (17)$$

Assuming steady uniform flow, there is no acceleration in the direction of flow and the equations of equilibrium[10] apply

$$\frac{\partial \sigma_{ij}}{\partial x_j} = 0 \quad \ldots\ldots\ldots\ldots\ldots\ldots (18)$$

---

[10] "Theory of Elasticity," by S. Timoshenko and J. N. Goodier, McGraw-Hill Book Co., Inc., New York, N. Y., 1951, Article 76.

This is equivalent to stating that by neglecting the inertia terms, the term $\partial\sigma_{ij}/\partial x_j$ vanishes and

$$\delta J = 2 \int_V \frac{\partial}{\partial x_j} \left(\sigma_{ij} \, \delta u_i \right) dv \quad \ldots\ldots\ldots\ldots (19)$$

By Green's theorem

$$\delta J = 2 \int_S \sigma_{ij} \, \alpha^j \, \delta u_i \, dS = 2 \int_S \sigma^i \, \delta u_i \, dS \quad \ldots\ldots\ldots (20)$$

in which α^j is the direction cosine of the outward normal to the surface element. The surface integral in Eq. 20 will vanish if

$$\delta u_i = 0 \quad \ldots\ldots\ldots\ldots\ldots\ldots (21a)$$

or if

$$\sigma^i = 0 \quad \ldots\ldots\ldots\ldots\ldots\ldots (21b)$$

on S. If either condition in Eqs. 21 is satisfied

$$\delta J = 0 \quad \ldots\ldots\ldots\ldots\ldots\ldots (22)$$

and the integral of Eq. 13 is an extremum.

If the boundary conditions specify the velocity on one part of the boundary S_1 and the traction on the remainder of the boundary S_2 the conditions of Eqs. 21 no longer hold on S_2 and the integral of Eq. 13 is not an extremum. However, Eq. 20 still holds and may be written as

$$\delta J = \delta \frac{1}{2} \int_V \sigma_{ij} \, e_{ij} \, dv = 2 \int_{S_1} \sigma^i \, \delta u_i \, dS + 2 \int_{S_2} \sigma^i \, \delta u_i \, dS \quad \ldots\ldots (23)$$

But because the boundary conditions specify the velocity on

$$S_1 \quad \delta u_i = 0 \quad \ldots\ldots\ldots\ldots\ldots\ldots (24)$$

on S_1, then

$$\delta \frac{1}{2} \int_V \sigma_{ij} \, e_{ij} \, dv = 2 \int_{S_2} \sigma^i \, \delta u_i \, dS \quad \ldots\ldots\ldots\ldots (25)$$

or

$$\delta \left\{ \frac{1}{2} \int_V \sigma_{ij} \, e_{ij} \, dv - 2 \int_{S_2} \sigma^i \, u_i \, dS \right\} = 0 \quad \ldots\ldots\ldots (26)$$

or

$$\delta I = 0 \quad \ldots\ldots\ldots\ldots\ldots\ldots (27)$$

which shows that the integral of Eq. 14 is an extremum for mixed boundary conditions.

The foregoing proof shows that I and J are extrema. Helmholtz[4] has shown that I and J tend to a unique and stable minimum.

EXAMPLES

In the subsequent material the velocity distribution for laminar flow in circular pipes will be obtained by variational technique and approximation of the velocity distribution for laminar flow in square and rectangular conduits obtained by the variational technique is compared to the exact solution. The same technique has been applied by D. F. Hays[11] to the problem of hydrodynamic lubrication of finite journal bearings.

Circular Pipe.—Consider a horizontal circular pipe of radius r_o, and let u be the velocity in the z-direction parallel to the axis of the pipe. The Navier-Stokes equation in cylindrical coordinates, in the z-direction, neglecting the inertia terms is (Fig. 3):

$$\frac{\partial^2 u}{\partial r^2} + \frac{1}{r}\frac{\partial u}{\partial r} + \frac{1}{r^2}\frac{\partial^2 u}{\partial \theta^2} = \frac{1}{\mu}\frac{\partial p}{\partial z} = C^* \quad \ldots\ldots\ldots\ldots (28)$$

Because of axial symmetry, the third term in Eq. 28 vanishes, and

$$\frac{d^2 u}{dr^2} + \frac{1}{r}\frac{du}{dr} = C^* \quad \ldots\ldots\ldots\ldots\ldots\ldots (29)$$

The boundary condition is

$$u = 0 \quad \ldots\ldots\ldots\ldots\ldots\ldots\ldots\ldots (30)$$

at $r = r_o$, and the pressure gradient as well as the viscosity are assumed to be given; that is, C^* is known.

An approximate solution of the differential equation (Eq. 29) along with the boundary condition of Eq. 30 can be obtained by use of the following steps:

1. Because the boundary conditions specify the velocity $u = 0$ at the wall of the pipe, and the head loss per unit length along the conduit is given by

$$\frac{\partial p}{\partial z} = \mu\, C^* \quad \ldots\ldots\ldots\ldots\ldots\ldots (31)$$

the problem falls into the category of mixed boundary conditions, and integral of Eq. 14 must be utilized. For the problem at hand the energy dissipation per unit time per unit volume is[12]

$$\phi = \mu \left(\frac{du}{dr}\right)^2 \quad \ldots\ldots\ldots\ldots\ldots\ldots (32)$$

---

11 "A Variational Approach to Lubrication Problems and the Solution of the Finite Journal Bearing," by D. F. Hays, Journal of Basic Engineering, ASME, Vol. 81, March, 1959.

12 "Fluid Mechanics," by V. L. Streeter, McGraw-Hill Book Co., Inc., New York, N. Y., 1958, p. 146.

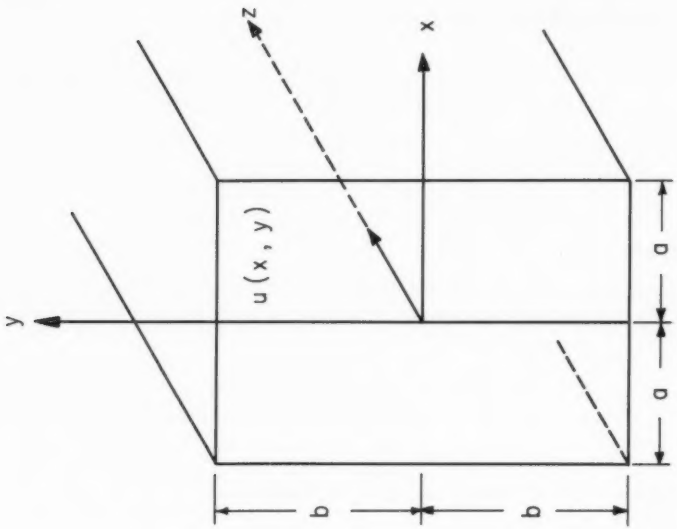

FIG. 4

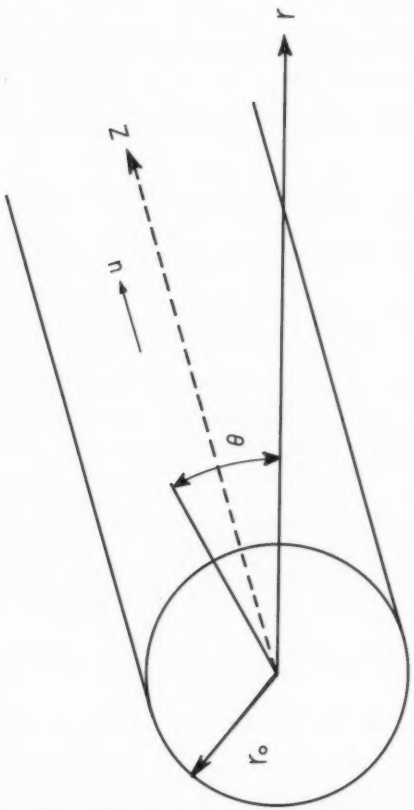

FIG. 3

The rate at which work is being done by the specified pressure forces per unit area on a fluid element of unit length is

$$\sigma^i u_i = \left[p - \left(p + \frac{dp}{dz} \right) \right] u = - u \frac{dp}{dz} \quad \ldots\ldots\ldots\ldots (33)$$

The integral of Eq. 14 may now be written

$$I = \int_V \mu \left(\frac{du}{dr} \right)^2 dv - 2 \int_{S_2} - u \left(\frac{dp}{dz} \right) dS \quad \ldots\ldots\ldots (34)$$

in which S_2 is the cross-sectional area at the ends of the element on which the pressure forces act. For an element of unit length in the z-direction, I may be rewritten

$$I = \int_0^{r_o} \int_0^{2\pi} \left[\mu \left(\frac{du}{dr} \right)^2 + 2 u \left(\frac{dp}{dz} \right) \right] r \, dr \, d\theta \quad \ldots\ldots\ldots (35)$$

The integrand of the foregoing variational integral is

$$F = r \left[\mu \left(\frac{du}{dr} \right)^2 + 2 \mu C^* u \right] = \mu r \left[u_r^2 + 2 C^* u \right] \quad \ldots\ldots (36)$$

in which the subscript r denotes derivative with respect to r.

2. The variational principle states that the integral I of Eq. 35 is a minimum. The velocity u(r) that minimizes Eq. 35 must also satisfy the Euler-Lagrange differential equation 5 (Eq. 10) which in circular coordinates becomes

$$\frac{\partial F}{\partial u} - \frac{d}{dr} \left(\frac{\partial F}{\partial u_r} \right) = 0 \quad \ldots\ldots\ldots\ldots\ldots (37a)$$

Performing the operations indicated in Eq. 37 with the value of F given in Eq. 36 one obtains

$$2 \mu r C^* - 2 \mu r \frac{d^2u}{dr^2} - 2 \mu \frac{du}{dr} = 0 \quad \ldots\ldots\ldots (37b)$$

which after dividing by $2 \mu r$ reduces to Eq. 29. This shows that solving the differential equation (Eq. 29) with its boundary condition (Eq. 30) is identical to finding the function u(r) that minimizes Eq. 35. This is the fundamental principle on which the variation technique is based.

3. A velocity distribution that satisfies the boundary condition (Eq. 30) is assumed. This is usually a polynomial or a truncated series. The variational technique yields the best set of coefficients for the polynomial or truncated series assumed. Further discussion on the selection of the assumed form of the velocity distribution will be given with the next example. Assume

$$u = \left(1 - R^2 \right) \left(A_0 + A_1 R^2 + A_2 R^4 \right) \quad \ldots\ldots\ldots (38a)$$

in which

$$R = \frac{r}{r_o} \quad \ldots\ldots\ldots\ldots\ldots\ldots \quad (38b)$$

This function obviously satisfies the boundary condition of Eq. 30.

4. The function F of Eq. 36 is now evaluated:

$$F = 4\ \mu\ r \left(A_1 \frac{r}{r_o^2} + 2\ A_2 \frac{r^3}{r_o^4} - A_0 \frac{r}{r_o^2} - 2\ A_1 \frac{r^3}{r_o^4} - 3\ A_2 \frac{r^5}{r_o^6} \right)^2$$

$$+ 2\ \mu\ C^*\ r \left(A_0 + A_1\ R^2 + A_2\ R^4 - A_0\ R^2 - A_1\ R^4 - A_2\ R^6 \right) \ldots (39)$$

which may be integrated to obtain the variational integral of Eq. 35:

$$I = 4\ \pi\ \mu \left[2 \left(\frac{1}{4} A_0^2 + \frac{1}{6} A_0\ A_1 + \frac{1}{12} A_0\ A_2 + \frac{1}{12} A_1^2 + \frac{7}{60} A_1\ A_2 + \frac{1}{2} A_2^2 \right) \right.$$

$$\left. + C^*\ r_o^2 \left(\frac{1}{4} A_0 + \frac{1}{12} A_1 + \frac{1}{24} A_2 \right) \right] \ldots\ldots\ldots\ldots (40)$$

5. Differentiating Eq. 40 with respect to each of the coefficients of the assumed function (Eq. 38a) and equating to zero will yield a set of simultaneous equations with the coefficients as the unknowns. The solution will yield the coefficients of Eq. 38a that will minimize Eq. 40:

$$\frac{\partial I}{\partial A_0} = 0 = A_0 + \frac{1}{3} A_1 + \frac{1}{6} A_2 + \frac{1}{4} C^*\ r_o^2 \quad \ldots\ldots\ldots (41a)$$

$$\frac{\partial I}{\partial A_1} = 0 = \frac{1}{3} A_0 + \frac{1}{3} A_1 + \frac{7}{30} A_2 + \frac{1}{12} C^*\ r_o^2 \quad \ldots\ldots\ldots (41b)$$

and

$$\frac{\partial I}{\partial A_2} = 0 = \frac{1}{6} A_0 + \frac{7}{30} A_1 + 2A_2 + \frac{1}{24} C^*\ r_o^2 \quad \ldots\ldots\ldots (41c)$$

Solving simultaneously yields

$$A_0 = -\frac{1}{4} C^*\ r_o^2 \quad \ldots\ldots\ldots\ldots\ldots\ldots (42a)$$

$$A_1 = 0 \quad \ldots\ldots\ldots\ldots\ldots\ldots (42b)$$

and

$$A_2 = 0 \quad \ldots\ldots\ldots\ldots\ldots\ldots (42c)$$

Substituting the coefficients into the assumed polynomial for u of Eq. 37b yields

$$u = \left(1 - R^2 \right) \left(-\frac{1}{4} C^*\ r_o^2 \right) = -\frac{1}{4} C^* \left(r_o^2 - r^2 \right) \quad \ldots\ldots (42d)$$

this is the well-known parabolic velocity distribution for laminar flow in pipes.

Although the foregoing example is trivial, and the variational technique is not the simplest method for obtaining the desired result, it illustrates the sequence of steps to follow. The method is actually a more powerful tool when the exact solution of the differential equation cannot be obtained or is extremely laborious to obtain. The variational techniques will yield the polynomial of best approximation of the form assumed.

Rectangular Conduit.—Consider a rectangular duct of sides 2 a and 2 b (Fig. 4). It is desired to obtain an approximate calculation of the velocity distribution for laminar flow of a fluid of absolute viscosity μ.

The differential equation governing the viscous flow in a rectangular duct, obtained by simplifying the Navier-Stokes equations (Eq. 10) is

$$\frac{\partial^2 u}{\partial x_2} + \frac{\partial^2 u}{\partial y_2} = \frac{1}{\mu}\frac{\partial p}{\partial z} = C^* \quad \ldots\ldots\ldots\ldots\ldots (43)$$

The boundary conditions are

$$\text{at} \quad X = \pm a \quad \text{and at} \quad y = \pm b, \quad u = 0 \quad \ldots\ldots\ldots (44)$$

The solution of the problem consists of the following steps:

1. The problem is again of the mixed boundary condition type and the integral of Eq. 14 applies. The dissipation function (Eq. 5) reduces to

$$\phi = \mu\left(\frac{\partial u}{\partial x}\right)^2 + \mu\left(\frac{\partial u}{\partial y}\right)^2 \quad \ldots\ldots\ldots\ldots\ldots (45)$$

and the rate at which work is being done by the specified pressure force on a unit area is

$$\sigma^i u_i = - u \frac{\partial p}{\partial z} \quad \ldots\ldots\ldots\ldots\ldots (46)$$

The dissipation integral (Eq. 14) becomes

$$I = \int_v \mu\left[\left(\frac{\partial u}{\partial x}\right)^2 + \left(\frac{\partial u}{\partial y}\right)^2\right] dv - 2\int_{S_2} - u\frac{\partial p}{\partial z}\, ds \quad \ldots\ldots\ldots (47)$$

that for an element of unit length in the z-direction may be written as

$$I = \int_{-a}^{a}\int_{-b}^{b}\left[\mu\left(\frac{\partial u}{\partial x}\right)^2 + \mu\left(\frac{\partial u}{\partial y}\right)^2 + 2\, u\frac{\partial p}{\partial z}\right] dx\, dy \quad \ldots\ldots (48)$$

or

$$I = \int_{-a}^{a}\int_{-b}^{b}\mu\left(u_x^2 + u_y^2 + 2\, C^* u\right) dx\, dy \quad \ldots\ldots\ldots (49)$$

in which the subscripts indicate partial derivatives.

The integrand is

$$F = \mu \left(u_x^2 + u_y^2 + 2\ C^*\ u \right) \quad \ldots\ldots\ldots\ldots\ldots (50)$$

Replacing F in the Euler-Lagrange equation (Eq. 12), Eq. 42d may be obtained. Once more this shows that solving the differential equation (Eq. 43) and the boundary conditions (Eq. 44) for u(x, y) is equivalent to finding the function u(x, y) that minimizes Eq. 49.

2. Velocity distribution that satisfies the boundary conditions is assumed.

Depending on the problem at hand the function u(x, y) may be assumed to be an algebraic series, or a trigonometric series. The Ritz method chooses u as a series of linear terms each of which satisfies the boundary conditions. That is

$$u = a_0\ u_0 + a_1\ u_1 + a_2\ u_2 + \ldots\ldots\ldots\ldots\ldots (51)$$

For the rectangular section, possible trial functions would be

$$u = \left(x^2 - a^2\right)\left(y^2 - b^2\right) \sum \sum A_{mn}\ x^{2m}\ y^{2n} \quad \ldots\ldots (52)$$

and

$$u = \sum_{m=1,3,5\ldots}^{\infty} \sum_{n=1,3,5\ldots}^{\infty} A_{mn} \cos \frac{m\ \pi\ x}{2\ a} \cos \frac{n\ \pi\ y}{2\ b} \ldots\ldots (53)$$

In general, if the conduit is bound by a convex polygon, of which the sides have the equations

$$A_n x + B_n y + C_n = 0 \qquad n = 1,\ 2,\ \ldots\ n \ldots\ldots\ldots (54)$$

a possible trial function would be

$$u = \left(A_1\ x + B_1\ y + C_1\right)\left(A_2\ x + B_2\ y + C_2\right) \ldots \left(A_n\ x + B_n\ y + C_n\right) \sum \sum A_{mn}\ X^m\ Y^n \ldots\ldots\ldots\ldots (55)$$

For the example to be considered herein a velocity distribution of the type of Eq. 52 has been selected:

$$u = \left(x^2 - a^2\right)\left(y^2 - b^2\right)\left[A_0 + A_1\ x^2\ A_2\ y^2 + A_3\ x^2\ y^2\right] \ldots\ (57)$$

3. The function F of Eq. 50 and the integral I of Eq. 49 are then determined. Differentiating I with respect to each of the coefficients contained in Eq. 57 and equating to zero one obtains the simultaneous equations

$$\frac{\partial I}{\partial A_0} = 0 \quad \ldots\ldots\ldots\ldots\ldots\ldots (58a)$$

$$\frac{\partial I}{\partial A_1} = 0 \quad \ldots\ldots\ldots\ldots\ldots\ldots \quad (58b)$$

and

$$\frac{\partial I}{\partial A_2} = 0 \quad \ldots\ldots\ldots\ldots\ldots\ldots \quad (58c)$$

Eqs. 58 written in detail are

$$M_1 A_0^1 + M_2 A_1^1 + M_3 A_2^1 + M_4 A_3^1 = -\frac{2}{9} \quad \ldots\ldots\ldots \quad (59a)$$

$$M_2 A_0^1 + M_5 A_1^1 + M_4 A_2^1 + M_6 A_3^1 = -\frac{2}{45} \quad \ldots\ldots\ldots \quad (59b)$$

$$M_7 A_0^1 + M_8 A_1^1 + M_9 A_2^1 + M_{10} A_3^1 = -\frac{2}{45} \quad \ldots\ldots\ldots \quad (59c)$$

and

$$M_8 A_0^1 + M_{11} A_1^1 + M_{10} A_2^1 + M_{12} A_3^1 = -\frac{2}{225} \quad \ldots\ldots\ldots \quad (59d)$$

in which

$$A_0^1 = \frac{A_0 a^2}{C^*} \quad \ldots\ldots\ldots\ldots\ldots\ldots \quad (60a)$$

$$A_1^1 = \frac{A_1 a^4}{C^*} \quad \ldots\ldots\ldots\ldots\ldots\ldots \quad (60b)$$

$$A_2^1 = \frac{A_2 a^4}{C^*} \quad \ldots\ldots\ldots\ldots\ldots\ldots \quad (60c)$$

and

$$A_3^1 = \frac{A_3 a^6}{C^*} \quad \ldots\ldots\ldots\ldots\ldots\ldots \quad (60d)$$

in which

$$M_1 = 2A\left(1 + r^2\right) \quad \ldots\ldots\ldots\ldots\ldots\ldots \quad (61a)$$

$$M_2 = Br^2 + C \quad \ldots\ldots\ldots\ldots\ldots\ldots \quad (61b)$$

$$M_3 = r^2\left(B + Cr^2\right) \quad \ldots\ldots\ldots\ldots\ldots\ldots \quad (61c)$$

$$M_4 = Dr^2\left(1 + r^2\right) \quad \ldots\ldots\ldots\ldots\ldots\ldots \quad (61d)$$

$$M_5 = 2\left(Er^2 + F\right) \quad \ldots\ldots\ldots\ldots\ldots\ldots \quad (61e)$$

$$M_6 = Hr^2 \quad \ldots\ldots\ldots\ldots\ldots\ldots \quad (61f)$$

$$M_7 = B + Cr^2 \quad \ldots\ldots\ldots\ldots\ldots\ldots \quad (61g)$$

$$M_8 = D\left(1 + r^2\right) \quad \ldots\ldots\ldots\ldots\ldots\ldots \quad (61h)$$

$$M_9 = 2r^2\left(E + Fr^2\right) \quad \ldots\ldots\ldots\ldots\ldots\ldots \quad (61i)$$

$$M_{10} = r^2\left(G + Hr^2\right) \quad \ldots\ldots\ldots\ldots\ldots\ldots \quad (61j)$$

$$M_{11} = Gr^2 + H \quad \ldots\ldots\ldots\ldots\ldots\ldots \quad (61k)$$

and

$$M_{12} = 2Kr^2\left(1 + r^2\right) \quad \ldots\ldots\ldots\ldots\ldots\ldots \quad (61l)$$

in which $r = b/a$ and in which the constants of integration obtained in performing the integration of Eq. 49 are:

A = 0.17777780	D = 0.01015873	G = 0.01596371
B = 0.07111110	E = 0.05587300	H = 0.00338625
C = 0.05079366	F = 0.00846561	K = 0.00266062

4. The simultaneous equations (Eqs. 58) were solved with help of the Datatron Digital Computer for several values of r. The obtained values of the coefficients A_0^1, A_1^1, A_2^1, A_3^1 are presented in Table 1. The velocity distribution

TABLE 1

r = b/a	A_0^1	A_1^1	A_2^1	A_3^1
1.0	-0.29190673	-0.05923733	-0.04665263	-0.08542354
2.0	-0.11216367	-0.00688249	-0.01755341	-0.00617324
4.0	-0.02974420	-0.00058096	-0.00290610	-0.00023508
8.0	-0.00710333	-0.00004145	-0.00027111	-0.00000536
12.0	-0.00309772	-0.00000845	-0.00005860	-0.00000051
20.0	-0.00110197	-0.00000111	-0.00000797	-0.00000003

may be obtained by substituting the values of A_0^1, A_1^1, A_2^1, and A_3^1 for the desired depth-to-width ratio into

$$u = \left(x^2 - a^2\right)\left(y^2 - b^2\right)\frac{C^*}{a^6}\left[A_0^1\, a^4 + A_1^1\, a^2\, x^2 + A_2^1\, a^2\, y^2 + A_3^1\, x^2\, y^2\right] \quad \ldots\ldots\ldots\ldots \quad (62)$$

which was obtained from Eq. 57 by introducing the coefficients of Eqs. 60.

The average velocity may be computed from

$$\bar{u} = \frac{1}{a\,b}\int_0^a \int_0^b u\, dx\, dy \quad \ldots\ldots\ldots\ldots \quad (63)$$

TABLE 2[a]

Value of R_1	$u/\bar{u}$, variational method	$u/\bar{u}$, exact method	u/u_{max}, variational method	u/u_{max}, exact method
0.00	2.07515550	2.09719040	1.00000000	1.00000000
0.05	2.07101770	2.09237840	0.99800605	0.99770557
0.10	2.05857290	2.07831860	0.99200899	0.99100148
0.15	2.03772630	2.05570450	0.98196323	0.98021844
0.20	2.00832010	2.02470940	0.96779259	0.96543905
0.25	1.97013300	1.98464360	0.94939055	0.94633457
0.30	1.92288090	1.93449860	0.92662016	0.92242394
0.35	1.86621620	1.87381840	0.89931395	0.89348998
0.40	1.79972850	1.80296170	0.86727410	0.85970347
0.45	1.72294410	1.72240950	0.83027230	0.82129386
0.50	1.63532580	1.63181130	0.78804982	0.77809407
0.55	1.53627370	1.52981360	0.74031746	0.72945862
0.60	1.42512460	1.41497020	0.68675561	0.67469802
0.65	1.30115200	1.28687110	0.62701422	0.61361677
0.70	1.16356620	1.14622580	0.56071281	0.54655306
0.75	1.01151460	0.99356904	0.48744039	0.47376169
0.80	0.84408114	0.82773494	0.40675562	0.39468755
0.85	0.66028682	0.64584733	0.31818667	0.30795837
0.90	0.45908934	0.44552387	0.22123129	0.21243844
0.95	0.23938325	0.22803567	0.11535678	0.10873389
1.00	0.00000000	$0.85574998 \times 10^{-7}$	0.00000000	$0.40804592 \times 10^{-7}$

[a] $r = b/a = 1.0$, $R_2 = y/b = 0.0$, values of A from Table 1.

which results in

$$\bar{u} = a^2 C^* r^2 \left(\frac{4}{9} A_0^1 + \frac{4}{45} A_1^1 + \frac{4}{45} A_2^1 r^2 + \frac{4}{225} A_3^1 r^2 \right) \quad \ldots . \quad (64)$$

Denoting

$$Z = r^2 \left(\frac{4}{9} A_0^1 + \frac{4}{45} A_1^1 + \frac{4}{45} A_2^1 r^2 + \frac{4}{225} A_3^1 r^2 \right) \quad \ldots . \quad (65a)$$

$$\frac{x}{a} = R_1 \quad \ldots . \quad (65b)$$

and

$$\frac{y}{b} = R_2 \quad \ldots . \quad (65c)$$

the velocity distribution may be written in dimensionless form as

$$\frac{u}{\bar{u}} = \frac{1}{Z} r^2 \left(R_1^2 - 1 \right) \left(R_2^2 - 1 \right) \left(A_0^1 + A_1^1 R_1^2 + A_2^1 r^2 R_2^2 + A_3^1 r^2 R_1^2 R_2^2 \right) \quad \ldots . \quad (66)$$

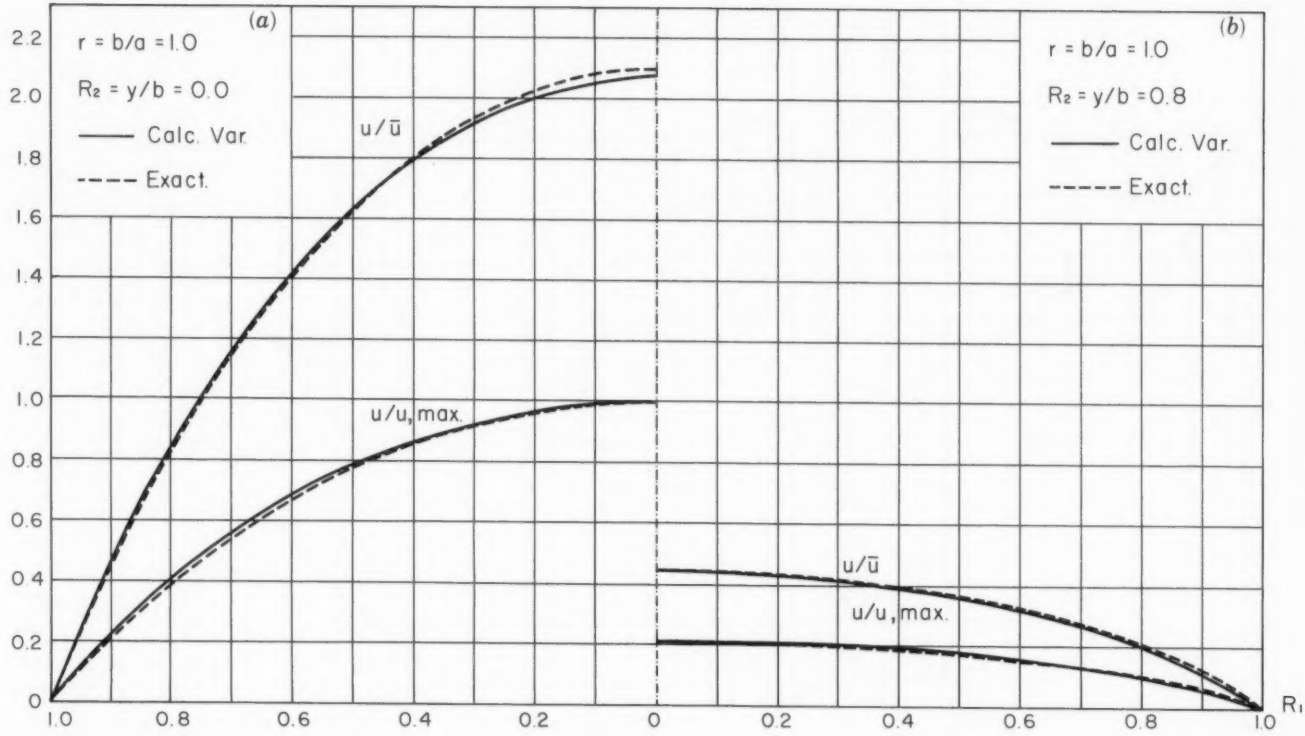
(a)
r = b/a = 1.0
R2 = y/b = 0.0
Calc. Var.
Exact.
u/ū
u/u, max.
(b)
r = b/a = 1.0
R2 = y/b = 0.8
Calc. Var.
Exact.
u/ū
u/u, max.
2.2
2.0
1.8
1.6
1.4
1.2
1.0
0.8
0.6
0.4
0.2
0
1.0
0.8
0.6
0.4
0.2
0
0.2
0.4
0.6
0.8
1.0
R1

FIG. 5

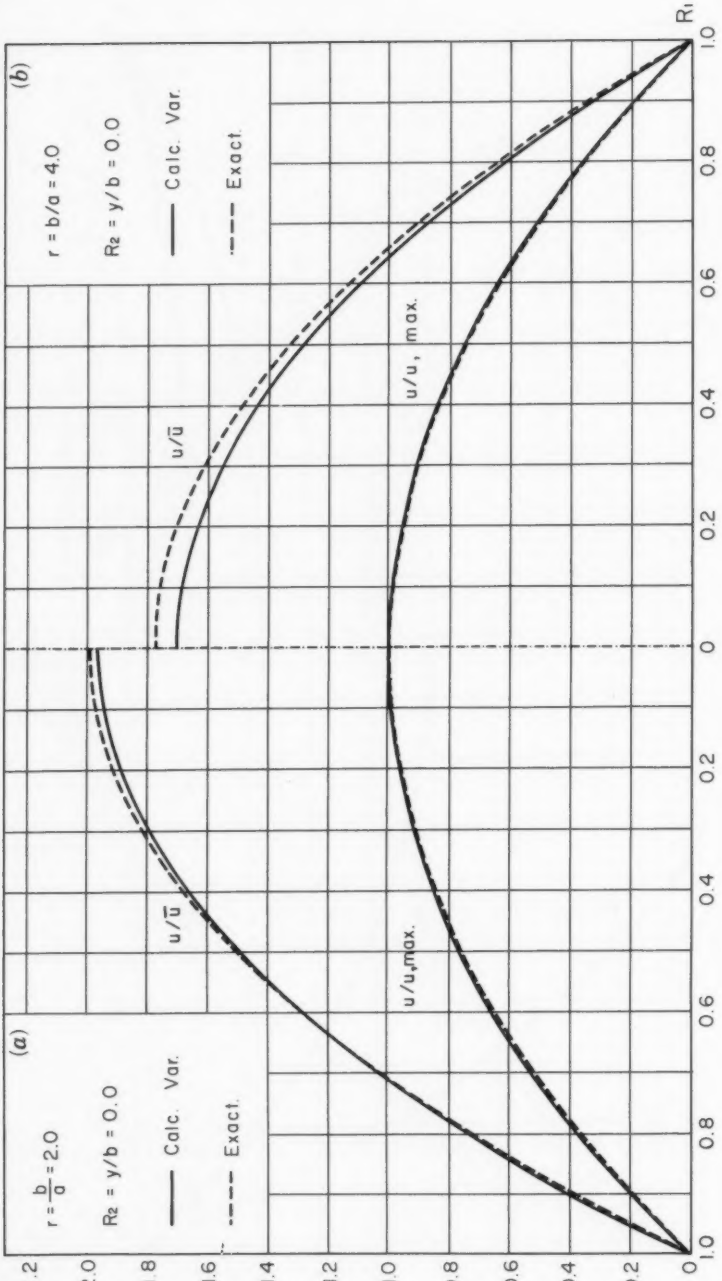
(a)
r = b/a = 2.0
R2 = y/b = 0.0
Calc. Var.
Exact
u/ū
u/u, max.
(b)
r = b/a = 4.0
R2 = y/b = 0.0
Calc. Var.
Exact
u/ū
u/u, max.
R1
2.2
2.0
1.8
1.6
1.4
1.2
1.0
0.8
0.6
0.4
0.2
0
1.0
0.8
0.6
0.4
0.2
0
0.2
0.4
0.6
0.8
1.0

FIG. 6

Similarly, when using u_{max} at $x = 0$, $y = 0$ and

$$u_{max} = A_0^1 \, C^* \, a^2 \, r^2 \quad \ldots\ldots\ldots\ldots\ldots\ldots \quad (67)$$

$$\frac{u}{u_{max}} = \frac{1}{A_0^1}\left(R_1^2 - 1\right)\left(R_2^2 - 1\right)\left(A_0^1 + A_1^1 \, R_1^2 + A_2^1 \, r^2 \, R_2^2 + A_3^1 \, r^2 \, R_1^2 \, R_2^2\right) \quad \ldots\ldots\ldots\ldots\ldots\ldots \quad (68)$$

The velocity distributions along the horizontal axis $(R_2 = 0)$ were determined by means of Eqs. 66 and 68 for several depth-to-width ratios r. In addition for the square conduit the velocity distribution was also computed for several values of R_2. The calculated values were compared to the exact solution,[13] and results are plotted in Figs. 5 and 6. Some of the calculated results are also summarized in Table 2. Figs. 5 and 6 show that for the square duct ($r = 1.0$) the agreement between the approximate solution by variational method, and the exact solution is good for both $u/\bar{u}$ and u/u_{max} plots. With increasing values of r, increasing deviations of $u/\bar{u}$ appear, whereas u/u_{max} remains in better agreement.

EXTENSIONS OF THE VARIATIONAL PRINCIPLE

The variational principle may be extended to non-Newtonian fluids for the case of a simple boundary condition. R. B. Bird[14] has shown that a similar procedure may be used for non-Newtonian fluids, with the same assumptions of steady flow, and negligible inertia terms. In the case of a non-Newtonian incompressible fluid the value of F in Eq. 13 is given by

$$F = \int_0^{\phi} \mu \, (\phi) \, d\phi \quad \ldots\ldots\ldots\ldots\ldots\ldots \quad (69)$$

where the viscosity is assumed to be a function of the dissipation function ϕ. For the case of a constant viscosity, Eq. 69 reduces to Eq. 14. Expressions for $\mu(\phi)$ for several non-Newtonian models are given by Bird, W. E. Stewart, and E. L. Lightfoot.[15]

CONCLUSIONS

The variational principle stated herein is applicable to the solution of the Navier-Stokes equations when the inertia terms may be neglected. The meth-

---

13 "Fluid Dynamics and Heat Transfer," by J. G. Knudsen and D. L. Katz, McGraw-Hill Book Co., Inc., New York, N. Y., 1958, Article 4.17.

14 "New Variational Principle for Incompressible Non-Newtonian Flow," by R. B. Bird, The Physics of Fluids, Vol. 3, No. 4, July-August, 1960, p. 539.

15 "Transport Phenomena," by R. B. Bird, W. E. Stewart, and E. L. Lightfoot, John Wiley and Sons, Inc., New York, N. Y., 1960, p. 103.

od is particularly useful where a closed-form solution of the differential equations governing the problem cannot be obtained. The sample calculations show that the method is particularly well suited for machine calculation, and that reliable solutions can be obtained. The method gives the polynomial of best approximation of the form assumed for the velocity distribution.

ACKNOWLEDGMENTS

The writers are indebted to Paul F. Chenea, Head of the School of Mechanical Engineering at Purdue University, Lafayette, Ind., whose ideas have contributed substantially to this paper. The writers are also grateful to D. F. Hays of the Research Laboratories at General Motors Corporation for his valuable suggestions. The calculations for the velocity distribution in square and rectangular ducts were made on the Datatron digital computer at Purdue University.

APPENDIX.—NOTATION

The following symbols have been adopted for use in this paper:

$A,B \ldots H,K$ = Constants of integration;

A_0,A_1,A_2 = coefficients, Eqs. 38 and 57;

A_0^1,A_1^1,A_2^1 = coefficients, Eq. 60;

a = half width of rectangular duct;

b = half depth of rectangular duct;

C^* = $\frac{1}{\mu}\frac{dp}{dz}$;

e_{ij} = rate of strain tension, Eq. 3;

F = integrand of variational integral;

I = variational integral;

i,j,k = subscripts in indicial notation;

J = variational integral;

$M_1,M_2, \ldots M_{12}$ = coefficients, Eq. 61;

p = pressure intensity;

R_1 = dimensionless coordinate, x/a;

R_2 = dimensionless coordinate, y/b;

r = radial coordinate in circular pipe and depth-to-width ratio in rectangular duct;

r_o = pipe radius;

S = area;

t = time;

u = velocity;

$\bar{u}$ = average velocity;

V = volume;

x,y,z = coordinates;

α^j = direction cosine;

δ = variation;

δ_{ij} = Kronecker delta = 1 if i = j, = 0 otherwise;

ϵ = parameter;

$\eta(x)$ = arbitrary differentiable function;

θ = tangential coordinate;

μ = absolute viscosity;

ρ = density;

σ_{ij} = stress tensor, Eq. 4;

σ^i = surface traction; and

ϕ = rate of dissipation of energy per unit of time per unit of vol., Eq. 5.

Journal of the
ENGINEERING MECHANICS DIVISION
Proceedings of the American Society of Civil Engineers

BUCKLING BEHAVIOR ABOVE THE TANGENT MODULUS LOAD

By Bruce G. Johnston,[1] F. ASCE

SYNOPSIS

The inelastic buckling behavior of a concentrically loaded strut having a reduced rectangular cross section as a mid-section is described in detail. The buckling model is similar to that originally used by F. R. Shanley.[2] In the Shanley model two localized points of area were assumed, whereas in the present model a solid rectangular cross section is introduced which permits a detailed exploration of stress distribution across the section. At various load levels the stress distributions that were described intuitively by Shanley, in his original paper, are determined quantitatively. The behavior of struts held so as to remain straight above the tangent modulus load is also studied, as well as other aspects of behavior that may lead to a better appreciation and understanding of inelastic buckling behavior. The great influence of very slight differences in the shape of the stress strain curve is demonstrated in connection with various aspects of inelastic column behavior.

INTRODUCTION

The results presented herein pertain to a series of simulated experiments on structural aluminum alloy struts of various lengths. Stress distribution across the section, load deflection curves, and other information are deter-

Note.—Discussion open until May 1, 1962. To extend the closing date one month, a written request must be filed with the Executive Secretary, ASCE. This paper is part of the copyrighted Journal of the Engineering Mechanics Division, Proceedings of the American Society of Civil Engineers, Vol. 87, No. EM 6, December, 1961.

[1] Prof. of Structural Engr., Civ. Engrg. Dept., Univ. of Michigan, Ann Arbor, Mich.

[2] "Inelastic Column Theory," by F. R. Shanley, Journal, Aero Science, Vol. 14, No. 5, May 1947, p. 261, including discussion by T. von Kármán.

mined by use of a computer. There are many advantages in simulated tests, carried out with the aid of a computer, in comparison with real tests in an actual testing machine. No machining is involved, no materials need be acquired, and there is no scatter in the test results! Moreover, the precision of results, although based on a simulated and idealized material, permits a study of details of behavior that is not possible in ordinary laboratory tests. It would be impossible to completely duplicate the observations that may be made on the basis of the simulated tests reported in this paper.

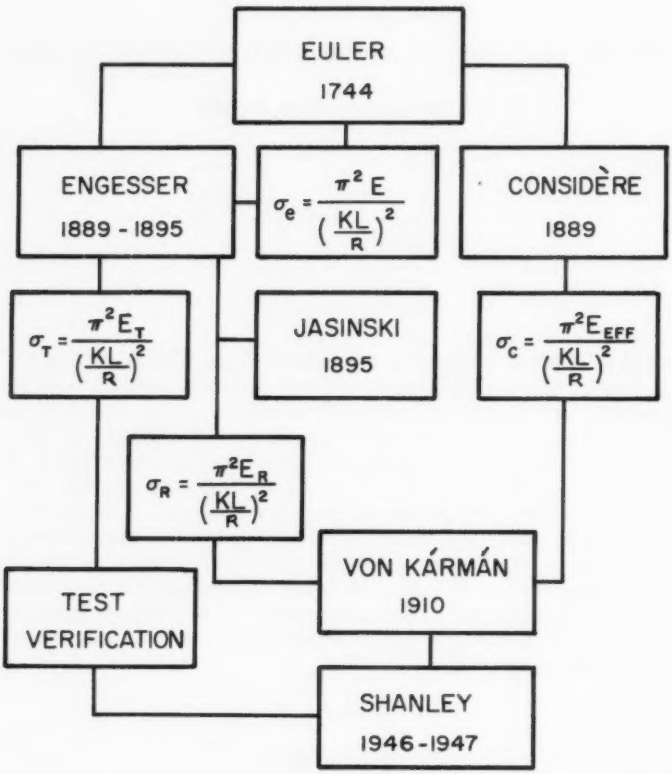

FIG. 1.—EVOLUTION OF THE COLUMN FORMULA

The maximum load (also termed "Shanley Load") is determined quantitatively for a concentrically loaded strut that starts to bend at the tangent modulus load. In properly examining the work of Shanley,[2] it is essential that the development of the Euler formula and its modifications be reviewed over the period of 203 years between it and Shanley's work. An excellent source for such a review has been provided by N. J. Hoff.[3] Fig. 1 summarizes the principal

3 "Buckling and Stability," by N. J. Hoff, Journal, Royal Aeronautics Society, Vol. 58, Aero Reprint No. 123, January, 1954.

developments in outline form. In 1744, Euler presented his evaluation of the average stress at which a slender axially loaded strut of constant cross section will develop bifurcation of equilibrium positions at a constant load. For many years Euler's formula was not generally applied to actual design because proof tests of structures indicated that columns frequently failed below the Euler load. In 1889, Considère indicated why Euler's formula had not been more useful to engineers. He conducted a series of thirty-two column tests and suggested that if buckling occurred above the proportional limit the elastic modulus, "E" should be replaced in the Euler formula by an "$E_{eff.}$" He correctly stated that this effective modulus should be somewhere between the elastic modulus E and the tangent modulus E_t.

Independently of Considère, during the same year, 1889, Engesser suggested that column strength in the inelastic range might be obtained by the substitution of E_t in place of E in the Euler formula. This is known today as the "tangent modulus formula" and has been adopted by Column Research Council[4] as the "proper basis for the establishment of working load formulas" for both ferrous and non-ferrous metals.

In 1895, Jasinski suggested that there was an apparent mistake in Engesser's formula in that the nonreversible characteristic of the stress-strain diagram in the inelastic range should be considered, as had been done in a very general way by Considère. Engesser proceeded, within the same year, to produce a "corrected" general formula for a "reduced modulus," and he stated that this reduced modulus depended not only on "E_t" and "E" but on the shape of the cross section as well.

In 1910, Theodor von Kármán, Hon. M. ASCE, derived explicit expressions for the "reduced modulus" for both the rectangular and the idealized H-section columns. For the rectangle

$$E_R = \frac{4\,E\,E_T}{\left(\sqrt{E}+\sqrt{E_T}\right)^2} \qquad \ldots\ldots\ldots\ldots\ldots \quad (1)$$

The reduced modulus is also called, appropriately, the "double modulus," and for about 35 years subsequent to von Kármán's work, a controversy was waged over the comparative merits of the tangent modulus and double modulus column formulas. From the classical instability concept the double modulus theory was correct, because it indicated the load at which a perfectly straight and centrally loaded column could have neighboring equilibrium configurations with no change in load. This is identical in concept to the Euler load in the elastic buckling range. However, many experimenters found that columns tested in the laboratory with utmost care usually buckled at loads just slightly above the tangent modulus load. For example, very careful tests were made in the 1930's by the Aluminum Research Laboratories.[5] One of their conclusions was: "The test data presented herein are in close agreement with Engesser's formula. . ." By this was meant the tangent modulus formula, even though Engesser himself had renounced it.

---

4 "Guide to Design Criteria for Metal Compression Members," Column Research Council, published by Column Research Council at the Univ. of Michigan, Ann Arbor, Mich. 1960.

5 "Column Strength of Various Aluminum Alloys," by R. L. Templin, R. G. Sturm, E. C. Hartmann, and M. Holt, Aluminum Research Labs., Technical Paper No. 1.

In 1946, Shanley[6] reconciled the controversy between the proponents of the tangent modulus and the double or reduced modulus theories. His explanation now seems simple in retrospect. Shanley showed that because it obviously was possible for a column to bend simultaneously with increasing axial load, without strain reversal, it was reasonable to conclude that such bending would start at the tangent modulus load. Thus, normally, for the usual stress-strain curves, the double modulus load never could be reached, because it is based on equilibrium configurations in the neighborhood of a perfectly straight column. In a letter published jointly with the 1947 Shanley paper, von Kármán[2] redefined the tangent modulus load in a way that may be paraphrased as follows:

> "The tangent modulus load is the smallest value of the axial load at which bifurcation of the equilibrium positions can occur regardless of whether or not the transition to the bent position requires an increase of the axial load."

Shanley showed intuitively that, after bending started, for any finite load increment above the tangent modulus load, there must be, to attain an equilibrium position, some strain reversal. Equilibrium in a bent configuration above the tangent modulus load obviously is not possible if everywhere across the section the stress-strain relationships have been governed only by the tangent modulus. This is true even if the tangent modulus suffers no decrease anywhere within the cross section.

In 1950, J. E. Duberg and T. W. Wilder III[7] applied the Shanley approach to the idealized H-section with flexibility over the full length of the column. The flanges were represented as in the Shanley model, by two point concentrations of area with an intervening web of zero area which could, nevertheless, transmit shear. The result is an important contribution to column theory, in that bending occurs under varying inelastic conditions all along the column. Duberg and Wilder confirm the Shanley concept that bending is initiated at the tangent modulus load:

> "If the behavior of a perfectly straight column is regarded as the limiting behavior of a bent column as its initial imperfection vanishes, the tangent-modulus load is the critical load of the column, -that is, the load at which bending starts."

In 1950, Tung-Hua Lin[8] presented results of his inelastic analysis of a slightly curved column, including effects of strain reversal, considering a rectangular section with distributed area.

Notation.—Terms used in this paper are defined where they first appear and are listed alphabetically, for convenience of reference, in the Appendix.

EVALUATION OF MAXIMUM COLUMN LOAD

A numerical procedure will be presented for the evaluation of the maximum (Shanley) load. Although the method is applied herein to an inelastic buckling

---

6 "The Column Paradox," by F. R. Shanley, Journal of Aero Science, Vol. 13, No. 5, December, 1946, p. 678.

7 "Column Behavior in the Plastic Stress Range," by J. E. Duberg, and T. W. Wilder III, Journal of Aero Science, Vol. 17, No. 6, June, 1950, p. 323, see also NACA T. N. 2267, January, 1951.

8 "Inelastic Column Buckling," by Tung-Hua Lin, Journal of Aero Science, Vol. 17, No. 3, March, 1950, p. 159.

model, with only a limited section at the center that undergoes bending, the method may readily be extended to more realistic columns with variable cross section. A digital computer will be required in such an undertaking, and at each successive equilibrium evaluation, the column configuration by the Newmark[9] numerical procedure will be determined.

After bending starts at the tangent modulus load, successive deflected equilibrium configurations must be established for which the increased column load and increased internal bending resistance are in equilibrium. The resisting internal moment and thrust resultants are determined by a pattern of stress across the cross section of the column that changes shape with each load increment. The calculation of a sequence of equilibrium positions for a succession of small load increments is essential, because over an appreciable portion of the column cross section the material experiences, first, an increase in stress under a continually changing tangent modulus, followed by a regression of strain that produces a stress reduction as determined by the elastic modulus.

The successive equilibrium configurations must be determined very precisely for a sequence of very small increments of unit rotation, with consideration of the continually changing values of tangent modulus. It is not practicable to use values of E_t obtained graphically from an experimental curve. It is necessary to use a mathematical expression that will simulate consistently both the tangent modulus and compressive stress as a function of strain to as great a numerical precision as may be required to give consistent numerical results. Duberg and Wilder[7] used the generalized stress-strain curves of W. Ramberg and W. R. Osgood.[10] These provide a wide variety of shapes with the added advantage that each curve throughout the entire range is represented by a single expression. The Ramberg-Osgood curves could readily be adapted to the procedure employed herein, but it was desired to take a very close look at the behavior near the transition from elastic to inelastic behavior. The Ramberg-Osgood curves have no truly elastic range and were not used in the present study.

The simulated properties for computer analysis correspond closely to the expected minimum properties quoted by the Aluminum Company of America for aluminum alloy 2014-T6. The minimum properties are shown by dashed lines in Fig. 2, and the simulated properties represented by various empirical relationships within the ranges indicated are shown on the same figure. The equations for stress and tangent modulus within the range $0.0032 < \epsilon < 0.0062$ are

$$\sigma = 14.08 + 6200\,\epsilon + 4.34175 \sin\left[\frac{\pi(\epsilon - 0.0032)}{0.0031}\right] \quad \ldots\ldots \quad (2)$$

and

$$E_T = \frac{d\sigma}{d\epsilon} = 6200 + 4400 + \cos\left[\frac{\pi(\epsilon - 0.0032)}{0.0031}\right] \quad \ldots\ldots \quad (3)$$

---

9 "Numerical Procedure for Computing Deflections, Moments, and Buckling Loads," by N. M. Newmark, Transactions, ASCE, Vol. 108, 1943, p. 1161.

10 "Description of Stress-Strain Curves by Three Parameters," by W. Ramberg, and W. R. Osgood, NACA T. N. No. 902, July, 1943.

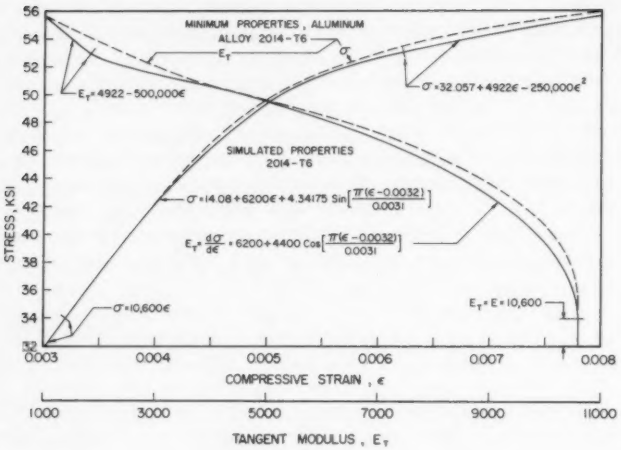

FIG. 2.—INELASTIC STRESS, STRAIN, AND TANGENT MODULUS RELATIONSHIPS

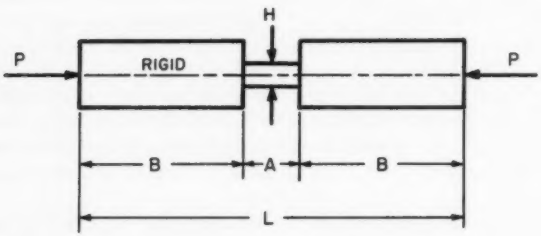

FIG. 3.—BUCKLING MODEL

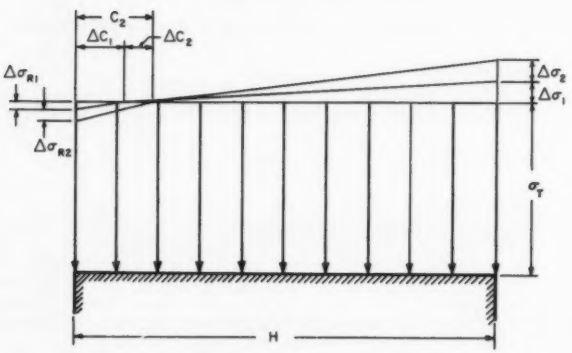

FIG. 4.—STRESS DISTRIBUTION JUST ABOVE THE TANGENT MODULUS LOAD

It is assumed that for stresses up to 33.92 ksi that the material is elastic with an elastic modulus of 10,600 kips per in squared. For $\epsilon > 0.0062$, additional expressions for σ and E_T are indicated on Fig. 2.

The buckling model to be considered herein is shown in Fig. 3. The central non-rigid segment is of square cross section with breadth H and length A, bounded on each end by rigid segments of equal length "B." It is assumed that during bending the reduced segment of length A has a parabolic bent shape for which a simple equilibrium evaluation in the deflected position, using the moment area procedure, gives the following buckling stress in the elastic range:

$$\sigma_C = \frac{E\,H^2}{A\left[6\,B + A\,\dfrac{\left(B + \dfrac{5}{16}A\right)}{\left(B + \dfrac{A}{4}\right)}\right]} \qquad \ldots\ldots\ldots \quad (4)$$

Eq. 4 for this buckling model corresponds to the Euler buckling stress for a column of uniform cross section. Eq. 4 is an approximation and, if B = 0, in which case the buckling model becomes a column of uniform square cross section with the length A, the buckling stress is

$$\sigma_C = \frac{0.8\,E}{\left(\dfrac{A}{H}\right)^2} \qquad \ldots\ldots\ldots\ldots\ldots \quad (5)$$

If Eq. 5 is written in terms of the radius of gyration of the cross section $R = H/\sqrt{12}$, the following approximation of the Euler buckling load for a square column of length A is derived:

$$\sigma_C = \frac{9.6\,E}{\left(\dfrac{A}{R}\right)^2} \qquad \ldots\ldots\ldots\ldots\ldots \quad (6)$$

The exact Euler buckling formula for the pin ended case is the well known equation

$$\sigma_C = \frac{\pi^2\,E}{\left(\dfrac{L}{R}\right)^2} \qquad \ldots\ldots\ldots\ldots\ldots \quad (7)$$

in which L is designated as the length of the column.

Although the buckling load by Eq. 6 is 2.7% less than the correct value by Eq. 7, the approximation in the case of the buckling model will improve, and the error grow less, as the length of the rigid segments increases. If the elastic modulus E in Eq. 4 is replaced by the tangent modulus E_T (corresponding to the identical stress level), the formula will correspond to the tangent modulus formula for column buckling. Similarly, if the reduced double modulus given by Eq. 1 is substituted in Eq. 4, the reduced modulus buckling stress will be obtained. In calculating E_R, the value of E_T corresponds, of course, to the higher reduced modulus load, σ_R.

The initial changes in stress distribution just above the tangent modulus load will now be examined. Fig. 4 shows the stress distribution as uniform at σ_T over the cross section.

If additional load above the tangent modulus load is now applied to the "inelastic buckling model" or "strut," as it will be denoted herein, the strut will start to bend. This bending will cause the stress on one side, as shown, to increase by $\Delta\sigma_1$. The subscript denotes this as the first increment of stress above the tangent modulus value. If $\Delta\sigma_1$ were thought of as an infinitesimal quantity $d\sigma$, in the limit, just as bending was initiated, in the limit, there would be no change in column load, and the tangent modulus would apply over the entire cross section. There would be no strain regression anywhere, and ΔC_1, as shown in the figure, would be zero. If, however, $\Delta\sigma_1$ is an actual finite difference in stress level, there will be a finite increase in column load above the tangent modulus load. If the tangent modulus governed the stress-strain relation over the entire cross section, any increase in load above the tangent modulus load would be supercritical; the tangent modulus load itself would be the maximum buckling load capacity, if the tangent modulus were to govern the stress-strain relationship over the entire cross section. Thus, if a finite $\Delta\phi$ is thought of as representing the first increment of unit curvature, the strut cross section at the point of maximum deflection will have to develop enough bending moment resistance to be in equilibrium with the resultant moment due to the external load P, increased by ΔP_1. This increase in bending resistance can occur only if some strain reversal takes place. Thus, if the tangent modulus stress is thought of as a new reference for stress changes, there will be in effect a movement of the "neutral axis" inward from the edge of the cross section by an amount ΔC_1, and there will be a stress regression on this convex side of the column as indicated by $\Delta\sigma_{R1}$.

If a second increment of rotation is permitted, corresponding to a further increase in axial column load and increase in internal resisting moment, there will be a further movement during this second increment somewhat smaller than the first one, as indicated in Fig. 4 by ΔC_2. This is the only way in which a positive increment in moment can be developed to offset the increase of external moment caused by the load $P + \Delta P_1 + \Delta P_2$. The increase in compressive stress indicated by $\Delta\sigma_2$ will be less than $\Delta\sigma_1$ in the case of the typical inelastic stress-strain curve in which the second derivative of σ with respect to ϵ is everywhere negative. In conducting calculations of this type, it will be assumed that the average tangent modulus during each increment of rotation governs the increase in stress that occurs during that particular rotation and load increment.

It is to be noted that within the region "C," the stress will first increase according to the local tangent modulus and thereafter, decrease according to the elastic modulus.

Now the change in rotation and its effect on axial load, moment, and "C" for the Nth increment of rotation must be considered; it is shown in Fig. 5 as the difference between the strain distribution at increment N and at the preceding increment N-1. An appreciable variation in tangent modulus will be realized over the cross section of the strut. However, the increments of load and moment, during any particular rotation increment, can be closely approximated if the tangent modulus is determined by a single value that decreases with each successive rotational increment but is determined by the actual strain one-quarter of the distance (H-C) in from the concave side of the column. If the

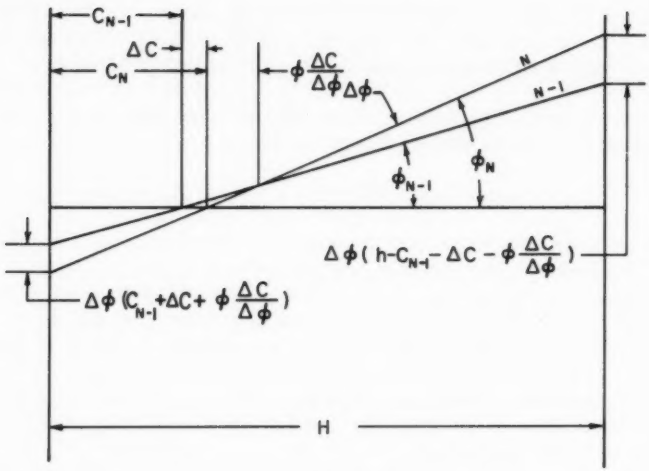

FIG. 5.—STRAIN INCREMENTS BETWEEN N-1 AND N EQUILIBRIUM POSITIONS

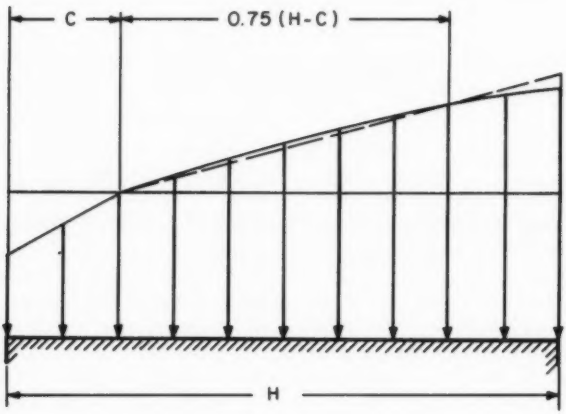

FIG. 6.—APPROXIMATION TO NON-LINEAR STRESS DISTRIBUTION

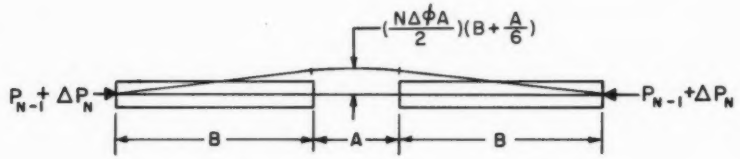

FIG. 7.—BENT EQUILIBRIUM CONFIGURATION

stress varied linearly throughout the increasing range, this would be the location at which the total force increment could be considered as concentrated, and this will give a close approximation for the nonlinear distribution that actually exists.

Thus, referring to Fig. 5, the strain that will be used as an index of the changing tangent modulus will be determined by

$$\epsilon_{N(AVG)} = \epsilon_T + 0.75\,(N - 0.5)\,(H - C_{N-1})\,\Delta\phi \quad \ldots\ldots \quad (8)$$

The actual strain distribution over the entire cross section will be assumed to vary linearly, and this index strain, given by Eq. 8, is merely for the purpose of evaluating a tangent modulus for which an assumed triangular distribution of increased compressive stress is assumed to represent satisfactorily the actual non-linear distribution of increased compressive stress for that particular load. The foregoing explanation is illustrated graphically in Fig. 6, which shows a possible stress distribution at a particular bent equilibrium position as a solid line. In the analysis, the curved solid line portion in the right portion of the stress distribution is replaced by the dashed-line which intersects the curved line at the location where the index strain has been determined.

Referring again to Fig. 5, the magnitude of loads, moment, and "C" will be determined after the Nth $\Delta\phi$ that is introduced as a result of bending that commences at the tangent modulus load. Thus,

$$P_N = P_{N-1} + (\Delta P)_N \quad \ldots\ldots\ldots\ldots \quad (9)$$

$$M_N = M_{N-1} + (\Delta M)_N \quad \ldots\ldots\ldots\ldots \quad (10)$$

and

$$C_N = C_{N-1} + (\Delta C)_N \quad \ldots\ldots\ldots\ldots \quad (11)$$

Each $\Delta\phi$ during a particular numeric step will be arbitrarily the same, thus ϕ_N may be considered as the independent variable in the solution of a particular equilibrium condition and

$$\phi_N = N\,\Delta\phi \quad \ldots\ldots\ldots\ldots\ldots\ldots \quad (12)$$

On the basis of the arbitrary rotation $\Delta\phi$, as shown in Fig. 5, the following equations may be written for ΔP_N and ΔM_N:

$$\Delta P_N = \frac{H\,\Delta\phi}{2}\left[(H-C_{N-1})^2\,E_{TN} - C_{N-1}^2\,E - 2N\left[(H-C_{N-1})\,E_{TN} + C_{N-1}\,E\right]\Delta C_N - N^2\,(E-E_{TN})\,\overline{\Delta C}_N^2\right] \quad \ldots\ldots\ldots \quad (13)$$

and

$$\Delta M_N = \frac{H\,\Delta\phi}{12}\left[(H-C_{N-1})^2\,(H+2\,C_{N-1})\,E_{TN} + C_{N-1}^2\,(3\,H-2\,C_{N-1})E\right.$$

$$+ 6N\,C_{N-1}\,(H-C_{N-1})\,(E-E_{TN})\,\Delta C_N + 3\,N^2\,(H-2\,C_{N-1})\,(E-E_{TN})\,\overline{\Delta C}_N^2$$

$$\left. - 2\,N^3\,(E-E_{TN})\,\overline{\Delta C}_N^3\right] \quad \ldots\ldots\ldots\ldots \quad (14)$$

In Eq. 13 values of C_{N-1} will have been determined in the preceding step, and E_{TN} will be determined in accordance with the index strain by Eq. 8. The same is true for Eq. 14. Thus, the only unknown quantity in Eqs. 13 and 14 is ΔC_N which appears in first, second and third powers. For very small values of N, when the strut just starts to bend, ΔC_N may be relatively large and, as bending proceeds, the quantity, $N\Delta C_N$, increases. It will be noted that in every term in which ΔC_N appears it is multiplied by N.

Eqs. 13 and 14 are combined into a single equation in terms of ΔC_N by means of the equilibrium equation for the Nth equilibrium position which may be written

$$(P_{N-1} + \Delta P_N)\left[\frac{N\,\Delta\phi\,A}{2}\left(B + \frac{A}{6}\right)\right] = M_{N-1} + \Delta M_N \quad \ldots\ldots \quad (15)$$

In Eq. 15 the quantity in brackets to the left of the equal sign is the maximum deflection at the center line of the column. The equilibrium condition that determines ΔC_N is also illustrated in Fig. 7.

RESULTS OF SIMULATED TESTS

Typical results of certain of the simulated tests conducted by means of the computer solution will now be presented and examined.

In the numerical example used in the simulated tests, dimension A (Fig. 3) was held constant at 2 in. and dimension H at 1 in. Thus, the reduced section has an area of 1 sq in., and the total strut load "P" is always identical with the average stress on the reduced section. Dimension B was varied in increments up to the value that would result in elastic buckling.

Stress Distribution.—The stress distributions across the breadth of the reduced section of the strut at increasing loads are shown in Figs. 8, 9, and 10, typical of short, intermediate, and long strut behavior. In Fig. 8 the space between each of the stress distribution lines covers ten different equilibrium evaluations at successively increasing loads. Thus, the $\Delta\phi$ used in the determinations of Fig. 8 was 0.00001 radians, whereas the plotted lines are for a $\Delta\phi$ of 0.0001 radians. As an indication of the fact that $\Delta\phi$ was taken sufficiently small in the computer input, the following tabulation shows results for L = 43

in. for various $\Delta\phi$'s:

$\Delta\phi$	Calculated maximum or Shanley load, in kips per square inch
0.000002	39.4570
0.000005	39.4566
0.000010	39.4557

It is obvious that in the range of $\Delta\phi$'s that were actually used in determining maximum loads the cited value of 0.00001 gave satisfactory accuracy.

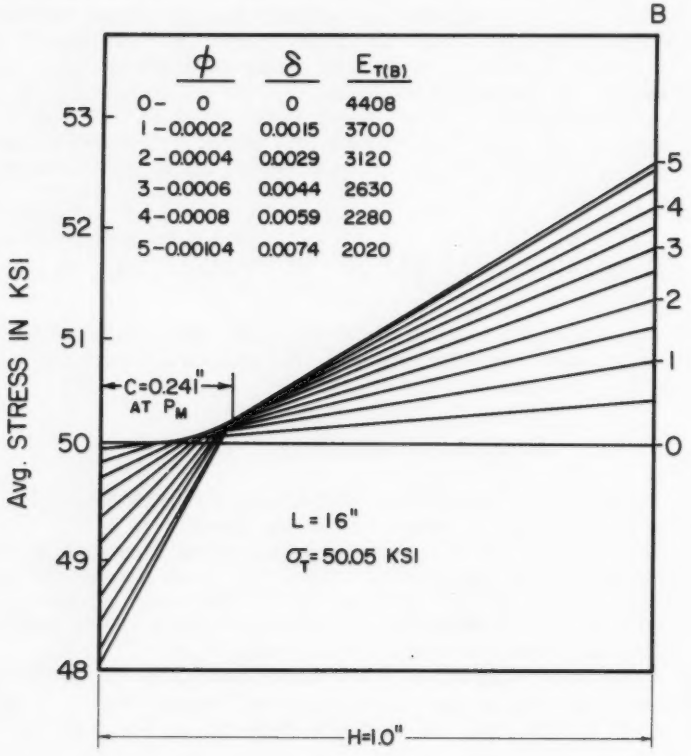

FIG. 8.—STRESS DISTRIBUTIONS $\sigma_T < \sigma < \sigma_M$ L = 16"

Referring again to Fig. 8, the gradual inward movement of C is noted, reaching a maximum of 0.241 in. at P_m (the Shanley load). There is a marked reduction in the index tangent modulus E_T. This demonstrates the necessity of considering the progressive change in tangent modulus as bending proceeds above the tangent modulus load. Also to be noted is the very small deflection in comparison with the column length at which the Shanley load is reached. The

maximum lateral deflection for this strut at the maximum load is less than one thousandth of the length of the strut. Although the constriction in the chosen model tends to accentuate these effects, the model is most nearly similar to an actual column in the short length range where the effects are most pronounced.

Fig. 9 presents the simulated test stress distributions for an intermediate length of a strut. The inward extent of region C is greater than in Fig. 8. The

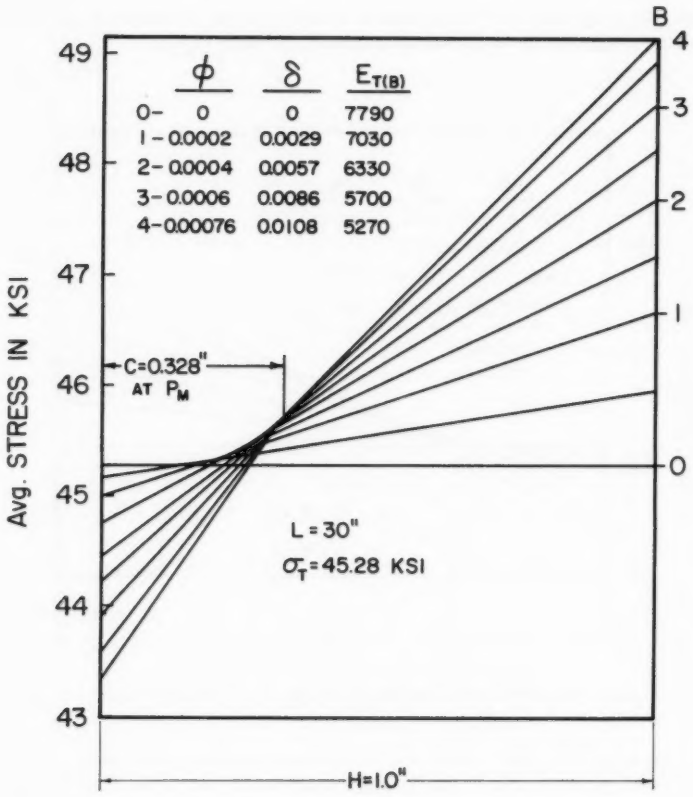

FIG. 9.—STRESS DISTRIBUTIONS $\sigma_T < \sigma < \sigma_M$ L = 30"

maximum deflection is considerably greater than for Fig. 8 at the maximum load but is still less than one thousandth of the strut length. The variation of E_T during bending above the tangent modulus load is large, but not so large as in the shorter strut.

Fig. 10 is for a relatively long strut that buckles just above the proportional limit. The tangent modulus at this load is nearly the same as for the elastic range. It is to be noted that the maximum extent of C at maximum load is more

than 80% of the way into the center of the column and that the deflection at maximum load is less in proportion to the length of the column than in the previous case. Obviously, in the elastic range there will be no load increment, as buckling will occur at constant load, and C will not move inward gradually but will be 0.5 at all times.

Load Deflection Curves.—Fig. 11 shows typical load versus lateral deflection curves plotted from the tangent modulus load out to the maximum or Shanley load for eight simulated tests of different strut lengths. The dashed line shows the limit of lateral deflections out to the maximum load. The deflection is zero at the proportional limit, below which elastic buckling will occur, and increases to a maximum in the intermediate column range.

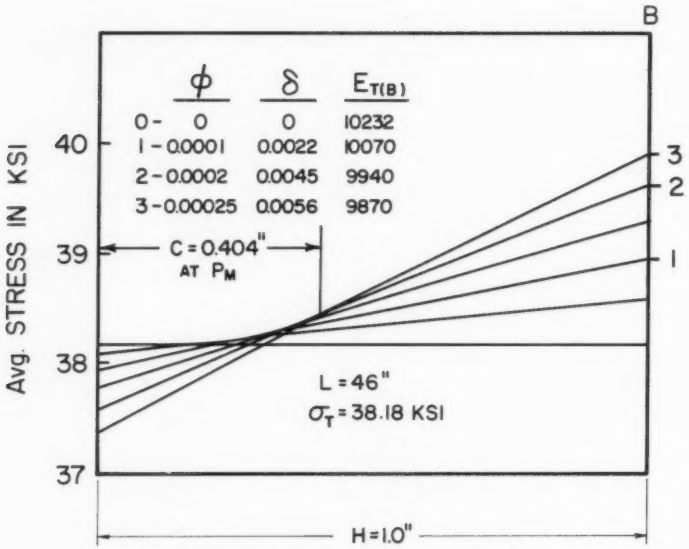

FIG. 10.—STRESS DISTRIBUTIONS $\sigma_T < \sigma < \sigma_M$ L = 46"

For a particular length L = 30 in., simulated tests were made in which the strut was held straight above the tangent modulus to various stress levels and then permitted to start bending. Results are shown in Fig. 12. The suggestion for this type of test dates from von Kármán's discussion of the second Shanley paper[2] in which, referring to the tangent modulus and reduced modulus loads, von Kármán stated

> ". . . One can construct sequences of equilibrium positions starting from any load between the two limiting values corresponding to the tangent modulus and the reduced moduli. The inclination of the equilibrium lines representing the load as a function of the deflection is steepest for the line starting from the lower limiting load and becomes zero for the line starting from the upper limiting load (i.e. the reduced modulus load).

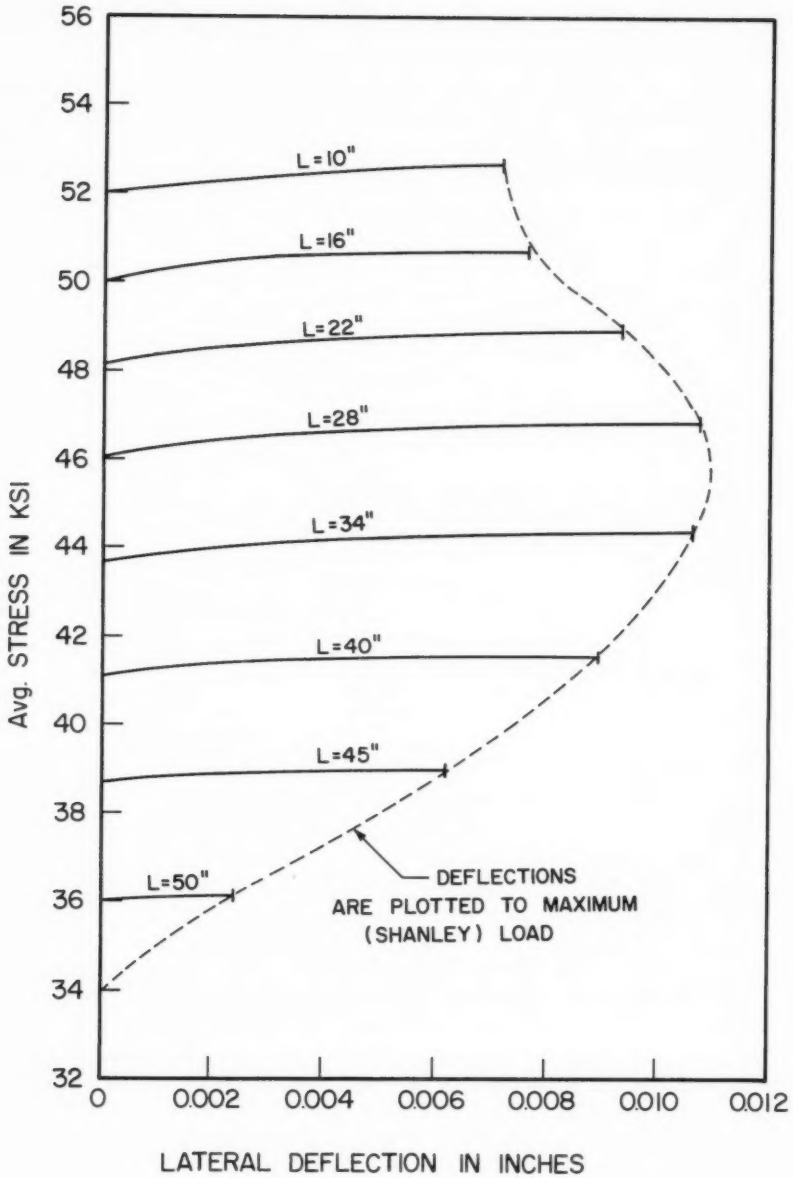

FIG. 11.—LATERAL DEFLECTION VS. AXIAL LOAD FOR VARIOUS LENGTH STRUTS

Equilibrium lines have an evelope that starts from the lower limiting load and--at least as long as the stress strain curve can be considered straight and the deflection small-approaches asymptotically the load computed with the reduced modulus."

The foregoing comment accurately describes the initial portion of the load deflection curves shown in Fig. 12. However, for the typical stress-strain curve used in this study, it is obvious that the comments regarding the asymptotic approach to the reduced modulus load have no real validity even though they

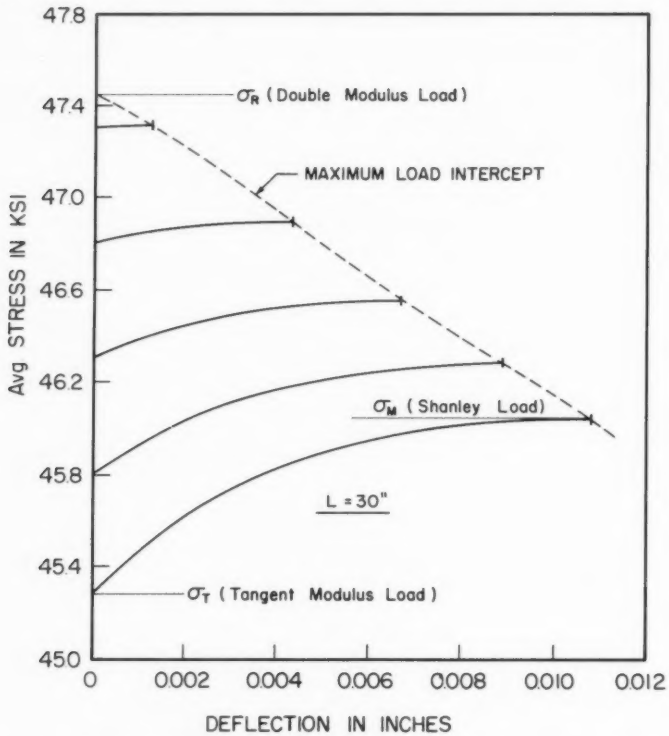

FIG. 12.—LATERAL DEFLECTION VERSUS AXIAL LOAD WITH STRUT HELD STRAIGHT TO VARIOUS STRESSES ABOVE TANGENT MODULUS LOAD

are correct for the assumption that the stress-strain curve would be straight above the tangent modulus load. If the stress-strain curve were straight, of course, such a fictitious reduced modulus load in the present case would be much greater than as calculated, as shown, at approximately 47.4 ksi. At 47.4 ksi the tangent modulus that determines the correct reduced modulus has substantially decreased from the tangent modulus at the tangent modulus load of about 45.3 ksi. But the slightest deviation from straightness has a marked effect on inelastic behavior.

To demonstrate the different load-deflection behavior that results when the stress-strain curve remains straight above the tangent modulus $(E_T = \text{const.})$ load, Fig. 13 should be compared with Fig. 12. In Fig. 13 the curve of Fig. 12

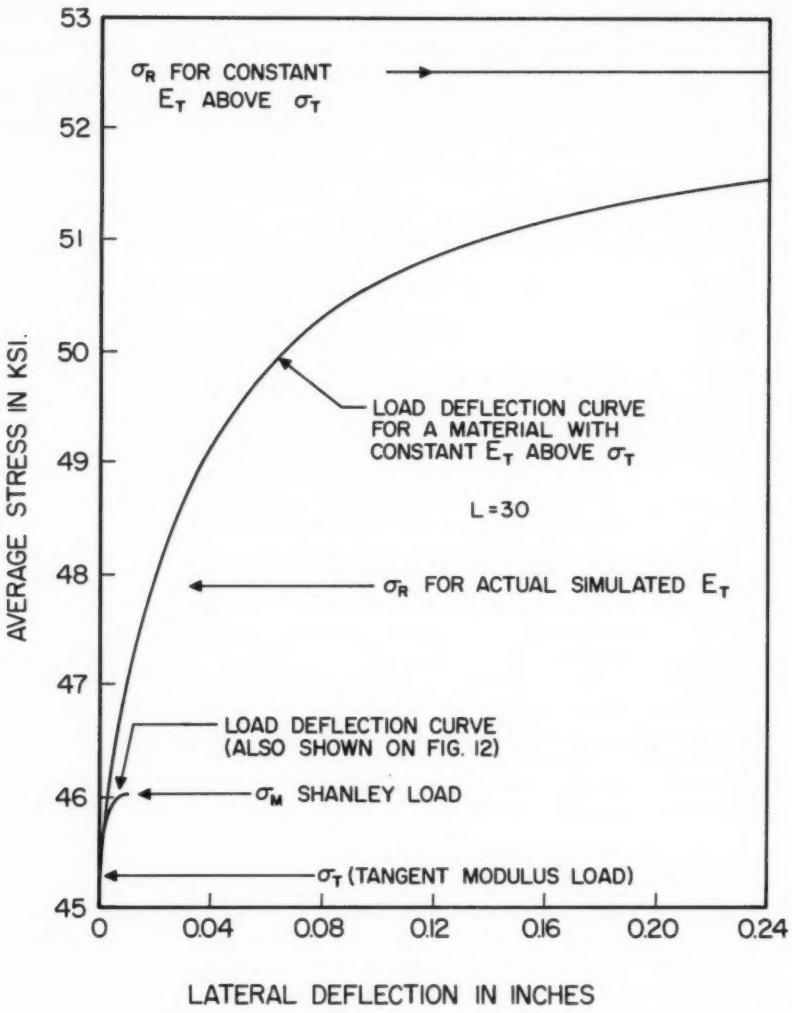

FIG. 13.—LATERAL DEFLECTION VERSUS AXIAL LOAD FOR ASSUMPTION OF CONSTANT E_T ABOVE σ_T

that determines the maximum (Shanley) load (bending initiated at σ_T) is redrawn to a new scale. The pseudo σ_R based on E_T at the tangent modulus load is indicated and is seen to be greatly in error and much too large. Although not shown herein, this error progressively increases as the strut is made

shorter. The great difference between behavior assuming constant E_T and predicted actual behavior leading to the Shanley load is graphically demonstrated. Whereas, with constant E_T, the lateral deflection and corresponding column load would both theoretically increase as much as the geometric limitations permit, the actual load differs but little from the tangent modulus load, and the Shanley load is reached at extremely small lateral deflection.

Column Strength Curve.—Fig. 14 shows the curve of strut length versus average stress (or load) at the various critical loads for the buckling model. These include the reduced modulus load, the maximum or Shanley load, and the tangent modulus load. Also, for comparative purposes, the reduced modulus

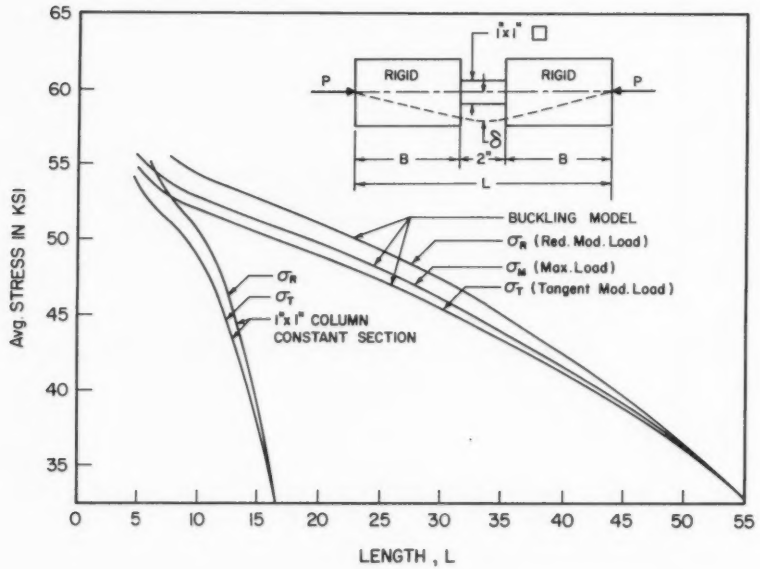

FIG. 14.—"COLUMN" - STRENGTH CURVES

load and tangent modulus load are given for a 1 in. by 1 in. column of constant section. The curves tend to join, as they should, at small lengths. Although the maximum or Shanley load is closer to the tangent modulus load than the reduced modulus load, no particular conclusion can be drawn from this relation because these simulated tests pertain to one particular material. The effort has not been so much to draw general conclusions, but rather to develop improved understanding of what actually occurs above the tangent modulus load.

SUMMARY

Although the simulated tests described herein have pertained to an inelastic buckling model with rigid bars adjacent to the center bending portion, it would

be possible with minor changes in the computer program to simulate somewhat more nearly actual column behavior by some arbitrary assumption as to the distribution of $M/(E\,I)$ along the column. This was not done because it was considered better to present a closely approximate solution of the model examined herein rather than an incorrect solution of a more realistic representation of a column. However, the present work is simply one step along the way toward the projected solution of columns with variable cross section in the inelastic range with correct evaluation of the buckled shape at the various load levels above the tangent modulus load. In such a study, errors in any assumed deflection configuration would be reduced by an iterative procedure making use of Newmark's[9] numerical method as adapted to inelastic buckling.

It has been the aim of the present paper simply to improve understanding of buckling behavior in the inelastic range and to clarify some concepts that relate to Shanley's important contributions. On the basis of the simulated tests conducted in this study and described herein the following statements may be made. These statements are restricted to a material for which $\frac{d^2\sigma}{d\epsilon^2}$ is continuous and negative above the proportional limit.

1. The inward movement of the termination point of strain regression from the convex side of the column, immediately above the tangent modulus load, as predicted by Shanley[2] in his Fig. 7, has been reproduced quantitatively for a specific aluminum alloy within a localized rectangular cross sectional constriction in an otherwise rigid strut.
2. The procedure is simple in concept, and the computer program can be adapted with minor alterations to any other stress-strain diagram or diagrams for which suitable mathematical expressions may be written.
3. The procedure presented herein is projected as the initial step toward the accurate evaluation of maximum inelastic buckling loads for columns of variable cross-section and arbitrary stress-strain properties.
4. In determining inelastic buckling equilibrium configurations and maximum loads above the tangent modulus load in members made of aluminum alloy, it is essential to consider the continuing decrease of tangent modulus in the region of increasing compressive stress.
5. The assumption of bilinear elasticity as an approximation of inelastic stress-strain properties may in some instances lead to grossly erroneous results if inelastic stability is involved in the case of a material such as structural aluminum alloy.
6. If a column is constrained to remain straight in the inelastic range, above the tangent modulus load, it will reach a maximum load that is greater than the Shanley load and less than the reduced modulus load. The deflection at the maximum load will be progressively less as the reduced modulus load is approached.
7. The maximum or Shanley load for an ideal column of a typical structural aluminum alloy in the inelastic range is reached at relatively small deflections relative to the column breadth.
8. Further validation is given to the significance of the tangent modulus load as a proper basis for the evaluation of column design formulas and the double

or reduced modulus load is seen to be of no practical significance for materials typified by the stress-strain curve for structural aluminum alloy used herein.

ACKNOWLEDGMENTS

The repeated solutions of the cubic equation in ΔC that results from the combination of Eqs. 13, 14, and 15 in successive equilibrium steps was carried out with the aid of the IBM 704 computer at the University of Michigan, Ann Arbor, Mich., utilizing MAD (Michigan Algorithm Decoder) programming. The work of programming and the conducting of all details of the actual numeric solution were handled by Rafi Hariri, a graduate student at the University of Michigan. The assistance of the Industry Program of the College of Engineering, University of Michigan, in the preparation of the drawings, is gratefully acknowledged.

APPENDIX.—NOTATION

The symbols adopted for use in this paper are listed here for convenience of reference and for the aid of discussers:

A = length of reduced section in buckling model;

B = length of rigid segment of model;

C_N = distance from convex face of bent segment to location where strain is neither increasing or decreasing with increasing load, at Nth equilibrium position;

E = elastic stress-strain modulus;

E_R = reduced modulus;

E_T = tangent modulus;

E_{TN} = effective tangent modulus near the concave side of the bent strut at the Nth increment of load during bending;

H = breadth of reduced section in buckling model;

M_N = maximum bending moment in bent segment at Nth increment of load during bending;

N = subscript integer denoting a particular load increment;

P_N = external column load on strut after Nth load increment during bending;

R = radius of gyration;

ΔC_N = increment of C_N during Nth load increment;

ΔM_N = Nth increment of bending moment;

ΔP_N = Nth increment of load during bending;

$\Delta\sigma_{RN}$ = increment of elastic stress regression at convex face during Nth load increment;

$\Delta\sigma_N$ = increment of stress increase at concave face during Nth increment of load;

$\Delta\phi$ = arbitrary increment of unit rotation;

δ = maximum deflection of strut centerline;

ϵ = normal strain;

ϵ_T = compressive strain at tangent modulus load;

σ = normal stress;

σ_C = critical stress;

σ_R = compressive stress at reduced modulus load; and

σ_T = compressive stress at tangent modulus load.

Journal of the
ENGINEERING MECHANICS DIVISION
Proceedings of the American Society of Civil Engineers

STABILITY IN A CONTINUOUSLY STRATIFIED FLUID

By Philip G. Drazin,[1] and Louis N. Howard[2]

SYNOPSIS

Techniques previously used by the writers for the study of stability in a homogeneous flow are applied to problems with density stratification. Results are restricted to instabilities of large wavelength but are given in a fairly explicit form. The effect of small density stratification in modifying the different types of instability of parallel flows of the shear-layer and jet types is considered, and simple approximate formulas for the long-wave stability characteristics are given.

INTRODUCTION

The stability of a two-dimensional horizontal parallel flow of a stratified inviscid fluid under gravity depends principally on three factors: The basic velocity field, the basic density field, and the presence of boundaries. The density field also enters the problem in two different ways, through its effect on the inertia of the fluid and through the buoyancy force. Because emphasis, herein, is on the velocity and density fields it will be assumed that the flow field is infinite and no boundaries are present. In addition, for simplicity, the effect of density variation on the inertia of the fluid will be neglected. This effect is a good approximation if the total change of density is small compared

Note.—Discussion open until May 1, 1962. To extend the closing date one month, a written request must be filed with the Executive Secretary, ASCE. This paper is part of the copyrighted Journal of the Engineering Mechanics Division, Proceedings of the American Society of Civil Engineers, Vol. 87, No. EM6, December, 1961.

[1] Dept. of Math., The Univ., Bristol, England, formerly Meteorology Dept., Massachusetts Inst. of Tech., Cambridge, Mass.

[2] Math. Dept., Massachusetts Inst. of Tech., Cambridge, Mass.

with the mean density, frequently the most interesting case physically. The methods presented here, however, can also be used without this approximation, at the expense of somewhat more complicated formulas.

The majority of the studies of stability in a stratified flow that have been made since the first extensive investigations in this field[3,4] have dealt with specific velocity and density fields. Taylor, in 1931, examined[3] the case of a shear flow with constant velocity gradient in a fluid with exponential density field, occupying a half-plane. This example was chosen in an attempt to model the stabilizing effect of cooling at the ground in the evening on wind-induced turbulence in the atmosphere. He found that there were no wave-like perturbations, either stable or unstable, when the Richardson number lies between 0 and 1/4. The Richardson number is defined as

$$J = - g \rho' \rho^{-1} (w')^{-2} \quad \ldots\ldots\ldots\ldots\ldots (1)$$

in which ρ and w are the basic density and velocity fields, and J is constant in the present case. When the Richardson number exceeds 1/4, only neutrally stable progressive waves are found, but he did not exclude the possibility of damped or self-excited waves. However, subsequent studies of this flow from the point of view of an initial value problem[5,6,7] have shown that it is stable for all $J \geq 0$, although neutrally stable waves do not exist for $0 \leq J < 1/4$, as found by Taylor.[3] This flow is unstable for $J < 0$, as is to be expected because this corresponds to density increasing upward.

Goldstein, in 1931, examined[4] a somewhat similar flow, in which w' and ρ'/ρ were constant in a finite interval, and zero outside it, w and ρ being continuous. This is a model for studying the stabilizing effect of a density gradient on a shear layer between two uniform streams. He found stability for $J > 1/4$, instability for $J < 1/4$, in which the value of J is determined by the density and velocity gradients in the shear layer. Note that this differs from the flow studied by Taylor, Eliassen, and Case in being actually unstable for $0 < J < 1/4$. Presumably, the fact that the density is constant outside the finite shear layer in Goldstein's case, but everywhere decreasing upward in Taylor's, is associated with the greater stability of the latter case.

Taylor and Goldstein also considered several examples of flows with constant shear, with layers of different constant densities. Other studies have considered various flows with piecewise constant velocity and density fields. Several examples of this sort are available.[8]

---

3 "Effect of Variation in Density on the Stability of Superposed Streams of Fluids," by G. I. Taylor, Proceedings, Royal Soc. of London, Series A, Vol. 132, 1932, p. 499.

4 "On the Stability of Superposed Streams of Fluids of Different Densities," by S. Goldstein, Proceedings, Royal Soc. of London, Series A, Vol. 132, 1932, p. 524.

5 "Two-Dimensional Perturbations of a Flow with Constant Shear of a Stratified Fluid," by Eliassen, et al., Inst. for Weather and Climate Research, Norwegian Academy of Science and Letters, Publication No. 1, 1953.

6 "Stability of an Idealized Atmosphere. I. Discussion of Results," by K. M. Case, Physics of Fluids, Vol. 13, March, April, 1960, p. 149.

7 Prik. Mat. Mech., L. A. Dikii, Vol. 24, No. 2, 1960, p. 240. English translation PMM, p. 357.

8 "Physikalische Hydronamik," by Bjerknes, Bjerknes, Solberg, and Bergeron, Springer, 1933.

An example of a flow with a smooth shear layer velocity profile was given by J. Drazin in 1958.[9] He studied the case

$$w = V \tanh \frac{y}{d} \quad \ldots\ldots\ldots\ldots\ldots\ldots (2)$$

constant ($-\infty < y < \infty$) and found that with

$$J = - g \rho' \rho^{-1} d^2 V^{-2} \quad \ldots\ldots\ldots\ldots\ldots\ldots (3)$$

(which is the minimum value of the local Richardson number

$$J(y) = - g \rho' \rho^{-1} (w')^{-2}) \quad \ldots\ldots\ldots\ldots\ldots\ldots (4)$$

the flow was stable for $J > 1/4$, unstable for some wavelengths for $0 < J < 1/4$. Specifically, he found neutrally stable waves of wavelength $2 \pi \alpha^{-1} d$ if $J = \alpha^2 (1 - \alpha^2)$.

J. W. Miles has unified this picture somewhat by proving[10] in general, for a flow with $w' < 0$ throughout, that if $J(y)$ is defined by Eq. 4 then a sufficient condition for stability is $J(y) > 1/4$ everywhere. The condition is not, however, necessary. This result is to be published.[10,11] Miles has emphasized a difficulty in the interpretation of many studies of this kind. This is that attention has sometimes been restricted to neutrally stable oscillations without sufficient study of the relation of these to actual instability. Thus, although in many cases a neutrally stable wave motion is adjacent to an unstable one, that is, it gives a point on the boundary between stable and unstable regions, this is not necessarily always the case. One need only recall the case of a density distribution decreasing upward, with no basic flow at all, where there are many neutrally stable oscillations (internal waves) and no unstable ones, to realize the importance of this objection and the consequent importance of the study of truly unstable waves.

In the present investigation the problem will be approached as follows: First, as mentioned previously, the effect of boundaries is suppressed by considering an infinite fluid; second, an attempt will be made to obtain results without assuming a specific form for the velocity and density fields, although it will always be assumed that the density is statically stable, that is, it is decreasing upwards. Third, there will be particular interest in actually unstable motions. In this connection the writers' point of view is to regard results for flows of a stratified fluid more as modifications of the stability characteristics of a homogeneous flow caused by the presence of density variation, than as modifications of internal waves in a stratified fluid at rest caused by the presence of a velocity field. Both points of view are of course legitimate as ways of relating results on inhomogeneous stability to more familiar situations, but the former tends to emphasize the possibilities for instability. This point of view is encouraged by the nature of the mathematical technique to be used,

---

9 "Fluid Mechanics," J. Drazin, No. 214, 1958.

10 "On the Stability of Homogeneous Shear Flows," by J. W. Miles, Journal of Fluid Mechanics, Vol. 11, 1961.

11 "Note on a Paper of John W. Miles," by L. N. Howard, Journal of Fluid Mechanics, Vol. 11, 1961.

which is a modification of methods used by the writers for the study of homogeneous stability problems.

Finally, attention will be restricted to the stability characteristics of long waves. This restriction is at the same time the key to this mathematical technique and the principal limitation on its results. It appears likely, however, that some such restriction is necessary if results are to be obtained for flows with more or less arbitrary density and velocity profiles. There is good reason to believe that some features of stability problems depend very sensitively on the details of the basic velocity and density profiles; this does not seem to be the case in the long wave region. It should perhaps be stated explicitly that all the results, like most other theoretical results in this field, are subject to the basic limitations of linearized inviscid stability theory. In particular, the possibility that some flows may be stable to infinitesimal perturbations but unstable to finite ones, or vice versa, cannot be examined.

MATHEMATICAL FORMULATION OF THE PROBLEM

The usual approach in stability problems of examining the growth properties of infinitesimal wave-like perturbations, by assuming a perturbation stream function of the form $\phi(y) \exp i\alpha(x - ct)$. Here y is the vertical coordinate, taken positive upwards, x the horizontal coordinate, α the wave number of the disturbance, c the complex wave speed. The flow is unstable to waves of length $2\frac{\pi}{\alpha}$ if the imaginary part of c is positive. The basic undisturbed flow is horizontal with velocity w(y) in the positive x direction and the basic density field is $\rho(y)$. The differential equation for ϕ is derived in most of the papers referred to[9] previously. Setting $W = w - c$ the differential equation can be written

$$\left[\rho W^2 \left(\frac{\phi}{W}\right)'\right]' - \alpha^2 \rho W^2 \left(\frac{\phi}{W}\right) - g\rho' \left(\frac{\phi}{W}\right) = 0 \quad \ldots\ldots (5)$$

The boundary conditions are that $\phi \to 0$ as $y \to \pm\infty$. The function $\frac{\phi}{W}$ has a simple physical interpretation, as has been pointed out by Miles. It can be regarded as the amplitude of the displacement, due to the perturbation, of the streamline which, in the undisturbed state, is at y. If the effect of density variation on the inertia of the fluid is neglected, Eq. 5 becomes

$$\left[W^2 \left(\frac{\phi}{W}\right)'\right]' - \alpha^2 W^2 \left(\frac{\phi}{W}\right) - \frac{g\rho'}{\rho} \left(\frac{\phi}{W}\right) = 0 \quad \ldots\ldots\ldots (6)$$

The following assumptions will be made concerning the velocity and density fields:

1. The velocity field, w, approaches finite limits as $y \to \pm\infty$. If these limits are the same, they may be taken to be zero by changing to a coordinate system moving with this common velocity. This is referred to as a "jet-type" velocity profile. If the limits are different it can be assumed that they are negatives of each other, by changing to a coordinate system moving with average velocity of the limits. This is denoted as a profile of "shear-layer" type. Typical jet and shear layer velocity profiles are shown in Fig. 1.

2. It is assumed that ρ is monotonically decreasing upwards and approaches finite limits as $y \to \pm \infty$. To be consistent with the use of Eq. 6 instead of Eq. 5, we also suppose that $\rho(-\infty) - \rho(+\infty)$ is small compared to $\rho(-\infty) + \rho(+\infty)$. A typical density profile is shown in Fig. 2.

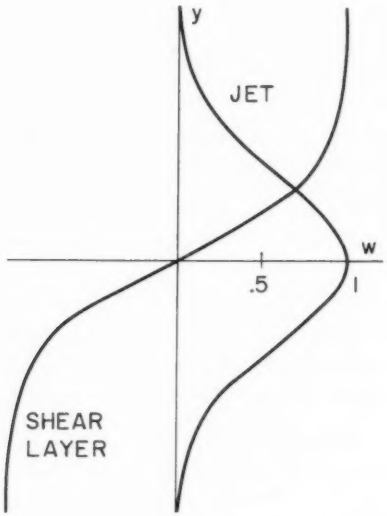

FIG. 1.—TYPICAL VELOCITY PROFILES

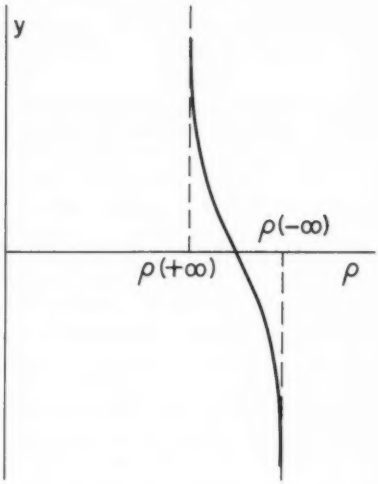

FIG. 2.—TYPICAL DENSITY PROFILE

L and V will be typical length and speed scales of the velocity profile and will be used to define dimensionless length, velocity, and time variables in the obvious way. Then in dimensionless terms, Eq. 6 becomes

$$\left[W^2 \left(\frac{\phi}{W}\right)' \right]' - \alpha^2 W^2 \left(\frac{\phi}{W}\right) + J \lambda' \left(\frac{\phi}{W}\right) = 0 \quad \ldots\ldots\ldots (7)$$

in which W, ϕ, α, y, and so on now refer to the dimensionless variables, and in which

$$\lambda(y) = \frac{\ln\left(\frac{\rho(-\infty)}{\rho(y)}\right) + \ln\left(\frac{\rho(+\infty)}{\rho(y)}\right)}{\ln\left(\frac{\rho(-\infty)}{\rho(+\infty)}\right)} \quad \ldots\ldots\ldots\ldots (8a)$$

and

$$J = \frac{1}{2} g \ln\left(\frac{\rho(-\infty)}{\rho(+\infty)}\right) \frac{L}{V^2} \quad \ldots\ldots\ldots\ldots\ldots (9a)$$

Assuming a relatively small total change of ρ, Eqs. 8a and 9a are approximately

$$\lambda(y) = \frac{\rho(-\infty) + \rho(+\infty) - 2\,\rho(y)}{\rho(-\infty) - \rho(+\infty)} \quad \ldots\ldots\ldots\ldots (8b)$$

and

$$J = g\,\frac{L}{V^2}\,\frac{\rho(-\infty) - \rho(+\infty)}{\rho(-\infty) + \rho(+\infty)} \quad \ldots\ldots\ldots\ldots\ldots (9b)$$

giving a somewhat more familiar form of the Richardson number, J. It should be noted that $\lambda(\pm\infty) = \pm 1$. The relation of this over-all Richardson number J and the local $J(y) = -g\,\rho'\,\rho^{-1}(w')^{-2}$ is, in terms of the present notation,

$$J(y) = J\left[L\,\lambda'(y)\right]\left[L\,V^{-1}\,w'\right]^{-2} \quad \ldots\ldots\ldots\ldots (10)$$

SKETCH OF METHOD OF SOLUTION

The mathematical problem is the determination of the conditions under which Eq. 7 has a non-trivial solution that approaches zero at $\pm\infty$. Such a solution will usually be possible only if c and α are properly related. The approach to finding this "eigenvalue relation" between c and α is first to find, essentially by means of an expansion in powers of α for fixed c, a solution ϕ_1 that satisfies the boundary condition $\phi_1(-\infty) = 0$. Similarly, ϕ_2 is found with $\phi_2(+\infty) = 0$. If now c is to have the correct value for each α to give an eigenfunction ϕ, K_1, $\phi_1 = \phi = K_2\,\phi_2$ for some constants K_1 and K_2, so that

$$K_1\,\phi_1(0) = K_2\,\phi_2(0) \quad \ldots\ldots\ldots\ldots\ldots (11a)$$

and

$$K_1\,\phi_1'(0) = K_2\,\phi_2'(0) \quad \ldots\ldots\ldots\ldots\ldots (11b)$$

Because ϕ is not identically zero, K_1 and K_2 cannot be zero and, therefore,

$$\phi_1(0)\,\phi'_2(0) = \phi_2(0)\,\phi_1'(0) \quad \ldots\ldots\ldots\ldots\ldots (12)$$

ϕ_1 and ϕ_2, of course, depend on α and c, and this condition then yields the eigenvalue relation. The problem is, thus, reduced to finding some representation for the functions ϕ_1 and ϕ_2. As $y \to -\infty$, the differential Eq. 7 becomes

$$\left(\frac{\phi}{W}\right)'' - \alpha^2\left(\frac{\phi}{W}\right) = 0 \quad \ldots\ldots\ldots\ldots\ldots (13)$$

because it has been assumed that $w \to$ constant and $\lambda' \to 0$. Thus, for $y \to -\infty$ the asymptotic form of the solution ϕ_1, which goes to zero at $-\infty$, can be taken to be $\rho_1 \sim e^{\alpha y}$. This shows that an attempt cannot be made to find ϕ_1 by a power series in α, because the convergence of the series must become increasingly worse as $y \to -\infty$. However, it turns out that such a power series can be used if the exponential factor is first split off by setting

$$\phi_1 = e^{\alpha\,y}\,\theta \quad \ldots\ldots\ldots\ldots\ldots (14)$$

and then expands θ. Similarly, ϕ_2 is found by setting

$$\phi_2 = e^{-\alpha y} \chi \quad \ldots\ldots\ldots\ldots\ldots\ldots (15)$$

and expanding χ in powers of α. In this way a representation of ϕ_1 is obtained which is valid except near $y = +\infty$ and a representation of ϕ_2 valid except near $y = -\infty$. It is because of the form of these representations that the eigenvalue relation is obtained by using the two functions and matching them in the middle at, for example, $y = 0$, rather than, for instance, trying to make ϕ_1 zero at $+\infty$. The representation of ϕ_1 fails to be usable at $+\infty$.

In the present problem, we must also deal with the term involving J. As mentioned in the introduction, our point of view in this paper is to look at the problem as a modification due to density variation of the homogeneous stability problem and, consequently, we regard J as small and actually find θ and χ in the form of double series in power of α and J, settling, for instance,

$$\theta = \theta_{00} + \alpha\,\theta_{10} + J\,\theta_{01} + \alpha^2\,\theta_{20} + \alpha\,J\,\theta_{11} + J^2\,\theta_{02} + \ldots (16)$$

Introducing θ and χ instead of ϕ in Eq. 7, expanding in powers of α and J, and using the normalizations $\theta/W \to 1$ as $y \to -\infty$ and $\chi/W \to 1$ as $y \to +\infty$, the following results are obtained:

$$\left[W_\infty = W(\infty)\ ,\ W_{-\infty} = W(-\infty)\right] \quad \ldots\ldots\ldots\ldots (17a)$$

$$\frac{\theta_{00}}{W} = 1 \quad \ldots\ldots\ldots\ldots\ldots\ldots (17b)$$

$$\frac{\theta_{10}}{W} = -\int_{-\infty}^{y} \left(1 - \frac{W_{-\infty}^2}{W^2}\right) dy' \quad \ldots\ldots\ldots\ldots (17c)$$

$$\frac{\theta_{01}}{W} = -\int_{-\infty}^{y} \frac{1+\lambda}{W^2}\, dy' \quad \ldots\ldots\ldots\ldots\ldots (17d)$$

$$\frac{\theta_{20}}{W} = \int_{-\infty}^{y} \frac{dy'}{W^2} \int_{-\infty}^{y'} \left(W^2 - W_{-\infty}^2\right) dy'' + \int_{-\infty}^{y} dy' \int_{-\infty}^{y'} \left(1 - \frac{W_{-\infty}^2}{W^2}\right) dy'' \quad \ldots (17e)$$

$$\frac{\theta_{11}}{W} = \int_{-\infty}^{y} \left(1 - \frac{W_{-\infty}^2}{W^2}\right) dy' \cdot \int_{-\infty}^{y} \frac{1+\lambda}{W^2}\, dy''$$

$$+ 2 \int_{-\infty}^{y} \frac{W_{-\infty}^2}{W^2}\, dy' \int_{-\infty}^{y'} \frac{1+\lambda}{W^2}\, dy'' \quad \ldots\ldots\ldots\ldots (17f)$$

$$\frac{\theta_{02}}{W} = -\int_{-\infty}^{y} \frac{dy'}{W^2} \int_{-\infty}^{y'} \frac{(1+\lambda)^2}{W^2}\, dy''$$

$$+ \int_{-\infty}^{y} \frac{(1+\lambda)dy'}{W^2} \int_{-\infty}^{y'} \frac{(1+\lambda)dy''}{W^2} \quad \ldots\ldots\ldots (17g)$$

$$\frac{\chi_{00}}{W} = 1 \quad \ldots\ldots\ldots\ldots\ldots\ldots (17h)$$

$$\frac{\chi_{10}}{W} = -\int_{y}^{\infty} \left(1 - \frac{W_\infty^2}{W^2}\right) dy' \quad \ldots\ldots\ldots\ldots (17i)$$

$$\frac{\chi_{01}}{W} = -\int_{y}^{\infty} \frac{1-\lambda}{W^2}\, dy' \quad \ldots\ldots\ldots\ldots (17j)$$

$$\frac{\chi_{20}}{W} = \int_{y}^{\infty} dy' \int_{y'}^{\infty} \left(1 - \frac{W_\infty^2}{W^2}\right) dy'' + \int_{y}^{\infty} \frac{dy'}{W^2} \int_{y'}^{\infty} \left(W^2 - W_\infty^2\right) dy'' \quad \ldots (17k)$$

$$\frac{\chi_{11}}{W} = \int_{y}^{\infty} \left(1 - \frac{W_\infty^2}{W^2}\right) dy' \cdot \int_{y}^{\infty} \frac{1-\lambda}{W^2}\, dy''$$

$$+ 2 \int_{y}^{\infty} \frac{W_\infty^2}{W^2}\, dy' \int_{y'}^{\infty} \frac{1-\lambda}{W^2}\, dy'' \quad \ldots\ldots\ldots (17m)$$

and

$$\frac{\chi_{02}}{W} = -\int_{y}^{\infty} \frac{dy'}{W^2} \int_{y'}^{\infty} \frac{(1-\lambda)^2}{W^2}\, dy'' + \int_{y}^{\infty} \frac{(1-\lambda)dy'}{W^2} \int_{y'}^{\infty} \frac{1-\lambda}{W^2}\, dy'' \quad \ldots (17n)$$

If these equations are now used in Eq. 12, the terms up to the second order in α and J are written down explicitly, the eigenvalue relation

$$\alpha \left[W_\infty^2 + W_{-\infty}^2\right] - 2J + \int_{-\infty}^{\infty} \left[\alpha\left(W^2 - W_\infty^2\right)\right.$$

$$\left. + J(1-\lambda)\right] \left[\alpha\left(W^2 - W_{-\infty}^2\right) + J(1+\lambda)\right] \frac{dy}{W^2} + \ldots\ldots = 0 \quad \ldots (18)$$

Notice that this is in a relatively explicit form in that it involves only integrals of functions which are completely known (in terms of the functions λ and w) except for the constant c.

COMPARISON WITH FAMILIAR RESULTS

The simplest example of a non-homogeneous stability problem is probably that of the stability of the interface between two parallel uniform streams of

different densities. The solution of this problem dates from the work of Helmholtz[12] and the eigenvalue relation in the ordinary dimensional form is:

$$c^2 = \frac{g}{\alpha}\frac{\rho(-\infty) - \rho(+\infty)}{\rho(-\infty) + \rho(+\infty)} - \frac{\rho(-\infty)\,\rho(+\infty)}{\left[\rho(-\infty) + \rho(+\infty)\right]^2}\left[w(\infty) - w(-\infty)\right]^2 \quad \ldots (19)$$

or, in terms of the dimensionless variables introduced previously, and assuming that the change of density is relatively small,

$$c^2 = \frac{J}{\alpha} - 1 \quad \ldots (20)$$

This case does not strictly fit into the scheme used because it has been assumed that the density field is differentiable. However, because the final formula, Eq. 18, does not involve derivatives of λ it is of interest to try it on this problem. In fact, Eq. 18 succeeds completely; it yields

$$w = \lambda = \mathrm{sgn}(y) \quad \ldots (21)$$

so that the second order terms vanish, and

$$W_\infty^2 + W_{-\infty}^2 = (1 - c)^2 + (1 + c)^2 = 2\left(1 + c^2\right) \quad \ldots (22)$$

Thus, Eq. 18 gives Eq. 20 exactly, at least to the order of approximation indicated. This is of course not surprising, for the Helmholtz flow, any wavelength is "long."

It will be noticed that w - c appears in the denominator of the integral in Eq. 18, which, thus, becomes difficult to interpret if c is real and in the range of w. For this reason Eq. 18 will, for the most part, be restricted to the unstable case, in which c is not real. There is one case, however, in which this difficulty does not occur, namely in which w = 0, and Eq. 18 then gives a formula for the speed of internal waves in a stratified fluid at rest, namely:

$$2\alpha c^2 - 2J + \frac{J^2}{c^2}\int_{-\infty}^{\infty}\left(1 - \lambda^2\right)dy + \ldots = 0 \quad \ldots (23)$$

The first approximation $c^2 - J/\alpha$ is easily verified to be the ordinary formula for internal waves on a density discontinuity, which thus holds in any case for long enough wavelength. The correction term gives

$$c^2 = J/\alpha - \frac{J}{2}\int_{-\infty}^{\infty}\left(1 - \lambda^2\right)dy \quad \ldots (24)$$

for the internal wave with $c^2 \sim J/\alpha$ as $\alpha \to 0$. Of course with a continuously stratified fluid there are an infinite number of different internal wave modes. The one just described is the fastest of these. To describe the others, more terms are needed, although Eq. 23 will also give the second mode as it stands.

---

12 "Hydrodynamics," by H. Lamb, Cambridge Univ. Press, 6th edition, article 232, 1932.

This can be checked, for instance, by examining the case of a three layer system.

STABILITY BOUNDARIES IN THE SHEAR-LAYER CASE

A velocity profile of the shear-layer type should now be considered with α small and J small, even fairly small compared to α. The Eq. 18 has the approximate solution

$$c^2 = -1 + \frac{J}{\alpha} \quad \ldots\ldots\ldots\ldots\ldots\ldots (25)$$

As a result the flow is unstable, the instability being essentially a weakened form of the instability of a shear layer in the absence of density gradients. So long as J/α is smaller than 1, c is, in first approximation, imaginary, and there is no difficulty about convergence of the integral. By using the first approximation to c in the integral, relatively simple formulas for the second approximation can be obtained. However, it is natural to look for the boundary of this region of instability: how large can J be made, for a given α, before the instability is suppressed? The first approximation of course gives for the stability boundary the equation $J = \alpha$. However, because this value of J makes c real (actually 0) in first approximation, the integrals that appear in the second approximation are not defined if this value of c is used in them; consequently, caution is required in investigating the stability boundary. Clearly, what is needed is the limiting value of the integral as c becomes real, that is, as the stability boundary is approached. This can be obtained, but the analytical details are somewhat lengthy. The result will be given in the simplest case, in which w is an odd function with $w' > 0$ and λ is odd. In this case, c approaches zero through pure imaginary values, and the second approximation to the equation of the stability boundary is

$$2\alpha - 2J - \frac{2}{w'(0)}(\alpha - J)^2 + \int_{-\infty}^{\infty} \left[\left(\alpha (w^2 - 1) + J\right)^2 - J^2 \lambda^2 - \frac{(\alpha - J)^2}{w'(0)} w'(y) \right] \frac{dy}{w^2} + \ldots = 0 \quad \ldots\ldots\ldots (26)$$

Solving this for J to second order gives

$$J = \alpha + \frac{\alpha^2}{2} \int_{-\infty}^{\infty} \frac{w^4 - \lambda^2}{w^2} dy + \quad \ldots\ldots\ldots\ldots (27)$$

Eq. 27 gives a remarkably simple representation of the stability boundary for essentially arbitrary odd profiles of the shear layer type. Examples will serve to illustrate its usefulness. The first is essentially a problem solved by Goldstein[4] in 1931:

$$w = \lambda = \begin{cases} -1 & y < -1 \\ y & -1 < y < 1 \\ 1 & y > 1 \end{cases}$$

In this case Eq. 27 yields

$$J = \alpha + \frac{\alpha^2}{2} \int_{-1}^{1} \left(y^2 - 1\right) dy + \ldots = \alpha - \frac{2}{3}\alpha^2 \ldots\ldots\ldots (28)$$

The problem can be solved exactly in terms of Bessel functions, with the result

$$J = \alpha - \frac{2}{3}\alpha^2 - \frac{4}{9}\alpha^3 - \frac{16}{45}\alpha^4 \ldots\ldots\ldots\ldots (29)$$

Thus, Eq. 27 gives a fairly good approximation for α smaller than about 1/3. If the quadratic approximation is taken literally, it is found that J has a maximum of 3/8 at $\alpha = 3/4$. Now for this problem the local Richardson number $J(y) = J$ in (-1,1) and is not defined for $|y| > 1$. However, Miles' condition for stability $\left(J(y) \geq \frac{1}{4}\right)$ can be replaced by the condition "$-g\rho' - \frac{1}{4}\rho w'^2 \geq 0$ everywhere implies stability,"[4] and in this form it can be seen that his condition gives stability for $J \geq \frac{1}{4}$ in this case. Thus, even though $\alpha + 3/4$ is much too large for validity of the quadratic approximation, the value 3/8 obtained from it does not hopelessly miss the absolute upper bound $\frac{1}{4}$ given by Miles' theorem.

The second example is $w = \lambda = \tanh y$. This problem was solved by J. Holmboe, in 1960,[13] with the exact result $J = \alpha(1 - \alpha)$. This appears to be a favorable case for the application of Eq. 27 because the exact result is quadratic in α. It yields

$$\int_{-\infty}^{\infty} \frac{w^4 - \lambda^2}{w^2}\, dy = \int_{-\infty}^{\infty} \left(\tanh^2 y - 1\right) dy = -\int_{-\infty}^{\infty} \operatorname{sech}^2 y\, dy = -2 \ldots (30)$$

so that Eq. 27 is actually exact in this case.

It is perhaps of interest to give the details of this example somewhat more fully. The local Richardson number is:

$$J(y) = J\,\lambda'(y)\left[w'(y)\right]^{-2} = J\cosh^2 y \ldots\ldots\ldots (31)$$

Thus, the condition that $J(y)$ be everywhere $\geq \frac{1}{4}$ is equivalent to $J \geq 1/4$.

The eigenfunction and eigenvalue relation are known exactly only in the case corresponding to the stability boundary in which $c = 0$. In this case, as mentioned previously, the eigenvalue relation reduces to $J = \alpha(1 - \alpha)$, and the corresponding eigenfunction is

$$\phi = \operatorname{sech}^{\alpha} y\, |\tanh y|^{1-\alpha} \ldots\ldots\ldots\ldots\ldots (32)$$

as is easily checked. This eigenfunction may be compared with that obtained from the formulas for the expansion coefficients θ_{kn}, χ_{kn}. It is sufficient to

---

13 Unpublished lecture notes by J. Holmbee, Univ. of California, Los Angeles, Calif.

give the results in the case of the χ_{kn}. Putting c = 0 and evaluating the integrals gives, (setting T = tanh y for short)

$$\chi_{00} = T \quad \ldots\ldots\ldots\ldots\ldots\ldots (33a)$$

$$\chi_{10} = 1 - T \quad \ldots\ldots\ldots\ldots\ldots\ldots (33b)$$

$$\chi_{01} = T - 1 - T \ln\left(\frac{2T}{1+T}\right) \quad \ldots\ldots\ldots\ldots (33c)$$

$$\chi_{20} = T - 1 \quad \ldots\ldots\ldots\ldots\ldots\ldots (33d)$$

$$\chi_{11} = (1+T)\ln\left(\frac{2T}{1+T}\right) + 2(1-T) + 2T\int_T^1 \ln\frac{2T'}{1+T'}\,\frac{dT'}{1-T'^2} \quad \ldots\ldots (33e)$$

and

$$\chi_{02} = 2(T-1) - (2T+1)\ln\frac{2T}{1+T} + \frac{T}{2}\left(\ln\frac{2T}{1+T}\right)^2 - 2T\int_T^1 \ln\frac{2T'}{1+T'}\,\frac{dT'}{1-T'^2} \quad \ldots\ldots\ldots\ldots (33f)$$

Because $J = \alpha - \alpha^2$ on the stability boundary,

$$\chi = \chi_{00} + \alpha\chi_{10} + (\alpha - \alpha^2)\chi_{01} + \alpha^2(\chi_{20} + \chi_{11} + \chi_{02}) \quad \ldots\ldots (34)$$

to order α^2.

Using the values given in Eqs. 33, to order α^2, yields

$$\chi = T - \alpha\left[T\ln\frac{2T}{1+T}\right] + \alpha^2\left[\frac{T}{2}\left(\ln\frac{2T}{1+T}\right)^2\right] + \quad \ldots\ldots (35)$$

To compare this with

$$\phi = \operatorname{sech}^{\alpha} y\,|\tanh y|^{1-\alpha} \quad \ldots\ldots\ldots\ldots\ldots (36)$$

the factor $e^{-\alpha y}$ must first be split off. Taking $y > 0$ yields

$$\phi = \left(\frac{e^y + e^{-y}}{2}\right)^{-\alpha} T^{1-\alpha} = e^{-\alpha y}\left(\frac{1+e^{-2y}}{2}\right)^{-\alpha} T^{1-\alpha}$$

$$= e^{-\alpha y}(1+T)^{\alpha} T^{1-\alpha} = 2^{\alpha} e^{-\alpha y} T\left(\frac{2T}{1+T}\right)^{-\alpha} \quad \ldots\ldots (37)$$

This shows that $\phi \sim 2^{\alpha} e^{-\alpha y}$ for $y \to \infty$, so that to make the normalization of ϕ agree with that used as a basis for our expansion formulas we must replace ϕ by $2^{-\alpha}\phi$. Because

$$T\left(\frac{2T}{1+T}\right)^{-\alpha} = T\,e^{-\alpha\ln\left(\frac{2T}{1+T}\right)}$$

$$= T - \alpha T\ln\frac{2T}{1+T} + \frac{\alpha^2}{2} T\ln\left(\frac{2T}{1+T}\right) + \quad \ldots\ldots\ldots (38)$$

it is seen that the expansion presented here agrees with the exact solution on the stability boundary. Because the exact solution is not known for $c \neq 0$, further comparisons cannot be made. However, the use of these formulas will be illustrated by obtaining the eigenvalue relation for Holmboe's example in the unstable range $J < \alpha(1 - \alpha)$, to second order in α. For this Eq. 18 will be used. After introducing $T = \tanh y$ as variable of integration, Eq. 18 becomes:

$$2\,\alpha(1+c^2) - 2J + \int_{-1}^{1} \left\{\alpha\left[(T-c)^2 - (1-c)^2\right] + J(1-T)\right\} \left\{\alpha\left[(T-c)^2 - (1+c)^2\right] + J(1+T)\right\} \frac{dT}{(T-c)^2\left(1-T^2\right)} + \ldots = 0 \quad \ldots (39)$$

Writing $c = c_r + i\,c_i$ and keeping in mind that it is assumed that $c_i > 0$, the integral is easily evaluated, giving

$$2\,\alpha(1+c^2) - 2J + \alpha^2 \left\{ -4 + c \ln\left[\frac{(1-c_r)^2 + c_i^2}{(1+c_r)^2 + c_i^2}\right] + 2\,ic\left[\tan^{-1}\left(\frac{1-c_r}{c_i}\right) + \tan^{-1}\left(\frac{1+c_r}{c_i}\right)\right] \right\}$$

$$+ \frac{4\alpha J}{1-c^2} - \frac{2J^2}{1-c^2} + \ldots = 0 \quad \ldots\ldots\ldots\ldots (40)$$

This eigenvalue relation can be written in a simpler form, because it can be shown that $c_r = 0$. This is physically fairly clear from the antisymmetry of the w and λ fields which shows that there is no preferred direction of propagation of unstable waves, and that one would, consequently, expect the instability to be simply an exponential growth of the initial sinuous perturbation, without propagation. Setting $c_r = 0$ yields

$$\alpha\left(1 - c_i^2\right) - J - 2\,\alpha^2 \left\{1 + c_i \tan^{-1}\left(\frac{1}{c_i}\right)\right\}$$

$$+ \frac{2\,\alpha J}{1+c_i^2} - \frac{J^2}{1+c_i^2} + \ldots = 0 \quad \ldots\ldots\ldots\ldots (41a)$$

or

$$J = \alpha\left(1 - c_i^2\right) + \alpha^2 \left\{ -2c_i \tan^{-1}\left(\frac{1}{c_i}\right) - 2 + \frac{1}{1+c_i^2} \right\} - \frac{(J-\alpha)^2}{1+c_i^2} + \quad \ldots\ldots\ldots\ldots\ldots (41b)$$

Because

$$J - \alpha = - \alpha c_i^2 \quad \ldots\ldots\ldots\ldots\ldots\ldots (42)$$

to first order, one obtains, to second order

$$J = \alpha\left(1 - c_i^2\right) - \alpha^2 \left\{ 2 c_i \tan^{-1}\left(\frac{1}{c_i}\right) + 1 + c_i^2 \right\} + \quad \ldots\ldots (43)$$

From Eq. 43 it is a simple matter to compute curves of constant c_i in the $J - \alpha$ plane. Of somewhat greater interest, however, are the curves of constant growth rate; αc_i = constant. Such curves are shown in Fig. 3. From the maxima of these curves one can determine the fastest growing wave number for any value of $J < 1/4$. This is the wave number one would expect to ob-

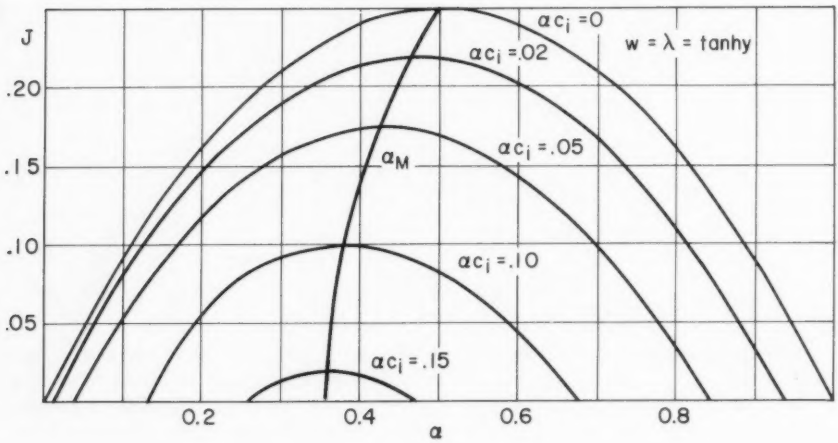

FIG. 3

serve in an experiment. The locus of these maxima is indicated by the curve marked α_M in Fig. 3.

It will be noticed that the general formula, Eq. 27 does not agree with the result of Drazin[9] mentioned in the introduction, which has J or order α^2 rather than α. The reason for this is that in that problem the density field was exponential in the whole plane and so the assumption that ρ approaches finite limits at $\pm$ is violated.

JET TYPE VELOCITY PROFILES

In a homogeneous fluid, velocity profiles of the simple jet type (where w(y) has a single maximum of, say, 1, and approaches zero at $\pm \infty$) have just two types of long wave instabilities. The nature of these two modes of disturbance

is indicated by Rayleigh's names for them; sinuousities and varicosities. Eq. 18 for the jet case and with J = 0 can be written

$$2\,\alpha\,c^2 = -\,\alpha^2 \int_{-\infty}^{\infty} \frac{w^2(w-2c)^2}{(w-c)^2}\,dy \quad \ldots\ldots\ldots (44)$$

The sinuous disturbance has $c \to 0$, through nearly pure imaginary values as $\alpha \to 0$, and to first approximation

$$c^2 = -\,\frac{\alpha}{2} \int_{-\infty}^{\infty} w^2\,dy \quad \ldots\ldots\ldots\ldots\ldots (45)$$

Thus the jet, although unstable to long waves, is less so than the shear layer, in the sense that the corresponding growth rate is smaller. Similarly, when density variation is present, J must be kept smaller in the jet case than in the shear layer case to stay in the unstable region. In fact, Eq. 18 shows that J must be small of the order of α^2 to do this, and as a first approximation to the equation of the stability boundary

$$J = \frac{\alpha^2}{2} \int_{-\infty}^{\infty} w^2\,dy \quad \ldots\ldots\ldots\ldots\ldots (46)$$

This refers to the sinuous instability. The varicose instability is a little more complicated. Here in the case J = 0, $c \to 1$ (the maximum of $w(y)$) through complex values, as $\alpha \to 0$. The precise behavior depends on the nature of $w(y)$ in the neighborhood of its maximum. In the presence of density variation a similar situation prevails. Eq. 7 shows that in the limit of $\alpha \to 0$ and $J \to 0$ $W^2(\phi/W)'$ can be expected to be constant, and because it is zero at ∞, actually zero. This implies that ϕ/W is constant throughout intervals in which $W \neq 0$, but this constant value may change at a point at which W = 0. If such a change occurs, ϕ will still be continuous because W = 0 at the jump in the constant, but ϕ' will not unless also $w' = 0$ there.

Thus if a discontinuity in vorticity is to be avoided, c must approach the maximum value taken on by w, as α and J approach zero. (Only the simplest jet-type case, in which w' vanishes at just one point, say y = 0, is considered here.) If c approaches the maximum of w, for example, 1, however, the integral in Eq. 18 diverges so that the second order terms are not really of second order. It can be shown, however, that the higher order terms that have been omitted in Eq. 18 are still of smaller order than those retained. If c is set equal to $1 + \gamma$, in which it is assumed that γ is a small complex number with $\epsilon \leq \arg\gamma \leq \pi - \epsilon$ for some $\epsilon > 0$, the integral in Eq. 18 can be estimated, and retaining only the largest term for small γ Eq. 18 yields

$$0 = 2\,\alpha - 2\,J + \left[-\,\alpha + J(1-\lambda(0))\right]\left[-\,\alpha + J(1+\lambda(0))\right] \frac{\pi\,\gamma^{-3/2}}{-\,2\,w''(0)} \quad \ldots\ldots (47)$$

in which, if $\gamma = |\gamma|\,e^{i\sigma}$, $\gamma^{-3/2}$ means $|\gamma|^{-3/2}\,e^{-3/2i\sigma}$.

Therefore,

$$|\gamma|^{3/2}\, e^{3/2i\sigma} = \frac{-\pi}{\sqrt{-2\,w''(0)}} \frac{\left[\alpha - J(1-\lambda(0))\right]\left[\alpha - J(1+\lambda(0))\right]}{2(\alpha - J)} \quad \ldots\ldots(48)$$

Thus if J is small enough in comparison to α, the right-hand side of Eq. 48 is negative; therefore, $\sigma = 2\pi/3$, and instability is obtained, with

$$c = 1 + e^{i\frac{2\pi}{3}} \left(\frac{\pi}{\sqrt{-2w''(0)}} \frac{\left[\alpha - J(1-\lambda(0))\right]\left[\alpha - J(1+\lambda(0))\right]}{2(\alpha - J)} \right)^{2/3} \quad \ldots\ldots(49)$$

It is clear also that the first approximation to the stability boundary is

$$J = \frac{\alpha}{1 - \lambda(0)} \quad \ldots\ldots(50a)$$

or

$$J = \frac{\alpha}{1 + \lambda(0)} \quad \ldots\ldots(50b)$$

whichever is larger.

ACKNOWLEDGMENTS

The research of the senior author was partially supported by the Office of Naval Research under contract N-onr 1841(18).

Journal of the
ENGINEERING MECHANICS DIVISION
Proceedings of the American Society of Civil Engineers

RANGE OF YIELD CONDITION IN IDEAL PLASTICITY

By R. M. Haythornthwaite,[1] M. ASCE

SYNOPSIS

The properties of ideal rigid-plastic solids are used to define bounding yield conditions that remain valid when test results are available for only one stress state, such as simple tension or simple shear. For material in which yield is insensitive to changes in mean stress, the bounding yield conditions are shown to be the maximum shear-stress criterion of Tresca and a new criterion designated as the maximum reduced stress criterion. Use of both criteria enables the best possible bounds to be obtained for the carrying capacity of a structure in the absence of further information. Parallel results are obtained for material in which yield strength is a linear function of the mean stress, and some examples are given.

INTRODUCTION

The powerful variational principles of the theory of ideally plastic solids have been used primarily in the development of approximate solutions to well-defined problems in which the yield properties of the material are supposed to be known exactly. The carrying capacity may then be bounded from above and below by means of the theorems of limit analysis, developed by A. A. Gvozdev[2]

Note.—Discussion open until May 1, 1962. To extend the closing date one month, a written request must be filed with the Executive Secretary, ASCE. This paper is part of the copyrighted Journal of the Engineering Mechanics Division, Proceedings of the American Society of Civil Engineers, Vol. 87, No. EM 6, December, 1961.

[1] Prof. of Engrg. Science, The Univ. of Michigan, Ann Arbor, Mich.

[2] "Determination of the Collapse Load for Statically Indeterminate Systems Undergoing Plastic Deformations," by A. A. Gvozdev, Proceedings, Conf. on Plastic Deformations, 1966. In Russian, edited by B. C. Galerkin, AN, SSSR, 1938, p. 19. English translation: Internatl. Journal of Mechanical Science, Vol. 1, 1960, p. 322.

and by D. C. Drucker, W. Prager, and H. J. Greenberg,[3] or by the use of escribed and inscribed yield conditions.[4] On the other hand, the question of finding approximate solutions when information about the yield condition is incomplete does not seem to have been investigated, despite its technological importance.

In this paper, the problem of finding upper and lower bounds to the yield load of a body is studied for the case when the yield strength of the material is known exactly for only one or two stress states. An isotropic material in which yield is independent of the mean stress is considered first, and then the analysis is extended to material in which the yield criterion is linearly dependent on the mean stress. The former model is widely used in the analysis of metals, whereas interest in the latter springs from attempts to apply the theory of plasticity to soils.[5,6]

Notation.—The letter symbols adopted for use in this paper are defined where they first appear, in the illustrations or in the text, and are arranged alphabetically, for convenience of reference, in Appendix II.

MATERIAL INSENSITIVE TO MEAN STRESS

For this paper, an ideally plastic, isotropic material, in which the yield criterion is independent of the mean stress, will be considered. In view of the property of isotropy, the orientation in space of the principal stress directions is unimportant, and the state of stress may be represented completely by the principal stress components σ_1, σ_2, and σ_3. It is then possible to represent the yield criterion by use of a surface in the principal-stress space having components σ_1, σ_2, and σ_3 as co-ordinates. In the case of yield criteria independent of the mean stress, this surface will be formed by generators at right angles to the planes

$$\sigma_1 + \sigma_2 + \sigma_3 = \text{constant} \quad \ldots\ldots\ldots\ldots \quad (1)$$

that is, parallel to the axis making equal angles with the co-ordinate directions, and any intersection of the surface with a plane represented by Eq. 1 will be typical.

Two cases of intersections of this type are shown in Fig. 1. One can first consider the case in which the results of tensile and compressive tests are available (Fig. 1(a)). In the case of metals, tensile and compressive yield strengths are often nearly equal, suggesting the additional assumption that will be made herein, that reversal of the sign of a stress does not alter the stress magnitude at yield. Test points are represented by the six small circles in Fig. 1(a), because any one of the three principal stresses can be taken as the non-zero component. Alternatively, considering a case in which the result of a shear test (such as simple torsion) is available, the six points indicated by the small circles in Fig. 1(b) will then have been determined experimentally.

---

3 "Extended Limit Design Theorems for Continuous Media," by D. C. Drucker, W. Prager and H. J. Greenberg, Quarterly of Applied Mathematics, Vol. 9, 1952, p. 381.

4 "A Theoretical Investigation of the Effect of Specimen Size in the Measurement of Hardness," by R. Hill, Philosophical Magazine, Vol. 41, 1951, p. 745.

5 "Soil Mechanics and Work-hardening Theories of Plasticity," by D. C. Drucker, R. E. Gibson, and D. J. Henkel, Proceedings, ASCE, Vol. 81, 1955, p. 791.

6 "Mechanics of the Triaxial Test for Soils," by R. M. Haythornthwaite, Proceedings, ASCE, Vol. 86, No. SM 5, 1960, p. 35.

The following question can now be considered: What are the largest and smallest yield surfaces that can be drawn through the test data in the two cases? When finding the smallest surfaces, it is sufficient to note the requirement of convexity for any yield surface associated with a stable plastic material,[7] in order to arrive at the two hexagons shown. The largest surfaces are found by noting, in addition, that the cross sections shown must have 30° symmetry, so that reversal of all three stress components does not influence yield.

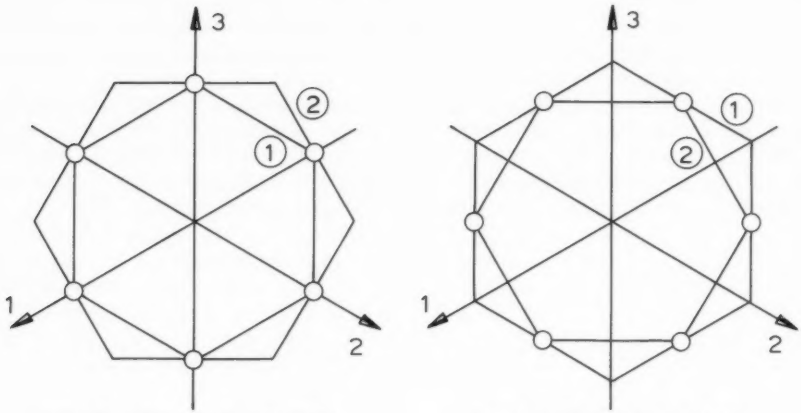

(*a*) TENSILE-TEST RESULTS AVAILABLE (*b*) SIMPLE SHEAR-TEST RESULTS AVAILABLE

FIG. 1.—BOUNDING YIELD CRITERIA FOR MATERIAL INSENSITIVE TO MEAN STRESS

The hexagons marked 1 in Fig. 1 will be recognized as representing the familiar maximum shear stress criterion of Tresca:

$$\max\left(|\sigma_1 - \sigma_2|, |\sigma_2 - \sigma_3|, |\sigma_3 - \sigma_1|\right) = \sigma_0 = 2\,\tau_0 \quad \ldots\ldots \quad (2)$$

in which σ_0 is the yield stress in simple tension, and τ_0 is the yield stress in simple shear. The hexagons marked 2 in Fig. 1 represent criteria in which a restriction is placed on the value of the maximum reduced stress (which in Fig. 1 is measured parallel to the stress axes):

$$\max\left(|\sigma_1 - \sigma|, |\sigma_2 - \sigma|, |\sigma_3 - \sigma|\right) = \tau_0 = \frac{2}{3}\,\sigma_0 \quad \ldots\ldots\ldots \quad (3)$$

in which

$$\sigma = \frac{\sigma_1 + \sigma_2 + \sigma_3}{3} \quad \ldots\ldots\ldots\ldots \quad (4)$$

---

7 "A More Fundamental Approach to Plastic Stress-Strain Relations," by D. C. Drucker, Proceedings, ASME, 1st U. S. Natl. Congress of Applied Mechanics, Chicago, Ill., 1951, p. 487.

The hexagons shown in Fig. 1 and represented analytically by Eqs. 2 and 3 owe their significance to the property that all possible yield conditions must lie between them. A lower bound obtained by the use of the inscribed hexagon will be a lower bound for all stable materials irrespective of the details of the yield condition, and an upper bound obtained by the use of the escribed hexagon will be similarly an upper bound in all cases.

R. Hill[8] has suggested Eq. 3 as a suitable linear approximation to von Mises' yield surface when the stress state is close to a uniaxial compression. D. D. Ivlev[9] introduced the hexagons shown in Fig. 1(a) and designated them as bounding hexagons, but did not make this property dependent on the availability of tensile test data. Neither writer anticipates the particular use of the criteria that is suggested here.

When determining upper bounds, the computations are greatly simplified, if a compact expression can be found for the rate of energy dissipation in terms of the strain rates. The theory of the generalized plastic potential[10] indicates that the associated strain-rate vectors coincide with the outward drawn normal to the yield surface when corresponding axes are superimposed. Thus,

$$\epsilon_{ij} = \sum_{p=1}^{n} \lambda_p \frac{\partial f_p}{\partial \sigma_{ij}} \quad \ldots\ldots\ldots\ldots \quad (5)$$

in which λ_p are positive constants and the f_p are regular functions, the equations of various parts of the yield surface being

$$f_p\left(\sigma_{ij}\right) = 0 \quad \ldots\ldots\ldots\ldots\ldots \quad (6)$$

It is then a simple matter to show that the rate of energy dissipation is

$$D = |\epsilon|_{max}\, \sigma_0 \quad \ldots\ldots\ldots\ldots\ldots \quad (7)$$

in the case of the maximum shear-stress criterion, and

$$D = |\gamma|_{max}\, \tau_0 \quad \ldots\ldots\ldots\ldots\ldots \quad (8)$$

in which γ is the shear strain, in the case of the maximum reduced stress criterion.

Still further restrictions on the range of the yield criterion can be made if the results of more than one type of test are available. If, for example, results for both tension and torsion tests were known and these results were consistent with the maximum shear-stress criterion, an examination of Fig. 1 reveals that the criterion must hold exactly for all other stress states. On the other hand, if these tests were consistent with the maximum reduced stress criterion,

---

8 "On the Inhomogeneous Deformation of a Plastic Lamina in a Compression Test," by R. Hill, Philosophical Magazine, Vol. 41, 1950, p. 733.

9 "On the Development of a Theory of Ideal Plasticity," by D. D. Ivlev, Prikladnaia Matematika i Mekhanika (AN, SSSR), Vol. 22, 1958, p. 850, (in Russian). English translation, Pergamon Press, Inc. p. 1221.

10 "Stress-strain Relations, Uniqueness and Variational Theorems for Elastic-plastic Materials with a Singular Yield Surface," by W. T. Koiter, Quarterly of Applied Mathematics, Vol. 11, 1953, p. 350.

that criterion would be the only possible one. In both cases, the range of possible criteria is reduced to a band of zero width.

In other cases, it is evident that additional results from only a very few combined stress tests would be sufficient to confine the yield surface for a stable material to an extremely narrow range.

As might be expected, application of the yield criteria developed previously leads to bounds on the carrying capacity which, in some cases, are much closer than can be obtained by a simple factoring process based on inscribed and escribed yield surfaces of the same shape. If tensile-test values are available, an upper bound based on the Tresca yield criterion must use the outer hexagon shown in Fig. 2, whereas an upper bound based on the maximum reduced stress criterion can use the inner hexagon. The latter will always be at least as favorable because, as a consequence of the lower-bound theorem of limit analysis,[3] increasing the yield strength of a body in any zone can never reduce the collapse load.

A Plane Stress Example.—A circular plate of radius R and thickness $t \ll R$, simply supported around the edge and subjected to a lateral pressure p uniformly distributed over the top surface will now be considered. Supposing the yield stress of the material in tension to be given, it is desired to find the closest upper and lower bounds to the carrying capacity. For the lower bound, a solution using the Tresca yield criterion will be appropriate. This has been given by H. G. Hopkins and Prager.[11] The corresponding solution for the reduced stress criterion will be developed herein.

In the analysis, the usual assumptions of plate theory will be adopted. If the effects of shear are neglected, and if the lateral pressure is small compared with the stresses in the plane of the plate, then the state of the plate will be approximately one of plane stress, the non-zero principal stresses lying in the plane of the plate. Adopting the maximum reduced-stress criterion, the yield curve drawn in terms of the radial moment per unit length, M_r, and the circumferential moment per unit length, M_θ, will be as shown in Fig. 3. Because M_r is zero at the outer edge and equal to M_θ at the center (by symmetry), the state points are expected to lie in the range ABC in Fig. 3. The equation of AB is

$$M_\theta - \frac{1}{2} M_r = M_0 \quad \ldots\ldots\ldots\ldots \quad (9)$$

and that of BC is

$$\frac{1}{2} M_\theta + \frac{1}{2} M_r = M_0 \quad \ldots\ldots\ldots\ldots \quad (10)$$

Eliminating the shear force from the radial-equilibrium equation by use of the transverse equilibrium equation,

$$\frac{d}{dr} (r M_r) - M_\theta + \frac{1}{2} p r^2 = 0 \quad \ldots\ldots\ldots\ldots \quad (11)$$

11 "The Load Carrying Capacities of Circular Plates," by H. G. Hopkins and W. Prager, Journal of the Mechanics and Physics of Solids, Vol. 2, 1953, p. 1.

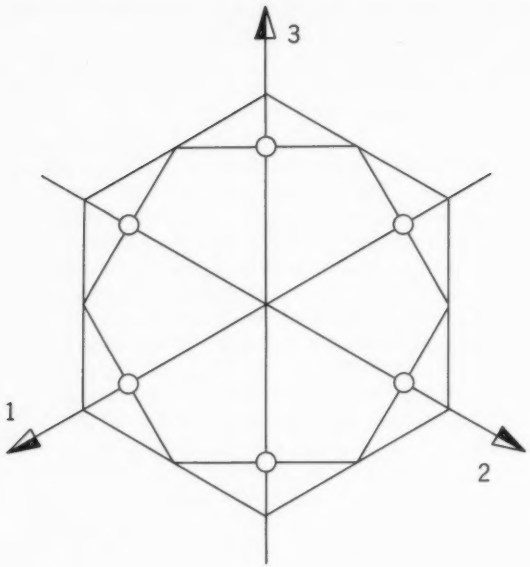

FIG. 2.—ALTERNATIVE ESCRIBED YIELD CRITERIA WHEN TENSILE-TEXT RESULTS ARE AVAILABLE

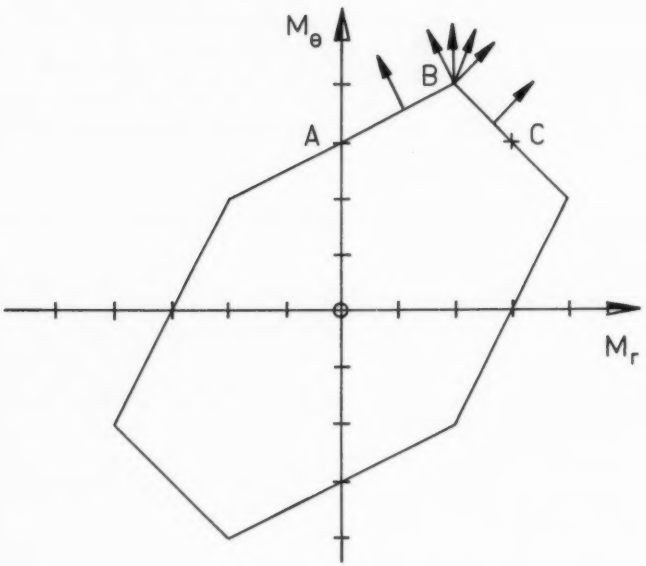

FIG. 3.—REDUCED STRESS CRITERION FOR PLATE BENDING (PLANE STRESS)

in which the signs have been assigned so that positive bending moments tend to induce sag of the plate in the same direction as the action of the pressure, p.

Substituting Eqs. 9 and 10 into 11 and integrating the resultant first-order ordinary differential equations,

$$M_r = 2\,M_0 - \frac{1}{5}\,p\,r^2 + c_1\,r^{-1/2} \quad \ldots\ldots\ldots (12a)$$

$$M_\theta = 2\,M_0 - \frac{1}{10}\,p\,r^2 + \frac{1}{2}\,c_1\,r^{-1/2} \quad \ldots\ldots\ldots (12b)$$

on AB and

$$M_r = M_0 - \frac{1}{8}\,p\,r^2 + c_2\,r^{-2} \quad \ldots\ldots\ldots\ldots (13a)$$

and

$$M_\theta = M_0 + \frac{1}{8}\,p\,r^2 - c_2\,r^{-2} \quad \ldots\ldots\ldots\ldots (13b)$$

on BC.

Substituting the boundary conditions $M_r = 0, M_\theta = M_0$ at $r = R$ and $M_r = M_\theta = M_0$ at $r = 0$, and equating the resultant expressions for M_r at $r = b = \beta R$, the following transcendental equation for β is obtained

$$6\,\beta^{2.5} - 15\,\beta^2 + 4 = 0 \quad \ldots\ldots\ldots\ldots (14)$$

The root in the range $1 \geq \beta \geq 0$ is $\beta = 0.6242$ which, on substitution into Eqs. 12 and 13 leads to

$$p = 6.852\,\frac{M_0}{R^2} \quad \ldots\ldots\ldots\ldots (15)$$

The pressure from Eq. 15 is statically admissible and so is a lower bound. It can be shown to be the actual collapse load by associating a velocity field.

The velocities are determined to within an arbitrary constant through the position of the state point in Fig. 3. According to the theory of plasticity for generalized stresses,[12] the generalized strains corresponding to M_r, M_θ will form a vector coinciding with the outwards drawn normal to the yield criterion, when corresponding axes are superimposed. The generalized strain rates corresponding to the moments are the curvature rates

$$\kappa_r = -\frac{d^2w}{dr^2} \quad \ldots\ldots\ldots\ldots (16a)$$

and

$$\kappa_\theta = -\frac{1}{r}\,\frac{dw}{dr} \quad \ldots\ldots\ldots\ldots (16b)$$

12 "General Theory of Limit Design," by W. Prager, Proceedings, 8th Internatl. Congress of Applied Mechanics, Istanbul, Vol. 2, 1952, p. 65.

in which w is the transverse velocity. The normal to the line described by Eq. 9 leads to the curvature components

$$\kappa_\theta = -\lambda \quad \ldots\ldots\ldots\ldots\ldots\ldots (17a)$$

and

$$\kappa_r = +\frac{1}{2}\lambda \quad \ldots\ldots\ldots\ldots\ldots\ldots (17b)$$

so

$$\kappa_\theta + 2\,\kappa_r = 0 \quad \ldots\ldots\ldots\ldots\ldots\ldots (18)$$

and, hence,

$$\frac{d^2w}{dr^2} + \frac{1}{2\,r}\frac{dw}{dr} = 0 \quad \ldots\ldots\ldots\ldots\ldots\ldots (19)$$

On integration, Eq. 19 becomes

$$w = c_3\, r^{1/2} + c_4 \quad \ldots\ldots\ldots\ldots\ldots\ldots (20)$$

and in a similar fashion the normal to Eq. 10 leads to

$$w = c_5\, r^2 + c_6 \quad \ldots\ldots\ldots\ldots\ldots\ldots (21)$$

Setting the deflection as zero at the supports, and noting that there must be continuity of deflection and slope at r = b,

$$w = 2.45\left(1 - \rho^{1/2}\right) w_0 \qquad 1 \geq \rho \geq \beta \quad \ldots\ldots\ldots (22a)$$

and

$$w = \left(1 - 1.240\,\rho^2\right) w_0 \qquad \beta \geq \rho \geq 0 \quad \ldots\ldots\ldots (22b)$$

in which w_0 is the deflection rate at the center. A velocity distribution has been associated with the statically admissible load, Eq. 15, and the solution is complete.

The estimates of collapse pressure obtained, using the two criteria, can now be compared. In the case of Tresca's yield criterion, the collapse pressure given by Hopkins and Prager[11] is

$$p = \frac{6\,M_0}{R^2} \quad \ldots\ldots\ldots\ldots\ldots\ldots (23)$$

and this will be the best lower bound. Comparing Eqs. 15 and 23

$$6.852 \geq \frac{p\,R^2}{M_0} \geq 6 \quad \ldots\ldots\ldots\ldots\ldots\ldots (24)$$

and the pressure is bound to within 14.2%.

In contrast, if the Tresca yield criterion were used to obtain the upper bound, the outer hexagon shown in Fig. 2 would be used and

$$8 \geq \frac{p\,R^2}{M_0} \geq 6 \qquad \ldots\ldots\ldots\ldots\ldots\ldots \quad (25)$$

and the pressure is bounded to within 33.3%.

MATERIAL SENSITIVE TO MEAN STRESS

An ideally plastic, isotropic material in which the stress level at yield is a linear function of the mean stress will now be considered. This constitutes a

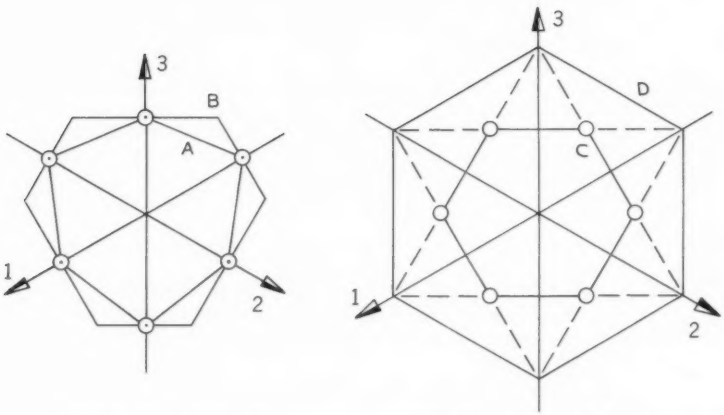

(*a*) TENSILE-TEST RESULTS AVAILABLE

(*b*) SIMPLE SHEAR-TEST RESULTS AVAILABLE

FIG. 4.—BOUNDING YIELD CRITERIA FOR MATERIAL SENSITIVE TO MEAN STRESS

first step in the generalization of the foregoing analysis. There is evidence that it may be appropriate for certain soils and possibly for some concretes and cast metals.

Intersections of the yield surfaces with the planes determined by Eq. 1 are shown in Fig. 4. Fig. 4(a) shows the case in which the results of tensile and compressive tests (represented by the circles) are available; Fig. 4(b) shows the case in which shear tests are available. The limiting lines are obtained by arguments parallel to those used previously.

When expressing the bounding criteria mathematically, it is convenient to introduce the cohesion, c, and the angle of internal friction, ϕ, in the fashion in which they are commonly used in statements of Coulomb's yield criterion. Any line that cuts the octahedral axis can then be defined in terms of c and ϕ, values

TABLE 1.—EXPRESSIONS FOR THE YIELD

SURFACE (1)	YIELD CRITERIA (2)
A	$(\alpha+\sin\phi)\sigma_1+(1-\alpha)\sigma_2-(1-\sin\phi)\sigma_3 = 2c\cos\phi$ where $2-\sin\phi \geq \alpha \geq (1-\sin\phi)/2$ $(\sigma_1 \geq \sigma_2 \geq \sigma_3;\ \alpha = \sin\phi/\sin\phi')$
	$\alpha = 2-\sin\phi$ $\max.(\sigma_1-\sigma, \sigma_2-\sigma, \sigma_3-\sigma) = 2(c\cos\phi-\sigma\sin\phi)/(3-\sin\phi)$ or $\sigma_1 = (\sigma_2+\sigma_3)(1-\sin\phi)/2 + c\cos\phi$ $(\sigma_1 \geq \sigma_2, \sigma_3)$
	$\alpha = (1-\sin\phi)/2$ $\min.(\sigma_1-\sigma, \sigma_2-\sigma, \sigma_3-\sigma) = 4(\sigma\sin\phi-c\cos\phi)/(3-\sin\phi)$
B	$(1+\sin\phi)(\sigma_1+\sigma_2)/2-(1-\sin\phi)\sigma_3 = 2c\cos\phi$ $(\sigma_2 \geq \sigma_2^c = [(2\alpha-1+\sin\phi)\sigma_1+(2-\alpha-\sin\phi)\sigma_3]/(1+\alpha))$ $(1-\sin\phi')(\sigma_1+\sigma_2)/2-(1+\sin\phi')\sigma_3 = -2c\cos\phi$ $(\sigma_2 < \sigma_2^c)$ $(\sigma_1 \geq \sigma_2 \geq \sigma_3;\ \alpha = \sin\phi/\sin\phi')$
C	$\max.(\lvert\sigma_1-\sigma\rvert, \lvert\sigma_2-\sigma\rvert, \lvert\sigma_3-\sigma\rvert) = c\cos\phi-\sigma\sin\phi$ or $(2-\sin\phi)\sigma_1-(1+\sin\phi)(\sigma_2+\sigma_3)+3c\cos\phi = 0$ $(\sigma_2 \geq (\sigma_1+\sigma_3)/2)$
D	$\max.(\lvert\sigma_1-\sigma_2\rvert, \lvert\sigma_2-\sigma_3\rvert, \lvert\sigma_3-\sigma_1\rvert) = 3(c\cos\phi-\sigma\sin\phi)$ or $(1+\sin\phi)\sigma_1+\sigma_2\sin\phi-(1-\sin\phi)\sigma_3 = 3c\cos\phi$ $(\sigma_1 > \sigma_2 > \sigma_3)$

CRITERIA ILLUSTRATED IN FIG. 4

STRAIN-RATE EQUATIONS
(3)

$$(1-\sin\phi)(\epsilon_1+\epsilon_2)+(1+\sin\phi)\epsilon_3 = 0 \qquad (\sigma_1 = \sigma_2 > \sigma_3)$$

$$(1-\sin\phi')\epsilon_1+(1+\sin\phi')(\epsilon_2+\epsilon_3) = 0 \qquad (\sigma_1 > \sigma_2 = \sigma_3)$$

$$\epsilon_1:\epsilon_2:\epsilon_3 = \alpha+\sin\phi:1-\alpha:\sin\phi-1 \qquad (\sigma_1 > \sigma_2 > \sigma_3)$$

$$(1-\sin\phi)(\epsilon_1+\epsilon_2)+(1+\sin\phi)\epsilon_3 = 0 \qquad (\sigma_1 = \sigma_2 > \sigma_3)$$

$$\epsilon_1:\epsilon_2:\epsilon_3 = 2/(1-\sin\phi):-1:-1 \qquad (\sigma_1 > \sigma_2 > \sigma_3)$$

$$(1-3\sin\phi)\epsilon_1+(1+\sin\phi)(\epsilon_2+\epsilon_3) = 0 \qquad (\sigma_1 > \sigma_2 = \sigma_3)$$

$$\epsilon_1:\epsilon_2:\epsilon_3 = 1:1:-2(1-\sin\phi)(1+\sin\phi) \qquad (\sigma_1 > \sigma_2 > \sigma_3)$$

$$(3-\sin\phi)(1-\sin\phi')\epsilon_1+[4\cos\phi\cos\phi'-(1+\sin\phi)(1-\sin\phi')]\epsilon_2+(1+\sin\phi)(3+\sin\phi')\epsilon_3 = 0 \qquad (\sigma_2 = \sigma_2^c)$$

$$\epsilon_1:\epsilon_2:\epsilon_3 = 1:1:-2(1-\sin\phi)/(1+\sin\phi) \qquad (\sigma_2 \geq \sigma_2^c)$$

$$\epsilon_1:\epsilon_2:\epsilon_3 = 1:1:-(1+\sin\phi')/2(1-\sin\phi') \qquad (\sigma_2 \leq \sigma_2^c)$$

$$(1+\sin\phi)\epsilon_1+\epsilon_2+(1-\sin\phi)\epsilon_3 = 0$$

$$(1-\sin\phi)(\epsilon_1+\epsilon_2)+(1+2\sin\phi)\epsilon_3 = 0 \qquad (\sigma_1 = \sigma_2 > \sigma_3)$$

$$(1-2\sin\phi)\epsilon_1+(1+\sin\phi)(\epsilon_2+\epsilon_3) = 0 \qquad (\sigma_1 > \sigma_2 = \sigma_3)$$

$$\epsilon_1:\epsilon_2:\epsilon_3 = 1+\sin\phi:\sin\phi:\sin\phi-1 \qquad (\sigma_1 > \sigma_2 > \sigma_3)$$

appropriate to the generalized Coulomb yield criterion that contains the line. The algebra is straightforward and will not be given herein; the resulting expressions for the various bounding criteria are summarized in Table 1. When tensile and compressive tests are available, these are not necessarily consistent with the same generalized Coulomb yield surface.[6] Therefore, values c and ϕ, corresponding to the compressive test results, and c' and ϕ' corresponding to the tensile test results, are introduced. The ratio $\alpha = \phi/\phi'$ is limited by the requirement of convexity to the range

$$2 - \sin\phi \geq \alpha \geq \frac{1 - \sin\phi}{2} \quad \ldots\ldots\ldots\ldots (26)$$

the extreme values representing the attainment of triangular cross sections to the yield surfaces A and B. When $\alpha = 1$, surface A reduces to the Coulomb yield surface (Table 1).

The flow equations in the Col. 3 of Table 1 are obtained by substituting the analytic expressions for the yield surfaces into Eq. 5 given in Col. 1.

At the point

$$\sigma_1 = \sigma_2 = \sigma_3 = c \cot\phi \quad \ldots\ldots\ldots\ldots (27)$$

which is the apex for all the yield surfaces, the rate of energy dissipation is

$$D = \sigma_{ij}\,\epsilon_{ij} = c \cot\phi \left(\epsilon_1 + \epsilon_2 + \epsilon_3\right) \quad \ldots\ldots\ldots (28)$$

which also applies to all other points on the surfaces; the apex can be considered as belonging to every side, and on any one side the projection of stresses in the direction normal to the side is always the same. In the case of surface C, the rate of energy dissipation can be written in the form

$$D = |\gamma|_{max}\, c \cos\phi \quad \ldots\ldots\ldots\ldots (29)$$

in which $|\gamma|_{max}$ is the value of the largest shear strain rate. Equally simple expressions do not appear to exist for the other surfaces, and Eq. 28 has to be used.

Plane Strain.—In the case of plane strain, all the bounding criteria introduced previously can be expressed in terms of equivalent Coulomb criteria, with a suitable choice of the constants. A solution that has used the Coulomb criterion can then be readily adapted to apply to any of the other criteria by a simple factoring process.

In plane strain, one principal strain rate is to be set equal to zero. The ordering $\epsilon_1 \geq \epsilon_2 \geq \epsilon_3$ is already established as a consequence of the ordering $\sigma_1 \geq \sigma_2 \geq \sigma_3$ adopted in Table 1, and it remains to determine which strain rate is to be zero. The dilatation is everywhere positive, so $\epsilon_1 \neq 0$. If $\epsilon_3 = 0$, then ϵ_1 and ϵ_2 are both greater than zero, but by the flow equations in Table 1 they are both of opposite sign in every case, which is a contradiction; hence, $\epsilon_2 = 0$.

For surface A, Fig. 4, substitution of $\epsilon_2 = 0$ in the flow equations, Table 1, corresponding to the two types of corner, gives

$$(1 - \sin\phi)\,\epsilon_1 + (1 + \sin\phi)\,\epsilon_3 = 0 \quad \ldots\ldots\ldots (30a)$$

when $\sigma_1 = \sigma_2 > \sigma_3$ and

$$(1 - \sin\phi')\ \epsilon_1 + (1 + \sin\phi')\ \epsilon_3 = 0 \quad \ldots\ldots\ldots (30b)$$

when $\sigma_1 > \sigma_2 = \sigma_3$. Examination of the plane stress cross section (not shown) reveals that Eq. 30(a) defines a vector lying between normals to adjacent flats providing $\phi \geq \phi'$ and Eq. 30(b) defines a similar vector providing $\phi \leq \phi'$. Substituting the stress conditions associated with Eqs. 30 in the equation for the yield surface given in Table 1 reduces the latter to

$$(1 + \sin\phi)\ \sigma_1 - (1 - \sin\phi)\ \sigma_3 = 2c \cos\phi \quad \ldots\ldots\ldots (31a)$$

when $\phi \geq \phi'$ and

$$(1 + \sin\phi')\ \sigma_1 - (1 - \sin\phi')\ \sigma_3 = 2c' \cos\phi' \quad \ldots\ldots\ldots (31b)$$

when $\phi \leq \phi'$. Thus, for plane strain, surface A reduces to Coulomb's criterion, the constants c and ϕ being used when $\phi \geq \phi'$ and c' and ϕ' when $\phi \leq \phi'$.

For surface B, Fig. 4, there is only one type of corner. Substituting the corresponding stress $\sigma_2 = \sigma_2^c$ in the yield criterion, Table 1, we obtain, after some reduction, an equivalent Coulomb yield criterion in which the effective values ϕ^* and c^* are defined by

$$\sin\phi^* = \frac{2(\sin\phi + \sin\phi')}{3 + \sin\phi - \sin\phi' + (\sin\phi \sin\phi')} \quad \ldots\ldots (32a)$$

and

$$\frac{c^*}{c} = 2\left(1 + \frac{\sin\phi'}{\sin\phi}\right)\left[\frac{1 - \sin\phi}{(3 + \sin\phi')(3 - \sin\phi)(1 - \sin\phi')}\right]^{1/2} \quad \ldots (32b)$$

For surface C, Fig. 4, the yield criterion in Table 1 reduces immediately to the Coulomb criterion when the value

$$\sigma_2 = \frac{\sigma_1 + \sigma_3}{2} \quad \ldots\ldots\ldots\ldots\ldots (33)$$

which holds at a corner, is substituted. This is as expected, because this value of σ_2 represents the state of simple shear for which the experimental data were available in the first place.

For surface D, Fig. 4, substitution of $\epsilon_2 = 0$ in the flow equations, Table 1, corresponding to the two types of corner, gives

$$(1 - \sin\phi)\ \epsilon_1 + (1 + 2\sin\phi)\ \epsilon_3 = 0 \quad \ldots\ldots\ldots (34a)$$

when $\sigma_1 = \sigma_2 > \sigma_3$ and

$$(1 - 2\sin\phi)\ \epsilon_1 + (1 + \sin\phi)\ \epsilon_3 = 0 \quad \ldots\ldots\ldots (34b)$$

when $\sigma_1 > \sigma_2 = \sigma_3$. Examination of the plane-stress cross section of the yield surface shows that Eq. 34a is inadmissible because it is not the normal to a supporting plane of the yield surface. Substituting $\sigma_2 = \sigma_3$ in the yield criterion, Table 1, an equivalent Coulomb yield criterion is obtained in which the effective values ϕ^{**} and c^{**} are defined by

$$\sin \phi^{**} = \frac{3 \sin \phi}{2 - \sin \phi} \quad \ldots\ldots\ldots\ldots (35a)$$

and

$$\frac{c^{**}}{c} = \frac{3}{2}\left[\frac{1 - 2 \sin \phi}{1 - \sin \phi}\right]^{1/2} \quad \ldots\ldots\ldots\ldots (35b)$$

As an alternative approach, the same effective values of c and ϕ for substitution in an equivalent Coulomb yield criterion can be found by comparing the corresponding flow equations given in Table 1.

All problems of plane strain have now been shown to reduce to equivalent problems formulated in terms of the Coulomb yield criterion. In the case of materials insensitive to mean stress, the parallel result is well known. However, it must be recalled that, in the presence of dilatation, the material is no longer in a state of simple shear and the argument used in the latter case is not applicable.

Plane-Strain Example.—Consider the identation of a half space by a long, rigid punch in the particular case when the tensile and compressive strengths have been measured and have been found to be consistent with the same constants in Coulomb's law, so that $\alpha = 1$. As stated by L. Prandtl,[13] the indentation pressure is

$$p = c \cot \phi \left(e^{\pi \tan^2 \phi} \tan^2\left(\frac{\pi}{4} + \frac{\phi}{2}\right) - 1\right) \quad \ldots\ldots\ldots (36)$$

Prandtl's solution is complete in the sense than an incipient velocity field can be associated with the stresses in the deformable zone, and the material can be shown to be necessarily rigid in the remainder of the half space.[14,15]

In plane strain, surface A, Fig. 4, reduces to the Coulomb criterion with the original constants c and ϕ, while surface B requires the new constants defined by Eq. 32 after setting $\phi' = \phi$. Surface C reduces to the Coulomb criterion with the original constants, and surface D requires the new constants defined in Eqs. 35.

Eq. 36 can be applied equally well using the modified values ϕ^* and c^* or ϕ^{**} and c^{**}, because the resultant stresses and velocities are consistent with the various yield surfaces of Fig. 4, in the plane-strain case. The resulting upper and lower bounds are shown in Fig. 5 for various ϕ, the range between

13 "Uber die Harte plastischer Korper," by L. Prandtl, Nachrichten von der Koniglichen Gesellschaft der Wissenschaften zu Gottingen, Mathematisch-Physikalische Klasse, 1920, p. 74.

14 "Mixed Boundary Value Problems in Soil Mechanics," by R. T. Shield, Quarterly of Applied Mathematics, Vol. 11, 1953, p. 61.

15 "Plastic Potential Theory and Prandtl Bearing Capacity Solution," by R. T. Shield, Transactions, ASME, Journal of Applied Mechanics, Vol. 21, 1954, p. 193.

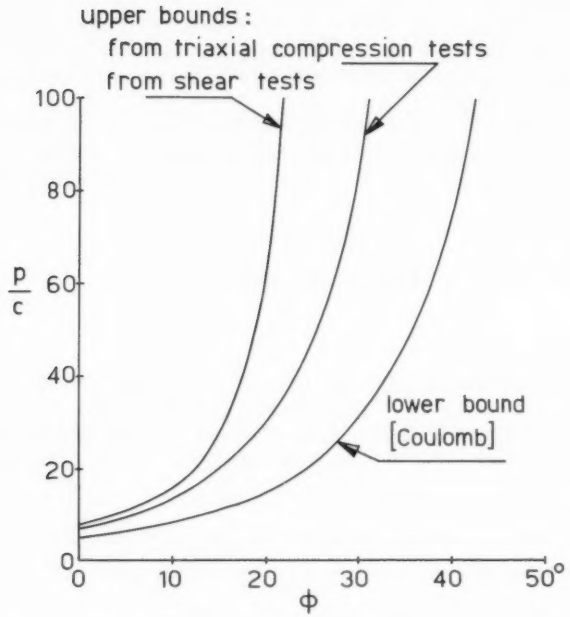

FIG. 5.—PUNCH INDENTATION (PLANE STRESS) FOR A MATERIAL SENSITIVE TO MEAN STRESS

the upper and lower curves representing the maximum variation in pressure that can occur with any convex, conical yield surface.

CONCLUSIONS

Certain yield criteria have been established as intrinsically suitable for engineering analysis because they lead to upper and lower bounds, as the case may be, without any reliance on a detailed knowledge of the actual yield criterion. All the criteria are piecewise linear, with the attendant simplifications of the analytical work that are well known.

It is perhaps worth emphasizing that results from a few tests may serve to define the yield criterion exactly, or nearly so, if the results fall close to one of the bounding criteria. If, for example, a metal develops yield strengths in tension, and torsion consistent with Tresca's criterion, no further testing is necessary to identify this as the correct criterion, providing there is sufficient other evidence to establish the metal as an ideally plastic material. A similar remark applies for the Coulomb criterion in the case of a material for which yield is a linear function of the main stress.

ACKNOWLEDGMENTS

This study was initiated in the course of work under contract AF 33(616)-6041 between the United States Air Force, Wright Air Development Division,

and The University of Michigan. The analysis for material sensitive to mean stress was completed in the course of work under contract DA-20-018-ORD-23276 between the United States Army Ordnance Corps, Land Locomotion Research Branch, and The University of Michigan, while the writer was at the University of Cambridge.

The contents of this paper formed the basis of a presentation before the Tenth International Congress of Applied Mechanics, in 1960, and an abstract, submitted in January, 1960, is to appear in the Proceedings of the Congress.

APPENDIX.—NOTATION

The following symbols, adopted for use in the paper, conform essentially with "Glossary of Terms and Definitions in Soil Mechanics," prepared by the Committee on Glossary of Terms and Definitions in Soil Mechanics of the Soil Mechanics and Foundations Division, Proceedings Paper 1826, October 1958:

b = radius of plate defined by Eq. 14;

c = cohesive stress computed from compression test;

c' = cohesive stress computed from extensional test;

c^*, c^{**} = effective values of cohesive stress;

D = energy dissipation;

f = yield function;

M_0 = yield moment per unit width of plate;

p = pressure intensity;

R = radius of plate;

r = cylindrical co-ordinate;

w = displacement;

z = cylindrical co-ordinate;

α = ϕ/ϕ';

β = b/R;

γ = shear strain;

ϵ = strain;

θ = cylindrical co-ordinate;

κ = curvature;

λ = positive constant;

ρ = r/R;

σ = stress;

τ = shear stress;

ϕ = angle of friction computed from compression test;

ϕ' = angle of friction computed from extensional test; and

ϕ^*, ϕ^{**} = effective values of angle of friction.

Journal of the
ENGINEERING MECHANICS DIVISION
Proceedings of the American Society of Civil Engineers

EFFECT OF JOINT ROTATION ON DYNAMICS OF STRUCTURES

By Moshe F. Rubinstein[1] and Walter C. Hurty[2]

SYNOPSIS

The results of a study on the effect of joint rotation on the dynamic characteristics of a multi-story steel-framed structure is analyzed under four levels of assumptions regarding joint rotations. The first ten normal modes and frequencies resulting from the analysis under each assumption are compared in figures and examined.

INTRODUCTION

The dynamic analysis of a multi-story rigid frame requires extensive numerical calculations. Because a multi-story framed structure normally consists of a number of such frames, the computational efforts increase greatly when a dynamic analysis of the entire strucutre is required. Therefore, it is desirable to introduce assumptions that will reduce the amount of computations, although result in a small sacrifice in accuracy.

One such assumption considers the mass of the building lumped, or concentrated, at the floor levels with three degrees of freedom of motion per floor with translation in two horizontal directions, and a rotation about a vertical axis. In the event that the foundation is not rigid enough to fix the building against rotation at the base, the building may also rotate about two horizontal axes.

Note.—Discussion open until May 1, 1962. To extend the closing date one month, a written request must be filed with the Executive Secretary, ASCE. This paper is part of the copyrighted Journal of the Engineering Mechanics Division, Proceedings of the American Society of Civil Engineers, Vol. 87, No. EM6.

[1] Asst. Prof. of Engrg., Univ. of California, Los Angeles, Calif.
[2] Prof. of Engrg., Univ. of California, Los Angeles, Calif.

An additional assumption, introduced by some investigators,[3] considers the girders of the building frames infinitely rigid, thus permitting no joint rotation and restricting the coupling between stories. This assumption simplifies the complex spring characteristics of the building frames. However, although lumping the mass at the floor levels is considered quite reasonable for a wide class of buildings, the assumption of infinitely rigid girders is questioned in the case of multi-story framed structures. The writer's experience is that in most cases the girders are far more flexible than the columns.

John E. Goldberg,[4] F. ASCE, proposed a dynamic analysis that assumes that all frame joints within a given floor undergo the same rotation.

Because computations are largely reduced by introducing restrictions on joint rotation, it is considered worthwhile to study the degree of accuracy sacrificed under such restrictions. The present paper is devoted to such a study. A nineteen-story steel-framed building is analyzed under four levels of assumptions regarding joint rotations. The dynamic analysis is carried out in one direction. The building consists of eight frames of three different types in that direction. Normal mode shapes and frequencies are computed under the following assumptions:

1. No joint rotation takes place (girders are assumed infinitely stiff).
2. All joints within a floor (for all frames) undergo an equal rotation.
3. All joints of a given type frame within a floor undergo an equal rotation.
4. No restriction on joint rotations.

The first ten modes and frequencies resulting from the analysis under each of the above assumptions are compared in figures. The analysis was carried out using the stiffness matrix approach.

METHOD OF ANALYSIS

Stiffness Matrix of a Rigid Frame.—Let all loads acting on a building frame be resolved into lateral loads, H_r, at the floor levels and moments, M_i, at the joints. The vector of loads $\begin{Bmatrix} M \\ H \end{Bmatrix}$ may be related to the corresponding vector of deformations $\begin{Bmatrix} \psi \\ y \end{Bmatrix}$ through a stiffness matrix

$$\begin{Bmatrix} M \\ H \end{Bmatrix} = [\rho] \begin{Bmatrix} \psi \\ y \end{Bmatrix} \quad \ldots\ldots\ldots\ldots\ldots\ldots (1)$$

in which $[\rho]$ is the stiffness matrix of the frame (see Appendix for the derivation of a stiffness matrix for a rigid frame), $\{\psi\}$ is the vector of joint rotations, and $\{y\}$ is the vector of floor displacements.

An element ρ_{ij} of the stiffness matrix $[\rho]$ has the following physical significance. It is the force required at i to permit a unit deformation at j only (no other deformation permitted). The terms force and deformation will mean lateral load or moment, and translation or rotation, respectively, as the case may be.

---

[3] "Earthquake Stresses in Shear Buildings," by M. G. Salvadori, Transactions, ASCE, Vol. 119, 1954, p. 171.

[4] "Forced Vibration and Natural Frequencies of Tall Building Frames," by J. E. Goldberg, J. L. Bogdanoff, and Z. L. Moh, Bulletin, Seismological Soc. of Amer., Vol. 49, January, 1959, p. 33.

With $[\rho]$ computed from the geometry of the frame and the properties of the sections and $\begin{Bmatrix} M \\ H \end{Bmatrix}$ established from the given loading conditions, the deformations may be solved for

$$\begin{Bmatrix} \psi \\ y \end{Bmatrix} = [\rho]^{-1} \begin{Bmatrix} M \\ H \end{Bmatrix} \quad \ldots\ldots\ldots\ldots\ldots\ldots (2)$$

in which $[\rho]^{-1}$ is the inverse of the stiffness matrix $[\rho]$.

Using the values of $\begin{Bmatrix} \psi \\ y \end{Bmatrix}$, all moments and shears for the individual frame members (columns and girders) may be computed.

Stiffness Matrix of a Frame with No External Joint Moments.—If the mass of the frame is concentrated at the floor levels and moving to the lateral direction, only lateral inertial forces result, and all inertial moments at the joints are zero, or

$$\{ M \} = \{ 0 \}$$

Substitute this moment value in Eq. 1 and partition the $[\rho]$ matrix to obtain

$$\begin{Bmatrix} 0 \\ \hline H \end{Bmatrix} = \left[\begin{array}{c:c} R_{11} & R_{12} \\ \hline R_{21} & R_{22} \end{array}\right] \begin{Bmatrix} \psi \\ y \end{Bmatrix} \quad \ldots\ldots\ldots\ldots\ldots (3)$$

Eq. 3 can be written in the form

$$\{ 0 \} = \left[R_{11} \right] \{ \psi \} + \left[R_{12} \right] \{ y \} \quad \ldots\ldots\ldots\ldots\ldots (4)$$

and

$$\{ H \} = \left[R_{21} \right] \{ \psi \} + \left[R_{22} \right] \{ y \} \quad \ldots\ldots\ldots\ldots\ldots (5)$$

From Eq. 4

$$\left[R_{11} \right] \{ \psi \} = - \left[R_{12} \right] \{ y \} \quad \ldots\ldots\ldots\ldots\ldots (6)$$

premultiply each side by $\left[R_{11} \right]^{-1}$ to yield

$$\{ \psi \} = - \left[R_{11} \right]^{-1} \left[R_{12} \right] \{ y \} \quad \ldots\ldots\ldots\ldots\ldots (7)$$

Substituting Eq. 7 in Eq. 5 yields

$$\{ H \} = \left(\left[R_{22} \right] - \left[R_{21} \right] \left[R_{11} \right]^{-1} \left[R_{12} \right] \right) \{ y \} \quad \ldots\ldots\ldots (8)$$

Let

$$[K] = \left(\left[R_{22} \right] - \left[R_{21} \right] \left[R_{11} \right]^{-1} \left[R_{12} \right] \right) \quad \ldots\ldots\ldots (9)$$

then

$$\{H\} = [K]\{y\} \quad \ldots\ldots\ldots\ldots\ldots\ldots (10)$$

in which [K] is the modified stiffness matrix of the frame under the assumption of no external moments at the joints. The order of matrix [K] is equal to the number of degrees of freedom in lateral motion.

It may be noted that the static analysis of the frame will still require the inversion of the $[\rho]$ matrix. However, now that $\left[R_{11}\right]^{-1}$ has been computed, it is worthwhile to take advantage of it and use the following relations for the inversion of a partitioned matrix.[5]

$$\text{For } [\rho] = \left[\begin{array}{c|c} R_{11} & R_{12} \\ \hline R_{21} & R_{22} \end{array}\right]$$

$$[\rho]^{-1} = \begin{bmatrix} R_{11}^{-1} + R_{11}^{-1} R_{12} B R_{21} R_{11}^{-1}, & -R_{11}^{-1} R_{12} B \\ -B R_{21} R_{11}^{-1} , & B \end{bmatrix} \quad \ldots\ldots (11)$$

in which

$$[B] = \left[R_{22} - R_{21} R_{11}^{-1} R_{12}\right]^{-1} \quad \ldots\ldots\ldots\ldots (12)$$

Lateral Stiffness Matrix of a Building.—A relation similar to Eq. 10 may be obtained for each frame of a building. Thus, for frames I and II in Fig. 1(b)

$$\{H_x\}_I = \left[K_I\right]\{x\}_I \quad \ldots\ldots\ldots\ldots\ldots (13a)$$

and

$$\{H_x\}_{II} = \left[K_{II}\right]\{x\}_{II} \quad \ldots\ldots\ldots\ldots\ldots (13b)$$

For the symmetrical building of Fig. 1(b)

$$\{x\} = \{x\}_I = \{x\}_{II} \quad \ldots\ldots\ldots\ldots\ldots (14)$$

in which $\{x\}$ is the vector of floor deformations in the x direction. Because there are two frames of each type, the vector of lateral forces $\{H_x\}$ for the building is

$$\{H_x\} = 2\{H_x\}_I + 2\{H_x\}_{II} \quad \ldots\ldots\ldots\ldots\ldots (15)$$

---

5 "Linear Structural Analysis," by P. B. Morice, Ronald Press, New York, 1959, p. 10,67.

Substitute $\{H_x\}_I$ and $\{H_x\}_{II}$ from Eq. 13 and using Eq. 14 yields

$$\{H_x\} = \left[2\ K_I + 2\ K_{II}\right]\{x\} \quad \ldots\ldots\ldots\ldots\ldots (16)$$

or

$$\{H_x\} = [K^*]\{x\} \quad \ldots\ldots\ldots\ldots\ldots (17)$$

in which elements of $[K^*]$ are obtained from the elements of $\left[K_I\right]$ and $\left[K_{II}\right]$

$$k^*_{ij} = 2\left\{(k_{ij})_I + (k_{ij})_{II}\right\} \quad \ldots\ldots\ldots\ldots\ldots (18)$$

The term $[K^*]$ is the modified stiffness matrix for the building in lateral motion in the x direction.

The Eigenvalue Problem.—In the building of Fig. 1, the mass concentrated at any floor r is denoted by m_r.

According to D'Alembert's principle, the inertial force associated with an acceleration of $\ddot{x}_r$ of m_r is

$$H_{x,r} = -\ m_r\ \ddot{x}_r \quad \ldots\ldots\ldots\ldots\ldots (19)$$

Postulating harmonic motion with angular frequency ω

$$\ddot{x}_r = -\ \omega^2\ x_r \quad \ldots\ldots\ldots\ldots\ldots (20)$$

Substitute Eq. 20 in Eq. 19

$$H_{x,r} = \omega^2\ m_r\ x_r \quad \ldots\ldots\ldots\ldots\ldots (21)$$

Writing Eq. 21 for each floor mass, the resulting set of equations becomes, in matrix form,

$$\{H_x\} = \omega^2\ \lceil m \rfloor\{x\} \quad \ldots\ldots\ldots\ldots\ldots (22)$$

in which $\lceil\ \rfloor$ designates a matrix with elements on the principal diagonal only.

From Eqs. 17 and 22

$$[K^*]\{x\} = \omega^2\ \lceil m \rfloor\{x\} \quad \ldots\ldots\ldots\ldots\ldots (23)$$

premultiply each side of Eq. 23 by $\lceil m \rfloor^{-1}$

$$\lceil m \rfloor^{-1}\ [K^*]\{x\} = \omega^2\ \{x\} \quad \ldots\ldots\ldots\ldots\ldots (24)$$

Let

$$[D] = \lceil m \rfloor^{-1}\ [K^*] \quad \ldots\ldots\ldots\ldots\ldots (25)$$

Eq. 24 then becomes

$$[D]\{x\} = \omega^2 \{x\} \quad \ldots\ldots\ldots\ldots\ldots\ldots (26)$$

or

$$\left([D] - \omega^2 [U]\right)\{x\} = \{0\} \quad \ldots\ldots\ldots (27)$$

in which [U] is the unit matrix.

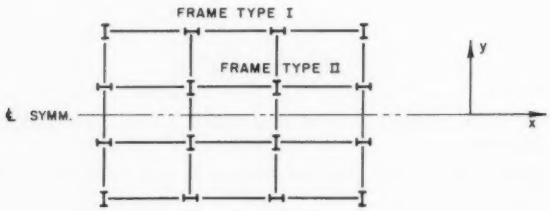

(b) Typical Floor Plan

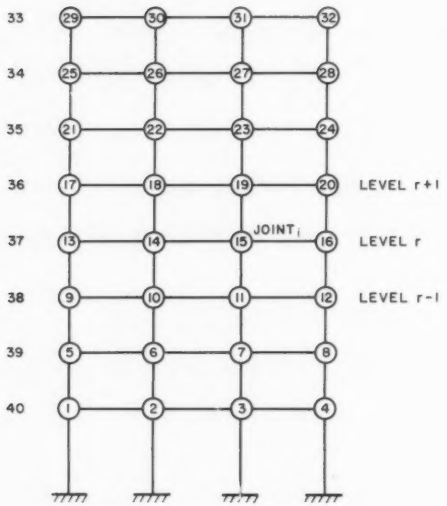

(a) Schematic Elevation of Frame I

FIG. 1

Eq. 25 represents the formulation of the classical eigenvalue problem. For a non-trivial solution $\{x\} \neq \{0\}$, the determinant, Δ, of the term within the brackets ( ) in Eq. 27 must vanish

$$\Delta = 0 \quad \ldots\ldots\ldots\ldots\ldots\ldots (28)$$

For tall multi-story buildings, Eq. 28 is a high order equation in ω. Thus, a trial and error solution is resorted to, or the iteration technique[6] may be used to solve Eq. 27. The non-trivial solution of Eq. 27 yields the natural frequencies and mode shapes of the building.

ASSUMPTIONS REGARDING JOINT ROTATIONS

No Restriction of Joint Rotation.—Consider the stiffness matrix

$$[\rho] = \left[\begin{array}{c|c} R_{11} & R_{12} \\ \hline R_{21} & R_{22} \end{array}\right] \quad \ldots\ldots\ldots\ldots\ldots (29)$$

for the frame of Fig. 1(a). R_{11} is a square matrix of order 32 equal to the number of degrees of freedom in joint rotations. R_{22} is a square matrix of order 8 equal to the number of degrees of freedom in horizontal translation. R_{12} and R_{21} (the coupling matrices) are of order 32-by-8 and 8-by-32, respectively.

The computations leading to the modified stiffness matrix [K] of the frame (Eq. 9)

$$[K] = \left(\left[R_{22}\right] - \left[R_{21}\right] \left[R_{11}\right]^{-1} \left[R_{12}\right] \right) \quad \ldots\ldots\ldots (9)$$

require the inversion of a matrix of order 32 $\left(\left[R_{11}\right] \right)$ when no restriction is placed on joint rotation.

No Joint Rotation Takes Place.—Substitute $\{ \psi \} = 0$ in Eq. 5 to obtain

$$\{ H \} = \left[R_{22}\right] \{ x \} \quad \ldots\ldots\ldots\ldots\ldots\ldots (30)$$

The modified stiffness matrix [K] is given by

$$[K] = \left[R_{22}\right] \quad \ldots\ldots\ldots\ldots\ldots\ldots (31)$$

and no matrix inversion is required.

All Joints of a Frame Within a Given Level r Undergo an Equal Rotation, ψ_r.—In Eq. 1 for frame I [Fig. 1(a)]

---

6 "Dynamics of Framed Structures," by G. L. Rogers, John Wiley and Sons, New York, 1959, p. 130.

$$\begin{pmatrix} M_1 \\ M_2 \\ M_3 \\ M_4 \\ M_5 \\ \vdots \\ M_{32} \\ \hline H_{33} \\ \vdots \\ H_{40} \end{pmatrix} = \left[\begin{array}{cccc|c|c} \rho_1, 1 & \rho 1,2 & \rho 1,3 & \rho 1,4 & \cdots \rho 1,32 & \rho 1,33 \cdots \rho 1,40 \\ \rho 2, 1 & & & & & \\ \rho 3, 1 & & & & & \\ \rho 4, 1 & \cdots & & \rho 4,4 & & \\ \hline \multicolumn{4}{c|}{} & & \\ \multicolumn{4}{c|}{} & & \\ \multicolumn{4}{c|}{} & & \\ \multicolumn{4}{c|}{} & & \\ \rho 32,1 & & & & \rho 32,32 & \\ \hline \multicolumn{4}{c|}{} & & \\ \multicolumn{4}{c|}{} & R_{22} & \\ \multicolumn{4}{c|}{} & & \end{array}\right] \begin{pmatrix} \psi_1 \\ \psi_2 \\ \psi_3 \\ \psi_4 \\ \psi_5 \\ \vdots \\ \psi_{32} \\ \hline X_{33} \\ X_{34} \\ \vdots \\ X_{40} \end{pmatrix}$$

set

$$\left.\begin{array}{lll} \phi_1 = \psi_i & \text{for} & i = 1, 2, 3, 4 \\ \phi_2 = \psi_i & \text{for} & i = 5, 6, 7, 8 \\ \vdots & \vdots & \vdots \\ \phi_8 = \psi_i & \text{for} & i = 29, 30, 31, 32 \end{array}\right\} \quad \cdots\cdots\cdots\cdots (32)$$

and

$$\left.\begin{array}{l} M_1^* = \sum_{i=1}^{4} M_i \\ M_2^* = \sum_{i=5}^{8} M_i \\ \vdots \\ M_8^* = \sum_{i=29}^{32} M_i \end{array}\right\} \quad \cdots\cdots\cdots\cdots\cdots\cdots (33)$$

Using Eqs. 32 in Eq. 1, Eqs. 33 become

$$
\left.
\begin{aligned}
M_1^* &= \phi_1 \sum_{i=1}^{4}\sum_{j=1}^{4} \rho_{ij} + \phi_2 \sum_{i=1}^{4}\sum_{j=5}^{8} \rho_{ij} + \ldots + \phi_8 \sum_{i=1}^{4}\sum_{j=29}^{32} \rho_{ij} \\
&\quad + x_{33} \sum_{i=1}^{4} \rho_{i,33} + x_{34} \sum_{i=1}^{4} \rho_{i,34} + \ldots + x_{40} \sum_{i=1}^{4} \rho_{i,40} \\
M_2^* &= \phi_1 \sum_{i=5}^{8}\sum_{j=1}^{4} \rho_{ij} + \phi_2 \sum_{i=5}^{8}\sum_{j=5}^{8} \rho_{ij} + \ldots + \phi_8 \sum_{i=5}^{8}\sum_{j=29}^{32} \rho_{ij} \\
&\quad + x_{33} \sum_{i=5}^{8} \rho_{i,33} + x_{34} \sum_{i=5}^{8} \rho_{i,34} + \ldots + x_{40} \sum_{i=5}^{8} \rho_{i,40} \\
&\vdots \\
M_8^* &= \phi_1 \sum_{i=29}^{32}\sum_{j=1}^{4} \rho_{ij} + \phi_2 \sum_{i=29}^{32}\sum_{j=5}^{8} \rho_{ij} + \ldots + \phi_8 \sum_{i=29}^{32}\sum_{j=29}^{32} \rho_{ij} \\
&\quad + x_{33} \sum_{i=29}^{32} \rho_{i,33} + x_{34} \sum_{i=29}^{32} \rho_{i,34} + \ldots + x_{40} \sum_{i=29}^{32} \rho_{i,40}
\end{aligned}
\right\} \quad \ldots \text{(34a)}
$$

Similarly, the lateral loads H_i, $i = 33, 34, \ldots, 40$, become

$$
\left.
\begin{aligned}
H_{33} &= \phi_1 \sum_{j=1}^{4} \rho_{33,j} + \phi_2 \sum_{j=5}^{8} \rho_{33,j} + \ldots + \phi_8 \sum_{j=29}^{32} \rho_{33,j} + \sum_{j=33}^{40} \rho_{33,j}\, x_j \\
H_{34} &= \phi_1 \sum_{j=1}^{4} \rho_{34,j} + \phi_2 \sum_{j=5}^{8} \rho_{34,j} + \ldots + \phi_8 \sum_{j=29}^{32} \rho_{34,j} + \sum_{j=33}^{40} \rho_{34,j}\, x_j \\
&\vdots \\
H_{40} &= \phi_1 \sum_{j=1}^{4} \rho_{40,j} + \phi_2 \sum_{j=5}^{8} \rho_{40,j} + \ldots + \phi_8 \sum_{j=29}^{32} \rho_{40,j} + \sum_{j=33}^{40} \rho_{40,j}\, x_j
\end{aligned}
\right\} \quad \ldots \text{(34b)}
$$

In matrix form Eqs. 34a and 34b become

$$\begin{Bmatrix} M^* \\ H \end{Bmatrix} = [\rho^*] \begin{Bmatrix} \phi \\ x \end{Bmatrix} \quad \ldots\ldots\ldots\ldots\ldots\ldots (35)$$

in which

$$[\rho^*] = \left[\begin{array}{c|c} R^*_{11} & R^*_{12} \\ \hline R^*_{21} & R_{22} \end{array}\right] \quad \ldots\ldots\ldots\ldots\ldots\ldots (36)$$

The elements of R^*_{11}, R^*_{12}, R^*_{21} are identified from Eqs. 34, and are obtained by adding blocks of ρ_{ij} coefficients in the original stiffness matrix $[\rho]$ (Eq. 1). The elements of R_{22} are the same as the corresponding elements of $[\rho]$. R^*_{11}, R^*_{12}, R^*_{21}, R_{22} are each of order 8-by-8, consequently a matrix of order 8-by-8 $\left[R^*_{11}\right]$ is inverted in computing [K] from Eq. 9.

If the building under consideration consists of a number of different type frames, one matrix of order 8-by-8 must be inverted in computing the stiffness matrix [K] for each frame. A linear combination of the elements k_{ij} of the [K] matrices for the different frames types will yield the lateral stiffness matrix for the building. (For example, Eq. 18 for the building of Fig. 1.)

All Joints Within a Floor (for all frames) Undergo an Equal Rotation.—An equation similar to Eq. 35 can be written for each frame in a building.

For instance, for frames I and II of Fig. 1(b),

$$\begin{Bmatrix} M^* \\ H \end{Bmatrix}_I = [\rho^*]_I \begin{Bmatrix} \phi \\ x \end{Bmatrix} \quad \ldots\ldots\ldots\ldots\ldots\ldots (37)$$

and

$$\begin{Bmatrix} M^* \\ H \end{Bmatrix}_{II} = [\rho^*]_{II} \begin{Bmatrix} \phi \\ x \end{Bmatrix} \quad \ldots\ldots\ldots\ldots\ldots\ldots (38)$$

Add Eqs. 35 and 38

$$\begin{Bmatrix} M^*_I + M^*_{II} \\ H_I + H_{II} \end{Bmatrix} = \left[\rho^*_I + \rho^*_{II}\right] \begin{Bmatrix} \phi \\ x \end{Bmatrix} \quad \ldots\ldots\ldots\ldots\ldots\ldots (39)$$

Let

$$[\gamma] = 2\left[\rho^*_I + \rho^*_{II}\right] \quad \ldots\ldots\ldots\ldots\ldots\ldots (40)$$

and

$$\begin{Bmatrix} M^* \\ H \end{Bmatrix} = 2 \begin{Bmatrix} M_I^* + M_{II}^* \\ H_I + H_{II} \end{Bmatrix} \quad \ldots\ldots\ldots\ldots\ldots\ldots (41)$$

then Eq. 39 becomes

$$\begin{Bmatrix} M^* \\ H \end{Bmatrix} = [\gamma] \begin{Bmatrix} \phi \\ x \end{Bmatrix} \quad \ldots\ldots\ldots\ldots\ldots\ldots (42)$$

$[\gamma] = \left[\begin{array}{c|c} \gamma_{11} & \gamma_{12} \\ \hline \gamma_{21} & \gamma_{22} \end{array}\right]$ is the stiffness matrix in the x direction for the entire building of Fig. 1. The modified stiffness matrix for the entire building under the assumption of no external joint moments is obtained from Eq. 9.

$$[K] = \left([\gamma_{22}] - [\gamma_{21}] [\gamma_{11}]^{-1} [\gamma_{12}] \right) \quad \ldots\ldots\ldots (9)$$

For the building of Fig. 1, matrices $\gamma_{11}, \gamma_{12}, \gamma_{21}$ and γ_{22} are each at order 8-by-8. Thus only one matrix of order equal to the number of floors in the building must be inverted in order to compute the modified stiffness matrix.

NORMAL MODES AND FREQUENCIES OF 19-STORY BUILDING

Preliminary Considerations.—The nineteen-story building of Figs. 2 and 3 is a rigid frame steel structure. The column and girder sections are indicated in Fig. 3. The structural properties of the framed members have been tabulated by the American Institute of Steel Construction (AISC).[7] The floors are constructed of 6 in. concrete slabs. Exterior walls and interior partitions are lightweight construction. The floor slabs are regarded as infinitely rigid in their own plane so that no girder change in length takes place. The building rests on rigid ground, and the columns are fixed against rotation at the first floor level. No foundation settlement occurs. The mass of the building is lumped at the floor levels.

The weight of a typical story $w_r = 1{,}235{,}200$ lb. The mass lumped at a typical floor (third through nineteenth inclusive)

$$m_r = \frac{w_r}{g} = 38.4 \ \frac{\text{kip-sec}^2}{\text{ft}}$$

$$r = 3, 4, 5, \ldots, 19$$

in which g = 32.2 ft per sec^2 is the acceleration due to gravity.

The second floor mass, including the mezzanine, and the twentieth floor mass, including the mechanical equipment, are each equivalent to 1.5 times the typical floor mass.

$$m_2 = m_{22} = 1.5 \ m_{\text{typical floor}}$$

---

[7] "Steel Construction," Amer. Inst. of Steel Constr., New York, 5th edition, 1947.

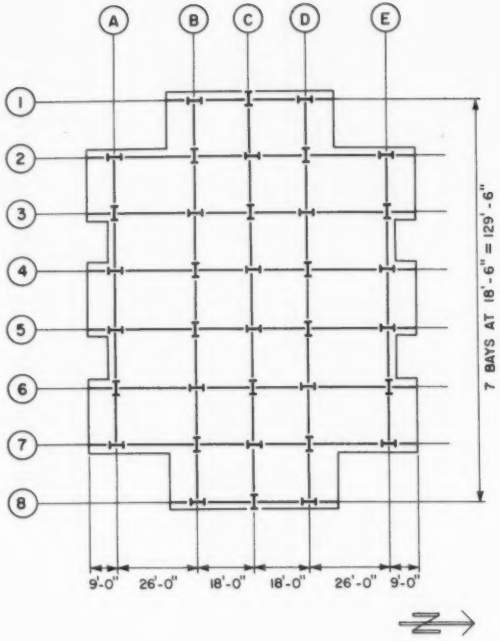

FIG. 2.—FLOOR PLAN OF A MULTI-STORY FRAMED STRUCTURE

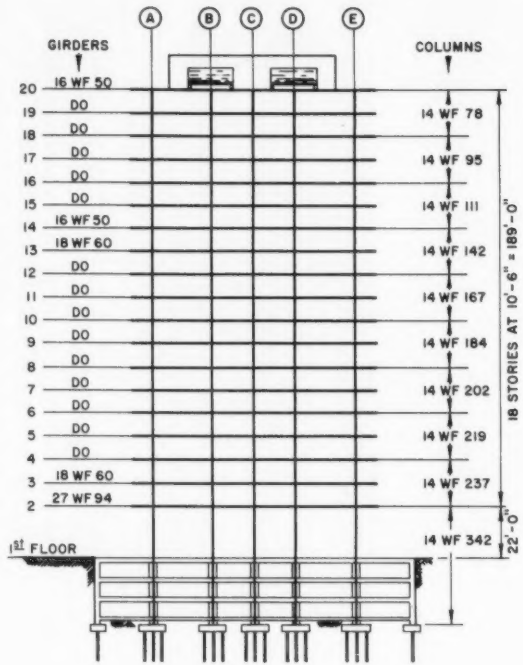

FIG. 3.—SCHEMATIC ELEVATION SHOWING COLUMN AND GIRDER SECTIONS OF A MULTI-STORY FRAMED STRUCTURE

The mass matrix $\lceil m \rfloor$ of the building then becomes

$$\lceil m \rfloor = \begin{bmatrix} 1.5 & & & & & & & & & & & & & & & & & & \\ & 1 & & & & & & & & & & & & & & & & & \\ & & 1 & & & & & & & & & & & & & & & & \\ & & & 1 & & & & & & & & & & & & & & & \\ & & & & 1 & & & & & & & & & & & & & & \\ & & & & & 1 & & & & & & & & & & & & & \\ & & & & & & 1 & & & & & & & & & & & & \\ & & & & & & & 1 & & & & & & & & & & & \\ & & & & & & & & 1 & & & & & & & & & & \\ & & & & & & & & & 1 & & & & & & & & & \\ & & & & & & & & & & 1 & & & & & & & & \\ & & & & & & & & & & & 1 & & & & & & & \\ & & & & & & & & & & & & 1 & & & & & & \\ & & & & & & & & & & & & & 1 & & & & & \\ & & & & & & & & & & & & & & 1 & & & & \\ & & & & & & & & & & & & & & & 1 & & & \\ & & & & & & & & & & & & & & & & 1 & & \\ & & & & & & & & & & & & & & & & & 1.5 & \end{bmatrix} \quad \ldots\ldots\ldots\ldots (43)$$

The dynamic analysis is carried out in the north-south direction. In this direction, the building consists of 8 frames (Fig. 2) of three different types. Frames on lines 1 and 8 are of one type, frames on lines 3 and 6 of a second type, and frames on lines 2, 4, 5, and 7 of a third type.

The normal modes and frequencies of the building in the north-south direction are computed for the following:

Case a. No joint rotation takes place (girders are assumed infinitely rigid).

Case b. All joints within a floor (for all frames) undergo an equal rotation.

Case c. All joints of a given type frame within a floor undergo an equal rotation.

Case d. No restriction on joint rotation.

Using Eq. 24 or Eq. 27 the mass matrix $\lceil m \rfloor$ of Eq. 43 is inverted in each case. This is, of course, a trivial matter because $\lceil m \rfloor$ is a diagonal matrix. No additional matrix inversion is required in the computations for Case a. A matrix of order 19 is inverted in the computations for Case b. Three matrices (one for each frame type) of order 19 are inverted in the computations for Case c. Two matrices of order 95 and one of order 57 are inverted in the computations for Case d. This is required because the interior type frames contain 95 joints each, and the exterior type frames contain 57 joints each. Only joints free to rotate are counted.

In all four cases, the normal modes and corresponding frequencies are obtained through the solution of an eigenvalue problem of order 19, equal to the number of degrees of freedom of motion of the building in the north-south direction. The natural frequencies are computed by trial and error from Eq. 28. For each frequency the corresponding mode shape is computed from Eq. 27.

All computations were done with the aid of an IBM 709 computer. Computation time for Case a was 2.39 min; for Case b, 2.64 min; for Case c, 2.69 min; and for Case d, 22.84 min.

RESULTS AND CONCLUSIONS

The first ten mode shapes and frequencies of the building computed for cases a, b, c, and d are compared in Figs. 4 through 13. The mode shapes of cases b, c, and d are so close that they are plotted as a single curve in the figures. Frequencies and frequency ratios are compared in Table 1.

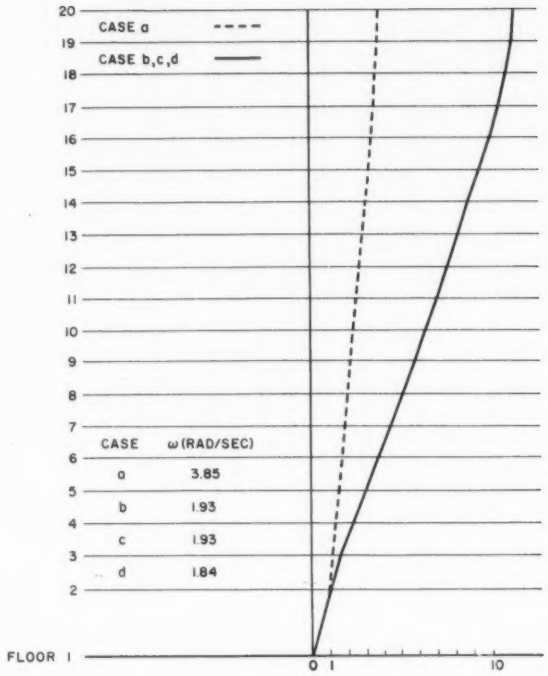

FIG. 4.—FIRST MODE SHAPES FOR THE STRUCTURE OF FIGURES 2, 3

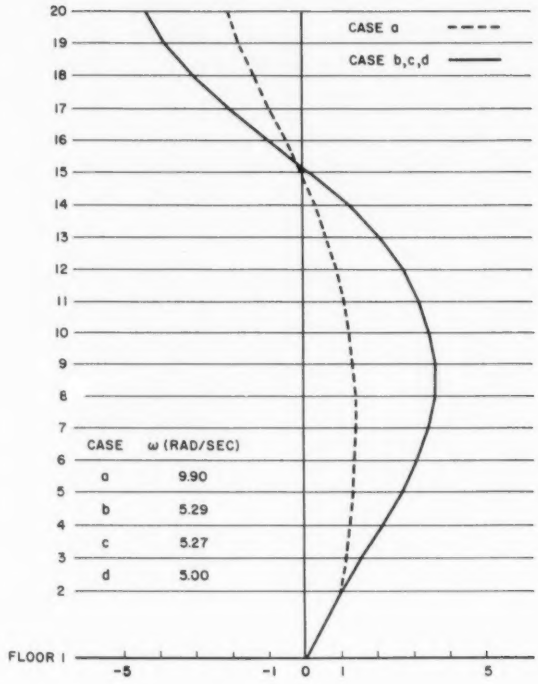

FIG. 5.—SECOND MODE SHAPES FOR THE STRUCTURE OF FIGURES 2, 3

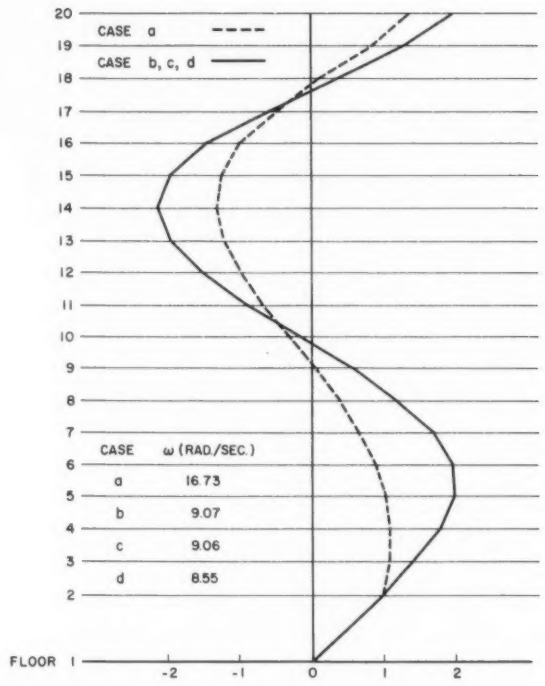

FIG. 6.—THIRD MODE SHAPES FOR THE STRUCTURE OF FIGURES 2, 3

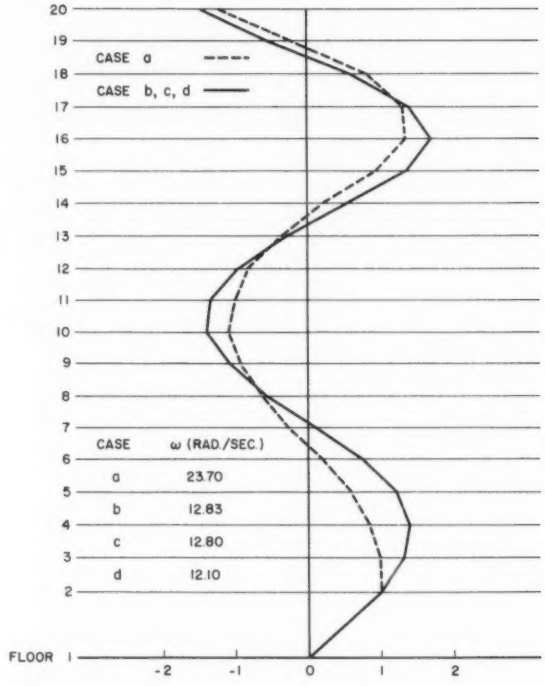

FIG. 7.—FOURTH MODE SHAPES FOR THE STRUCTURE OF FIGURES 2, 3

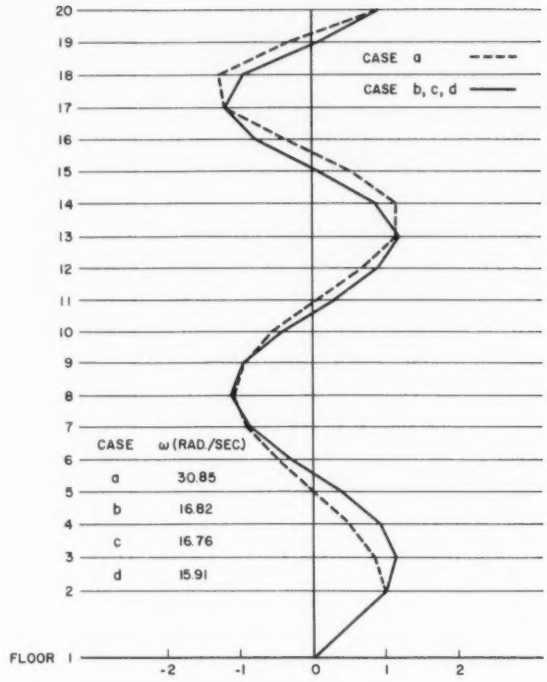

FIG. 8.—FIFTH MODE SHAPES FOR THE STRUCTURE OF FIGURES 2, 3

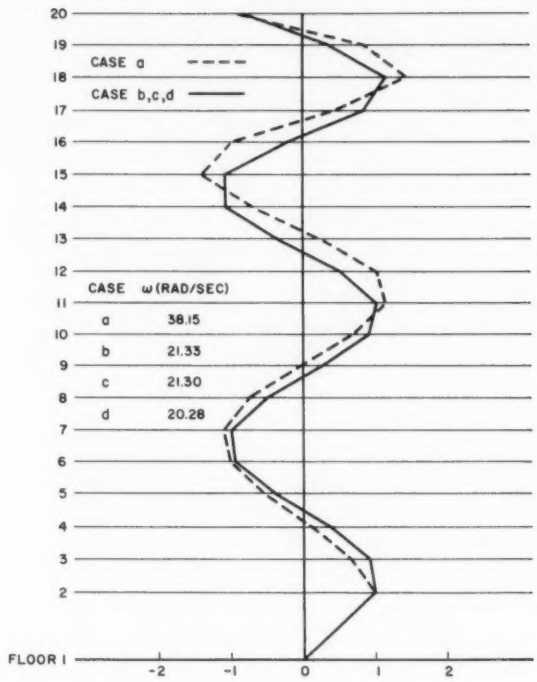

FIG. 9.—SIXTH MODE SHAPES FOR THE STRUCTURE OF FIGURES 2, 3

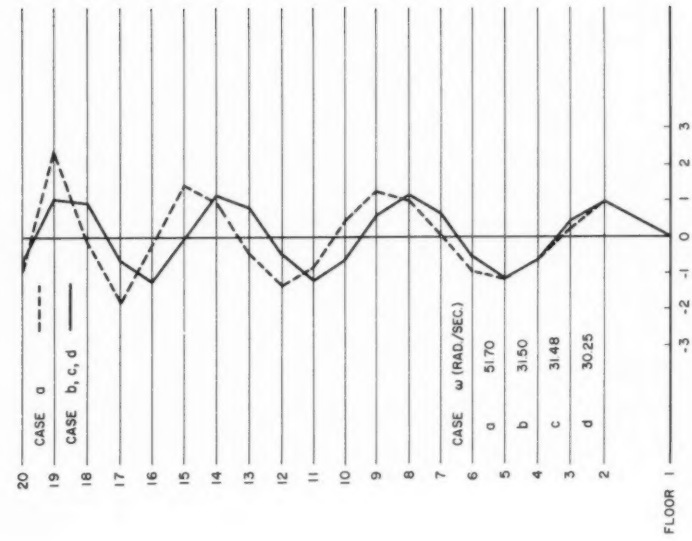

FIG. 11.—EIGHTH MODE SHAPES FOR THE STRUCTURE OF FIGURES 2, 3

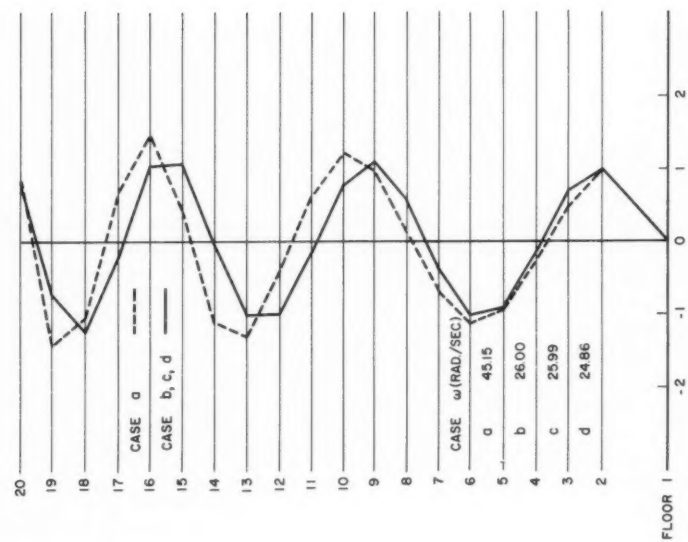

FIG. 10.—SEVENTH MODE SHAPES FOR THE STRUCTURE OF FIGURES 2, 3

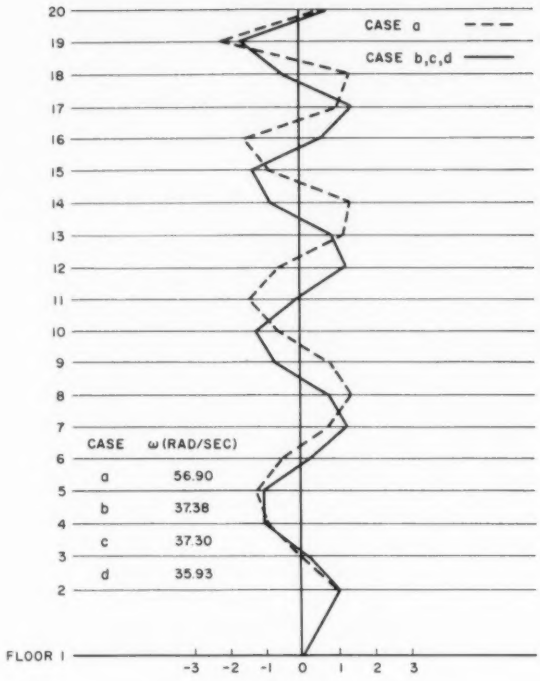

FIG. 12.—NINTH MODE SHAPES FOR THE STRUCTURE OF FIGURES 2, 3

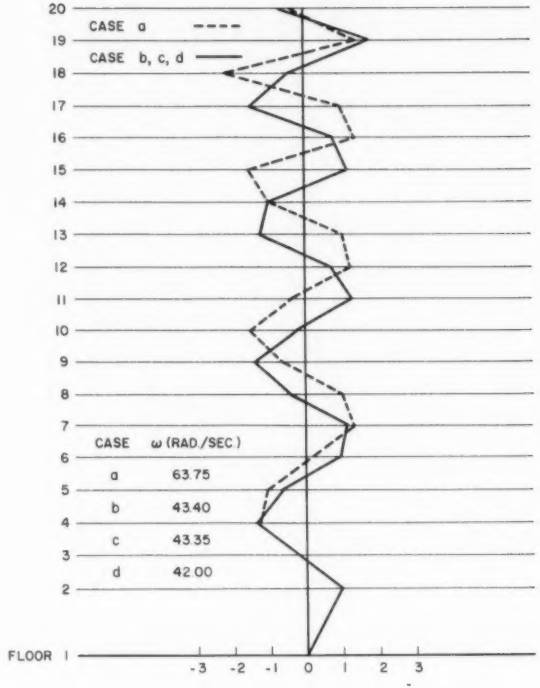

FIG. 13.—TENTH MODE SHAPES FOR THE STRUCTURE OF FIGURES 2, 3

Mode shapes for case a differ from those of case d. The difference is most pronounced in the first, second, and third modes. This is expected, because the effect of joint rotation diminishes in the higher modes; it is conceivable that the joints in a given floor may not rotate at all in a high mode.

The frequencies for case a differ from the corresponding frequencies of case d. The deviation is largest in the first natural frequency (109%). Deviations become smaller for the higher frequencies, as the effect of joint rotation diminishes.

The frequencies for cases b and c are the same, for all practical purposes. This is explained by the fact that the largest difference in joint behavior is between exterior and interior joints. Once this difference is reconciled by assuming an equal rotation for the joints within a floor, it makes little difference whether this rotation is considered an average joint rotation per floor for a single frame type, or for all frames.

The deviations of the frequencies computed for cases b and c from those computed for d are in the order of 3% to 6% for the first ten modes, with the deviation decreasing for the higher frequencies.

TABLE 1.—FREQUENCIES AND FREQUENCY RATIOS FOR THE STRUCTURE OF FIGS. 2 AND 3

Mode Number	Frequencies (Radians per Second)				Frequency Ratios		
	ω_a Case a	ω_b Case b	ω_c Case c	ω_d Case d	$\frac{\omega_a}{\omega_d}$	$\frac{\omega_b}{\omega_d}$	$\frac{\omega_c}{\omega_d}$
1	3.85	1.93	1.93	1.84	2.09	1.05	1.05
2	9.90	5.29	5.27	5.00	1.98	1.06	1.05
3	16.73	9.07	9.06	8.55	1.96	1.06	1.06
4	23.70	12.83	12.80	12.10	1.96	1.06	1.06
5	30.85	16.82	16.76	15.91	1.94	1.06	1.05
6	38.15	21.33	21.30	20.28	1.88	1.05	1.05
7	45.15	26.00	25.99	24.86	1.82	1.05	1.05
8	51.70	31.50	31.48	30.25	1.71	1.04	1.04
9	56.90	37.38	37.30	35.93	1.58	1.04	1.04
10	63.75	43.50	43.35	42.00	1.52	1.03	1.03

The frequencies computed for case a are consistently largest in value; those computed for case d are smallest in value; and frequencies of cases b and c lie between these two extremes. This is expected, because frequency increases with stiffness. In case a, the assumption of rigid joints attributes a high stiffness to the structure; consequently, high frequencies are obtained. In cases b, c, and d, the assumption of rigid joints is progressively relaxed, and, consequently, the computed frequencies are reduced in value progressively from case a to b to c to d (see Table 1). All mode shapes and frequencies were computed to an accuracy of six significant figures.

In comparing the results of cases a, b, and c with those of case d, it is concluded that the assumption of no joint rotation results in mode shapes and frequencies, with a discrepancy in the order of 100% for the lower frequencies. Cases b and c yield very satisfactory results, with only a 5% to 6% discrepancy for the low modes. Because case b requires less computations than case c, and the results obtained for these two cases are practically the same, it is

suggested that the assumption of equal joint rotation for all joints within a floor be introduced in computing the dynamic characteristics of a multi-story framed structure. This considerably reduces the computational efforts or computer time (a reduction of about 900% in the example in this paper) with a rather small sacrifice in accuracy of results (6%).

All computations in this paper were carried out with the aid of the IBM 709 computer at the Western Data Processing Center, University of California, Los Angeles, Calif. Without the aid of the computer, this study would not have been undertaken.

APPENDIX.—DERIVATION OF THE STIFFNESS MATRIX $[\rho]$ FOR A RIGID FRAME

Consider Fig. 14. Fig. 14(c) is a linear combination of Figs. 14(a) and 14(b). The member ik is moved as a rigid body from position ik to il and then a unit rotation is applied in the clockwise direction to each end. The stiffness, K_{ik}, of member ik at end i is defined as the moment required at end i to rotate that end through a unit rotation with end k restrained against rotation. The carry-over factor, C_{ik}, at end i is defined as the ratio of the moment induced at end k to the moment applied at end i, when end i is free to rotate and end k is fixed. K_{ki} and C_{ki} for end k of member ik are defined in a similar way.

In deriving the stiffness matrix for a rigid frame, such as shown in Fig. 1(b), three assumptions are introduced here:

1. There is no change in length of columns or girders.
2. There is no settlement of frame supports.
3. Joints are rigid; namely, all ends of members framing into a joint rotate an amount equal to the joint rotation.

The total number of degrees of freedom of motion of the frame is then equal to the total number of joints and horizontal girder lines (floor levels) in the frame.

To obtain the stiffness matrix for the frame, it is necessary to calculate the forces required to permit a unit deformation of a single joint or floor at one time.

Forces Required to Permit a Unit Rotation at a Frame Joint.—Apply a unit rotation at joint i = 5 (Fig. 15), with all other joints and floors restrained. From the definition of stiffness of a member, the carry-over factor, and an element ρ_{ik} of the stiffness matrix, it follows that

$$\rho_{ii} = M_i = \sum_k K_{ik} \quad \ldots\ldots\ldots\ldots\ldots\ldots (44)$$

and

$$\rho_{ki} = M_k = C_{ik}\ K_{ik} \quad \ldots\ldots\ldots\ldots\ldots\ldots (45)$$

in which

$$k = 4, 8, 6, 2$$

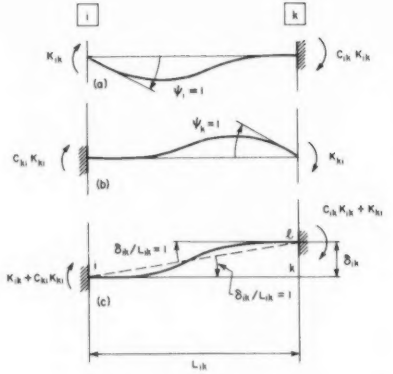

FIG. 14.—FRAME MEMBER SUBJECTED TO UNIT DEFORMATIONS

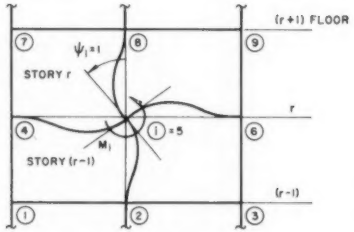

FIG. 15.—UNIT ROTATION APPLIED AT A FRAME JOINT

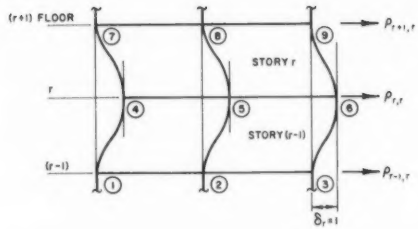

FIG. 16.—UNIT LATERAL DISPLACEMENT APPLIED AT A FRAME FLOOR

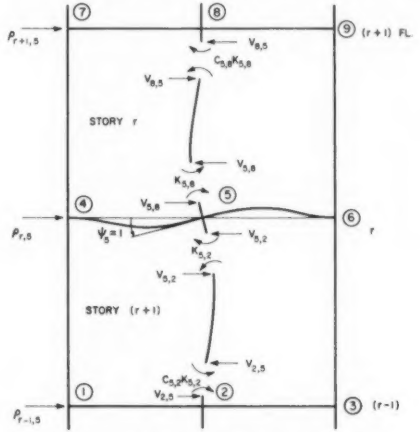

FIG. 17.—LATERAL FORCES DUE TO UNIT ROTATION

To calculate the restraining forces at the (r - 1), r, and (r+1) floors of Fig. 15, consider Fig. 17. From elementary equilibrium conditions for columns 5, 8 and 5, 2, and the frame

$$\rho_{r+1,5} = V_{8,5} = K_{5,8} \frac{1 + C_{5,8}}{L_{5,8}} \quad \ldots\ldots\ldots\ldots (46)$$

$$\rho_{r-1,5} = - V_{5,2} = - K_{5,2} \frac{1 + C_{5,2}}{L_{5,2}} \quad \ldots\ldots\ldots (47)$$

and

$$\rho_{r,5} = - \left(\rho_{r+1,5} + \rho_{r-1,5}\right) \quad \ldots\ldots\ldots\ldots (48)$$

Forces Required to Permit a Unit Lateral Deformation Along a Girder Line.— Apply a unit lateral deformation at level r of Fig. 16 with all other floors and joints restrained. At end 8 of column 5, 8

$$\rho_{8,r} = M_{8,5} = - K_{8,5} \left(1 + C_{8,5}\right) \quad \ldots\ldots\ldots\ldots (49)$$

[see Fig. 14(c)]. Similarly

$$\rho_{2,r} = M_{2,5} = - K_{2,5} \left(1 + C_{2,5}\right) \quad \ldots\ldots\ldots\ldots (50)$$

and finally

$$\rho_{5,r} = - \left(M_{5,8} + M_{5,2}\right) = - \left[K_{5,8} \left(1 + C_{5,8}\right) + K_{5,2} \left(1 + C_{5,2}\right)\right] \quad \ldots (51)$$

Similar expressions can be written for ρ_{kr} in which k = 1,3,4,6,7,9 (see Fig. 16).

To obtain $\rho_{r+1,r}$ of Fig. 16, equate it to the r^{th} story shear:

$$\rho_{r+1,r} = \sum \frac{M_{ik} + M_{ki}}{L_{ik}} \quad \ldots\ldots\ldots\ldots\ldots (52)$$

in which the summation extends over all columns ik in the r^{th} story.

Similarly,

$$\rho_{r-1,r} = \sum \frac{M_{ik} + M_{ki}}{L_{ik}} \quad \ldots\ldots\ldots\ldots\ldots (53)$$

in which the summation extends over all columns ik of the $(r - 1)^{st}$ story.

To satisfy equilibrium of external forces in Fig. 16

$$\rho_{r,r} = - \left(\rho_{r+1,r} + \rho_{r-1,r}\right) \ldots\ldots\ldots\ldots\ldots (54)$$

must be satisfied.

Applying Betti's Law[5] to the various load deformation systems used in deriving the stiffness matrix, it may be established that

$$\rho_{ij} = \rho_{ji} \quad \ldots\ldots\ldots\ldots\ldots\ldots \quad (55)$$

This reciprocity relation makes it possible to derive the stiffness matrix $[\rho]$ by computing only $\frac{n\,(n+1)}{2}$ terms out of a total of n^2 terms.

Journal of the
ENGINEERING MECHANICS DIVISION
Proceedings of the American Society of Civil Engineers

DISCUSSION

Note.—This paper is a part of the copyrighted Journal of the Engineering Mechanics Division, Proceedings of the American Society of Civil Engineers, Vol. 87, No. EM 6, December, 1961.

BEARING CAPACITY OF FLOATING ICE SHEETS[a]

Closure by G. G. Meyerhof

G. G. MEYERHOF,[25] F. ASCE.—Both H. G. Hopkins and R. H. Wood enquire about the extent to which the mechanical behavior of ice can be approximated by a rigid-plastic material obeying the Tresca yield criterion. Because ice is an elastic-plastic material, it is necessary to distinguish between long-time and short-time stress applications. For long duration of stressing and slow rates of loading, the behavior of ice is similar to that of a ductile material with a yield stress in shear of approximately one-half of the yield stress in tension (12),[2] thus approximating the Tresca theory of strength.

Under this condition, ice may be represented by a rigid-plastic material with an adequate moment-rotation capacity in bending under the limit moment M_O, which obtains in practice for long-time parked vehicles or aircraft and for storage loads on floating ice sheets. Although combined loading tests on ice would be required to check the yield function, the writer believes, from an analogy with other ductile materials, that, at least for long-time loading, the Tresca yield condition applies and is preferable to the simpler Rankine criterion of maximum principal stress or moment ("square" failure condition). Moreover, previous computations by the writer for concentrated loads at the center and edge of plates on an elastic foundation have shown that the Rankine failure criterion gives much greater theoretical collapse loads that are not confirmed by observations on ice sheets. The Tresca yield condition was also chosen with a view to applying the proposed theoretical analysis to other related problems in practice, such as the collapse load of steel plates and shells loaded over small areas.

Under short duration of stressing and rapid rates of loading, however, ice behaves like a brittle material with a shear strength of about one-half of the bending tensile strength (21), which is again consistent with the Tresca theory of failure. Because the corresponding moment-rotation capacity under the yield moment M_y is limited, the moment redistribution in plates is believed to be small and can be neglected in practice for short-time loads on floating ice sheets. The theoretical collapse load for this condition has, therefore, been estimated on the assumption that the ice sheet has either radial cracks or a circumferential crack, in the case of concentrated loads, or a longitudinal crack, in the case of strip loads. Whereas both assumptions give practically the same theoretical collapse load for concentrated loads, the actual collapse mechanism favors the assumption of radial cracks. In these cases, the Tresca

---

[a] October 1960, by G. G. Meyerhof (Proc. Paper 2627).

[2] Numerals in parentheses refer to corresponding items in the Appendix Bibliography in the original paper and this closure.

[25] Head, Dept. of Civ. Engrg., Nova Scotia Tech. College, Halifax, N. S., Canada.

yield criterion has also been used and would indirectly be supported by the good agreement between the proposed theory and the observations of loading tests presented by L. W. Gold.

Gold's additional information, obtained from field surveys of ice roads and landings of pulp and paper companies, is most welcome, and these observations of normal, maximum, and failure loads fall in the same regions as those indicated in Fig. 8. Using the high values of the flexural strength f_b deduced from the maximum working loads and the low values of this strength deduced from the failure loads, the various field observations give a range of f_b from about 100 psi to 300 psi, which is within the customary variation of the strength of fresh-water ice under short-time loads. To the various factors mentioned by Gold in connection with failures of normally adequate ice thicknesses in practice may be added the effect of a sudden drop in air temperature and extremely cold weather; such weather conditions may lead to cracking of ice sheets due to great thermal contraction. Under such conditions the bearing capacity of ice is theoretically about one-half of that of an uncracked sheet (see Fig. 4); this would be confirmed by recent field data (22). Before thermal cracks have time to heal, a half load limit should be used on the ice as a precaution.

In view of the continued absence of published results of full-scale loading tests on ice to failure, the series of model tests on floating ice sheets by Gold is particularly valuable. His test results show that the maximum tensile stress deduced from the yield load at first cracking of the sheets agrees closely with the flexural strength of the ice deduced from the collapse load and the proposed equations for central loads. Practically the same flexural strength of the ice has been deduced from the collapse under edge and corner loads on sectorial sheets that failed at a load in almost direct proportion to the center angle of the sheet and with a crack pattern, as had been suggested in the theoretical analysis. The average observed radius of the circumferential crack of about 0.4 L at failure of the ice sheets is also consistent with the average value of approximately 0.3 L estimated from the proposed theory for narrow wedges. This radius also supports the assumed collapse mechanism of radially-cracked sheets.

In this connection, the results of another model loading test are of interest (23). A floating ice sheet of 8.4 in. thickness and 26 ft-by-26 ft wide was loaded at the center over an area of 30 in. diameter, the test being made in 5 hr at a temperature of 15°F. The first radial crack in the sheet was observed at a load of 7,840 lb, when the maximum tensile stress s_r is calculated to be 235 psi (Eq. 1) for a characteristic length L of 200 in. A circumferential crack with a radius of about 0.6 L developed at a load of 18,300 lb, for which the flexural strength f_b of the ice is deduced to be 215 psi (Eq. 38) with a theoretical crack radius of 0.5 L. Complete collapse of the sheet occurred at a load of 20,600 lb, for which f_b is estimated to be 240 psi. The values of f_b and s_r are in good agreement and are of the same order of magnitude as those of Gold's tests. The observed deflection pattern is also found to be consistent with the theoretical shape (Eq. 45).

The influence of the geometry of loading on the collapse of ice sheets has been referred to only briefly in the paper, and most solutions were obtained for single circular and strip loads. The analysis for concentrated loads at the edge of semi-infinite plates was, however, derived for a semi-circular area [Fig. 5(a)] so that an equivalent radius of $\sqrt{2}$ a should be used for a circular load of radius a tangent to the edge of an ice sheet before entering Fig. 4(a).

Similarly, wedge plates were analysed for a sector load (Fig. 6) so that an equivalent radius of 2 a should be used for a circular load of radius a adjacent to the corner (90° wedge) of an ice sheet before entering Fig. 4(a). Moreover, where the radius of the loaded area is of the same order of magnitude as the thickness h of the sheet, an equivalent contact radius at the mid-surface of the ice sheet can be used. Thus, for thick sheets ($a \leq 2\ h$) the effective load radius may be taken as $a + h/2$, as in the case of punching failure.

Regarding the bearing capacity of floating ice sheets under combined loads, the writer agrees with Gold that under normal loading conditions, the collapse load may be estimated from an equivalent circle enclosing the wheel space of a single vehicle or aircraft or from an equivalent strip, in the case of a load train. This is shown by the comparison between estimated and observed collapse and working loads of single units in Fig. 8, whereas for the usual contact range of a/L between 0.1 and 0.2, the theoretical radius of the circumferential

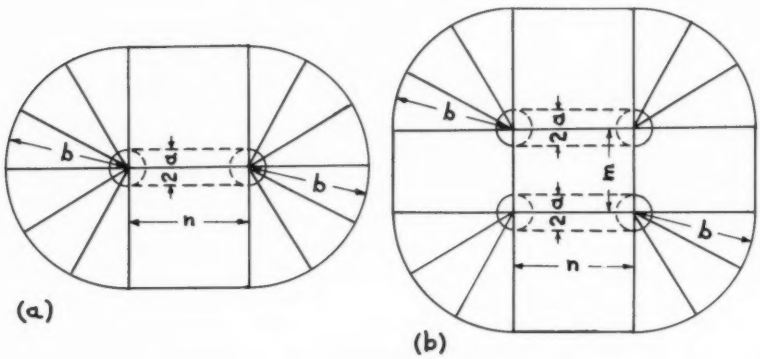

FIG. 18.—INFINITE PLATE UNDER COMBINED LOADS

crack of about 0.5 L to 0.7 L at failure (using the theory proposed for narrow wedges) compares well with the observed variation of this radius (19). However, where the wheels or tracks of a unit have a wider spacing in relation to the characteristic length L of the sheet or where a load train is relatively short, a more accurate estimate of the collapse load is to be preferred, and the following additional expressions are presented for central loads of various common types. The bearing capacity of edge and corner loads may be taken approximately as one-half and one-quarter, respectively, of that of corresponding central loads.

Circular Loads.—For two loads of the same radius a and center spacing n on an infinite ideally-plastic plate, the combined theoretical flow field is shown in Fig. 18(a). In the semi-circular end zones the collapse load may be estimated from Eqs. 4 to 6, whereas in the rectangular central zone of length n, the collapse load per unit length may be estimated from Eq. 9. The corresponding total collapse load is, therefore, approximately,

$$P_O = \left(2\,\pi + 3.6\,\frac{n}{L}\right) M_O \qquad \text{(for } a = 0\text{)} \qquad \ldots\ldots (104)$$

and

$$P_o = \left[3.3\,\pi \left(1 + 3\,\frac{a}{2}\,L\right) + \frac{3.6\,n}{L - \frac{a}{2}} \right] M_o \left(\text{for } 0.05 < \frac{a}{L} < 1\right) \quad ..(105)$$

Under short-time loading conditions on large floating ice sheets, in practice, Eqs. 104 and 105 may be replaced by the following conservative formulas in accordance with Eqs. 38 to 40:

$$P_o = \left[2\,\pi \left(1 + 2\,\frac{a}{L}\right) + \frac{3\,n\left(1 + \frac{a}{L}\right)}{L} \right] M_u \quad .....(106)$$

or, approximately,

$$P_o = \left(1 + \frac{n}{2}\,L\right) f_b\,h^2 \text{ (for } a \geq h) \quad .....(107)$$

As the load spacing n increases, Eqs. 104 to 107 approach the upper limit of the collapse load, which is given by the sum of the collapse loads of the individual circular areas.

Similarly, for four equal loads of radius a and center spacing m and n in both rectangular directions on an infinite plate, the combined flow field is shown in Fig. 18(b), and the total collapse load is, approximately,

$$P_o = \left[2\,\pi + 3.6\,\frac{(m + n)}{L} \right] M_o \quad \text{(for } a = 0) \quad .....(108)$$

and

$$P_o = \left[3.3\,\pi \left(1 + \frac{3a}{2L}\right) + \frac{3.6\,(m + n)}{L - \frac{a}{2}} \right] M_o \left(\text{for } 0.05 < \frac{a}{L} < 1\right) \quad ..(109)$$

Further, the total collapse load of large floating ice sheets under short-time loads is, approximately,

$$P_o = \left[2\,\pi \left(1 + 2\,\frac{a}{L}\right) + \frac{3\,(m + n)\left(1 + \frac{a}{L}\right)}{L} \right] M_u \quad .....(110)$$

or,

$$P_o = \left[1 + \frac{(m + n)}{2\,L} \right] f_b\,h^2 \text{ (for } a \geq h) \quad .....(111)$$

As the load spacings m and n increase, Eqs. 108 to 111 approach the upper limit of the sum of the collapse loads of the individual circular areas. If the radius of these areas differs, an average radius a may be used in the above expressions.

Rectangular Loads.—For a load applied over a short strip of width 2 a and length n with semi-circular ends of radius a, the theoretical flow field at collapse is identical to that shown in Fig. 18(a) so that the collapse load is, approximately, given by Eqs. 104 to 107. Similarly, for two short strip loads of the same size as above and center line spacing m, the theoretical flow field at collapse is identical to that shown in Fig. 18(b) so that the total collapse load

is, approximately, given by Eqs. 108 to 111. As the center line spacing increases, the total collapse load approaches the sum of the collapse loads of the individual strips.

Wood, N. C. Lind, and D. T. Wright refer to the influence of deflections on the collapse loads of plates. Membrane action, change in geometry, and shearing deformation of the plates have been neglected in the proposed analysis, because trial computations by the writer indicated that their effects would be relatively small for floating ice sheets in practice. Only where deflections are greater than the approximate thickness of the ice would the theoretical collapse loads be increased significantly, and until supported by field evidence, it seems best to neglect this increase.

G. Y. Sebastyan and F. Penner have made an extensive series of loading tests on concrete pavements of airfields having various subgrades, bases, and slab thicknesses. Static plate bearing tests have been carried out at free, keyed, and dowelled corners and at the center of pavements when the corners and edges were curled down. The test results show that the yield or first cracking loads are much greater than according to the conventional (elastic) method of design. For the free corner case, the observed collapse loads agree fairly well with the estimates based on the proposed method of analysis, whereas for the dowelled and keyed corners, the actual collapse loads are generally greater than the theoretical value for edge-loaded slabs. Under central loads, however, collapse occurred at considerably greater loads than estimated. This difference appears to be largely due to the different yield criterion for concrete and the variable foundation modulus for soils, which may require a modification of the method of analysis and that it is proposed to consider in a subsequent paper. It is of interest to note that the observed punching loads give a theoretical tensile strength (Eq. 36) of about one-half of the flexural strength, which is in accordance with the usual laboratory test results on concrete.

A. Assur discusses the author's assumptions of the position of the yield hinge circle and the extent of the hydrostatic reaction pressure in relation to some unpublished results of large-scale loading tests on floating ice sheets. These tests show that after collapse the hydrostatic reaction is essentially confined to the yield hinge circle in which a circumferential crack occurs near the location of the estimated maximum elastic radial bending moment. As mentioned in the paper, a complete solution of this problem requires an elastic-plastic analysis based on the actual mechanical properties of the ice. In view of mathematical difficulties, such an analysis is not yet (1961) available. The author's approach is, therefore, based on plastic theory for a rigid plate, which necessarily implies zero deflection at the yield hinge circle. This method, in which an allowance is made for the limited moment-rotation capacity of ice under short-time loads, furnishes simple solutions for the collapse load under various loading and boundary conditions, and expressions for combined loads have been added above, as requested by some of the discussers.

Although the actual radius of the yield hinge circle of an ice sheet at collapse is smaller than the radius of the deflection dish, the latter value has been adopted in the paper as a safe approximation for the effective radius b in estimating the ultimate load from the proposed theory. If the former radius is used, as preferred by Assur, the theoretical collapse loads deduced from Fig. 3 will be greater, but the difference is relatively small for the usual range of contact areas. Further, an assumption that the hydrostatic reaction at collapse

extends beyond the yield hinge circle gives similar estimates, if the effect of shearing stresses on the limit moment is taken into account. Assur's modification of Johansson's theory tends to give excessive estimates for concentrated loads, and for a central point load it gives twice the collapse load estimated from the present theory. This difference is due to the use of the Rankine failure criterion in the former theory, which does not apply to ice, as indicated previously. On the other hand, the corresponding location of the circumferential crack of an ice sheet at collapse is of the same order of magnitude as estimated from the equation $r = 1.63 \sqrt{a\,L}$, based on the author's theory of a radially-cracked center-loaded sheet. The most useful check of the present theory may, however, be obtained from a comparison of the estimated collapse loads with the results of loading tests on floating ice sheets. In this respect, the evidence presented in the paper and in the tests by Gold and Linell show good agreement between the proposed formulas and observations. A full publication of the results of the large-scale loading tests by the laboratory with which Assur is associated would, therefore, be most welcome.

The author is grateful to the various discussers for their kind comments and for adding important experimental evidence; both have helped to assess the proposed approach to a complex problem of considerable practical interest.

ADDITIONAL REFERENCES

21. "Bending and Shear Tests on Lake Ice," by J. T. Wilson and J. M. Horeth, Transactions, Amer. Geophysical Union, 1948, Vol. 29, p. 909.

22. "Field Study on the Load Bearing Capacity of Ice Covers," by L. W. Gold, Woodlands Review, Pulp and Paper Magazine of Canada, Vol. 61, 1960, p. 11.

23. "Use of Ice as a Load-Supporting Surface," by K. A. Linell, presented at the 1951 ASCE Convention at New York, N. Y.

DYNAMIC ELASTIC-PLASTIC ANALYSIS OF STRUCTURES[a]

Closure by M. L. Baron, H. H. Bleich, and P. Weidlinger

MELVIN L. BARON,[12] A. M. ASCE, HANS H. BLEICH,[13] F. ASCE, and PAUL WEIDLINGER,[14] F. ASCE.—The last paragraph of A. A. Eremin's discussion begins with the statement, . . . "In the illustrative example the interval was assumed . . .

$$k = 0.50\ T"$$

This statement seems to be based on some misinterpretation of the text by the discusser. The paper nowhere makes such a statement, and much smaller intervals were used. (As explained in the Appendix, stability of the integration requires $k < T_4/\pi$, in which T_4 is the shortest period of the beam with lumped masses. As T_4 is much smaller than the fundamental frequency T, an analysis with $k = 0.50\ T$ would be unstable and impossible.) At the beginning of the numerical example it is stated that the decay constant of the pressure wave in the example in Table 1 is

$$t_o = T/2$$

that may be the origin of the misunderstanding.

Finally, the writers cannot agree with Eremin's statement, ". . . it is hardly necessary to refer to the period of natural vibration," because the decay constant t_o of the applied pressure must be defined, and its natural (dimensionless) definition is the ratio of t_o to the period T.

The writers would like to acknowledge that this paper is the result of investigations sponsored by The RAND Corporation under contract with Paul Weidlinger, Consulting Engineer.

---

[a] February 1961, by Melvin L. Baron, Hans H. Bleich, and Paul Weidlinger (Proc. Paper 2731).

[12] Assoc., Paul Weidlinger, Cons. Engr., New York, N. Y., and Adjunct Assoc. Prof. of Civil Engrg., Columbia Univ., New York, N. Y.

[13] Dir., Inst. of Flight Structures, Columbia Univ., New York, N. Y.

[14] Cons. Engr., New York, N. Y.

MOIRÉ FRINGES AS A MEANS OF ANALYZING STRAINS[a]

Closure by C. A. Sciammarella and A. J. Durelli

CESAR A. SCIAMMARELLA[16] and AUGUST J. DURELLI.[17]—Morse has touched on five areas of comment:

1. Objective of the paper (first paragraph);
2. Limitations of the method (second paragraph);
3. Use of Eulerian and Lagrangian equations (second paragraph);
4. Mathematical errors (second and third paragraphs); and
5. The use of classical large strain displacement theory for moire analysis, as opposed to the more direct "geometric approach" with the use of the 8 measurements he describes (fourth, fifth, and sixth paragraphs).

Each point will be considered in turn.

1. Apparently, Morse has missed the objective of the paper. Noting that the mathematical theory of deformations has its starting point in the displacement field, it was the objective of the paper to present Moiré data in terms of this displacement field and so allow the computation of the deformations from moire data. No "new method of measurement . . . with greater precision" was presented or implied.

2. Both large displacement and small displacement equations were presented in the paper, and it is the judgment of the writers that there are many cases in which the small displacement equations may be used. The question of what amount of strain is necessary to produce fringes depends on the line density of the available grid, the geometry to be analyzed, and the maximum allowable strain for the material used. Further examples of problems with large strains and large rotations are needed before definite conclusions may be drawn as to whether Eq. 15 or 16 should be used, rather than Eqs. 20 and 21.

3. The distinction between the Eulerian and Lagrangian descriptions is made in the section "Fundamental Properties of the Moiré Fringes" and the pages following.

4. The correction of Eq. 19, although not changing any of the conclusions, does help in the understanding of the presentation.

5. In comparing the "geometric approach" with the use of Eqs. 15 and 16, it should first be pointed out that the field of u and v values completely defines the strain field, and that the field of $\partial u/\partial x$, $\partial u/\partial y$, $\partial v/\partial x$, $\partial v/\partial y$ also defines the strain field; thus, the four other measurements Morse describes are supplemental in the same sense that a hypotenuse and an angle are supplemental

---

[a] February 1961, by C. A. Sciammarella and A. J. Durelli (Proc. Paper 2736).

[16] Argentine Atomic Energy Comm., Buenes Aires, Argentina.

[17] Prof., Civ. Engrg., Catholic Univ. of America, Washington, D. C.

to the two legs of a right triangle in construction of the triangle. Either set is sufficient to construct the triangle.

The one advantage of the geometric method, cited by Morse, is the use of one photograph to determine some values of strain. This advantage results from a simplification.

The only assumptions implicit in Eqs. 15 and 16 are homogeneity, isotropy, and a uniform strain field at the point of analysis. In order to analyze strains with one photo, it must be further assumed that rotations are negligible. Obviously, if there is rotation, a shearing strain along the model grid lines would not affect the fringe pattern, but would change the value of strain perpendicular to the master grid. In other words, the u-field does not uniquely determine ϵ_{xx}^{E} if there is rotation.

Thus, it is obvious that regardless of the approach, generally, both displacement fields are necessary to compute strains. In the special case of no rotations, as on lines of symmetry, either approach may be used to determine strains from one photograph.

WIND INDUCED VIBRATIONS IN ANTENNA MEMBERS[a]

Closure by William Weaver, Jr.

WILLIAM WEAVER, JR.,[4] M. ASCE.—The writer agrees with Woodruff that there appears to be no "critical" velocity above a Reynolds number of approximately 3 by 10^5.

The values of $\overline{C}_K$ reported in the experiments were obtained by direct force measurements for stationary cylinders. Values of $\overline{C}_K$ for oscillating cylinders and flexural members were calculated using the incremental load factors (ILF) defined in detail in the paper. The value of 0.20 for large stacks quoted by Woodruff corresponds fairly well with the writer's results.

With regard to Woodruff's remarks concerning the frequency of oscillation, all responses of cylinders and flexural members were observed to be at natural frequencies only.

A question was raised about the numerical value of R in Appendix I, but the writer can find no discrepancy:

$$R = \frac{V D}{\nu} = \frac{v d}{1.564 \times 10^{-4}} \frac{(44)}{(30)(12)} = 780\, v\, d \quad \ldots\ldots \quad (32)$$

in which, R refers to the Reynolds number; V is the velocity, in feet per second; D denotes the diameter, in feet; v is the velocity, in miles per hour; d describes the diameter, in inches; and ν = is the kinematic viscosity of air, in square feet per second.

---

[a] February 1961, by William Weaver, Jr. (Proc. Paper 2748).

[4] Asst. Prof. of Civ. Engrg., Stanford Univ., Stanford, Calif.

RESPONSE OF MULTI-STORY STRUCTURES TO EARTHQUAKE[a]

Discussion by John A. Blume

JOHN A. BLUME,[15] F. ASCE.—Work in the detailed response of inelastic multi-storied buildings to earthquake motion should be encouraged. Glenn V. Berg, F. ASCE, is to be commended for his efforts in this complex field. The problem is one of many parameters, but carefully controlled research may lead to the isolation and evaluation of the basic factors. Although many of these parameters have been considered by other investigators, and analysis techniques have been proposed to include the effects of damping, multi-story behavior, inelastic response, and the combined participation of frames, shear walls, and other building elements, more data are needed to refute, substantiate, or modify the proposals and to provide a needed background of reference material.

The fact that most structures respond to major earthquakes in the inelastic range and that this response should be considered either directly or implicitly in design practice is gradually being more generally recognized. There still is a great tendency, however, for many designers to assume that damping, or perhaps a few shear walls, will take care of all the problems. The numerical evaluation of these and other important factors is thus desirable not only for basic research but also to help overcome inertia in the practice of building design.

The author's models are idealized, as they should be. It may be well to consider the implications of the simplifications and to compare the model characteristics with those of actual buildings. The zero damping situation does not, of course, occur in structures. However, it has been found[5,6,11,16] that damping at small amplitudes is not great, and values of 5% to 10% of critical damping have been proposed as applicable to the non-damaged state.[6,17] Although greater energy dissipation that that represented by the 5% to 10% viscous damping occurs in the inelastic range, it seems desirable to differentiate between a nominal viscous type damping, in which energy is converted to heat without damage to or permanent distortion of the structure, and the inelastic range of cracking, yielding, or other damage. Berg has used viscous damping conditions that result in 14.8% of critical for the first mode of the four-story

---

[a] April 1961, by Glenn V. Berg (Proc. Paper 2790).

15 Pres., John A. Blume & Assocs., Engrs., San Francisco, Calif.

16 "A Structural-Dynamic Investigation of Fifteen School Buildings Subjected to Simulated Earthquake Motion," by John A. Blume, Sharpe, and Elsesser, prepared for the State of California, Dept. of Public Works, Div. of Architecture, distributed by Printing Div., Documents Sect., Sacramento 14, Calif.

17 "A Reserve Energy Technique for the Design and Rating of Structures in the Inelastic Range," by John A. Blume, Proceedings, Second World Conf. on Earthquake Engrg., Tokyo, Japan, July, 1960.

model and the other 6.25% of critical for the eight-story model. Because a nominal value of 5% seems applicable to the frame and from 5% to 10% for the shear walls, depending on detailed conditions, the values used are not significantly greater than those often considered applicable. However, it would seem well to include a slightly damped frame among the elasto-plastic models.

The use of zero damping values is necessary to compare the author's response of the elastic and inelastic frames. This is unfortunate, not only because zero damping is not directly applicable to structures, but also because undamped response to earthquake motion may lead to much greater peaks and valleys and irregularities than for a more typical value such as 5% of critical, that "irons out" many of the irregularities of response.

Berg notes fundamental periods of 2.01 sec for the four-story frame and 1.45 sec for the same frame with the added shear walls. These are extremely long periods for any four-story building and, in fact, are longer than the traditional type fifteen-story building, studied by the writer, and longer than a modern fifteen-story building, for which periods were carefully determined all through construction.[18] The height squared divided by the width of the four-story building is approximately 45. Building periods in this category[19] of height-to-width generally range from 0.3 sec to 0.8 sec and usually would not exceed 0.4 sec to 0.6 sec.

An attempt was made by the writer to compute natural periods from the data shown in Figs. 1 and 2. Assuming all columns oriented with their greatest moments of inertia in the direction parallel to the bents illustrated, and neglecting all resistance but the steel frame, the following fundamental periods were obtained, using a portal method and the Rayleigh procedure:[20]

Four-story frame	1.55 sec
Four-story frame with 30 kips per in. shear wall stiffness added to each story	1.24 sec
Eight-story frame	1.84 sec

The eight-story period also seems very long in comparison with average buildings. It would be well for Berg to list his shear spring constants and elastic limit shear values so that readers would have available the same dynamic properties that were used in the experiments.

Although the author's periods are quite long for actual buildings of corresponding stories with floors, fireproofing, stairways, and other elements included, this does not detract from the value of the response data obtained for multi-mass dynamic systems of specific characteristics. It does indicate, however, that the results should not be considered typical for four and eight-story buildings. The models might be "extended" to approximate dynamically equivalent buildings of more stories. The procedure of coupling stories was

---

18 "Periods of a Modern Multi-Story Office Building During Construction," by John A. Blume and R. W. Binder, Proceedings, Second World Conf. on Earthquake Engrg., Tokyo, Japan, July, 1960.

19 "Lateral Forces of Earthquake and Wind," by Arthur W. Anderson, John A. Blume, Henry J. Degenkolb, Harold B. Hammill, Edward M. Knapik, Henry L. Marchand, Henry C. Powers, John E. Rinne, George A. Sedgwick, and Harold O. Sjoberg, Transactions, ASCE, Vol. 117, 1952, Fig. 8, p. 732.

20 "Earthquake Stresses in Shear Buildings," discussion by John A. Blume, Transactions, ASCE, Vol. 119, 1954, p. 194.

used in a recent research effort[6] to reduce a twenty-story building to a ten-mass equivalent system that could be accommodated in the available electric analog. The writer has taken the liberty of doing the opposite with the author's four-story frame, as shown in Fig. 11, where, as indicated by the dash lines, it is arbitrarily "uncoupled" or "extended" to represent a twelve-story structure.

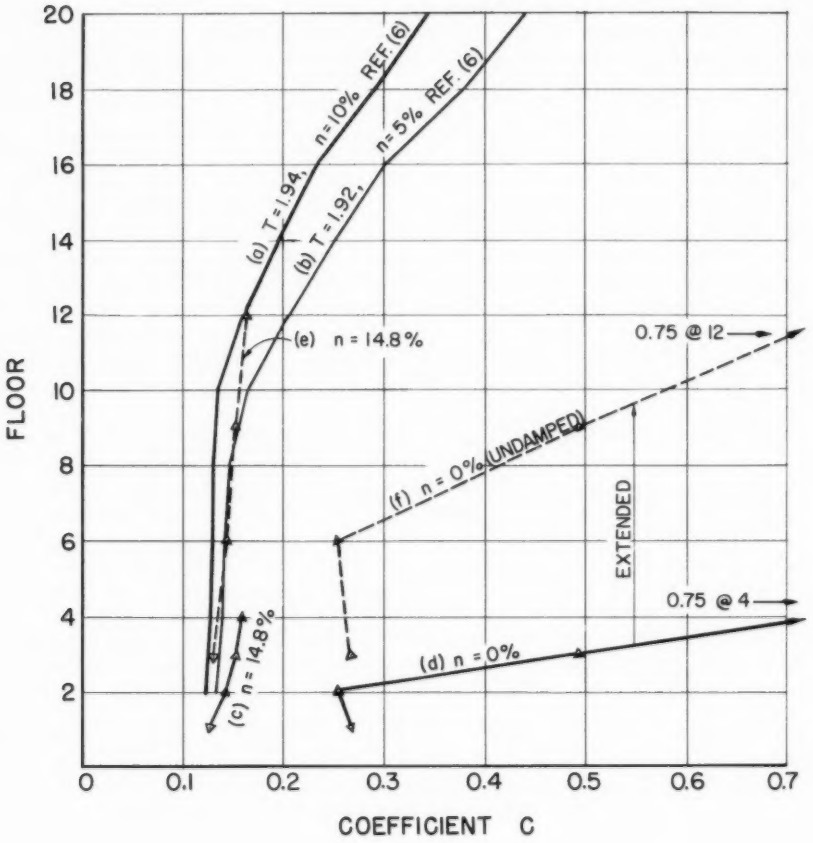

FIG. 11.—ELASTIC ACCELERATIONS

Fig. 11 shows elastic acceleration coefficients from two sources for the 1940 El Centro (N-S) earthquake. Only "all-mode" results are plotted. The natural periods of the systems are basic factors, of course, in the response and must be considered in making comparisons. There is good reconciliation between the shapes and values of the various elastic responses, when all factors are

considered. It is to be noted, however, that the elastic accelerations for models of shorter period would be considerably greater.[16,17,20,21,22]

It is important to obtain response data for all possible multi-mass systems, especially under inelastic behavior. Moreover, every effort should be made to analyze and compare all available data. A few comparisons will be made herein:

The upper three stories of the four and eight-story framed structures are identical in weight and dimensions and vary only slightly in column properties. The response of these stories, as shown in Table 1 for the Helena earthquake, is considerably greater for the eight-story undamped model than for the four-story model; this is as would be expected. It is noted, however, that the damped

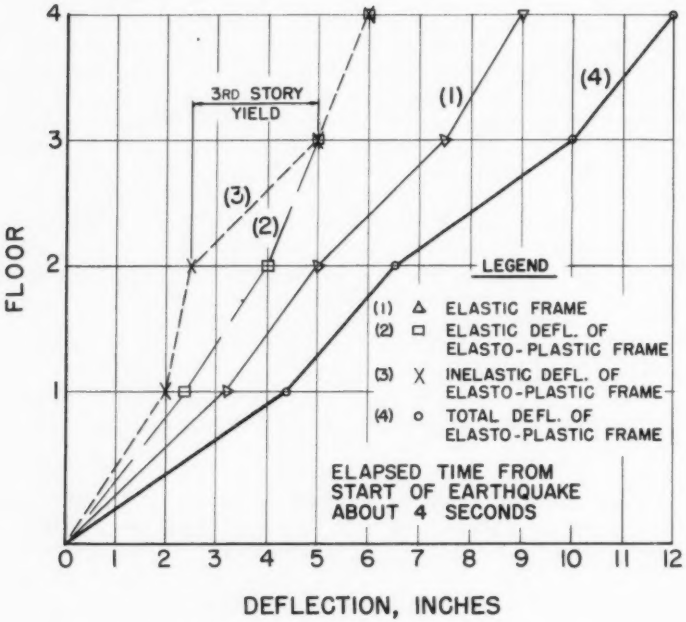

FIG. 12.—FOUR-STORY UNDAMPED FRAMES (RESPONSE TO EL CENTRO MOTION AT FIRST YIELDING)

frame of the four-story model (damped to 14.8% of critical, whereas the eight-story is only damped to 6.25%) has essentially equal or greater seismic coefficients, in spite of lesser deflections. These particular damped results seem to have some inconsistency.

The elasto-plastic response in Berg's paper is limited to the four-story models under the 1940 El Centro N-S ground motion. Col. 4 of Table 1 gives

21 Discussion by John A. Blume of "Behavior of Structures During Earthquakes," Proceedings, ASCE, Vol. 86, No. EM 3, June, 1960.

22 "Dynamic Response of Elasto-Plastic Frames," by Joseph Penzien, Proceedings, ASCE, Vol. 86, No. ST 7, July, 1960.

the maximum deflections and accelerations for the undamped elasto-plastic frames; these values are less than for the undamped completely elastic frame, as shown in the second column. This is interesting when questioning[13,17] whether deflection preservation or energy preservation better represents elasto-plastic response phenomena. In this case, as the author notes, the maximum deflections under elasto-plastic response are greater than for the corresponding earthquake exposure of the elastic system. However, this comparison is not direct, because the maxima may not occur at the same time and the elasto-plastic yieldings may be confused by cumulative effects. In order to explore this problem and also to attempt to evaluate the relative energy demands, the writer has scaled values from Figs. 9 and 10 for one instant of time and for all stories. The peak values occurring at about 4 sec elapsed time were selected, because this apparently represents the first excursion beyond the yield point and is thus uncomplicated by prior lurches and any cumulative effects. Fig. 12 indicates the results.

Although no great accuracy was possible or is claimed for Fig. 12 and the related results, it is believed that the general trend is apparent. It is noted that the completely elastic system shown as curve (1) consistently has less total deflection than the elasto-plastic system of curve (4). Curve (3), that is the deflection beyond the yield point for the elasto-plastic frame, is interesting because it shows inelastic response in all four stories, although the second and fourth stories had minor inelastic response as compared to the first and third stories.

Fig. 13 indicates the shear and deformation relationships obtained for the same (4-sec elapsed time) instant. Obviously, the work done in the inelastic range, for this case at least, varies considerably between stories. The term C' represents the seismic coefficient at which yield occurs as obtained by this scaling procedure, with the aid of the elastic spring constants represented by the slopes in the figure. The low yield value of the third story seems inconsistent with the other stories and may be due to the difficulty of scaling or the model characteristics.

The dash line in Fig. 13 roughly represents a mode or distortion shape, because the deflection scale is the same for all stories. This appears to be a fourth mode of vibration, whereas a line connecting the yield points would indicate a third mode. Such modes are, of course, reinforcing the fundamental mode motion. These conjectures are not too unreasonable, considering the facts that the spectral peak of the El Centro earthquake is in the period range of 0.2 sec to 0.3 sec, the third or fourth mode of this flexible model would be in the same general spectural region, and Figs. 9 and 10 plainly indicate short period motion, as well as the 2 sec fundamental-mode motion.

Story strain energy and inelastic work were computed by the writer for the conditions shown in Figs. 12 and 13; that is, for the instantaneous deflected position. In addition, strain energy for the elastic response of Fig. 9 was computed for the same instant; results are shown in Table 2.

Table 2 indicates that there is somewhat more energy in the elasto-plastic case when it is not completely elastic, especially in the lower story. The differences are not great, however, in view of the scaling and perhaps other inaccuracies. Moreover, energy is assumed to affect design as a square foot rather than as a direct function.

The reserve-energy technique[6,17,23] for inelastic analysis and design reduces elastic spectral accelerations to equivalent inelastic values in normal code terms, with allowance for energy absorption during excursions into the inelastic range. For an ideal elasto-plastic case, such as Berg has assumed, the value of R, the reduction factor, for a single mass system becomes simply

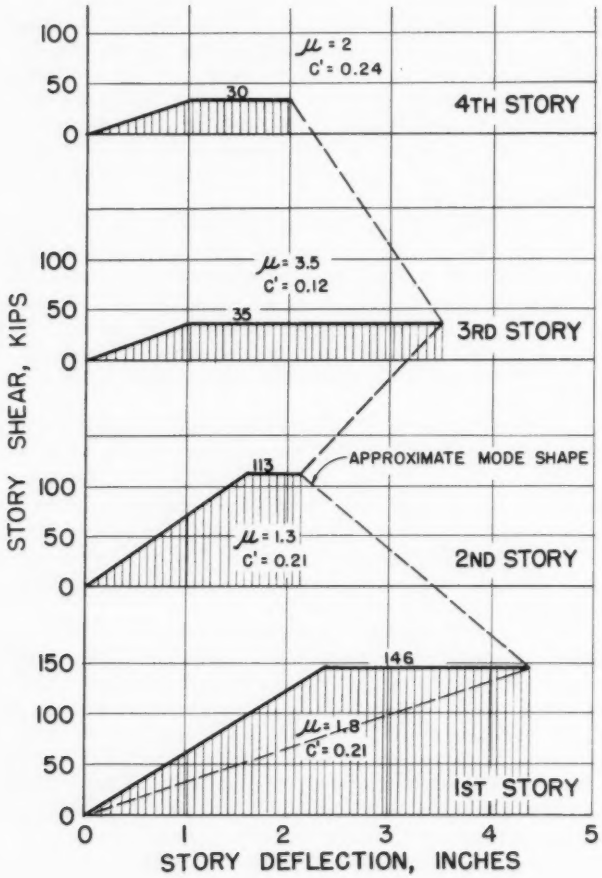

FIG. 13.—STORY SHEAR AND DEFORMATION AT FIRST YIELDING

$1/\sqrt{2\mu - 1}$, in which μ is the total deformation divided by the yield point deformation. Such values are shown in Table 3 for the data obtained for the same 4-sec instant of time.

23 "Electrical Analog for Earthquake Yield Spectra," discussion by John A. Blume, Proceedings, ASCE, Vol. 86, No. EM 3, June, 1960.

The tabulations in Cols. 6 and 7 of Table 3 are made under the assumption that each story is a discrete or independent dynamic system, that is, of course, not the case, except in the fourth mode, in which this approximation may have some merit. It is interesting to note, however, that the values of Col. 6 are not much different than those of Col. 4 and, also, that the Col. 6 energy values fall closer to the test data of Col. 4 at all stories than do the values in Col. 7, that are based on deformation, rather than energy preservation, in the inelastic range. This concept of stories being treated as independent inelastic systems deserves further exploration. It has been suggested[17] for first stories, under some conditions, but not for other stories. It would seem that, generally, for Berg's results, energy preservation more closely represents the test data than displacement preservation.

TABLE 2.—ENERGY DEVELOPMENT, IN KIP-INCHES, AT 4 SEC ELAPSED TIME

Story	Undamped Elastic Frame	Undamped Elasto-Plastic Frame		
		Elastic	Inelastic	Total
4	34	15	30	45
3	110	18	88	106
2	114	90	57	147
1	310	175	292	467
Total	568	298	467	765

TABLE 3.—ACCELERATIONS AND REDUCTION FACTORS

	Experimental Data			Calculated Values		
Story	Elastic Acceleration α, in g units	Yield Value, or C'	$R = \frac{C'}{\alpha}$	μ	$\frac{1}{\sqrt{2\mu - 1}}$	$\frac{1}{\mu}$
(1)	(2)	(3)	(4)	(5)	(6)	(7)
4	0.37	0.24	0.65	2	0.58	0.50
3	0.29	0.12	0.41	3.5	0.41	0.28
2	0.26	0.23	0.88	1.3	0.79	0.76
1	0.28	0.21	0.75	1.8	0.62	0.56

A basic problem in multi-story building considerations in the inelastic range is how much the energy dissipation in other stories helps or affects each story under consideration. Is the total energy capacity above each story effective, or should it be reduced because of the improbability of all above stories participating at full capacity? Is the value of stories below the one under consideration also effective and, if so, in what degree? There is no simple answer, especially since time-history of performance is a factor, unless, perhaps, the discrete story consideration noted previously might be found to have practical application under certain conditions. The reserve-energy technique considers the total of all energy values above each level, but it reduces this capacity in accordance with various probability factors. The assumption of a straight line

deflection shape, but without probability reduction for energy, produced a first-story R factor of 0.78 in this case, as compared to the 0.75 found. The R-factors for the upper stories were found to be greater than the experimental, as would be expected for such low ductility factors or such minor excursions into the inelastic range.

It is obvious that extensive research is needed to provide complete answers and values for these and other related problems. The inelastic type of work done by the author, by Joseph Penzien,[22] in New Zealand,[24] and in Japan should be correlated with actual field conditions and structures, considerably extended, and the data should be analyzed in great detail. The writer's approximate analyses presented herein are not intended to offer or to imply any sweeping conclusions from this limited work but to suggest types of detailed considerations, taken step by step, that seem to be needed in this problem. Unfortunately, in the current state of progress, with different investigators using so many different parameters, comparison and reconciliation cannot be made effectively. For example, Berg used four and eight story models of specific periods and the north-south component of the 1940 El Centro record, whereas Penzien[22] used the east-west component and six-story models. A coordinated program could, no doubt, lead to earlier isolation and evaluation of the many parameters.

It is recognized that there are several types of damping in a building and that truly viscous damping may account for but a small part of the total energy absorption. However, it seems desirable to continue with the mathematically convenient concept of viscous damping, but to confine the values to the low amounts found at small amplitudes (perhaps 5% to 10% of critical) and to allow for greater energy consumption by friction, grinding, and so forth, in the damaging or yielding range, as another parameter, that is, work done. This is convenient, traditional, less confusing, and is compatible with much work that has been done. It is not necessary to use equivalent viscous damping, as the author implies, to analyze structures with the aid of response spectra. The reserve energy technique[5,16,17,23] may be used with any spectrum desired and any viscous damping value, although 5% of critical is generally recommended, and convenient smoothed spectra are provided. Although this technique needs refinement and more test data before its general use or its use as an exclusive design procedure on multi-story buildings would be considered, it is general in application, yet quite simple and adaptable, and has been used extensively in the analysis of all types of buildings. One of its benefits is that it separates damping, damage or yield, and deterioration. By combining these into some such broad term as equivalent damping, identification is lost, and designers lose the art or "the feeling" of design.

There may be little residual doubt of, but perhaps some reluctance to accept, the fact that most multi-story buildings will have to enter the inelastic range to resist major earthquakes. The principal problem is, and this has been developed extensively,[6] that modern buildings without the aid of "non-calculated" walls, partitions, concrete fireproofing, and so forth cannot be expected to have the reserve energy capacity of the traditional type buildings or to perform so well as they did. Not only is more research needed, but also more general acceptance of the facts of structural dynamics and more realistic design analyses, at least for special cases. Deformation and energy are basic

---

24 "Electrical Analog for Earthquake Yield Spectra," by G. N. Bycroft, M. J. Murphy, and K. J. Brown, Proceedings, ASCE, Vol. 85, No. EM 5, October, 1959.

considerations, in addition to strength, but these must be evaluated in terms not only of primary loads but also of secondary effects, eccentricities, and buckling tendencies under severe story deformations. The interaction and the value of various building materials and elements are not new considerations, but when contemporary architectural design deletes most of these elements and materials from the buildings, the design professions are faced with a serious problem. Modern buildings require more advanced earthquake designs than their predecessors, if they are to survive severe earthquakes. The codes and code coefficients along may not be expected, nor are they intended, to supersede good engineering judgment based upon all available and pertinent facts.

This somewhat extensive discussion is not intended to be critical of this excellent research effort but to emphasize certain factors considered important in the basic, but little-recognized, subject of inelastic response of multistory buildings to earthquake motion, to encourage more efforts in this field, and to attempt to make a better and more effective climate in which those interested may work for the public welfare.

CONTINUOUS BEAM-COLUMNS ON ELASTIC FOUNDATION[a]

Closure by S. L. Lee, T. M. Wang, and J. S. Kao

SENG LIP LEE,[12] M. ASCE, T. M. WANG,[13] and J. S. KAO.[14]—The three-moment equation for continuous beam-columns on elastic foundation derived by Lu, Eq. 60, defines the relationship between the end moments and deflections. In comparison, the use of the slope-deflection equations, Eqs. 18a and 18b or Eq. 22, as the case may be, yields the relationship between the end slopes and deflections. The former leads, in general, to a system of simultaneous equations that involves more unknowns than the latter. For the problem treated in Example 1, for instance, Eqs. 62, 63, and 64 contain three unknowns M_a, M_b, and y_b, whereas Eqs. 30a and 30b involve only two unknowns θ_b and y_b.

The proposed method may be extended to the analysis of continuous plane frames with members which are elastically restrained. In this case, the use of the slope-deflection equations generally introduces three unknown displacement components per joint, the rotation and two deflection components. On the other hand, the application of the four-moment equation, which may be derived in similar fashion as Eq. 60, involves more unknowns per joint, with the exception of joints with only two members. For example, a four-member joint introduces five unknowns, three moments, and two deflection components, the fourth moment being expressed a priori in terms of the other three. On the standpoint of the number of unknowns involved, therefore, it must be concluded that the use of the slope-deflection equations is preferable.

As stated at the end of the conclusions of the paper, the moment-distribution method should be used when large number of joints are involved. In this respect, the stiffness influence coefficients contained in the slope-deflection equations furnish the distribution and carry-over factors, whereas the fixed-end moments give the residuals in the joints to be balanced by successive approximation.

The foregoing discussion takes nothing away from the significance of Eq. 60, which gives the general form of the three-moment equation and should be useful in cases in which it is desirable, for some practical reasons, to formulate the problem in terms of the end moments, instead of the joint rotations.

---

[a] April 1961, by Seng-Lip Lee, T. M. Wang, and J. S. Kao (Proc. Paper 2801).

[12] Prof. of Civ. Engrg., Northwestern Univ., Evanston, Ill.

[13] Asst. Prof. of Civ. Engrg., Univ. of New Hampshire, Durham, N. H.

[14] Walter P. Murphy Research Fellow, Civ. Engrg. Dept., Northwestern Univ., Evanston, Ill.

HYDRODYNAMICS OF FLOW INTO CURB-OPENING INLETS[a]

Discussion by James A. Liggett

JAMES A. LIGGETT,[8] A. M. ASCE.—The writer finds Wasley's division of zones I and II rather strange. The disturbance created by the end of the curb does not only travel in the transverse direction but in all directions. It is for this reason that the author was forced to restrict his solution to supercritical flows. Therefore, the equation introducing the small wave velocity Eq. 6 should read

$$c = \frac{ds^*}{dt} = \sqrt{gz^*} \quad \ldots\ldots\ldots\ldots\ldots\ldots (19)$$

where s^* is the length of the line element normal to the dividing line.

Actually, the author is trying to find the equation of the characteristic line (line along which small disturbances propagate) that begins at the end of the curb. The equation should be simply

$$\frac{dy^*}{dx^*} = \frac{c}{\sqrt{\bar{u}^2 - c^2}} \quad \ldots\ldots\ldots\ldots\ldots\ldots (20)$$

for $\bar{v} = 0$. Eq. 20 follows directly from the definition of the small wave angle[9]

$$\beta = \arcsin \frac{1}{F} \quad \ldots\ldots\ldots\ldots\ldots\ldots (21)$$

in which F is the local Froude number $\left(\text{in this case } F = \frac{C_o}{\sqrt{g}} \right)$. A short analysis of the author's development will show that he has neglected the c in the denominator of Eq. 20. Thus, the end of the curb will affect the flow upstream of the line that he has indicated.

Using Eqs. 2 and 19 to integrate Eq. 20, one obtains

$$x^* = \sqrt{\frac{C_o^2}{g} - 1}\ y^* \quad \ldots\ldots\ldots\ldots\ldots\ldots (22)$$

---

[a] August 1961, by Richard J. Wasley (Proc. Paper 2880).

8 Asst. Prof. of Civ. Engrg., Cornell Univ., Ithaca, N. Y.

9 "Elementary Fluid Mechanics," by J. K. Vennard, John Wiley and Sons, Inc., New York, 4th edition, p. 366.

which would replace the author's Eq. 10. Accepting the author's analysis in Eqs. 13 through 16, Eqs. 17 and 18 would be, respectively,

$$x = y_o \left(\frac{C_o}{\sqrt{2\,g}} + \sqrt{\frac{C_o^2}{g} - 1} \right) - \frac{C_o}{\sqrt{2\,g}}\, y \quad \ldots\ldots\ldots \quad (23)$$

and

$$X_{o\text{theo}} = y_o \left(\frac{C}{\sqrt{2\,g}} + \sqrt{\frac{C_o^2}{g} - 1} \right) \quad \ldots\ldots\ldots\ldots \quad (24)$$

The corresponding equations in the second column of Table 1 (under "Dimensional") would also change, but the equations in the third column remain the same. Hence, the author's non-dimensional plot (Fig. 9) is correct for the theoretical points, but the experimental points would be plotted at

$$\hat{x} = \frac{x}{y_o \left(\frac{C_o}{\sqrt{2\,g}} + \sqrt{\frac{C_o^2}{g} - 1} \right)} \quad \ldots\ldots\ldots\ldots \quad (25)$$

instead of using Eq. 18 as the normalizing function in the x- direction.

It would be interesting to see if the present analysis brings the experimental work into closer agreement with the theory. The change seems to move the plotted experimental points outward on the $\hat{x}$- axis.

CONJUGATE BEAM SIMULATED BY ELECTRIC CURRENTS[a]

Discussion by Campbell Massey

CAMPBELL MASSEY.[5]—The analogue suggested by Freiberg for obtaining influence lines of moment, shear, rotation, and deflection in beams is much more versatile if the resistors R', used to join the beam and conjugate beam strips, are variable rather than fixed in value. A beam varying in flexural rigidity along its length may then be treated by the analogue simply by setting the values of R' proportional to $(E\,I)/(ds)$ of the relevant structural element.

It may be of interest to report that an analogue similar to that described in the paper was designed and built in the Civil Engineering Department of the University of Western Australia during 1958 and described in a paper presented at the Congress of the Australian and New Zealand Association for the Advancement of Science, held in Adelaide, South Australia, in August of that year. Full details were subsequently presented by R. Leicester,[6] whose paper was reviewed in Applied Mechanics Reviews[7] and who extended the argument to include arch analysis.

The analogue is used for undergarduate instruction in the University of Western Australia.

---

[a] August 1961, by S. Freiberg (Proc. Paper 2909).

[5] Senior Lecturer in Civ. Engrg., Univ. of Wastern, Australia.

[6] "Resistance Analogue of Beams and Arches," by R. Leicester, Journal, Inst. Engrs. of Australia, Vol. 32, No. 4-5, April-May, 1960.

[7] Review 1401, Applied Mechanics Reviews, Vol. 14, No. 3, March, 1961.